# SYNTHESIS AND CHARACTERIZATION OF CHARGED POLYETHERS FOR MEMBRANE MATERIALS AND TO STUDY POLYELECTROLYTE SELF-ASSEMBLY

By

Gouree Vijaykumar Kumbhar

#### A DISSERTATION

Submitted to
Michigan State University
in partial fulfillment of the requirements
for the degree of

Chemical Engineering – Doctor of Philosophy

2023

#### **ABSTRACT**

Epoxides are a promising polymer materials platform because of their diverse functionality, ease of synthesis, availability, and ring strain favoring polymerization. Recently reported mono(μ-alkoxo)bis(alkylaluminum) (MOB) based polymerization technique provides controlled molecular weight polymers for wide variety of functional epoxides without chain transfer. We want to use this facile polymerization platform to create polymers with orthogonally addressable pendant groups to precisely tune polymer properties. Specifically, this work focuses on incorporation of charged moieties through post polymerization modification of functional pendent groups to investigate their transport and self-assembly properties.

We have demonstrated control over molecular weight, composition, and architecture via copolymerization of propargyl glycidyl ether (PGE) and epichlorohydrin (ECH), with functional alkyne and chloromethyl groups respectively. Molecular weights up to 100 kg/mol with narrow distributions were achieved. Copolymer composition was varied by incorporating increasing ratios of PGE (20-80%) in the polymerization feed. In situ <sup>1</sup>H NMR kinetic study was performed using two different systems that is MOB and separate initiator-catalyst to determine reactivity ratios. With the use of Meyer-Lowry method reactivity ratios were calculated as  $r_{PGE} = 0.69$  and  $r_{ECH} = 1.43$  for MOB system, and  $r_{PGE} = 0.72$  and  $r_{ECH} = 1.48$  for separate initiator-catalyst system. So, in both cases  $r_{PGE} \times r_{ECH} \approx 1$  which confirms the statistical nature of the copolymer with preferred addition of ECH to growing chain end regardless of polymerization technique.

These precursor copolymers were further modified with various charged groups such as imidazole and sulfonate via orthogonal chemistry through the chloromethyl and alkyne moieties. This will be beneficial in achieving tuned compositional control of structure—property relationships in a polyether materials platform. These functional polyethers were then used to create economical

crosslinked networks to prepare amphoteric ion exchange membranes (AIEMs). Nafion ion exchange membranes have been used in vanadium redox flow batteries (VRFB) applications owing to their good ionic conductivity and excellent chemical and mechanical stability. But nafion's high cost, excessive swelling and low ion selectivity limits its use for commercialization. AIEMs have potential for preventing vanadium ion penetration thus increasing ion selectivity. Membranes were synthesized by grafting of novel ECH and PGE-based charged copolymer S-P(PGE-stat-ECH) to the PVDF-co-HFP membrane matrix. We studied the physicochemical, electrochemical, and surface properties of these membranes to investigate candidacy of this novel membrane for VRFB application.

Next, we used a homopolymer of allyl glycidyl ether (PAGE) as a unifying platform for polyelectrolyte design. With the use of click chemistry we created polyether based polyanions and polycations to study effect of charge and molecular weight on self-assembly. We studied effect of NaCl and LiCl salt as well on polyelectrolyte self-assembly with varying polyanions to polycation ratios. Coacervation formations was studied using absorbance measurements on UV-vis spectrophotometer. With the use of MOB polymerization platform, we can synthesize variety of polymers, and this will be useful in exploring effects of counter-ions, polymer architecture, charge densities in future. Our synthetic platform provides control over different governing parameters separately which will be impactful in giving insights on polyelectrolyte self-assembly from fundamental standpoint. We expect the broader impacts of this research to encompass innovation in polyelectrolyte design and application. In conclusion, we demonstrated control over factors such as molecular weight, polymer architecture, charge density, monomer sequence, and counter-ions independently with the use of this platform. We have utilized these materials to further develop AIEMs for electrochemical application and to study charged polymer self-assembly.

Copyright by GOUREE VIJAYKUMAR KUMBHAR 2023 Dedicated to Aai and baba- Vijaya & Vijaykumar Kumbhar

#### **ACKNOWLEDGEMENTS**

First and foremost, I would like to express my deepest gratitude to my advisor, Prof. Robert C. Ferrier, Jr. for giving me this opportunity to work on this exciting research in his laboratory at the Michigan State University. He has pruned me to become a researcher that I am today. I am thankful to the MSU and particularly the department of Chemical Engineering and Materials Science (CHEMS) for the excellent resources they continue to provide. The entire CHEMS staff and the Ferrier group has always been helpful and resourceful, encouraging personal development to take on new challenges and responsibilities from day one.

I am especially grateful to my doctoral guidance committee members Prof. Ramani Narayan, Prof. Caroline Szczepanski, Prof. Volodymyr Tarabara for their support to present my ideas and research, for reviewing my progress and suggesting corrective measures at every stage of my research. I am also thankful to Prof. Scott Barton, Prof. David Hickey, Prof. Andre Lee, and Prof. Shiwang Cheng for their constructive feedback.

I would also like to thank my friends who have made East Lansing as my second home, my exroommate Sneha with whom I started my memorable journey at MSU; my never-was-a-roommatebut-still-shared-the-same-apartment roommate Apoorva; fellow adventure partner Manali; great
trip planner, fellow pumpkin spice latte enthusiast and match-making guru Aditya; a good friend,
philosopher and guide Affan (aka Juan); the power couple Renu and Sushanta for being the perfect
example of calm, excited and motivated people also thank you for introducing us to our own baby
Yoda Siddhanta; and finally to Shalin, who thinks he is humorous but is just not and also for
constantly reminding of finishing my thesis in time (which obviously I didn't). Thank you all for
being there for me always, for bearing me through all these years and making this journey
mesmerizing.

I am also grateful to all my lab mates, Danielle, Geetanjali, Mayson, Niloofar, Shaylynn for being such good friends and great co-workers, and I learned a lot from them during my time at Ferrier lab. I would like to extend my gratitude to all my friends in CHEMS Chase, Denghao, Sabrina, Swayam, Yan, Sharmila, Sunanda with whom I have enjoyed working, planning events, potlucks and many more fun activities.

Finally, I am incredibly grateful to my parents Vijaykumar Kumbhar and Vijaya Kumbhar who have been incredibly supportive and encouraging to pursue my dreams. Thank you for providing me with unwavering support throughout my journey here at MSU.

# TABLE OF CONTENTS

Chapter 1. Introduction	1
BIBLIOGRAPHY	
Chapter 2. Development of novel polyether synthesis platform from the facile	
(co)polymerization of functional epoxides using organo-aluminum catalyst-initiator system	
BIBLIOGRAPHYAPPENDIX	
AT ENDIA	<del>4</del> 7
Chapter 3. Post polymerization modification to obtain tunable ion-containing polyether using	-
thiol click chemistryBIBLIOGRAPHY	
APPENDIX	
Chapter 4 Dely(vinylidene diffuenide as heyeflyeremenylene) crefted with nevel polyether	_
Chapter 4. Poly(vinylidene difluoride-co-hexafluoropropylene) grafted with novel polyether amphoteric ion exchange membranes for redox flow batteries	
BIBLIOGRAPHY	
APPENDIX	
Chapter 5. Design of tunable polyelectrolytes to study and control its self-assembly behavior	r 122
BIBLIOGRAPHY	
APPENDIX	142
Chapter 6. Conclusions and future work	145

# Chapter 1. Introduction

# 1.1 Polyethers and their properties

Polyethers are a class of polymeric materials obtained by polymerizing epoxides containing aliphatic polar backbone chain and varying functional pendent groups. The most used polyether is polyethylene glycol (PEG) which is obtained by polymerizing ethylene oxide. Properties of these polyethers vary depending on presence of functional groups in backbone as well as on side chains. Chemical and physical properties of any polymer depend on functionality of polymer backbone and pendent groups hence they are often tuned to obtain desired functionality.<sup>2,3</sup> Polyethers are specifically known for their good water solubilities, excellent flexibility, low toxicity, and good low temperature properties. For example, PEG has polar backbone chain with oxygen atom which gives synergetic hydrogen bonding effect leading to good water solubilities. 4-6 PEG is also biocompatible allowing us to design materials for biomedical applications.<sup>7</sup> These PEGs and its and its derivatives are widely used in food, cosmetics, consumer products industry.<sup>8</sup> In addition, functional polyethers are used for more advanced application such as solid polymer electrolytes in batteries<sup>9</sup>, separation membranes<sup>10,11</sup>, drug delivery<sup>12,13</sup> and to develop antifouling coatings<sup>14–16</sup>. They are also used in the production of polyurethane foams, which are used in cushions, mattresses, and insulation.<sup>17</sup> Overall, functional polyethers are versatile materials that have a wide range of uses across many different industries. Hence study of these polyethers holds supreme importance in polymer science field.

# 1.2 Polymerization methodology

Epoxide polymerization involves ring opening polymerization techniques using various catalytic and ionic methodologies. Ethylene oxide (EO) has high ring strain energies of 110 kJ/mol which favors ring opening polymerization following SN<sup>2</sup> mechanism. <sup>18</sup> EO polymerization methodology was first introduced back in 1863. Since then, we are equipped with modern polymerization techniques capable of producing controlled high molecular weights polyethers with narrow polydispersities for range of functional epoxides. Commercially used catalytic method is using vandenberg's catalyst, but it has drawbacks due to uncontrolled polymerization resulting in high molecular weight and polydispersities. 19-22 Anionic or cationic ring opening polymerizations are also popular ionic methods, but it gives low molecular weight polyethers with limited functionality.<sup>23,24</sup> None of these is universal method for polymerization of functional epoxides. Recently reported polymerization technique developed by Lynd and Ferrier using mono(μalkoxo)bis(alkylaluminum) (MOB) system solves this problem.<sup>25</sup> This method inspired from vandenberg's catalyst uses combined ionic and catalytic approach and provides us with controlled polymerization technique for wide variety of functional epoxides. This synthetic route follows coordination insertion mechanism to obtain functional polyethers in controlled manner. This novel universal polymerization platform can facilitate polymerization of any epoxide with ease of operation, cost-effectively and sustainably.<sup>25–29</sup> All these parameters are critical in designing sustainable polymers with required properties.

MOB system offers good tolerance for functional groups such as halides, pendant alkenes, or alkyne without chain transfer. In addition, it follows green chemistry principles (Figure 1), especially with respect to atom economy, as we polymerize up to 99% of the starting materials using solvent-free reaction conditions. Additionally, the starting epoxides are derived from

renewable feedstocks like glycerin. With the use of MOB system, we can significantly reduce the reaction times while enabling the use of moderate or ambient reaction temperatures. This platform follows most of the green chemistry goals making it a prime methodology for epoxide polymerization.



Figure 1: Green chemistry principles for sustainable technology development

# 1.3 Necessity of functional epoxides polymerization platform

Historically it was challenging to synthesize functional polyethers using conventional anionic ring opening polymerization (AROP) methodology involving complex post polymerization modification steps.<sup>30</sup> This was limiting use of these cheaper polyethers for advanced applications. We will utilize MOB polymerization system to obtain various functional polyethers for

engineering application. Using MOB system, we can polymerize epoxides with diverse functionality such as halides, alkenes and alkyne groups. In this thesis work we have focused on preparation of charged polyethers using epoxides allyl glycidyl ether (AGE), propargyl glycidyl ether (PGE) and epichlorohydrin (ECH) and propylene oxide (PO).

The charged groups are often introduced through the addition of ionic monomers during polymerization, resulting in a polyether with a net positive or negative charge or by post polymerization modification. Chloromethyl group from ECH as a starting epoxide provides handle for post polymerization modification to obtain positively charged moieties. In case of epoxides, AGE and PGE pendent alkene or alkyne functional groups can be modified using radical click chemistries to obtain charged pendent groups with increased loading capacities. Residual methyl group from PO polymerization is useful in controlling the hydrophobicity and crystallinity of polyethers. Each of these groups brings unique characteristics which we will utilize to design materials for specific application. (Figure 2)

Charged polymers contain ionic groups as a part of their side chains. The presence of charged groups imparts unique properties to these polymers such as high-water solubilities, hydrophilicity, excellent electrochemical properties for ion transport, biocompatibility, and surface functionality to enhance antifouling performance. Due to these outstanding characteristics charged polymer are often used for diverse application in drug delivery and biomaterials<sup>7,13,38,39</sup>, coatings<sup>40,41</sup>, ion exchange membranes<sup>10,11</sup> and energy storage devices<sup>42</sup>.

With the use of MOB system, we can design charged material platform using cheaper but sustainable starting materials and lesser reaction steps. Material properties are dependent on presence of different functional groups and its distribution across the polymer chain which we can

tailor using charged polyethers to obtain desired characteristics and innovate better technologies in future.

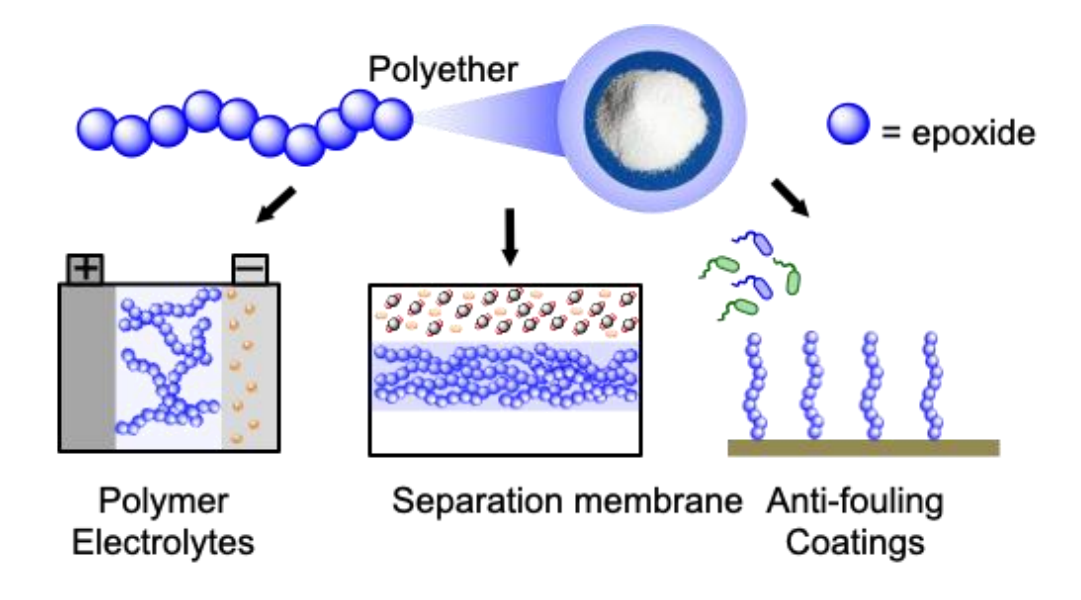


Figure 2: Graphical representation for charged polyether uses

# 1.4 Thesis summary

For the first study, we have demonstrated a tunable polymer platform from the facile (co)polymerization of allyl glycidyl ether (AGE), propargyl glycidyl ether (PGE) and epichlorohydrin (ECH) and propylene oxide (PO), with functional alkene, alkyne, chloromethyl and methyl groups respectively. Copolymerization of propargyl glycidyl ether (PGE) and epichlorohydrin (ECH), with functional alkyne and chloromethyl groups respectively was studied in detail for effect of molecular weight, monomer sequence, architecture, and composition. (Figure 3) This is essential in obtaining compositional control of structure—property relationships in a polyether materials platform.

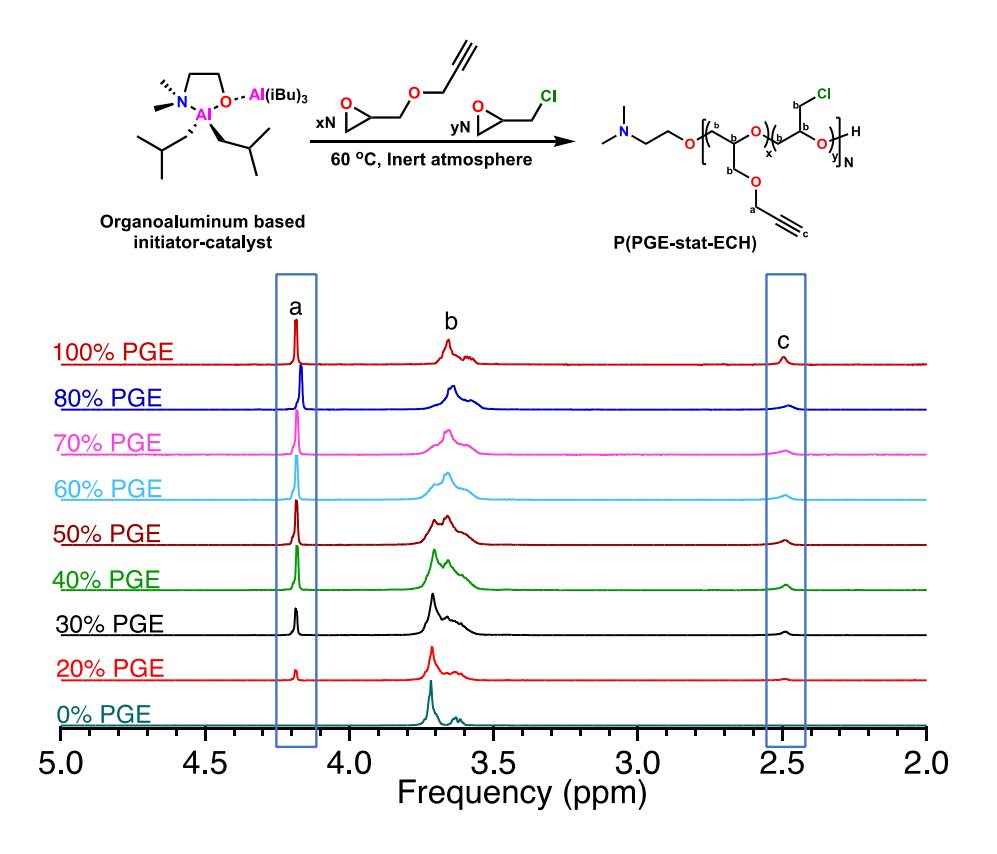


Figure 3: Stacked <sup>1</sup>H NMR spectra of P(PGE-*stat*-ECH) with varying composition along with synthesis scheme

Next, we modified P(PGE-*stat*-ECH) using click chemistry reaction to control charged groups and densities. The high functional group tolerance of thiol-yne chemistry makes this methodology applicable to the synthesis of a wide range of functionalized polymers by further modifications.<sup>43–45</sup> Chloromethyl group was also modified using simple substitution reactions using imidazole to introduce more charged moieties. These modified materials were then used to prepared amphoteric ion exchange membrane as shown in Figure 4 and Figure 5.

This novel AIEM is prepared from a partially fluorinated membrane matrix using PVDF-co-HFP grafted with a functional polyether of epichlorohydrin (ECH) and propargyl glycidyl ether (PGE) will serve as low-cost alternative to Nafion. By adjusting molecular weight as well as composition of ECH and PGE in the matrix we can obtained good balance of cationic and anionic species. The resulting homogeneous polymer membrane was tested for physicochemical, surface, and

electrochemical properties. This novel AIEM with promising thermal, mechanical, and electrochemical properties with low cost have a potential candidacy to use in VRFB system.

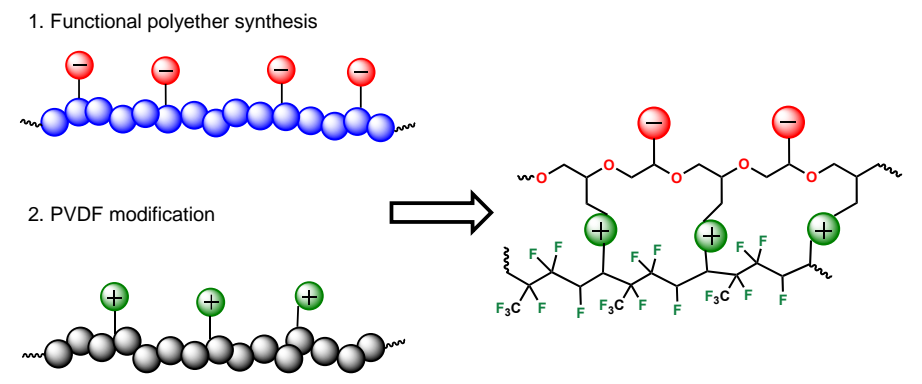


Figure 4: Simplified representation of charged material development

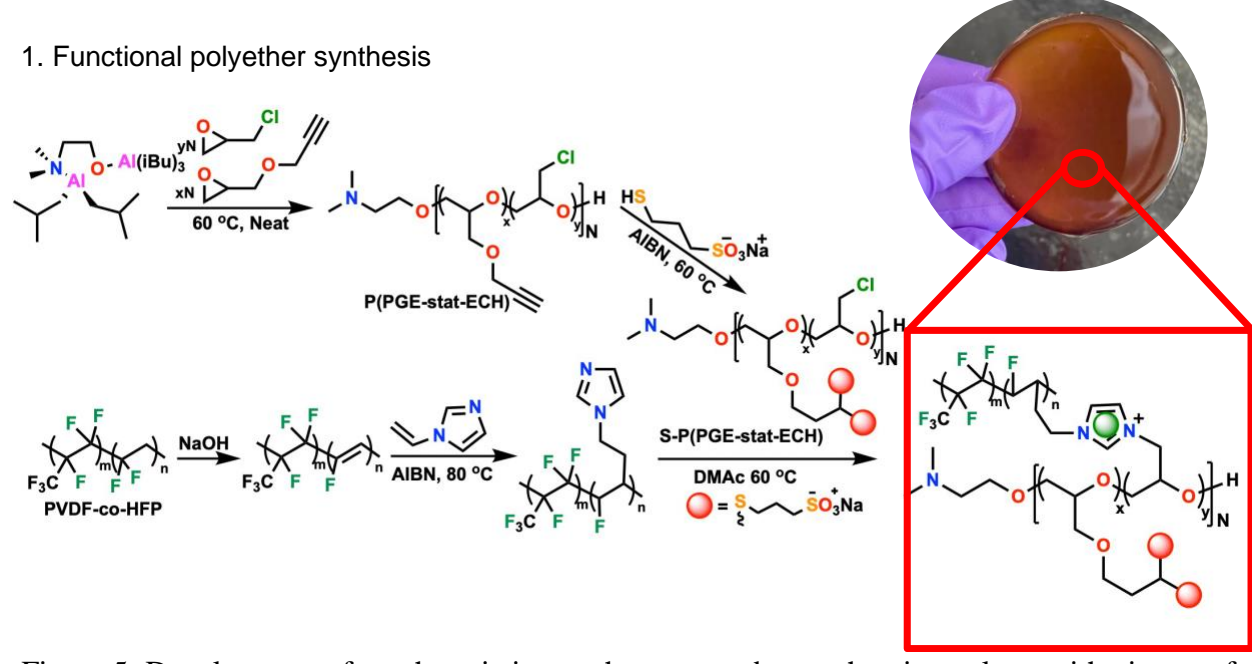


Figure 5: Development of amphoteric ion exchange membrane chemistry along with picture of representative membrane sample

Finally, we designed a polyelectrolyte system using a homopolymer PAGE with varying molecular weight to study coacervation phenomena. (Figure 6)

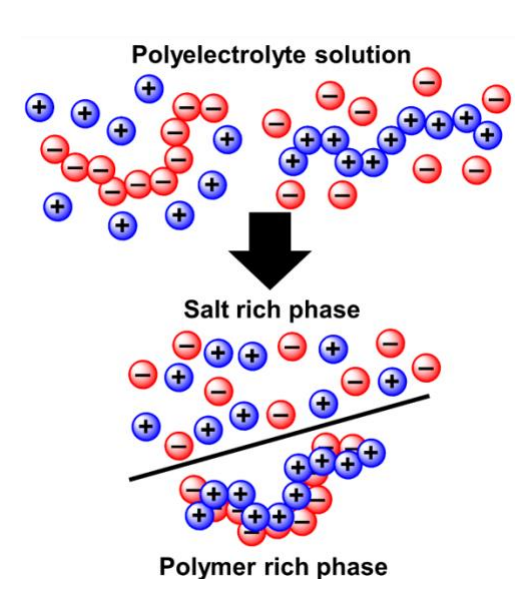


Figure 6: Depiction of complex coacervation phenomena

Using simple click chemistry, we created polyether based polyanions and polycations to study effect of charge and molecular weight on self-assembly through turbidity measurements. We studied effect of NaCl and LiCl salt as well on polyelectrolyte self-assembly with varying polyanions to polycation ratios. With the use of MOB polymerization platform, we can synthesize variety of polymers, and this will be useful in exploring effects of counter-ions, polymer architecture, charge densities in future. This synthetic platform will be useful in providing insights into polyelectrolyte design and control for future innovations.

Ongoing research in development of novel charged polyether field involves exploration of new ways to design and synthesize materials with tailored properties for specific applications.

#### BIBLIOGRAPHY

- (1) Herzberger, J.; Niederer, K.; Pohlit, H.; Seiwert, J.; Worm, M.; Wurm, F. R.; Frey, H. Polymerization of Ethylene Oxide, Propylene Oxide, and Other Alkylene Oxides: Synthesis, Novel Polymer Architectures, and Bioconjugation. *Chemical Reviews*. American Chemical Society December 29, 2016, pp 2170–2243. https://doi.org/10.1021/acs.chemrev.5b00441.
- (2) Chochos, C. L.; Choulis, S. A. How the Structural Deviations on the Backbone of Conjugated Polymers Influence Their Optoelectronic Properties and Photovoltaic Performance. *Progress in Polymer Science (Oxford)*. October 2011, pp 1326–1414. <a href="https://doi.org/10.1016/j.progpolymsci.2011.04.003">https://doi.org/10.1016/j.progpolymsci.2011.04.003</a>.
- (3) Jutemar, E. P.; Jannasch, P. Influence of the Polymer Backbone Structure on the Properties of Aromatic Ionomers with Pendant Sulfobenzoyl Side Chains for Use as Proton-Exchange Membranes. *ACS Appl Mater Interfaces* 2010, 2 (12), 3718–3725. https://doi.org/10.1021/am1008612.
- (4) Kjellander, R.; Ebba Florin, Water Structure and Changes in Thermal Stability of the System Poly (ethylene oxide)-Water; *J Chem Soc, Faraday Trans.* 1981; Vol. 77.
- (5) Shikata, T.; Okuzono, M.; Sugimoto, N. Temperature-Dependent Hydration/Dehydration Behavior of Poly(Ethylene Oxide)s in Aqueous Solution. *Macromolecules* 2013, 46 (5), 1956–1961. <a href="https://doi.org/10.1021/ma3026282">https://doi.org/10.1021/ma3026282</a>.
- (6) Israelachvili, J. Commentary The Different Faces of Poly(Ethylene Glycol); 1997; Vol. 94. <a href="https://www.pnas.org">www.pnas.org</a>.
- (7) Thomas, A.; Müller, S. S.; Frey, H. Beyond Poly(Ethylene Glycol): Linear Polyglycerol as a Multifunctional Polyether for Biomedical and Pharmaceutical Applications. *Biomacromolecules*. American Chemical Society June 9, 2014, pp 1935–1954. <a href="https://doi.org/10.1021/bm5002608">https://doi.org/10.1021/bm5002608</a>.
- (8) Dingels, C.; Schömer, M.; Frey, H. Die Vielen Gesichter Des Poly(Ethylenglykol)s: Von Der Kosmetik Zum Ionenleiter. *Chemie in Unserer Zeit* 2011, 45 (5), 338–349. <a href="https://doi.org/10.1002/ciuz.201100551">https://doi.org/10.1002/ciuz.201100551</a>.
- (9) Vallbe, A.; Besner, S.; Prud'homme, J. comparative study of poly(ethylene oxide) electrolytes made with lin(cf, so,), licf, so, and liclo,: thermal properties and conductivity behaviour; Vol. 37.
- (10) Rodriguez, C. G.; Chwatko, M.; Park, J.; Bentley, C. L.; Freeman, B. D.; Lynd, N. A. Compositionally Controlled Polyether Membranes via Mono(μ-Alkoxo)Bis(Alkylaluminum)-Initiated Chain-Growth Network Epoxide Polymerization: Synthesis and Transport Properties. *Macromolecules* 2020, *53* (4), 1191–1198. <a href="https://doi.org/10.1021/acs.macromol.9b02318">https://doi.org/10.1021/acs.macromol.9b02318</a>.

- (11) Luo, S.; Stevens, K. A.; Park, J. S.; Moon, J. D.; Liu, Q.; Freeman, B. D.; Guo, R. Highly CO2-Selective Gas Separation Membranes Based on Segmented Copolymers of Poly(Ethylene Oxide) Reinforced with Pentiptycene-Containing Polyimide Hard Segments. 

  ACS Appl Mater Interfaces 2016, 8 (3), 2306–2317. 

  https://doi.org/10.1021/acsami.5b11355.
- (12) Veronese, F. M. Peptide and Protein PEGylation: A Review of Problems and Solutions; 2001; Vol. 22.
- (13) Pasut, G.; Veronese, F. M. State of the Art in PEGylation: The Great Versatility Achieved after Forty Years of Research. *Journal of Controlled Release*. July 20, 2012, pp 461–472. <a href="https://doi.org/10.1016/j.jconrel.2011.10.037">https://doi.org/10.1016/j.jconrel.2011.10.037</a>.
- (14) Kang, T.; Banquy, X.; Heo, J.; Lim, C.; Lynd, N. A.; Lundberg, P.; Oh, D. X.; Lee, H. K.; Hong, Y. K.; Hwang, D. S.; Waite, J. H.; Israelachvili, J. N.; Hawker, C. J. Mussel-Inspired Anchoring of Polymer Loops That Provide Superior Surface Lubrication and Antifouling Properties. *ACS Nano* 2016, *10* (1), 930–937. <a href="https://doi.org/10.1021/acsnano.5b06066">https://doi.org/10.1021/acsnano.5b06066</a>.
- (15) Patterson, A. L.; Wenning, B.; Rizis, G.; Calabrese, D. R.; Finlay, J. A.; Franco, S. C.; Zuckermann, R. N.; Clare, A. S.; Kramer, E. J.; Ober, C. K.; Segalman, R. A. Role of Backbone Chemistry and Monomer Sequence in Amphiphilic Oligopeptide- and Oligopeptoid-Functionalized PDMS- and PEO-Based Block Copolymers for Marine Antifouling and Fouling Release Coatings. *Macromolecules* 2017, *50* (7), 2656–2667. <a href="https://doi.org/10.1021/acs.macromol.6b02505">https://doi.org/10.1021/acs.macromol.6b02505</a>.
- (16) Shin, E.; Lim, C.; Kang, U. J.; Kim, M.; Park, J.; Kim, D.; Choi, W.; Hong, J.; Baig, C.; Lee, D. W.; Kim, B. S. Mussel-Inspired Copolyether Loop with Superior Antifouling Behavior. *Macromolecules* 2020, 53 (9), 3551–3562. <a href="https://doi.org/10.1021/acs.macromol.0c00481">https://doi.org/10.1021/acs.macromol.0c00481</a>.
- (17) Engels, H. W.; Pirkl, H. G.; Albers, R.; Albach, R. W.; Krause, J.; Hoffmann, A.; Casselmann, H.; Dormish, J. Polyurethanes: Versatile Materials and Sustainable Problem Solvers for Today's Challenges. *Angewandte Chemie International Edition*. September 2, 2013, pp 9422–9441. <a href="https://doi.org/10.1002/anie.201302766">https://doi.org/10.1002/anie.201302766</a>.
- (18) Dudev, T.; Lim, C. Ring Strain Energies from Ab Initio Calculations; 1998. <a href="https://pubs.acs.org/sharingguidelines">https://pubs.acs.org/sharingguidelines</a>.
- (19) Vandenberg, E. J. Epoxide Polymers: Synthesis, Stereochemistry, Structure, and Mechanism. *J Polym Sci A1* 1969, 7 (2), 525–567. <a href="https://doi.org/10.1002/pol.1969.150070210">https://doi.org/10.1002/pol.1969.150070210</a>.
- (20) Vandenberg, E. J. Some Aspects of the Bimetallic M-oxo-alkoxides for Polymerizing Epoxides to Polyether Elastomers. *J Polym Sci A Polym Chem* 1986, 24 (7), 1423–1431. <a href="https://doi.org/10.1002/pola.1986.080240701">https://doi.org/10.1002/pola.1986.080240701</a>.

- (21) Vandenberg, E. J. Organometallic Catalysts for Polymerizing Monosubstituted Epoxides. *Journal of Polymer Science* 1960, 47 (149), 486–489. <a href="https://doi.org/10.1002/pol.1960.1204714947">https://doi.org/10.1002/pol.1960.1204714947</a>.
- (22) Vandenberg, E. J. High Polymers from Symmetrical Disubstituted Epoxides. *Journal of Polymer Science* 1960, 47 (149), 489–491. https://doi.org/10.1002/pol.1960.1204714948.
- (23) Biedron, T.; Kubisa, P.; Penczek, S. Polyepichlorohydrin Diols Free of Cyclics: Synthesis and Characterization. *J Polym Sci A Polym Chem* 1991, 29 (5), 619–628. <a href="https://doi.org/10.1002/pola.1991.080290502">https://doi.org/10.1002/pola.1991.080290502</a>.
- (24) Carlotti, S.; Labbé, A.; Rejsek, V.; Doutaz, S.; Gervais, M.; Deffieux, A. Living/Controlled Anionic Polymerization and Copolymerization of Epichlorohydrin with Tetraoctylammonium Bromide-Triisobutylaluminum Initiating Systems. *Macromolecules* 2008, *41* (19), 7058–7062. <a href="https://doi.org/10.1021/ma801422c">https://doi.org/10.1021/ma801422c</a>.
- (25) Ferrier, R. C.; Imbrogno, J.; Rodriguez, C. G.; Chwatko, M.; Meyer, P. W.; Lynd, N. A. Four-Fold Increase in Epoxide Polymerization Rate with Change of Alkyl-Substitution on Mono-μ-Oxo-Dialuminum Initiators. *Polym Chem* 2017, 8 (31), 4503–4511. <a href="https://doi.org/10.1039/c7py00894e">https://doi.org/10.1039/c7py00894e</a>.
- (26) Rodriguez, C. G.; Ferrier, R. C.; Helenic, A.; Lynd, N. A. Ring-Opening Polymerization of Epoxides: Facile Pathway to Functional Polyethers via a Versatile Organoaluminum Initiator. *Macromolecules* 2017, 50 (8), 3121–3130. https://doi.org/10.1021/acs.macromol.7b00196.
- (27) Safaie, N.; Smak, J.; DeJonge, D.; Cheng, S.; Zuo, X.; Ohno, K.; Ferrier, R. C. Facile Synthesis of Epoxide-Co-Propylene Sulphide Polymers with Compositional and Architectural Control. *Polym Chem* 2022. https://doi.org/10.1039/d2py00005a.
- (28) Imbrogno, J.; Ferrier, R. C.; Wheatle, B. K.; Rose, M. J.; Lynd, N. A. Decoupling Catalysis and Chain-Growth Functions of Mono(μ-Alkoxo)Bis(Alkylaluminums) in Epoxide Polymerization: Emergence of the N-Al Adduct Catalyst. ACS Catal 2018, 8 (9), 8796–8803. https://doi.org/10.1021/acscatal.8b02446.
- (29) Safaie, N.; Rawal, B.; Ohno, K.; Ferrier, R. C. Aluminum-Based Initiators from Thiols for Epoxide Polymerizations. *Macromolecules* 2020, 53 (19), 8181–8191. https://doi.org/10.1021/acs.macromol.0c00464.
- (30) Shukla, G.; Ferrier, R. C. The Versatile, Functional Polyether, Polyepichlorohydrin: History, Synthesis, and Applications. *Journal of Polymer Science*. John Wiley and Sons Inc November 15, 2021, pp 2704–2718. https://doi.org/10.1002/pol.20210514.
- (31) Herzberger, J.; Frey, H. Epicyanohydrin: Polymerization by Monomer Activation Gives Access to Nitrile-, Amino-, and Carboxyl-Functional Poly(Ethylene Glycol).

- *Macromolecules* 2015, 48 (22), 8144–8153. https://doi.org/10.1021/acs.macromol.5b02178.
- (32) Herzberger, J.; Leibig, D.; Langhanki, J.; Moers, C.; Opatz, T.; Frey, H. "Clickable PEG" via Anionic Copolymerization of Ethylene Oxide and Glycidyl Propargyl Ether. *Polym Chem* 2017, 8 (12), 1882–1887. https://doi.org/10.1039/c7py00173h.
- (33)Sprafke, J. K.; Spruell, J. M.; Mattson, K. M.; Montarnal, D.; McGrath, A. J.; Pötzsch, R.; Miyajima, D.; Hu, J.; Latimer, A. A.; Voit, B. I.; Aida, T.; Hawker, C. J. Revisiting Thiol-Yne Chemistry: Selective and Efficient Monoaddition for Block and Graft Copolymer Formation. JPolym Sci $\boldsymbol{A}$ Polym Chem 2015. 53 (2),319-326. https://doi.org/10.1002/pola.27345.
- (34) Krannig, K. S.; Huang, J.; Heise, A.; Schlaad, H. Photochemical Thiol-Yne Functionalization of Polypeptide Scaffolds. *Polym Chem* 2013, *4* (14), 3981–3986. <a href="https://doi.org/10.1039/c3py00428g">https://doi.org/10.1039/c3py00428g</a>.
- (35) Obermeier, B.; Frey, H. Poly(Ethylene Glycol-Co-Allyl Glycidyl Ether)s: A PEG-Based Modular Synthetic Platform for Multiple Bioconjugation. *Bioconjug Chem* 2011, 22 (3), 436–444. https://doi.org/10.1021/bc1004747.
- (36) Mangold, C.; Dingels, C.; Obermeier, B.; Frey, H.; Wurm, F. PEG-Based Multifunctional Polyethers with Highly Reactive Vinyl-Ether Side Chains for Click-Type Functionalization. *Macromolecules* 2011, *44* (16), 6326–6334. <a href="https://doi.org/10.1021/ma200898n">https://doi.org/10.1021/ma200898n</a>.
- (37) Hamaide, T.; Goux, A.; Llauro, M.-F.; Spitz, R.; Guyot, A.; Hamaide, T.; Goux, A.; Llauro, M.-F.; Spitz, R.; Guyot, A. *Stat-Poly(Ethylene Oxide-Co-Propylene Oxide) Synthesis, NMR Characterization and Crystallinity Studies. Correlation with Monte Carlo Simulation*; 1996; Vol. 237.
- (38) Love, B. Polymeric Biomaterials. In *Biomaterials*; Elsevier, 2017; pp 205–238. <a href="https://doi.org/10.1016/B978-0-12-809478-5.00009-2">https://doi.org/10.1016/B978-0-12-809478-5.00009-2</a>.
- (39) Fruijtier-Pölloth, C. Safety Assessment on Polyethylene Glycols (PEGs) and Their Derivatives as Used in Cosmetic Products. *Toxicology*. October 15, 2005, pp 1–38. <a href="https://doi.org/10.1016/j.tox.2005.06.001">https://doi.org/10.1016/j.tox.2005.06.001</a>.
- (40) Nayak, K.; Kumar, A.; Tripathi, B. P. Molecular Grafting and Zwitterionization Based Antifouling and Underwater Superoleophobic PVDF Membranes for Oil/Water Separation. *J Memb Sci* 2022, *643*. https://doi.org/10.1016/j.memsci.2021.120038.
- (41) Choi, W.; Park, S.; Kwon, J. S.; Jang, E. Y.; Kim, J. Y.; Heo, J.; Hwang, Y. D.; Kim, B. S.; Moon, J. H.; Jung, S.; Choi, S. H.; Lee, H.; Ahn, H. W.; Hong, J. Reverse Actuation of Polyelectrolyte Effect for in Vivo Antifouling. *ACS Nano* 2021, *15* (4), 6811–6828. <a href="https://doi.org/10.1021/acsnano.0c10431">https://doi.org/10.1021/acsnano.0c10431</a>.

- (42) Xue, Z.; He, D.; Xie, X. Poly(Ethylene Oxide)-Based Electrolytes for Lithium-Ion Batteries. *Journal of Materials Chemistry A*. Royal Society of Chemistry July 17, 2015, pp 19218–19253. https://doi.org/10.1039/c5ta03471j.
- (43) Huynh, V. T.; Chen, G.; Souza, P. De; Stenzel, M. H. Thiol-Yne and Thiol-Ene "Click" Chemistry as a Tool for a Variety of Platinum Drug Delivery Carriers, from Statistical Copolymers to Crosslinked Micelles. *Biomacromolecules* 2011, *12* (5), 1738–1751. <a href="https://doi.org/10.1021/bm200135e">https://doi.org/10.1021/bm200135e</a>.
- (44) Hoogenboom, R. Thiol-Yne Chemistry: A Powerful Tool for Creating Highly Functional Materials. *Angewandte Chemie International Edition* 2010, 49 (20), 3415–3417. <a href="https://doi.org/10.1002/anie.201000401">https://doi.org/10.1002/anie.201000401</a>.
- (45) Huynh, V. T.; Chen, G.; Souza, P. De; Stenzel, M. H. Thiol-Yne and Thiol-Ene "Click" Chemistry as a Tool for a Variety of Platinum Drug Delivery Carriers, from Statistical Copolymers to Crosslinked Micelles. *Biomacromolecules* 2011, *12* (5), 1738–1751. https://doi.org/10.1021/bm200135e.

Chapter 2. Development of novel polyether synthesis platform from the facile (co)polymerization of functional epoxides using organo-aluminum catalyst-initiator system

#### Abstract

Epoxides are a promising polymer materials platform because of their diverse functionality, ease of synthesis, availability, and indiscriminate ring strain driving force for polymerization. Recently developed mono(µ-alkoxo)bis(alkylaluminum) (MOB) initiators gives controlled molecular weight polymers without chain transfer for a range of functional epoxides. We have demonstrated a tunable polymer platform from the facile copolymerization of propargyl glycidyl ether (PGE) and epichlorohydrin (ECH), with functional alkyne and chloromethyl groups respectively. This platform allows for control over parameters such as molecular weight, composition, monomer sequence, and polymer architecture independently. Molecular weights up to 100 kg/mol with narrow distributions were achieved. Copolymer composition was varied by incorporating increasing ratios of PGE (20-80%) in the polymerization feed. Reactivity ratios were calculated as rpge= 0.69 and rech= 1.43 using in situ <sup>1</sup>H NMR kinetic study which confirms the statistical nature of the copolymer. In conclusion, we have numerous practical and conceptual tools to understand and control macromolecular architecture in polyethers. These precursor polymers were further modified with various charged groups such as imidazole and sulfonate via orthogonal chemistry through the chloromethyl and alkyne moieties (will be discussed in chapter 3). This will be useful in providing true compositional control of structure-property relationships in a macromolecular materials platform. We will utilize these materials to further study charged polymer self-assembly and to develop amphoteric ion exchange membrane for electrochemical application.

#### 2.1 Introduction

Epoxides are ideal starting materials for polymerization due to their low cost and sustainable manufacturing methods. Macromolecules obtained by polymerizing these epoxides are known as polyethers. These polyethers have diverse applications ranging from pharmaceutical<sup>1-4</sup>, food<sup>5</sup>, cosmetics<sup>6</sup>, automobile industry<sup>7</sup> to many advanced applications such as antifouling coatings<sup>8-11</sup>, solid polymer electrolytes<sup>12,13</sup>, separation membranes<sup>14</sup>, etc. Researchers have employed different catalytic and ionic techniques to carry out polymerization of functional epoxides. Popularly used catalytic method is using vandenberg's catalyst, but it has drawbacks due to uncontrolled polymerization resulting in high molecular weight and polydispersities.<sup>15</sup> Ionic methods such as cationic ring opening polymerization leads to low molecular weight polyethers while anionic ring opening polymerization gives high molecular weight polyethers for selective epoxides.<sup>16,17</sup> None of these is a universal method for polymerization of functional epoxides. Recently reported polymerization technique developed by Lynd and Ferrier solves this problem. This method inspired from vandenberg's catalyst uses combined ionic and catalytic approach and provides us with controlled polymerization technique for wide variety of functional epoxides.<sup>18–22</sup>

This polymerization platform offers good tolerance for functional groups such as halides, pendant alkenes, or alkynes without chain transfer. It follows green chemistry principles, especially with respect to atom economy, as we polymerize up to 99% of the starting materials using solvent-free reaction conditions. Additionally, the starting epoxides are derived from renewable feedstocks like glycerin.<sup>23,24</sup> With the use of MOB system we can significantly reduce the reaction times while enabling the use of moderate or ambient reaction temperatures.

Motivation for this work originates from requirement of facile tunable polymerization platform for diverse functionality epoxides. Polyethylene oxide is the widely used polyether inherently lacks

functionality which limits its applications. Hence, researchers are exploring innovative techniques to increase its functionality.<sup>25,26</sup> In this work we have demonstrated a tunable polymer platform from the facile (co)polymerization of allyl glycidyl ether (AGE), propargyl glycidyl ether (PGE) and epichlorohydrin (ECH) and propylene oxide (PO), with functional alkene, alkyne, chloromethyl and methyl groups respectively. Using in situ <sup>1</sup>H NMR kinetic study we determined polymer structure as well in case of copolymer synthesis. This platform allows for control over parameters such as molecular weight, charge density, monomer sequence, polymer architecture, and counter-ions independently through novel polymer synthesis. Alkene and alkyne functionality can further be tuned using click chemistry reaction to control charged groups and densities. The high functional group tolerance of thiol-yne chemistry makes this methodology applicable to the synthesis of a wide range of functionalized polymers by further modifications.<sup>27–29</sup> Chloromethyl group provides handle for post polymerization modification to achieve required material properties through composition control. Methyl group will be useful in controlling the hydrophobicity and glass transition temperatures of the final polymer. Each of these groups brings unique characteristics which we will utilize to design materials for specific application. In addition, we are using benign epoxides compared to toxic ethylene oxide-based copolymers developed before in literature. 1,25,30 In summary, conventional polyether polymerization methodologies lack ability to polymerize functional epoxides. But with the use aluminum-based catalyst-initiator system (MOB) we have obtained polymers with multifunctionalities with ease.

# 2.2 Experimental section

#### 2.2.1 Materials

Propargyl alcohol (Sigma-Aldrich, 99%), sodium hydroxide pellets (Fisher Chemical), epichlorohydrin (Sigma-Aldrich, 99%) used for monomer propargyl glycidyl ether synthesis. Allyl glycidyl ether (Sigma-Aldrich, ≥99%) used as a starting monomer for polymerization. Tri-isobutyl aluminum (1.0 M in hexanes, Sigma-Aldrich), dimethyl aminoethanol (Sigma-Aldrich, >98%), benzyl alcohol (Sigma-Aldrich) tri-methyl aluminum (2.0 M in hexanes, Sigma-Aldrich), triethyl amine (Sigma-Aldrich) and anhydrous hexane (Sigma-Aldrich >99%) were all used for preparing catalyst and initiator for polymerization in glovebox without any modification. CDCl₃ (Cambridge Isotope Laboratories, Inc. 99.8%) were used for preparing NMR samples without any alteration.

Methanol (MeOH, Fisher, Certified ACS), hexane (Fisher, Certified ACS) and dichloromethane (DCM, Fisher, Certified ACS) were used for clean polymers by removing unreacted monomers and catalyst. Glovebox was used to carry out all moisture and oxygen sensitive reactions under nitrogen environment.

#### 2.2.2 Instrumentation

<sup>1</sup>H NMR and <sup>13</sup>C NMR spectroscopy was performed on Agilent DDR2 500 MHz NMR spectrometer using deuterated solvents at room temperature. The chemical shifts are reported in parts per million (ppm) and are referenced using the residual <sup>1</sup>H peak from the deuterated solvent. All Diffusion Ordered Spectroscopy (DOSY) measurements were performed on a Bruker Advance III HD 500 MHz spectrometer operating at 499.96 MHz at 25 °C. It was equipped with a 5mm X-nuclei-optimized double resonance broad banded probe capable of producing gradients in the Z direction with a maximum strength of 50 G/cm. All DOSY measurements were run using the

convection compensated dstebpgp3s pulse sequence with 64 scans and 16 increments with gradient strengths from 1 to 42 G/cm. First gradient amplitude of 2% and final gradient amplitude of 94% was used. The diffusion times of 100-200 ms and gradient pulse of 2-4 ms was used. The gel permeation chromatography (GPC) was performed on the Malvern OMNISEC system with an isocratic pump, degasser, and temperature-controlled column oven operated at 35 °C containing 2 Viscotek 300×8.0 mm columns (T3000 and T4000) with an exclusion limit of 400 kDa. Triple detection with light scattering, viscometer, and refractive index has been used for determining absolute molecular weight of polymers. Calibration was carried out using polystyrene standards (from scientific polymer) in THF (Sigma-Aldrich 99.8%).

Differential scanning calorimetric (DSC) tests were carried out on a TA250 instrument with a heating rate of 10 °C min<sup>-1</sup> under a N<sub>2</sub> atmosphere, and the data from the second heating curve was used for further analysis.

Thermogravimetric Analysis (TGA) was performed using a TGA 500 (TA Instruments, USA). A sample (about 10 mg) was heated to 800 °C with a heating rate of 10 °C /min.

Fourier Transform Infrared (FT-IR) spectra were taken using Shimadzu IRAffinity-1 spectrometer equipped with MIRacle ATR attachment. The spectra were recorded between the wavelength on 500-4000 cm<sup>-1</sup> in absorption mode.

#### 2.2.3 Methods

#### Synthesis of propargyl glycidyl ether (PGE)

Reactants propargyl alcohol (15.0 g, 0.268 mol), epichlorohydrin (68.9 g, 0.745 mol), and sodium hydroxide pellets (10.7 g, 0.268 mol) were charged in a round bottom flask with a magnetic stirrer. The reaction scheme is shown in. This is an exothermic reaction hence the flask was submerged in an ice water bath and stirred at 300 rpm overnight while warming to room temperature. Next

day stopped stirring let it separate into two phases. Then decanted supernatant into a clean round bottom flask and purified using a rotary evaporator under vacuum at 45 °C, 100 rpm. The mixture was kept under vacuum to remove remaining epichlorohydrin overnight and distilled at 50 °C under reduced pressure to obtain pure PGE. The reaction scheme is shown in Figure 7. The purified product (yield 60-70%) was characterized using ¹H and ¹³C NMR spectroscopy.¹8 ¹H NMR (CDCl₃, 500 MHz) δ 2.44 (m, epoxide Cℍ₂–O–CH–), 2.61 (m, epoxide Cℍ₂–O–CH–), 2.78 (m, epoxide Cℍ₂–O–Cℍ–), 3.15 (m, ℍℂ≡ℂℂℍ₂O–), 3.46 (m, –Oℂℍ₂CH–), 3.80 (m, –Oℂℍ₂CH–), 4.19 (m, Hℂ≡ℂℂℍ₂O–)

<sup>13</sup>C NMR (CDCl<sub>3</sub>, 125 MHz) δ 43.85 (epoxide <u>C</u>H<sub>2</sub>–O–CH–), 50.16 (epoxide CH<sub>2</sub>–O–<u>C</u>H–),58.06 (HC≡C<u>C</u>H<sub>2</sub>O–), 70.1 (–O<u>C</u>H<sub>2</sub>CH–), 74.74 (H<u>C</u>≡CCH<sub>2</sub>O–), 79.13 (HC≡<u>C</u>CH<sub>2</sub>O–) (Figure 8 A & B).

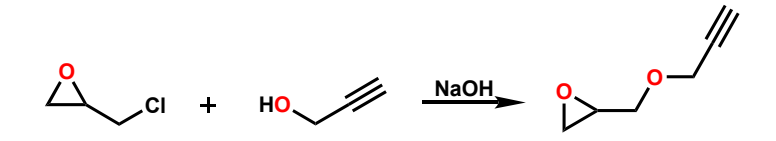


Figure 7: Synthesis route for propargyl glycidyl ether (PGE)

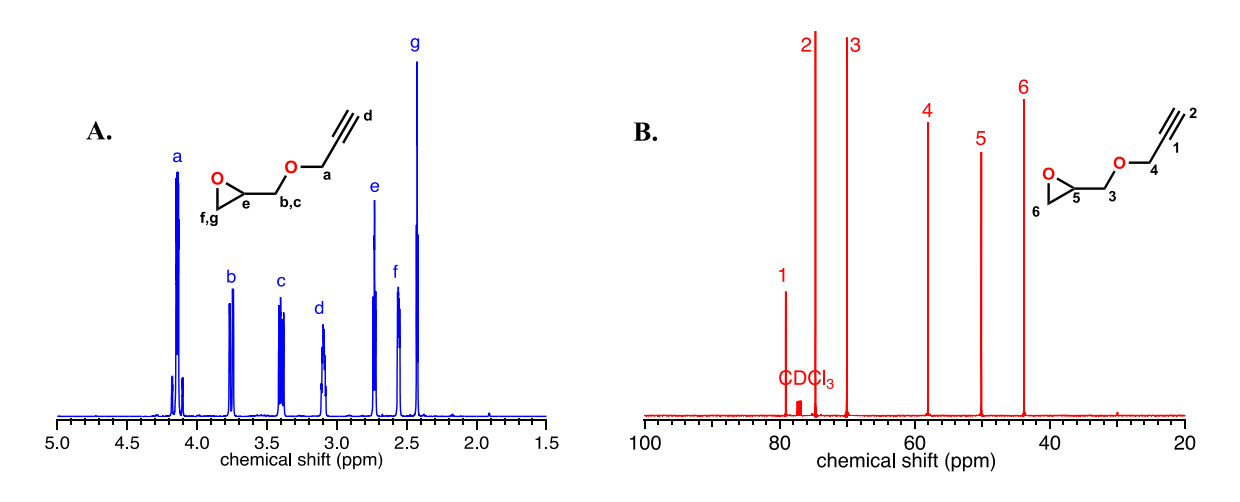


Figure 8: A. <sup>1</sup>H NMR B. <sup>13</sup>C NMR spectra of purified PGE in CDCl<sub>3</sub>

# $Synthesis\ of\ triis obutyla luminum\ adduct\ of (2-dimethylamino) ethoxy-diis obutyla luminum\ (MOB)$

1.0 M tri-isobutylaluminum in hexane (12.7 mL, 12.7mmol) was added to a reaction vial with magnetic stirrer and cooled to −78°C using liquid nitrogen blanket under dry nitrogen environment inside glovebox. To this vial a ligand dimethylaminoethanol (4.7 mmol, 0.5 mL) was added dropwise. The reaction was carried out by continuous stirring until it warms to room temperature overnight. Next day stopped stirring and cooled down the reaction mixture again to −40°C to crystallize the desired product. These crystals were then washed with anhydrous hexanes three times to remove excess reactant and dried under vacuum.<sup>18</sup>

<sup>1</sup>H NMR (CDCl<sub>3</sub>, 500 MHz) δ 0.12 to -0.15 (m, -Al[-CH<sub>2</sub>-CH-(CH<sub>3</sub>)<sub>2</sub>]<sub>2</sub>, and m, -Al[-CH<sub>2</sub>-CH-(CH<sub>3</sub>)<sub>2</sub>]<sub>3</sub>), 0.92 (m, -Al[-CH<sub>2</sub>-CH-(C<u>H</u><sub>3</sub>)<sub>2</sub>]<sub>2</sub>, and m, -Al[-CH<sub>2</sub>-CH-(C<u>H</u><sub>3</sub>)<sub>2</sub>]<sub>3</sub>), 1.82 (m, -Al[-CH<sub>2</sub>-C<u>H</u>-(CH<sub>3</sub>)<sub>2</sub>]<sub>2</sub>, and m, -Al[-CH<sub>2</sub>-CH-(CH<sub>3</sub>)<sub>2</sub>]<sub>3</sub>), 2.59 (s, N-(C<u>H</u><sub>3</sub>)<sub>2</sub>), 2.87 (t, N-C<u>H</u><sub>2</sub>-CH<sub>2</sub>-CH<sub>2</sub>-O), 3.97 (t, N-CH<sub>2</sub>-C<u>H</u><sub>2</sub>-O) (Figure 9)

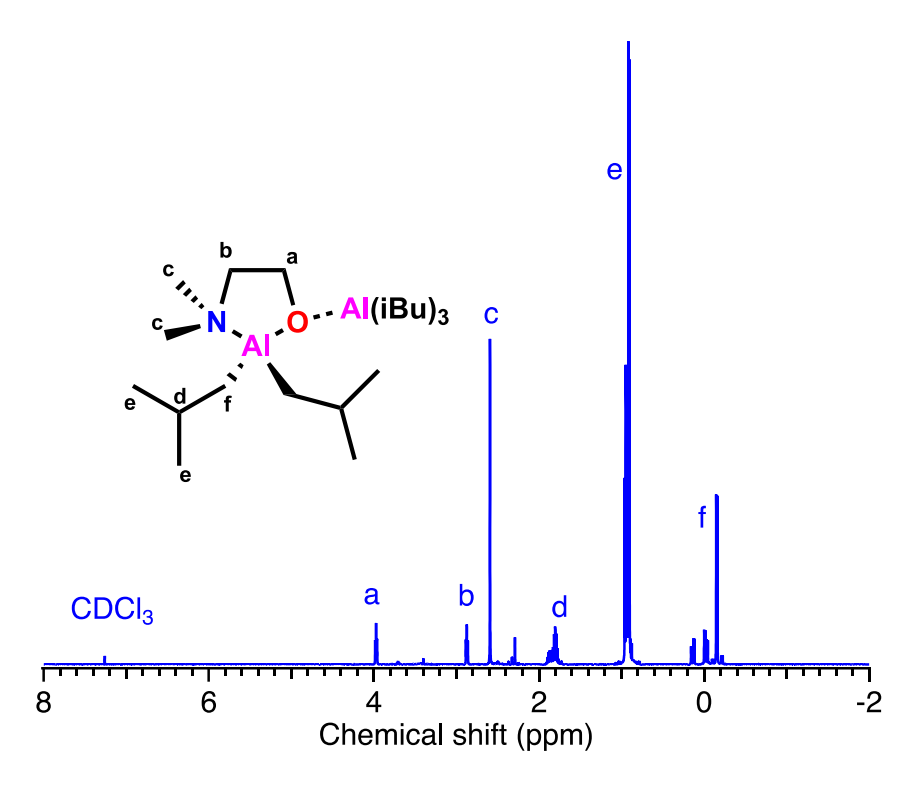


Figure 9: <sup>1</sup>H NMR of MOB in CDCl<sub>3</sub>

#### Synthesis of trimethylaluminum and triethylamine adduct (NAI Catalyst synthesis)

A reaction vial was charged with a stir bar, 6.35 mL anhydrous hexanes, and 2.0 M trimethylaluminum in hexane (6.35 mL, 12.7 mmol) and cooled to  $-78^{\circ}$ C in a dry nitrogen glovebox. To this vial triethylamine (12.7 mmol) was added slowly. The reaction is exothermic so add triethylamine dropwise. The solution was set to stir and warm to room temperature overnight. The reaction mixture was then cooled down again to  $-40^{\circ}$ C to crystallize the desired product. These crystals were then washed with anhydrous hexanes three times to remove excess reactant and dried under vacuum.

<sup>1</sup>H NMR (CDCl<sub>3</sub>, 500 MHz) δ -0.89 (s, Al–C<u>H</u><sub>3</sub>), 1.18 (t, N–CH<sub>2</sub>–C<u>H</u><sub>3</sub>), 2.8 (q, N–C<u>H</u><sub>2</sub>–CH<sub>3</sub>)

<sup>13</sup>C NMR (CDCl<sub>3</sub>, 125 MHz) δ 9.11 (Al–<u>C</u>H<sub>3</sub>), 46.25 (N–CH<sub>2</sub>–<u>C</u>H<sub>3</sub>), 47.68 (N–<u>C</u>H<sub>2</sub>–CH<sub>3</sub>).

(Figure 10 A & B)

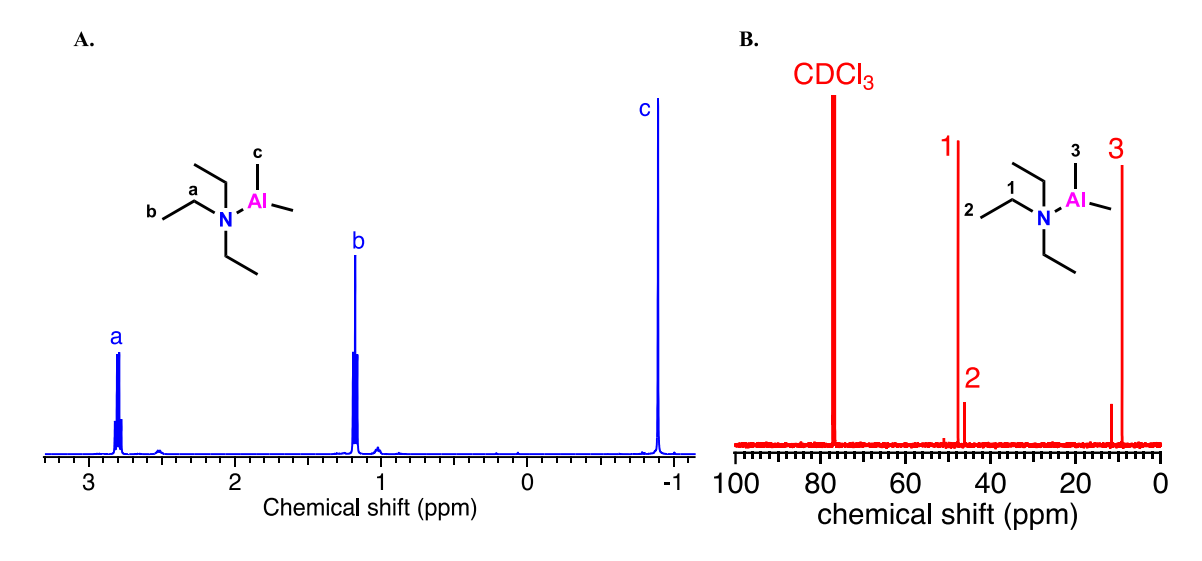


Figure 10: A. <sup>1</sup>H NMR B. <sup>13</sup>C NMR spectra of NAl catalyst in CDCl<sub>3</sub>

# Synthesis (benzyloxy) dimethyl aluminum (benzyl initiator)

A reaction vial was charged with a stir bar, 6.35 mL anhydrous hexanes, and 2.0 M trimethylaluminum in hexane (6.35 mL, 12.7 mmol) and cooled to – 78°C in a dry nitrogen glovebox. To this vial a ligand, benzyl alcohol (12.7 mmol), was added dropwise. The solution was set to stir and warm to room temperature overnight. The reaction mixture was then cooled down again to –40°C to crystallize the desired product. These crystals were then washed with anhydrous hexanes three times to remove excess reactants and undesired products. Finally, the desired crystals were dried under vacuum.

<sup>1</sup>H NMR (CDCl<sub>3</sub>, 500 MHz) δ -0.79 (s, Al–C<u>H</u><sub>3</sub>), 5.08 (s, –Ph–C<u>H</u><sub>2</sub>–O), 7.46-7.28 (m, –<u>Ph</u>–CH<sub>2</sub>–O), <sup>13</sup>C NMR (CDCl<sub>3</sub>, 125 MHz) δ 51.26 (Al–<u>C</u>H<sub>3</sub>), 65.6 (–Ph–<u>C</u>H<sub>2</sub>–O), 129.96-126.68, 138 (–<u>Ph</u>–CH<sub>2</sub>–O). (Figure 11 A & B)

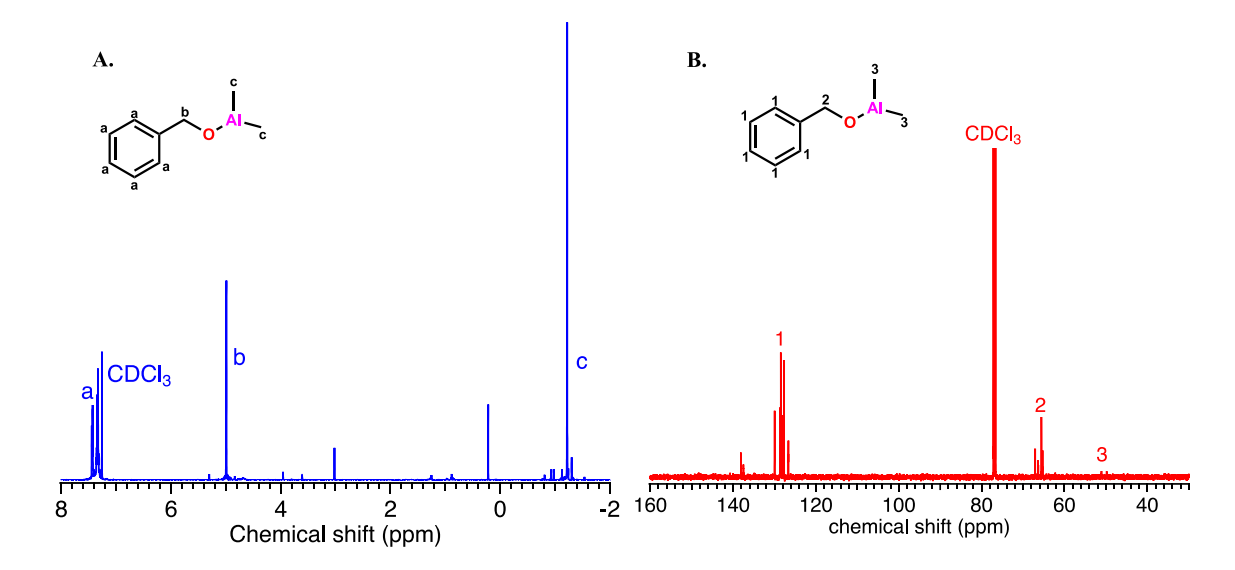


Figure 11: A. <sup>1</sup>H NMR B. <sup>13</sup>C NMR spectra of benzyl initiator in CDCl<sub>3</sub>

#### General procedure for polymerization using MOB system

All polymerizations were performed neat in a septum-capped 20mL reaction vial under inert atmosphere in glovebox. The vials were charged with a stir bar, a monomer(s) and initiator-catalyst or separate initiator and catalyst to prepare 2 g of final polymer weight. Initiator-catalyst amount was decided depending on targeted molecular weight. The solutions were then heated to the final reaction temperature (50-60 °C, dependent on monomer) and polymerizations were carried out for 48 hours-5 days (until its >90% polymerized). Reactions were quenched with methanol and dissolved in dichloromethane to remove aluminum. The resulting solution was added dropwise into hexane to precipitate out the desired polymer product. The supernatant was removed, and then again washed the polymer with hexane (or any poor solvent) three times to remove residual catalyst. The polymer was first dried using rotary evaporator and then kept under vacuum overnight to remove excess solvent. Mn was determined using GPC with triple detection system and using <sup>1</sup>H NMR by end group analysis for polymers prepared with the use of initiator (benzyloxy) dimethyl aluminum.

#### **Kinetics and reactivity ratios calculation**

Kinetics study of polymerization of epichlorohydrin and propargyl glycidyl ether was conducted to determine reactivity ratios. A vial was charged with the catalyst and monomers ECH and PGE in desired quantity and heated to 60 °C. Small aliquots were taken out at specific times and dissolved in CDCl<sub>3</sub> to perform <sup>1</sup>H NMR. The conversion of monomer was calculated based on the integration of unreacted monomers compared with polymer backbone integration. These aliquots were taken periodically throughout the experiment (up to 24 hrs.). After complete polymerization resulting polymer was characterized using <sup>1</sup>H NMR and <sup>13</sup>C NMR spectroscopy after cleaning.

#### 2.3 Result and discussion

Functional monomers such as ECH, AGE, PO and PGE can be controllably homopolymerized with MOB catalysts. Before attempting copolymerization of these monomers, we sought to determine the capacity for homopolymerization of these sometimes difficult to polymerize monomers. To do this we first polymerized AGE and PGE and characterized before further modifications.

#### 2.3.1 Synthesis of precursor poly(allyl glycidyl ether) (PAGE)

All polymerizations were performed neat in a septum-capped reaction vial. The vials were charged with a stir bar, a monomer allyl glycidyl ether, and TIBA in an inert environment. The solutions were then heated to the final reaction temperature (50 °C, dependent on monomer) and polymerizations were carried out for 48 hours. Reactions were quenched with methanol and dissolved in dichloromethane to remove aluminum. The resulting solution was then washed with a poor solvent like hexane to precipitate the desired polymer product. The supernatant was removed, and the polymer was dried in vacuo. Reaction scheme for synthesis of poly-(allyl glycidyl ether) (PAGE) is shown in Figure 12. The final product was stored in refrigerator at low

temp to avoid any crosslinking reaction within the polymer.  $^{1}H$  NMR (CDCl<sub>3</sub>, 500 MHz)  $\delta$  3.38–3.71 (broad m,–O–CH<sub>2</sub>–CH(CH<sub>2</sub>–O–CH<sub>2</sub>–CH=CH2)–O–), 3.99 (d,–O–CH<sub>2</sub>–CH=CH<sub>2</sub>), 5.16/5.27 (dd,–O–CH<sub>2</sub>–CH=CH<sub>2</sub>), 5.91 (m,–O–CH<sub>2</sub>–CH=CH<sub>2</sub>),

<sup>13</sup>C NMR (CDCl<sub>3</sub>, 125 MHz) δ 69.79 (–O–<u>C</u>H<sub>2</sub>–CH(CH<sub>2</sub>–O–CH<sub>2</sub>–CH=CH<sub>2</sub>)–O–,) 69.97–70.36 (–O–<u>C</u>H<sub>2</sub>–CH(<u>C</u>H<sub>2</sub>–O–CH<sub>2</sub>–CH=CH<sub>2</sub>)–O–, m), 72.38 (–O–<u>C</u>H<sub>2</sub>–CH=CH<sub>2</sub>), 78.93 (–O–CH<sub>2</sub>–CH=CH<sub>2</sub>), CH(CH<sub>2</sub>–O–CH<sub>2</sub>–CH=CH<sub>2</sub>)–O–),116.8(–O–CH<sub>2</sub>–CH=<u>C</u>H<sub>2</sub>), 134.9 (–O–CH<sub>2</sub>–<u>C</u>H=CH<sub>2</sub>) (Figure 13 A & B).

$$\begin{array}{c|c} & & & & \\ & & & \\ & & & \\ & & & \\ & & & \\ & & & \\ & & & \\ & & & \\ & & & \\ & & \\ & & \\ & & \\ & & \\ & & \\ & & \\ & & \\ & & \\ & & \\ & & \\ & & \\ & & \\ & & \\ & & \\ & & \\ & & \\ & & \\ & & \\ & & \\ & & \\ & & \\ & & \\ & & \\ & & \\ & & \\ & & \\ & & \\ & & \\ & & \\ & & \\ & & \\ & & \\ & & \\ & & \\ & & \\ & & \\ & & \\ & & \\ & & \\ & & \\ & & \\ & & \\ & & \\ & & \\ & & \\ & & \\ & & \\ & & \\ & & \\ & & \\ & & \\ & & \\ & & \\ & & \\ & & \\ & & \\ & & \\ & & \\ & & \\ & & \\ & & \\ & & \\ & & \\ & & \\ & & \\ & & \\ & & \\ & & \\ & & \\ & & \\ & & \\ & & \\ & & \\ & & \\ & & \\ & & \\ & & \\ & & \\ & & \\ & & \\ & & \\ & & \\ & & \\ & & \\ & & \\ & & \\ & & \\ & & \\ & & \\ & & \\ & & \\ & & \\ & & \\ & & \\ & & \\ & & \\ & & \\ & & \\ & & \\ & & \\ & & \\ & & \\ & & \\ & & \\ & & \\ & & \\ & & \\ & & \\ & & \\ & & \\ & & \\ & & \\ & & \\ & & \\ & & \\ & & \\ & & \\ & & \\ & & \\ & & \\ & & \\ & & \\ & & \\ & & \\ & & \\ & & \\ & & \\ & & \\ & & \\ & & \\ & & \\ & & \\ & & \\ & & \\ & & \\ & & \\ & & \\ & & \\ & & \\ & & \\ & & \\ & & \\ & & \\ & & \\ & & \\ & & \\ & & \\ & & \\ & & \\ & & \\ & & \\ & & \\ & & \\ & & \\ & & \\ & & \\ & & \\ & & \\ & & \\ & & \\ & & \\ & & \\ & & \\ & & \\ & & \\ & & \\ & & \\ & & \\ & & \\ & & \\ & & \\ & & \\ & & \\ & & \\ & & \\ & & \\ & & \\ & & \\ & & \\ & & \\ & & \\ & & \\ & & \\ & & \\ & & \\ & & \\ & & \\ & & \\ & & \\ & & \\ & & \\ & & \\ & & \\ & & \\ & & \\ & & \\ & & \\ & & \\ & & \\ & & \\ & & \\ & & \\ & & \\ & & \\ & & \\ & & \\ & & \\ & & \\ & & \\ & & \\ & & \\ & & \\ & & \\ & & \\ & & \\ & & \\ & & \\ & & \\ & & \\ & & \\ & & \\ & & \\ & & \\ & & \\ & & \\ & & \\ & & \\ & & \\ & & \\ & & \\ & & \\ & & \\ & & \\ & & \\ & & \\ & & \\ & & \\ & & \\ & & \\ & & \\ & & \\ & & \\ & & \\ & & \\ & & \\ & & \\ & & \\ & & \\ & & \\ & & \\ & & \\ & & \\ & & \\ & & \\ & & \\ & & \\ & & \\ & & \\ & & \\ & & \\ & & \\ & & \\ & & \\ & & \\ & & \\ & & \\ & & \\ & & \\ & & \\ & & \\ & & \\ & & \\ & & \\ & & \\ & & \\ & & \\ & & \\ & & \\ & & \\ & & \\ & & \\ & & \\ & & \\ & & \\ & & \\ & & \\ & & \\ & & \\ & & \\ & & \\ & & \\ & & \\ & & \\ & & \\ & & \\ & & \\ & & \\ & & \\ & & \\ & & \\ & & \\ & & \\ & & \\ & & \\ & & \\ & & \\ & & \\ & & \\ & & \\ & & \\ & & \\ & & \\ & & \\ & & \\ & & \\ & & \\ & & \\ & & \\ & & \\ & & \\ & & \\ & & \\ & & \\ & & \\ & & \\ & & \\ & & \\ &$$

Figure 12: Reaction scheme for synthesizing PAGE

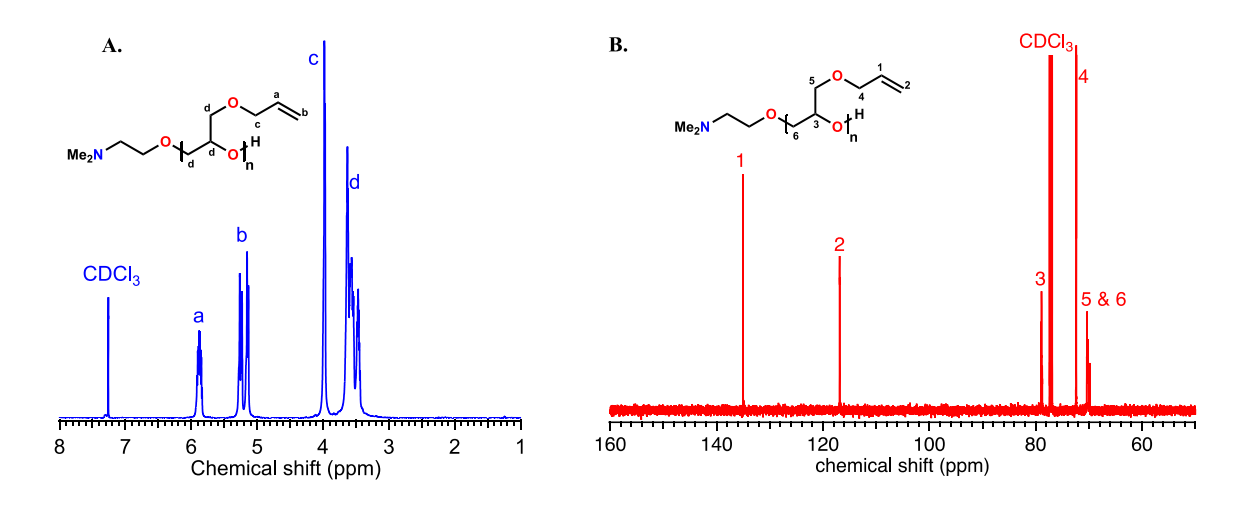


Figure 13: A. <sup>1</sup>H NMR B. <sup>13</sup>C NMR spectra of PAGE in CDCl<sub>3</sub>

 $M_n$  was determined using SEC with refractive index, multiangle light scattering, and viscosity detectors. GPC trace using RI detector for PAGE is shown in Figure 14. The  $M_n$  and D was determined to be 40.7 kg/mol and 1.26.

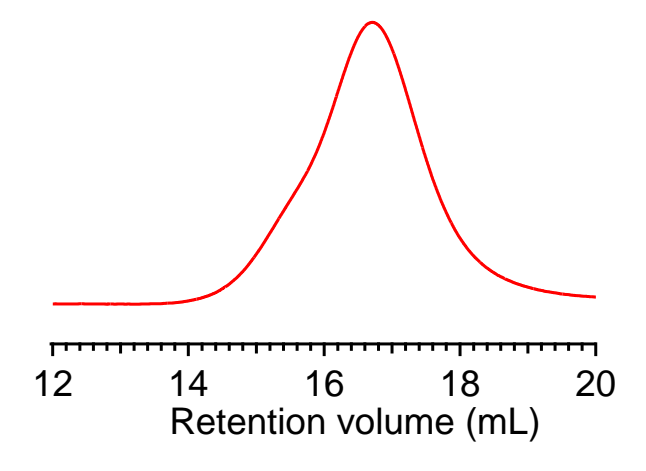


Figure 14: GPC trace for PAGE

The thermal properties of polymers were determined using DSC and TGA. Glass transition temperature was determined using DSC. DSC plot shows  $T_g = -78^{\circ}$ C for PAGE in Figure 15 A. The thermal degradation of polymer was studied using TGA. The first weight loss observed around 300-390 °C is due to cleavage of C-O, C-C and C=C from pendant polymer chain whereas the weight loss beyond 400 °C is due to the polymer backbone degradation as shown in Figure 15 B.

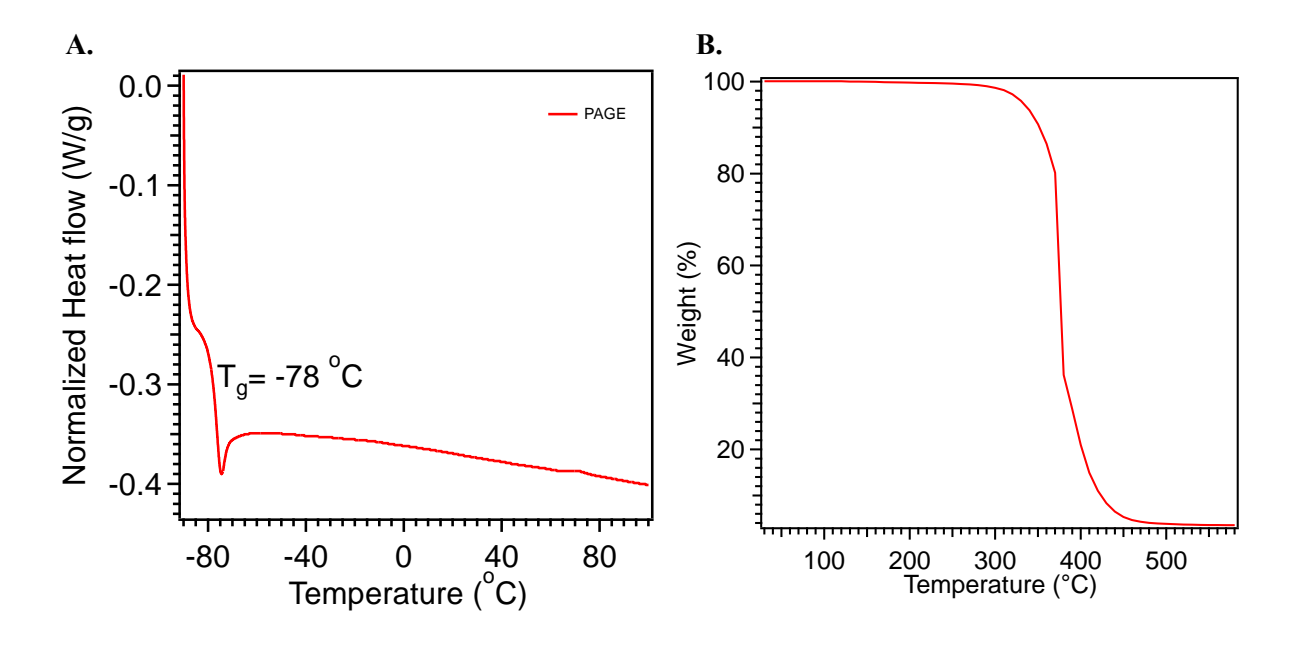


Figure 15: A. DSC trace for PAGE indicating T<sub>g</sub> at around -78°C B. TGA plot for PAGE showing weight loss as a function of temperature

### 2.3.2 Synthesis of precursor poly(propargyl glycidyl ether) (PPGE)

AGE with terminal alkyne group was polymerized successfully as discussed in earlier section. Now we attempted polymerizing PGE with terminal alkyne group. This polymerization is often difficult due to acidic proton on alkyne end using conventional anionic ring opening methodologies as it leads to premature reaction terminations. We carried out PGE polymerization using conditions same as discussed earlier for PAGE. Reaction scheme for synthesis of poly(propargyl glycidyl ether) (PPGE) is shown in Figure 16.

<sup>13</sup>C NMR (CDCl<sub>3</sub>, 125 MHz) δ 58.49 (–O–CH<sub>2</sub>–C≡CH), 69.26–70.35(–O–CH<sub>2</sub>–CH(CH<sub>2</sub>–O–CH<sub>2</sub>–C=CH)–O–), 74.39(–O–CH<sub>2</sub>–C≡CH), 78.56 (–O–CH<sub>2</sub>–CH(CH<sub>2</sub>–O–CH<sub>2</sub>–C≡CH)–O–), 79.95 (–O–CH<sub>2</sub>–C≡CH) (Figure 17 A & B).

Figure 16: Reaction scheme for synthesizing PPGE

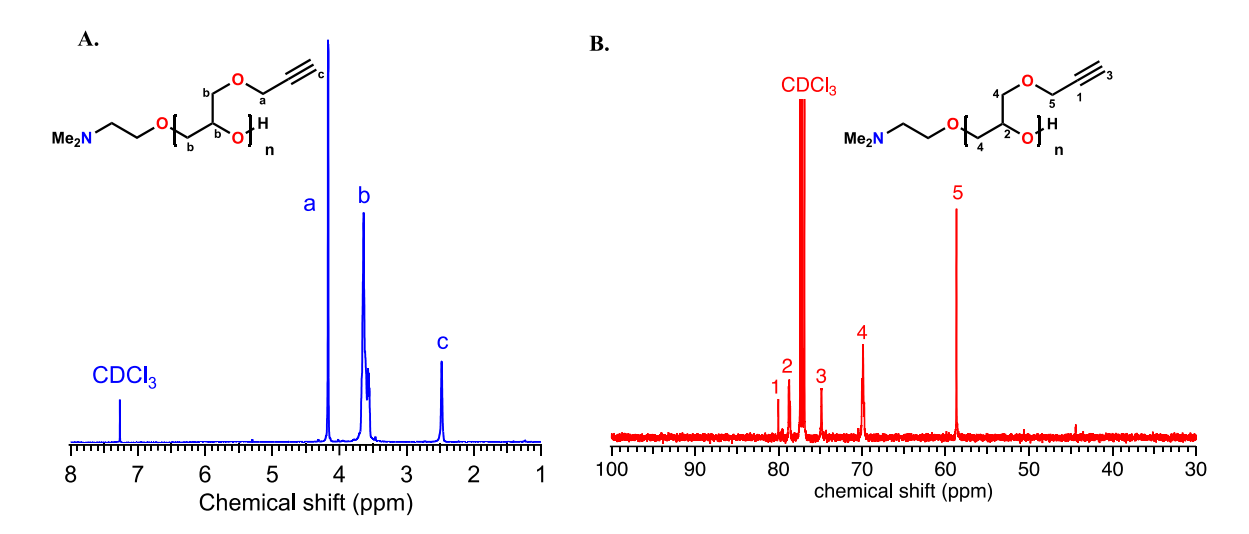


Figure 17: A. <sup>1</sup>H NMR B. <sup>13</sup>C NMR spectra of PPGE in CDCl<sub>3</sub>

GPC using RI detector for PPGE is shown in Figure 18. The  $M_n$  and D was determined to be 23 kg/mol and 1.46.

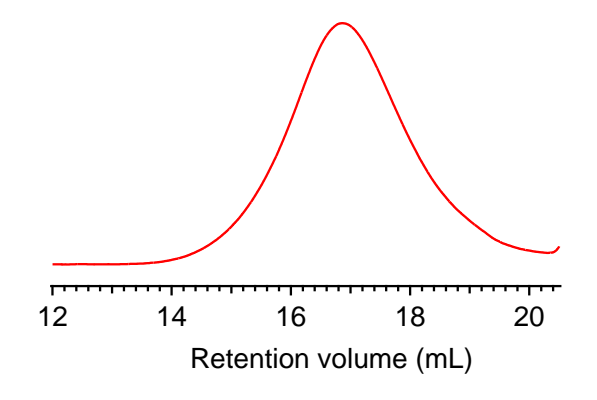


Figure 18: GPC trace for PPGE

The thermal properties of PPGE were determined using DSC and TGA. Glass transition temperature was determined using DSC. DSC plot shows  $T_g = -36^{\circ}\text{C}$  for PPGE in Figure 19 A. The thermal degradation of polymer was studied using TGA. The first weight loss observed around 300-390 °C is due to cleavage of C-O, C-C and C $\equiv$ C from pendant polymer chain whereas the weight loss beyond 400 °C is due to the polymer backbone degradation as shown in Figure 19 B.

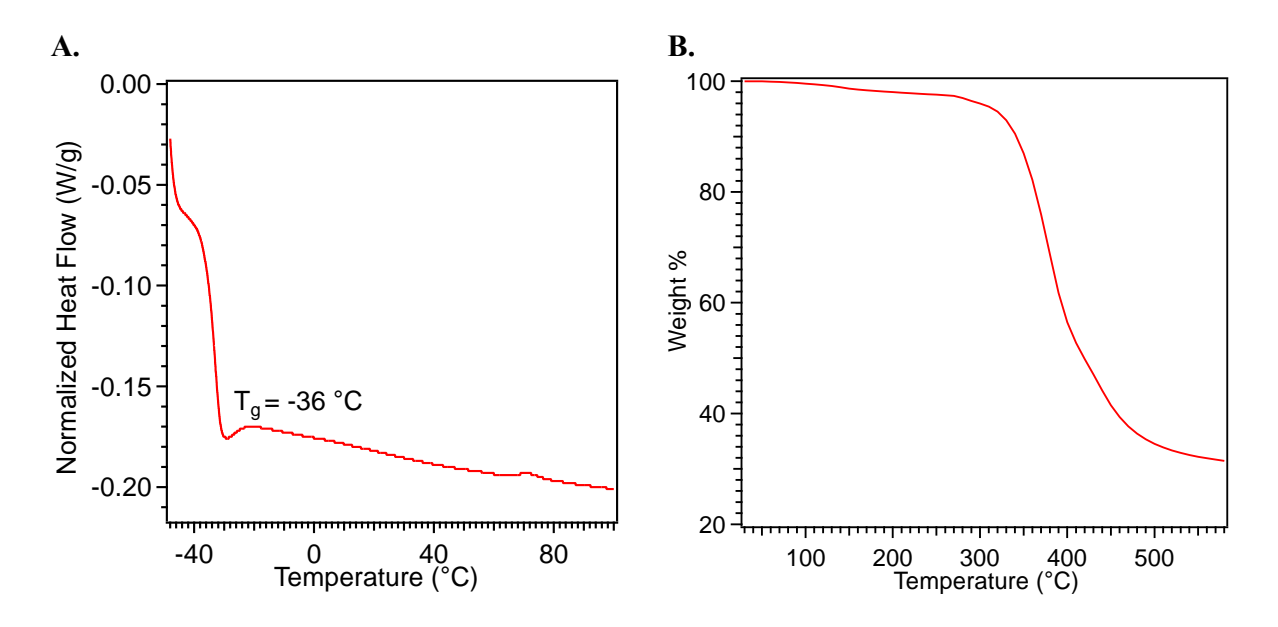


Figure 19: A. DSC trace for PPGE indicating T<sub>g</sub> at around -36°C B. TGA plot for PPGE showing weight loss as a function of temperature

# 2.3.3 Synthesis of P(PGE-b-ECH) copolymer

Now we attempted first copolymerization reaction using ECH and PGE. Block copolymer was synthesized using similar strategy as homopolymerizations. Instead of adding ECH and PGE monomers all at the same time we use sequential addition methodology. The vials were charged with a stir bar, the first monomer PGE, and MOB in an inert environment. The solutions were then heated to the final reaction temperature (50 °C, dependent on monomer) and polymerizations were carried out for 48 hours or until fully polymerized (checked by taking crude proton NMR). Then second monomer ECH was added and polymerized completely before quenching it. The resulting polymer was cleaned following general method described in methods section to obtain final polymer.

 $^{1}H \ NMR \ (CDCl_{3}, 500 \ MHz) \ \delta \ 2.48 \ (s, -O-CH_{2}-C\equiv C\underline{H}), 3.54-3.70 \ (broad \ m, -O-C\underline{H}_{2}-C\underline{H}(C\underline{H}_{2}-C\underline{H})) \ (C\underline{H}_{2}-C\underline{H}_{2}-C\underline{H}_{2}-C\underline{H}_{2}-C\underline{H}_{2}-C\underline{H}_{2}-C\underline{H}_{2}-C\underline{H}_{2}-C\underline{H}_{2}-C\underline{H}_{2}-C\underline{H}_{2}-C\underline{H}_{2}-C\underline{H}_{2}-C\underline{H}_{2}-C\underline{H}_{2}-C\underline{H}_{2}-C\underline{H}_{2}-C\underline{H}_{2}-C\underline{H}_{2}-C\underline{H}_{2}-C\underline{H}_{2}-C\underline{H}_{2}-C\underline{H}_{2}-C\underline{H}_{2}-C\underline{H}_{2}-C\underline{H}_{2}-C\underline{H}_{2}-C\underline{H}_{2}-C\underline{H}_{2}-C\underline{H}_{2}-C\underline{H}_{2}-C\underline{H}_{2}-C\underline{H}_{2}-C\underline{H}_{2}-C\underline{H}_{2}-C\underline{H}_{2}-C\underline{H}_{2}-C\underline{H}_{2}-C\underline{H}_{2}-C\underline{H}_{2}-C\underline{H}_{2}-C\underline{H}_{2}-C\underline{H}_{2}-C\underline{H}_{2}-C\underline{H}_{2}-C\underline{H}_{2}-C\underline{H}_{2}-C\underline{H}_{2}-C\underline{H}_{2}-C\underline{H}_{2}-C\underline{H}_{2}-C\underline{H}_{2}-C\underline{H}_{2}-C\underline{H}_{2}-C\underline{H}_{2}-C\underline{H}_{2}-C\underline{H}_{2}-C\underline{H}_{2}-C\underline{H}_{2}-C\underline{H}_{2}-C\underline{H}_{2}-C\underline{H}_{2}-C\underline{H}_{2}-C\underline{H}_{2}-C\underline{H}_{2}-C\underline{H}_{2}-C\underline{H}_{2}-C\underline{H}_{2}-C\underline{H}_{2}-C\underline{H}_{2}-C\underline{H}_{2}-C\underline{H}_{2}-C\underline{H}_{2}-C\underline{H}_{2}-C\underline{H}_{2}-C\underline{H}_{2}-C\underline{H}_{2}-C\underline{H}_{2}-C\underline{H}_{2}-C\underline{H}_{2}-C\underline{H}_{2}-C\underline{H}_{2}-C\underline{H}_{2}-C\underline{H}_{2}-C\underline{H}_{2}-C\underline{H}_{2}-C\underline{H}_{2}-C\underline{H}_{2}-C\underline{H}_{2}-C\underline{H}_{2}-C\underline{H}_{2}-C\underline{H}_{2}-C\underline{H}_{2}-C\underline{H}_{2}-C\underline{H}_{2}-C\underline{H}_{2}-C\underline{H}_{2}-C\underline{H}_{2}-C\underline{H}_{2}-C\underline{H}_{2}-C\underline{H}_{2}-C\underline{H}_{2}-C\underline{H}_{2}-C\underline{H}_{2}-C\underline{H}_{2}-C\underline{H}_{2}-C\underline{H}_{2}-C\underline{H}_{2}-C\underline{H}_{2}-C\underline{H}_{2}-C\underline{H}_{2}-C\underline{H}_{2}-C\underline{H}_{2}-C\underline{H}_{2}-C\underline{H}_{2}-C\underline{H}_{2}-C\underline{H}_{2}-C\underline{H}_{2}-C\underline{H}_{2}-C\underline{H}_{2}-C\underline{H}_{2}-C\underline{H}_{2}-C\underline{H}_{2}-C\underline{H}_{2}-C\underline{H}_{2}-C\underline{H}_{2}-C\underline{H}_{2}-C\underline{H}_{2}-C\underline{H}_{2}-C\underline{H}_{2}-C\underline{H}_{2}-C\underline{H}_{2}-C\underline{H}_{2}-C\underline{H}_{2}-C\underline{H}_{2}-C\underline{H}_{2}-C\underline{H}_{2}-C\underline{H}_{2}-C\underline{H}_{2}-C\underline{H}_{2}-C\underline{H}_{2}-C\underline{H}_{2}-C\underline{H}_{2}-C\underline{H}_{2}-C\underline{H}_{2}-C\underline{H}_{2}-C\underline{H}_{2}-C\underline{H}_{2}-C\underline{H}_{2}-C\underline{H}_{2}-C\underline{H}_{2}-C\underline{H}_{2}-C\underline{H}_{2}-C\underline{H}_{2}-C\underline{H}_{2}-C\underline{H}_{2}-C\underline{H}_{2}-C\underline{H}_{2}-C\underline{H}_{2}-C\underline{H}_{2}-C\underline{H}_{2}-C\underline{H}_{2}-C\underline{H}_{2}-C\underline{H}_{2}-C\underline{H}_{2}-C\underline{H}_{2}-C\underline{H}_{2}-C\underline{H}_{2}-C\underline{H}_{2}-C\underline{H}_{2}-C\underline{H}_{2}-C\underline{H}_{2}-C\underline{H}_{2}-C\underline{H}_{2}-C\underline{H}_{2}-C\underline{H}_{2}-C\underline{H}_{2}-C\underline{H}_{2}-C\underline{H}_{2}-C\underline{H}_{2}-C\underline{H}_{2}-C\underline{H}_{2}-C\underline{H}_{2}-C\underline{H}_{2}-C\underline{H}_{2}-C\underline{H}_{2}-C\underline{H}_{2}-C\underline{H}_{2}-C\underline{H}_{2}-C\underline{H}_{2}-C\underline{H}_$ 

 $^{13}C$  NMR (CDCl<sub>3</sub>, 125 MHz)  $\delta$  43.79, 58.71, 69.84, 74.89, 78.72, 79.16, 80 (Figure 20 A & B).

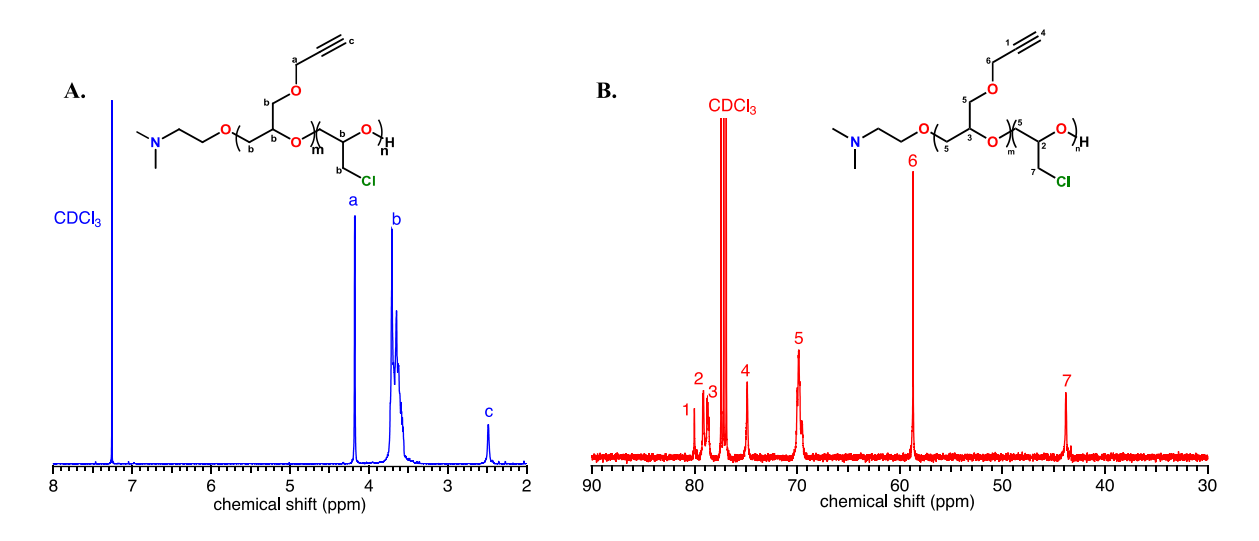


Figure 20: A. <sup>1</sup>H NMR B. <sup>13</sup>C NMR spectra of P(PGE-b-ECH) in CDCl<sub>3</sub>

# 2.3.4 Synthesis of P(PGE-stat-PPO) copolymer

Next, copolymer with different polymer structure was prepared by adding PGE and PO at the start of the reaction. This technique leads to statistical copolymer formation where we obtain random addition of epoxides in the final polymer chain. For polymerization followed general polymer synthesis method by adding PGE (40%) and PO (60%) together at the start of the reaction. This novel copolymer was then characterized using <sup>1</sup>H and <sup>13</sup>C NMR spectroscopy.

<sup>1</sup>H NMR (CDCl<sub>3</sub>, 500 MHz) δ 1.13 (d, C<u>H</u><sub>3</sub>), 2.44 (s, -O-CH<sub>2</sub>-C≡C<u>H</u>), 3.33–3.74 (broad m, -O-C<u>H</u><sub>2</sub>-C<u>H</u>(C<u>H</u><sub>2</sub>-O-CH<sub>2</sub>-C≡CH)-O-), 4.16 (s, -O-C<u>H</u><sub>2</sub>-C≡CH)

<sup>13</sup>C NMR (CDCl<sub>3</sub>, 125 MHz) δ 17.36, 58.56, 70.32, 73.2, 75.30, 78.9, 79.5, 80 (Figure 21 A & B).

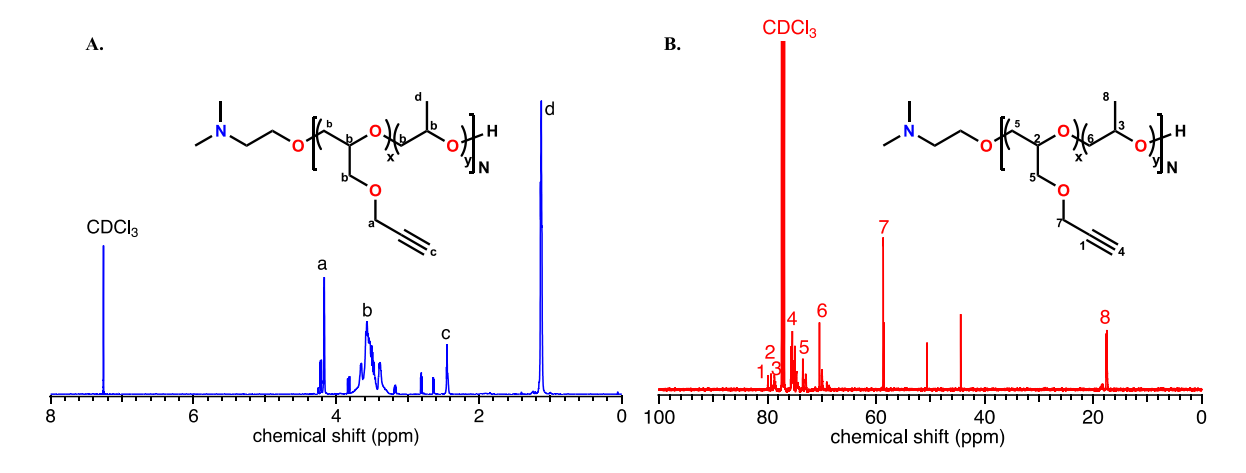


Figure 21: A. <sup>1</sup>H NMR B. <sup>13</sup>C NMR spectra of P(PGE-stat-PO) in CDCl<sub>3</sub>

# 2.3.5 Synthesis of P(PGE-*stat*-ECH) copolymer

In this study we attempted a novel copolymer synthesis using starting epoxides PGE and ECH. This synthesis followed same technique as homopolymerization with only difference in addition of monomers where both epoxides were added simultaneously at the start of the reaction. Both PGE and ECH were taken in equal quantities. The structure and <sup>1</sup>H NMR of purified P(PGE-*stat*-ECH) is as shown in Figure 22 and Figure 23 A & B.

<sup>1</sup>H NMR (CDCl<sub>3</sub>, 500 MHz) δ 2.48 (s, -O-CH<sub>2</sub>-C≡CH), 3.54–3.70 (broad m, -O-CH<sub>2</sub>-CH(CH<sub>2</sub>-O-CH<sub>2</sub>-C=CH) – O-) and -O-CH<sub>2</sub>-CH(CH<sub>2</sub>-Cl)-O-, 4.17 (s, -O-CH<sub>2</sub>-C=CH)

<sup>13</sup>C NMR (CDCl<sub>3</sub>, 125 MHz) δ 43.83, 58.56, 68.97-69.95, 74.86, 78.57, 78.87, 79.86.

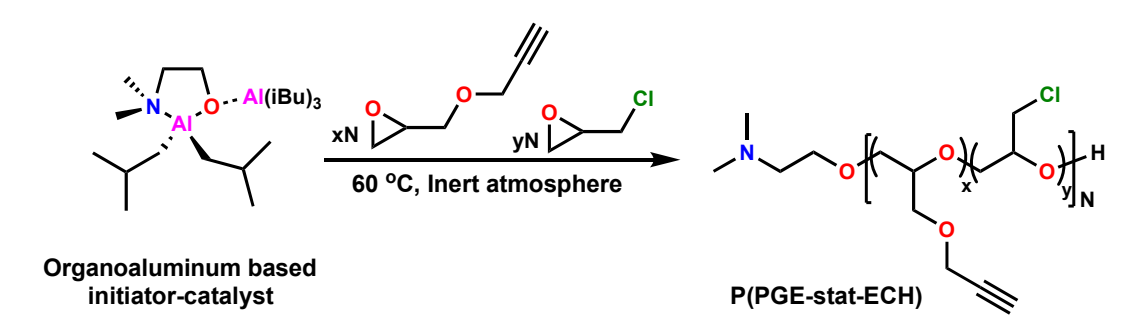


Figure 22: Reaction scheme for synthesizing P(PGE-*stat*-ECH)

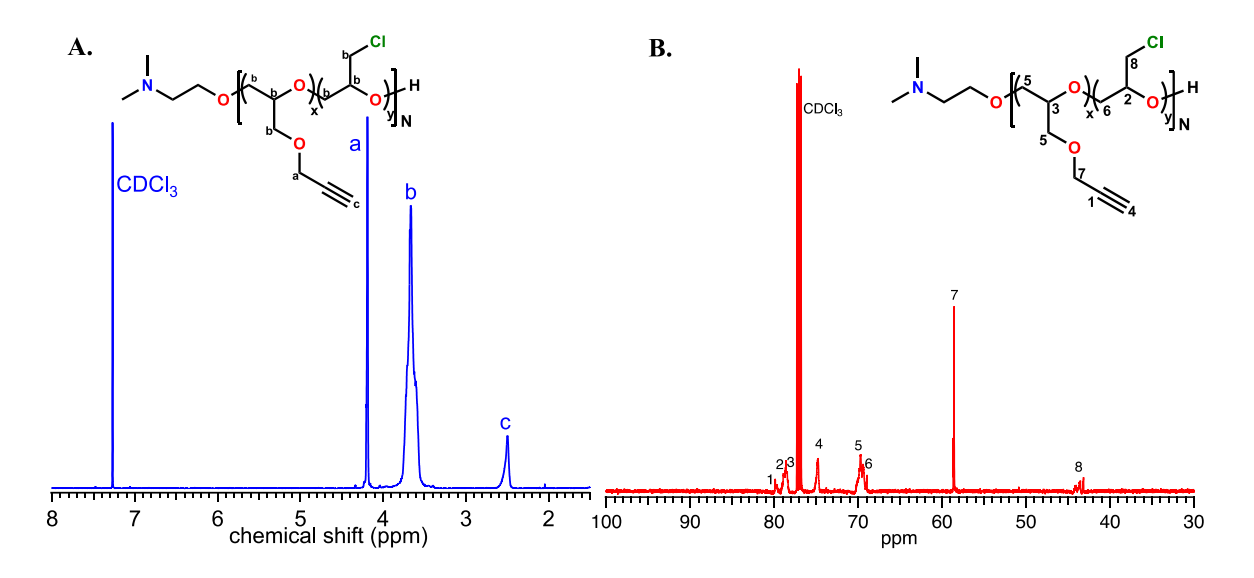


Figure 23: A. <sup>1</sup>H NMR B. <sup>13</sup>C NMR spectra of P(PGE-stat-PO) in CDCl<sub>3</sub>

The P(PGE-stat-ECH) copolymer was further characterized by size-exclusion chromatography (SEC) with triple detection, revealing a molecular weight of 25.5 kg/mol and D=1.43, which is consistent with the targeted molecular weight of 20 kg/mol. (Figure 24) The relatively high polydispersity is likely due to the difficult ring opening polymerization of the two epoxides. Chain transfer reactions of acidic proton from PGE leads to formation of mixture of different molecular weight polymers and high polydispersity.

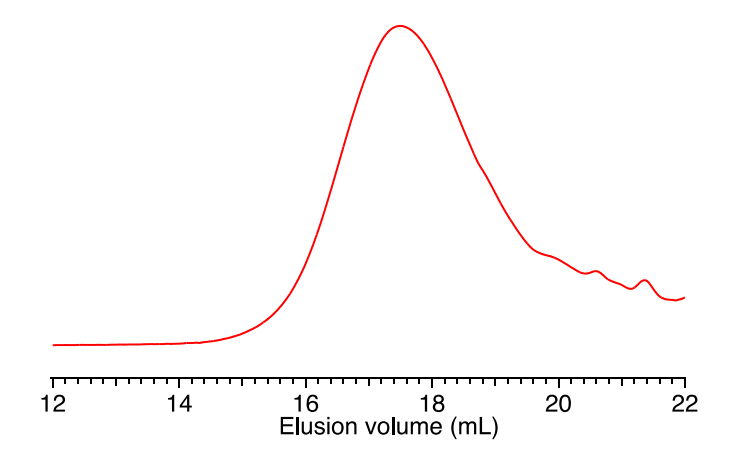


Figure 24: GPC trace for P(PGE-stat-ECH)

Finally, we performed DSC which revealed a single  $T_g$  at -31 °C consistent with a 50-50 statistical copolymer of these two epoxides. (Figure 25 A) The thermal degradation behavior of the prepared P(PGE-*stat*-ECH) were also examined using TGA (Figure 25 B). For this analysis, a sample (approximately 10 mg) was heated to 800 °C at a heating rate of 10°C /min under N<sub>2</sub> environment. The TGA shows three step weight loss for the P(PGE-*stat*-ECH). The weight loss near 100-150 °C is due to solvent or moisture trapped in the membrane. The second step weight loss is observed around 300-390 °C and is due to cleavage of C-O, C-C, C=C and C-Cl from pendant polymer chain whereas the third step weight loss beyond 400 °C is due to the degradation of polymer backbone.

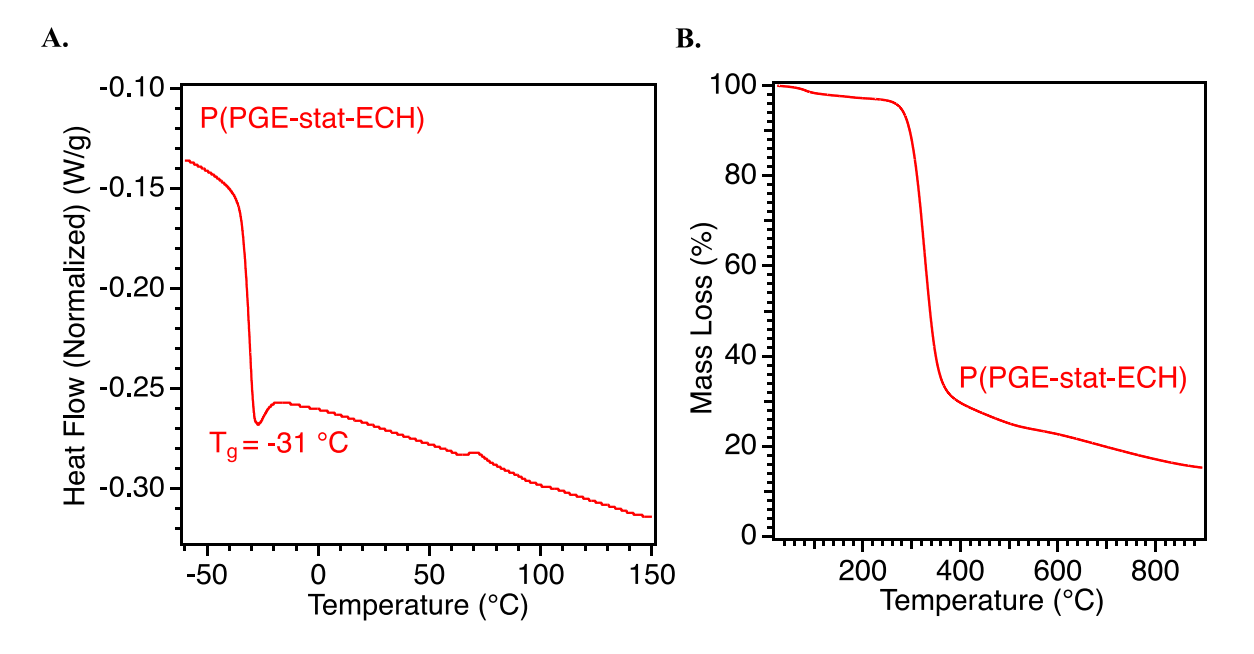


Figure 25: A. DSC trace for P(PGE-*stat*-ECH) indicating T<sub>g</sub> at around -31°C B. TGA plot for P(PGE-*stat*-ECH) showing weight loss as a function of temperature

The chemical composition of a copolymers was characterized through FTIR spectroscopy. (Figure 26) A clear CH stretch peak at 3296 cm<sup>-1</sup> and 2112 cm<sup>-1</sup> can be seen, which confirms the presence of the alkyne group. The sharp band around 750 cm<sup>-1</sup> for P(PGE-*stat*-ECH) is consistent with C-Cl stretching, indicating that the chloromethyl group is present as well.

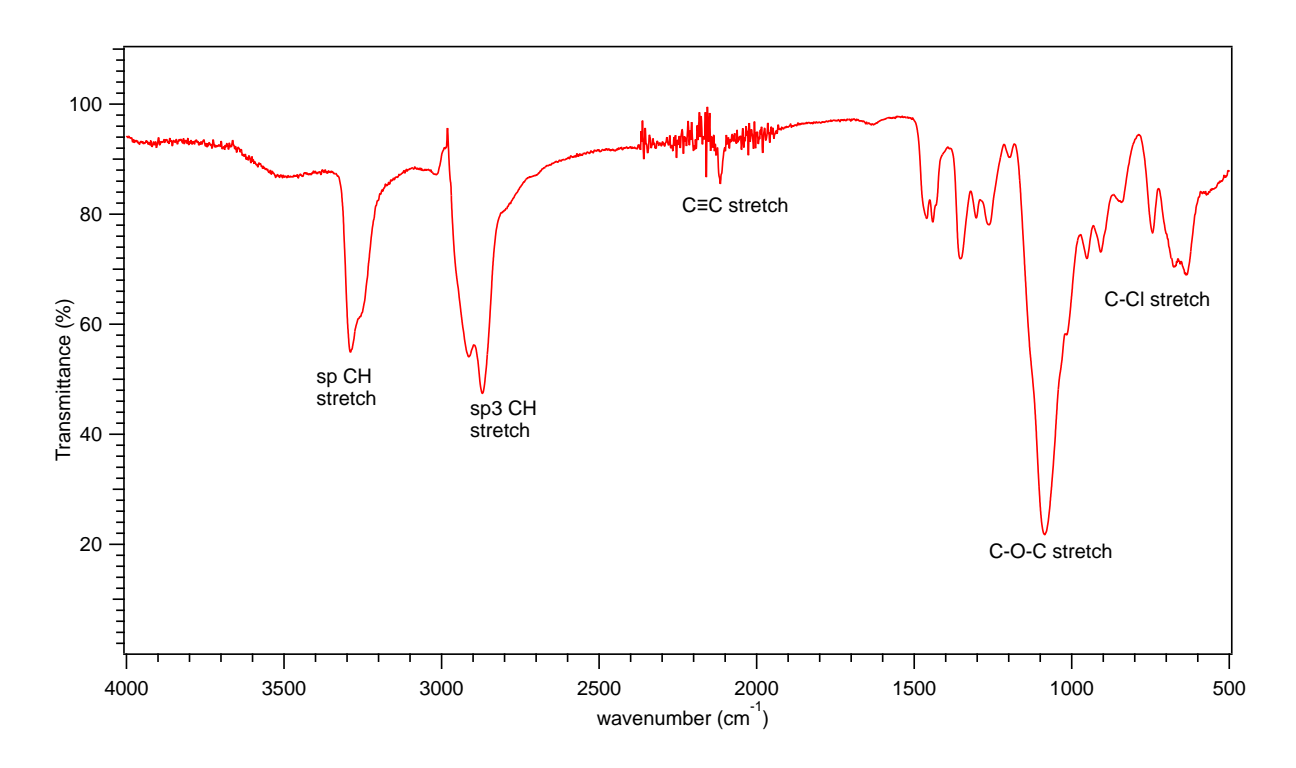


Figure 26: FTIR spectra of P(PGE-stat-ECH)

This copolymer holds huge importance in developing tunable charged polymers for advanced uses. With chloromethyl and alkyne functionality we can practically introduce any charged moieties using simple chemistries after polymerizations. We will be focusing on study of this functional copolymer and its uses in this thesis.

# 2.3.6 Kinetics and reactivity ratios calculation

Reactivity ratios are an important factor to determine randomness addition of two or more monomers into polymeric backbone chain. The knowledge about reactivity ratios is very helpful to understand polymer structure completely. To determine reactivity ratios, we need to combine experimental data and need to fit it using different models. If we have two monomers A and B for copolymerization, they will be added to the chain end with a certain probability. This will depend on the affinity between growing chain end and the monomers. So, reactivity ratio of A (r<sub>A</sub>) is indicator of how likely it will add to the chain end with A. r<sub>A</sub>=k<sub>AA</sub>/k<sub>AB</sub> where k<sub>AA</sub> and k<sub>AB</sub> are the

propagation rate constants for the A terminal chain end and the A and B monomers. If A is prone to add to A chain end, we get blocky copolymer. If both monomer A and B are competing to add to A chain end, we will get random copolymer. In general, if  $r1 \times r2 = 1$  statistical copolymer,  $r1 \times r2 = 0$  alternating copolymer,  $r1 \times r2 > 1$  block copolymer forms.<sup>34</sup>

Kinetics study of polymerization of epichlorohydrin and propargyl glycidyl ether was conducted to determine reactivity ratios. The targeted molecular weight of these polymers is 20 kg/mol for both the studies. Sample conversion calculation for copolymerization is given in appendix.

For the first study, we used triisobutylaluminum adduct of (2-dimethylamino)ethoxy-diisobutylaluminum (MOB). For this study 75% PGE and 25% ECH was used. We have used Meyer-Lowry method to model reactivity ratios.<sup>34</sup> It has been found out that  $r_{ECH}$ = 1.43,  $r_{PGE}$ = 0.69 (Figure 27) So  $r_{ECH} \times r_{PGE} \approx 1$ . This confirms random addition of both monomers in the resulting copolymer to obtain statistical copolymer.

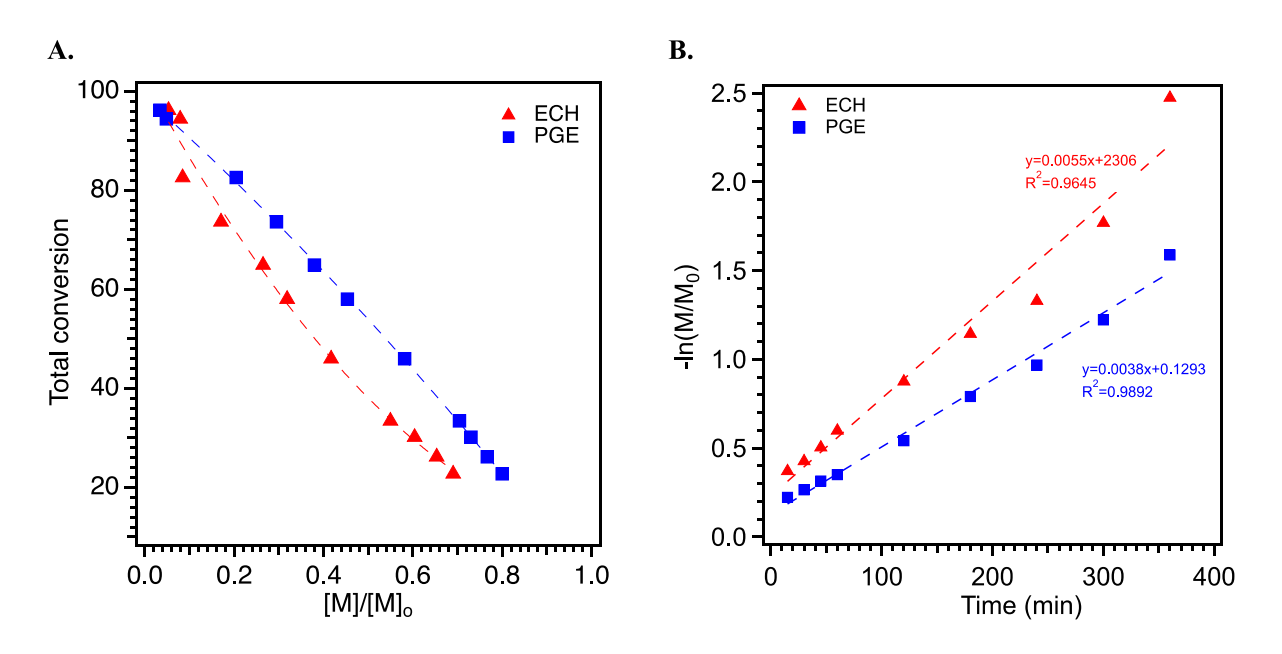


Figure 27: A. Plot of conversion vs normalized monomer concentration B. plot of -ln([M]/[Mo]) vs time of polymerization for PGE and ECH using MOB

Stacked <sup>1</sup>H NMR spectra for P(PGE-*stat*-ECH) showing evolution of polymer peaks in Figure 28 as reaction progresses using MOB system.

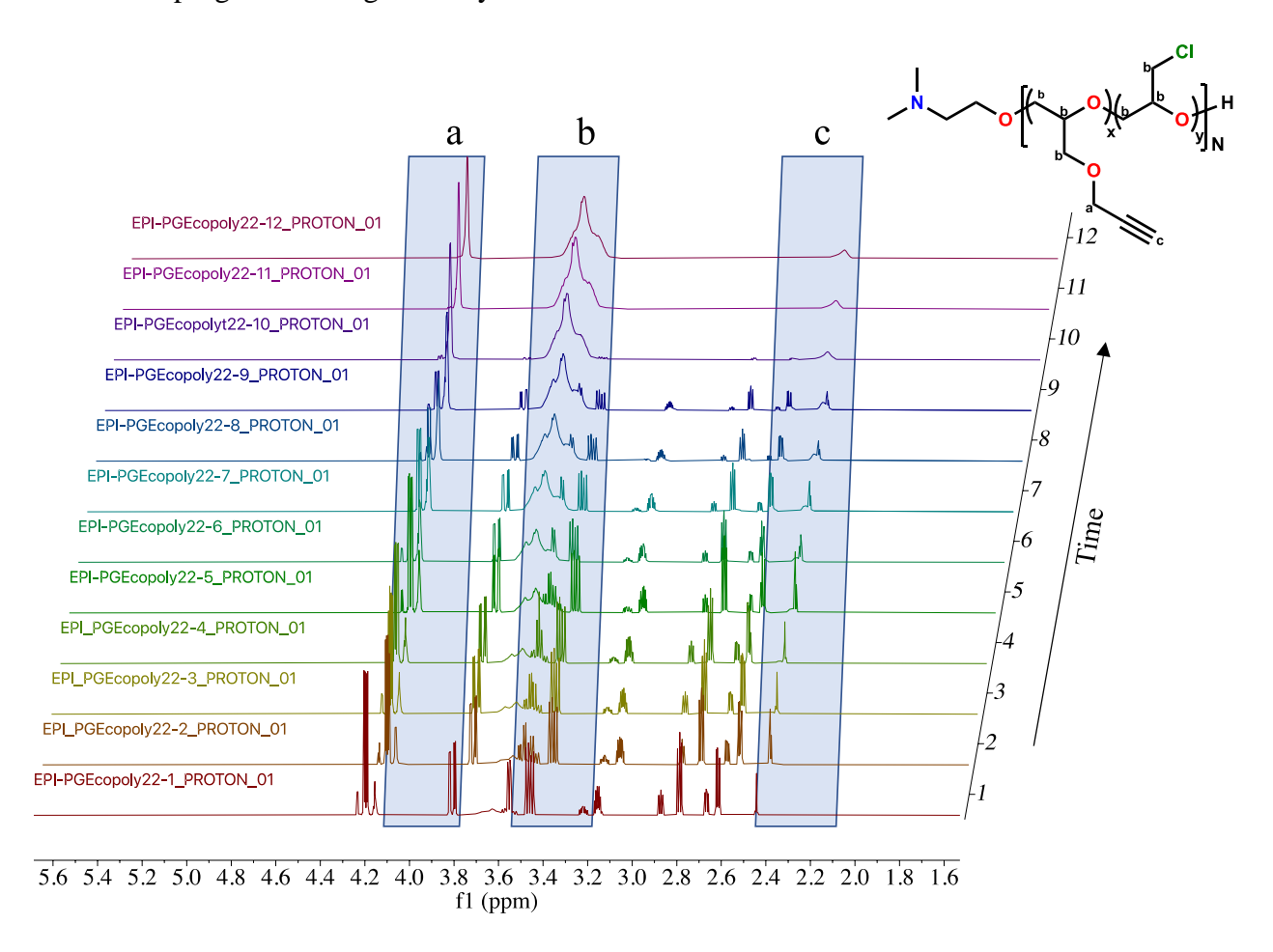


Figure 28: Stacked <sup>1</sup>H NMR spectra for P(PGE-stat-ECH) showing evolution of polymer peaks as reaction progresses using MOB system

For the second study, we used separate initiator and catalyst system for polymerization of mixture of 50% PGE and 50% ECH. Again, using Meyer-Lowry method we calculated reactivity ratios to be rech= 1.48, rpge= 0.72. So rech×rpge≈1. (Figure 29) This confirms random addition of both monomers to obtain statistical copolymer. Hence, we can conclude that regardless of system of initiator and catalyst we achieve final product which is statistical copolymer. This copolymer is novel, and no such polymer has been reported in literature before.

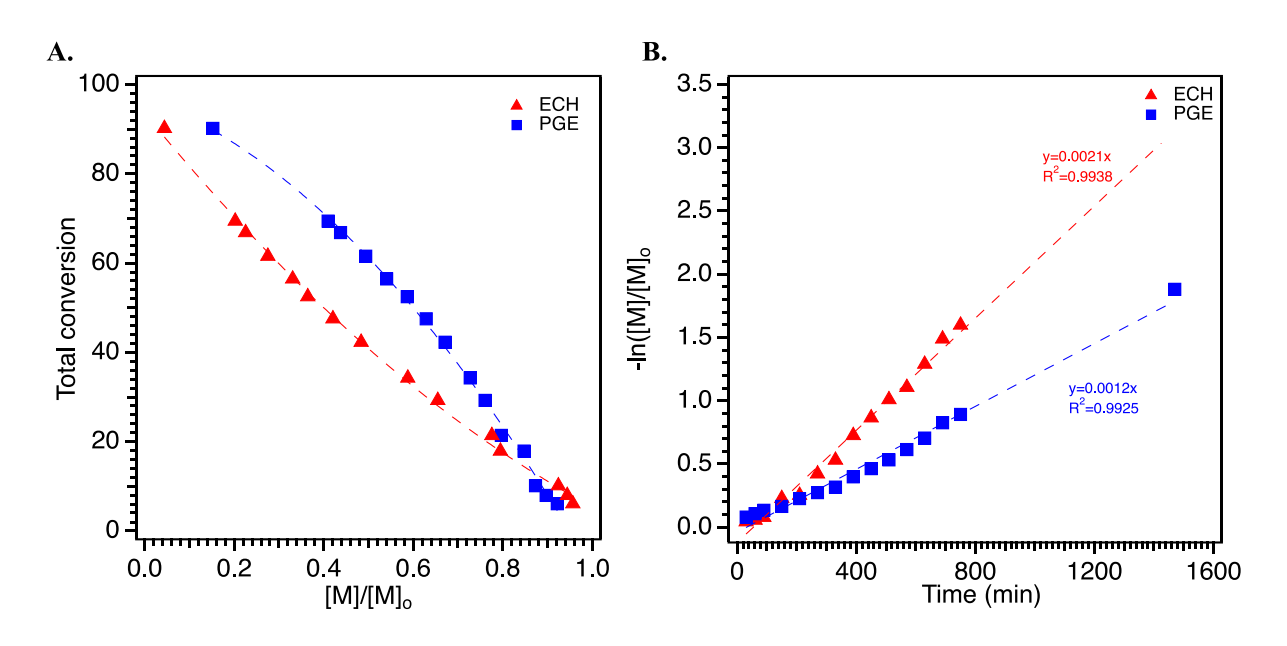


Figure 29: A. Plot of conversion vs normalized monomer concentration B. plot of -ln([M]/[Mo]) vs time of polymerization for PGE and ECH using NAI and benzyl initiator system

Stacked <sup>1</sup>H NMR spectra for P(PGE-*stat*-ECH) showing evolution of polymer peaks as reaction progresses using NAl and benzyl initiator system is given in Figure 30.

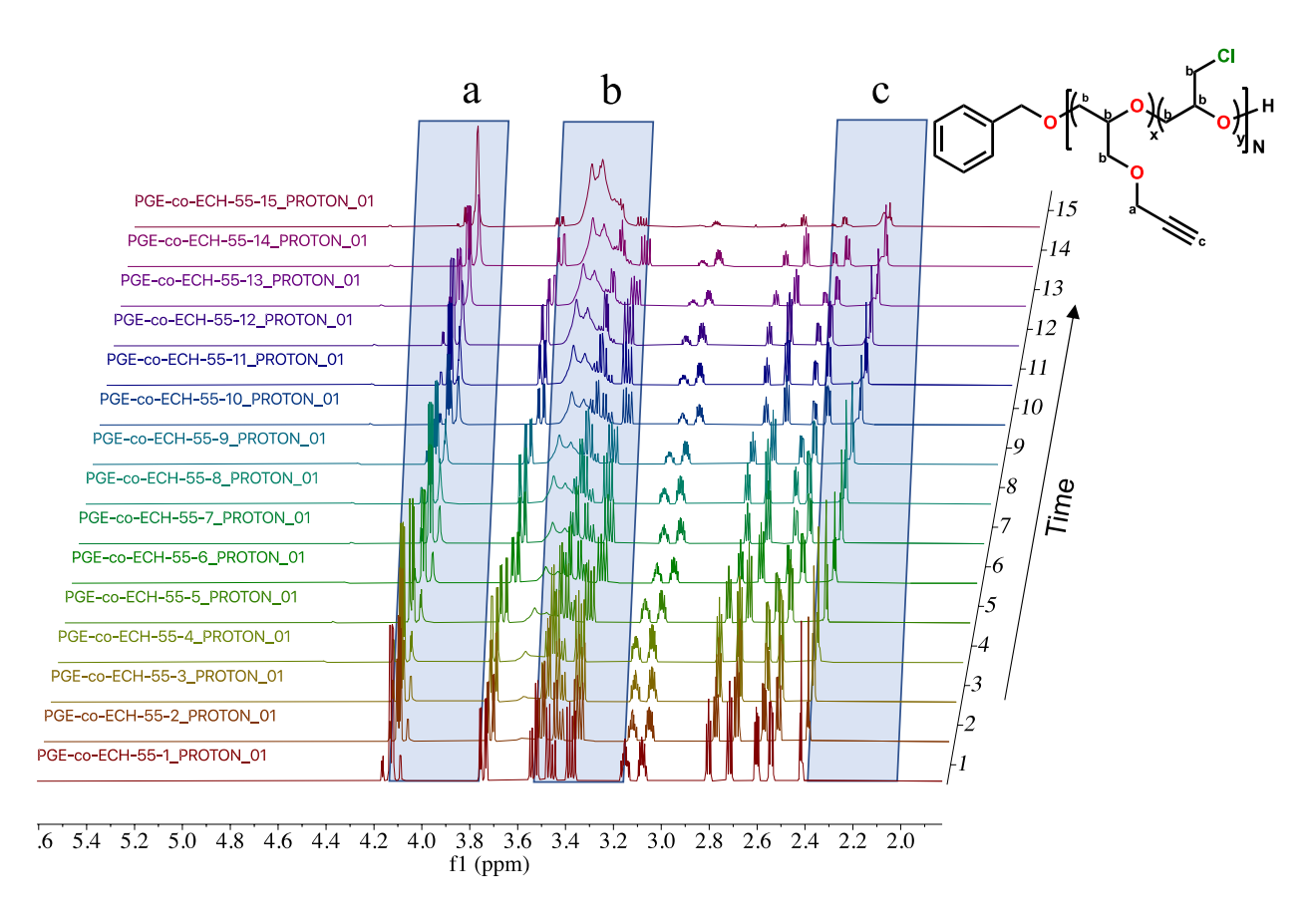


Figure 30: Stacked <sup>1</sup>H NMR spectra for P(PGE-stat-ECH) showing evolution of polymer peaks as reaction progresses using NAI and benzyl initiator system

# **Composition variation**

A statistical copolymer of PGE and ECH can be considered a key factor for the synthesis of multifunctional charged polymers. In this study copolymer composition was varied by incorporating increasing ratios of PGE (20-80%) in the polymerization feed. This will be crucial in developing a platform to explore new charged polymers in different contexts to better understand antifouling properties, ion exchange membranes for separations and charge polymer self-assembly. We used MOB system for carrying out these set of polymers. The reaction scheme is shown in Figure 31.

Figure 31: Reaction scheme for synthesizing P(PGE-stat-ECH) using MOB

All the polymers were characterized using <sup>1</sup>H NMR spectroscopy. Figure 32 shows a stacked plot of these polymers clearly showing evolution of peaks a and c corresponding to the peaks emerging from PGE part of copolymer. Sample calculation for determining ECH and PGE composition in copolymer has been detailed in appendix.

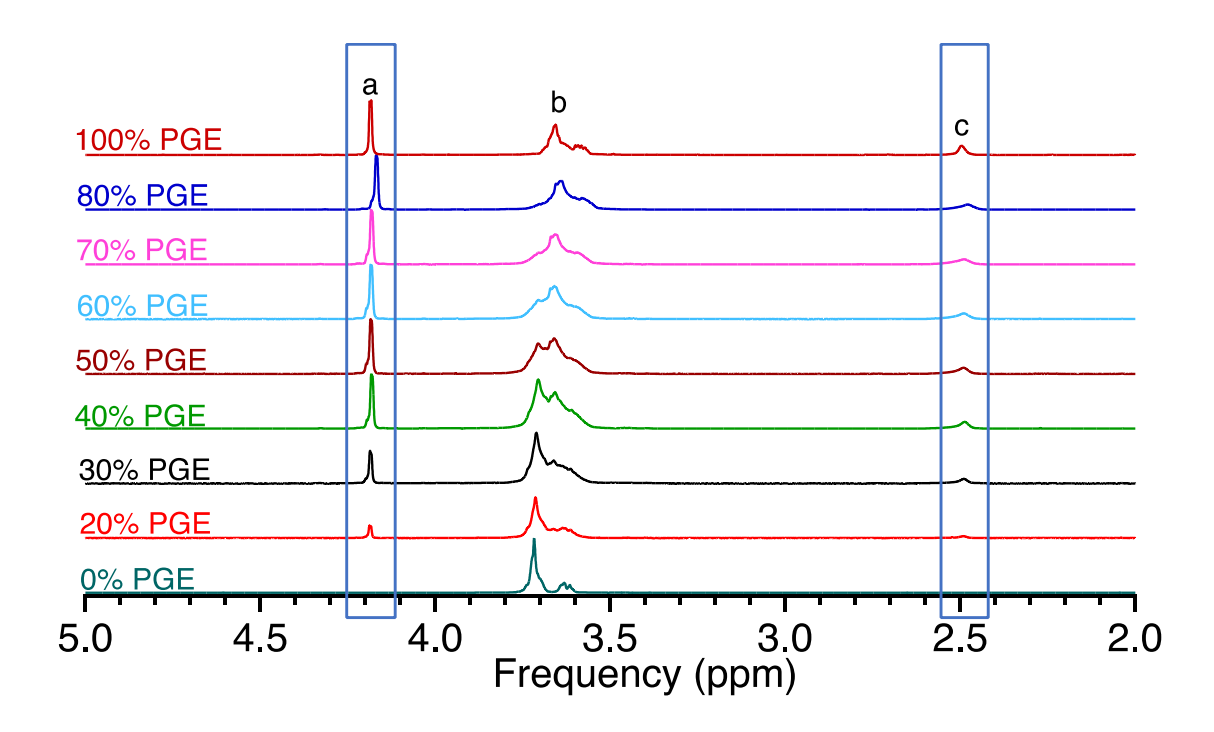


Figure 32: Stacked <sup>1</sup>H NMR spectra for P(PGE-*stat*-ECH) with varied PGE:ECH composition with fixed M<sub>n</sub> of 20 kg/mol

DSC experiments were performed to determine  $T_g$  of these polymers. For homopolymer with ECH  $T_g$  is -22 °C and for homopolymer with PGE that is PPGE  $T_g$  is -36 °C. As we get a statistical copolymer, we get a net property of the both the polymers. So, in this case We get  $T_g$  as a combined  $T_g$  of two of these monomers. This can be fitted using Fox equation as a function of PGE composition. Comparison plot of  $T_g$  experimental vs  $T_g$  from fox equations is shown in Figure 33.

Fox equation 
$$\frac{1}{T_g} = \frac{x_1}{T_{g1}} + \frac{x_2}{T_{g2}}$$

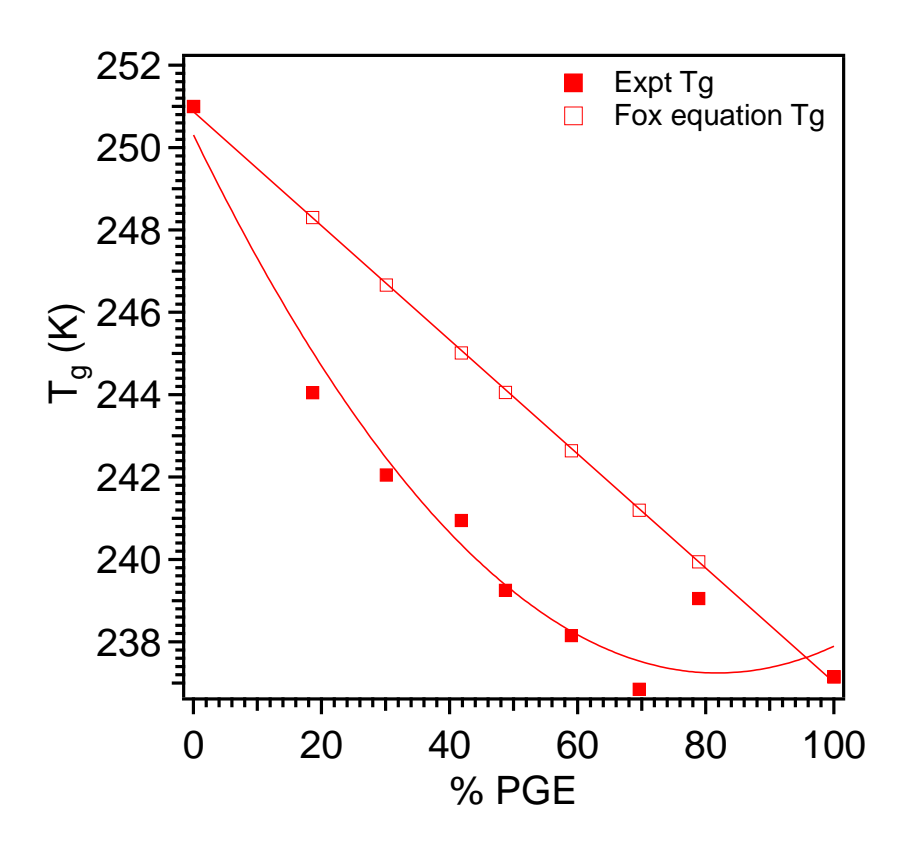


Figure 33: Variation in  $T_g$  of P(PGE-stat-ECH) with increase in PGE content measured using DSC experiments compared with  $T_g$  calculated from Fox equation

DOSY spectroscopy was performed to confirm copolymer formation. Figure 34 A-F shows plots shows plots of various P(PGE-*stat*-ECH) polymers with single diffusion coefficient for each polymer protons. This verifies formation of statistical copolymer. All results from this study are tabulated in Table 1.

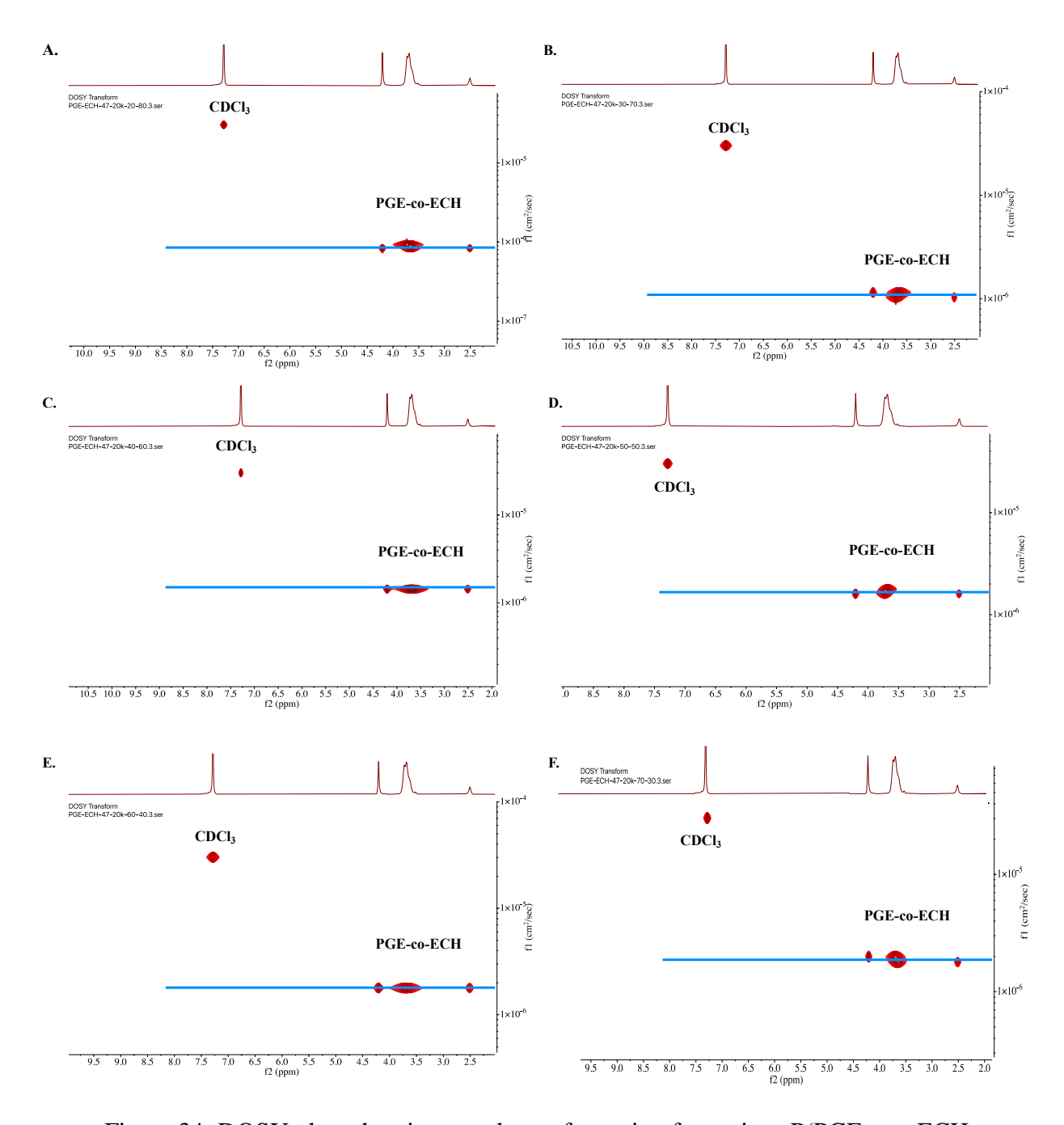


Figure 34: DOSY plots showing copolymer formation for various P(PGE-stat-ECH polymers)A.PGE:ECH=20:80 B. PGE:ECH=30:70 C. PGE:ECH=40:60 D. PGE:ECH=50:50 E. PGE:ECH=60:40 F. PGE:ECH=70:30

Table 1: Summary table for P(PGE-co -ECH) polymers with varying composition and molecular weights

Copolymer	Composition theoretical (mol %PGE)	Composition actual (PGE mol %)	M <sub>n</sub>	M <sub>n</sub> ¹H NMR	T <sub>g</sub> (°C)
	20	18.6	20k	-	-29.1
	30	30.1	20k	-	-31.1
PGE-co-ECH	40	41.8	20k	-	-32.2
composition	50	48.7	20k	-	-33.9
variation	60	59	20k	-	-35
V 661 1862 O 11	70	69.6	20k	-	-36.3
	80	78.9	20k	-	-34.1
	50	48.1	10k	11.9k	-33.8
	50	47.8	20k	19.5k	-34.3
PGE-co-ECH	50	48	40k	51.3k	-34.5
M <sub>n</sub> variation	50	48.9	60k	66.3k	-35.8
172 <sub>11</sub> + 32 1401012	50	48.5	80k	62.9k	-35.9
	50	48.3	100k	105.1k	-39.59

# Molecular weight variation keeping composition same

For this study separate initiator (benzyl initiator) and catalyst (NAI) system was used. (Figure 35) By tuning initiator composition, we can achieve control over molecular weight. This platform will allow us to control molecular weight, composition, monomer sequence, and polymer architecture. Number average molecular weights were determined using end group analysis. (Sample calculation is provided in the appendix). Molecular weights up to 100 kg/mol with narrow distributions were achieved.

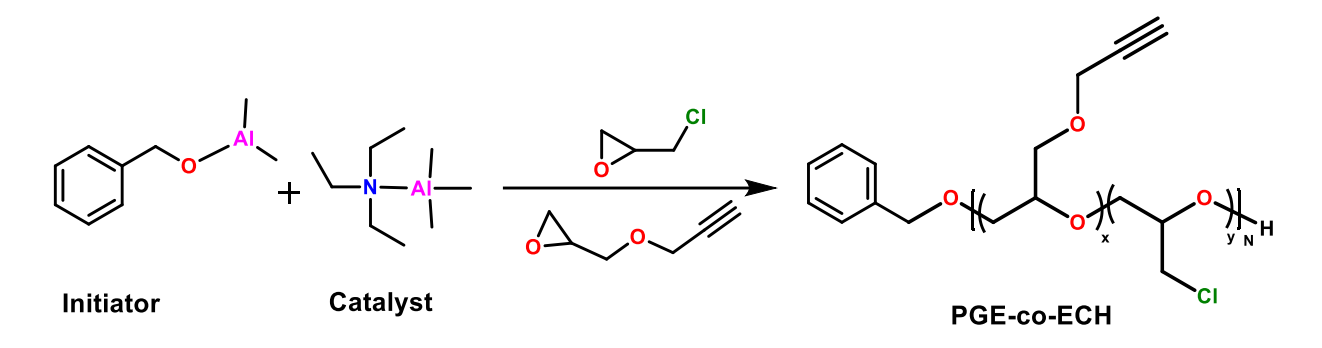


Figure 35: Reaction scheme for synthesizing P(PGE-stat-ECH) using NAI and benzyl initiator DOSY spectroscopy was performed to confirm copolymer formation. Figure 36 A-D shows plots of various P(PGE-*stat*-ECH) polymers with single diffusion coefficient for each polymer protons. This signifies all polymer protons are diffusing at the same time and verifies formation of statistical copolymer.

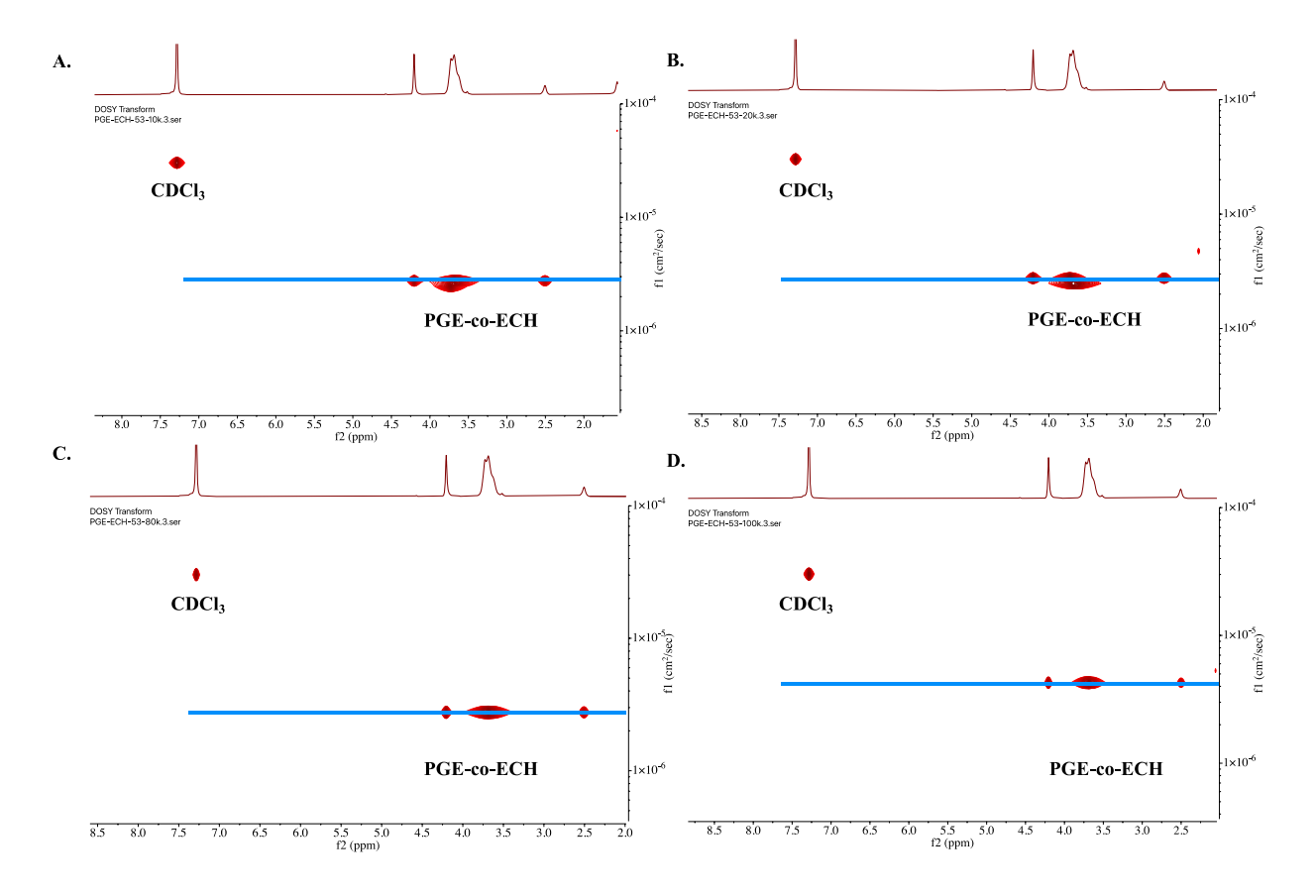


Figure 36: DOSY plots confirming copolymer formation for various P(PGE-*stat*-ECH polymers)A. M<sub>n</sub>= 10 kg/mol B. M<sub>n</sub>= 20 kg/mol C. M<sub>n</sub>= 80 kg/mol D. M<sub>n</sub>= 100 kg/mol

All results from this study are tabulated in Table 1.

#### 2.4 Conclusion

In conclusion, obtaining multifunctional polyethers was challenging using conventional methodologies. Alkyne functional polyethers were usually prepared by modifying polyethylene oxide as the acidic proton interferes during polymerization process causing early chain termination. But we demonstrated relatively higher molecular weights and good polydispersities for these functional polyethers without any need for post polymerization modification. We studied the polymerization kinetics for copolymerization of PGE and ECH and found out that we obtain gradient statistical copolymer with more favorable addition of ECH over PGE. With the use this synthesis route we didn't require to protect alkyne pendant groups and so minimizing extra reaction step. The benefit of having pendant alkene, alkyne or chloride is that we can modify these polymers for further applications. With the use of MOB system, we have developed tunable polymerization platform providing us with good structure—property relationships control for further application. We are equipped with this versatile platform through which we can understand and control macromolecular architecture in polyethers. We will utilize it to develop amphoteric ion exchange membrane and to study charged polymer self-assembly.

#### BIBLIOGRAPHY

- (1) Obermeier, B.; Frey, H. Poly(Ethylene Glycol-Co-Allyl Glycidyl Ether)s: A PEG-Based Modular Synthetic Platform for Multiple Bioconjugation. *Bioconjug Chem* 2011, 22 (3), 436–444. https://doi.org/10.1021/bc1004747.
- (2) Knop, K.; Hoogenboom, R.; Fischer, D.; Schubert, U. S. Poly(Ethylene Glycol) in Drug Delivery: Pros and Cons as Well as Potential Alternatives. *Angewandte Chemie International Edition*. August 23, 2010, pp 6288–6308. https://doi.org/10.1002/anie.200902672.
- (3) Pasut, G.; Veronese, F. M. State of the Art in PEGylation: The Great Versatility Achieved after Forty Years of Research. *Journal of Controlled Release*. July 20, 2012, pp 461–472. <a href="https://doi.org/10.1016/j.jconrel.2011.10.037">https://doi.org/10.1016/j.jconrel.2011.10.037</a>.
- (4) Knop, K.; Hoogenboom, R.; Fischer, D.; Schubert, U. S. Poly(Ethylene Glycol) in Drug Delivery: Pros and Cons as Well as Potential Alternatives. *Angewandte Chemie International Edition*. August 23, 2010, pp 6288–6308. <a href="https://doi.org/10.1002/anie.200902672">https://doi.org/10.1002/anie.200902672</a>.
- (5) Dingels, C.; Schömer, M.; Frey, H. Die Vielen Gesichter Des Poly(Ethylenglykol)s: Von Der Kosmetik Zum Ionenleiter. *Chemie in Unserer Zeit* 2011, 45 (5), 338–349. <a href="https://doi.org/10.1002/ciuz.201100551">https://doi.org/10.1002/ciuz.201100551</a>.
- (6) Schmolka, I. R. A Review of Block Polymer Surfactants.
- (7) Engels, H. W.; Pirkl, H. G.; Albers, R.; Albach, R. W.; Krause, J.; Hoffmann, A.; Casselmann, H.; Dormish, J. Polyurethanes: Versatile Materials and Sustainable Problem Solvers for Today's Challenges. *Angewandte Chemie International Edition*. September 2, 2013, pp 9422–9441. <a href="https://doi.org/10.1002/anie.201302766">https://doi.org/10.1002/anie.201302766</a>.
- (8) Mcpherson, T.; Kidane, A.; Szleifer, I.; Park, K. Prevention of Protein Adsorption by Tethered Poly(Ethylene Oxide) Layers: Experiments and Single-Chain Mean-Field Analysis; 1998. <a href="https://pubs.acs.org/sharingguidelines">https://pubs.acs.org/sharingguidelines</a>.
- (9) Ba, C.; Economy, J. Preparation and Characterization of a Neutrally Charged Antifouling Nanofiltration Membrane by Coating a Layer of Sulfonated Poly(Ether Ether Ketone) on a Positively Charged Nanofiltration Membrane. *J Memb Sci* 2010, *362* (1–2), 192–201. <a href="https://doi.org/10.1016/j.memsci.2010.06.032">https://doi.org/10.1016/j.memsci.2010.06.032</a>.
- (10) Sagle, A. C.; Van Wagner, E. M.; Ju, H.; McCloskey, B. D.; Freeman, B. D.; Sharma, M. M. PEG-Coated Reverse Osmosis Membranes: Desalination Properties and Fouling Resistance. *J Memb Sci* 2009, 340 (1–2), 92–108. https://doi.org/10.1016/j.memsci.2009.05.013.

- (11) Louie, J. S.; Pinnau, I.; Ciobanu, I.; Ishida, K. P.; Ng, A.; Reinhard, M. Effects of Polyether-Polyamide Block Copolymer Coating on Performance and Fouling of Reverse Osmosis Membranes. *J Memb Sci* 2006, 280 (1–2), 762–770. <a href="https://doi.org/10.1016/j.memsci.2006.02.041">https://doi.org/10.1016/j.memsci.2006.02.041</a>.
- (12) Berthier, C.; Gorecki, W.; Minier, M.; Armand, M. B.; Chabagno, J. M.; Rigaud, P. *Solid State Ionics* 11 (1983) 91-95 Microscopic Investigation Of Ionic Conductivity In Alkali Metal Salts-Poly(Ethylene Oxide) Adducts.
- (13) Barteau, K. P.; Wolffs, M.; Lynd, N. A.; Fredrickson, G. H.; Kramer, E. J.; Hawker, C. J. Allyl Glycidyl Ether-Based Polymer Electrolytes for Room Temperature Lithium Batteries. *Macromolecules* 2013, *46* (22), 8988–8994. <a href="https://doi.org/10.1021/ma401267w">https://doi.org/10.1021/ma401267w</a>.
- (14) Wang, P.; Tan, K. L.; Kang, E. T.; Neoh, K. G. Plasma-Induced Immobilization of Poly(Ethylene Glycol) onto Poly(Vinylidene Fluoride) Microporous Membrane; 2002; Vol. 195.
- (15) Vandenberg, E. J. Organometallic Catalysts for Polymerizing Monosubstituted Epoxides. *Journal of Polymer Science* 1960, 47 (149), 486–489. https://doi.org/10.1002/pol.1960.1204714947.
- (16) Biedron, T.; Kubisa, P.; Penczek, S. Polyepichlorohydrin Diols Free of Cyclics: Synthesis and Characterization. *J Polym Sci A Polym Chem* 1991, 29 (5), 619–628. <a href="https://doi.org/10.1002/pola.1991.080290502">https://doi.org/10.1002/pola.1991.080290502</a>.
- (17) Carlotti, S.; Labbé, A.; Rejsek, V.; Doutaz, S.; Gervais, M.; Deffieux, A. Living/Controlled Anionic Polymerization and Copolymerization of Epichlorohydrin with Tetraoctylammonium Bromide-Triisobutylaluminum Initiating Systems. *Macromolecules* 2008, *41* (19), 7058–7062. <a href="https://doi.org/10.1021/ma801422c">https://doi.org/10.1021/ma801422c</a>.
- (18) Ferrier, R. C.; Imbrogno, J.; Rodriguez, C. G.; Chwatko, M.; Meyer, P. W.; Lynd, N. A. Four-Fold Increase in Epoxide Polymerization Rate with Change of Alkyl-Substitution on Mono-μ-Oxo-Dialuminum Initiators. *Polym Chem* 2017, 8 (31), 4503–4511. https://doi.org/10.1039/c7py00894e.
- (19) Rodriguez, C. G.; Ferrier, R. C.; Helenic, A.; Lynd, N. A. Ring-Opening Polymerization of Epoxides: Facile Pathway to Functional Polyethers via a Versatile Organoaluminum Initiator. *Macromolecules* 2017, 50 (8), 3121–3130. <a href="https://doi.org/10.1021/acs.macromol.7b00196">https://doi.org/10.1021/acs.macromol.7b00196</a>.
- (20) Safaie, N.; Smak, J.; DeJonge, D.; Cheng, S.; Zuo, X.; Ohno, K.; Ferrier, R. C. Facile Synthesis of Epoxide-Co-Propylene Sulphide Polymers with Compositional and Architectural Control. *Polym Chem* 2022. <a href="https://doi.org/10.1039/d2py00005a">https://doi.org/10.1039/d2py00005a</a>.
- (21) Imbrogno, J.; Ferrier, R. C.; Wheatle, B. K.; Rose, M. J.; Lynd, N. A. Decoupling Catalysis and Chain-Growth Functions of Mono(μ-Alkoxo)Bis(Alkylaluminums) in Epoxide

- Polymerization: Emergence of the N-Al Adduct Catalyst. *ACS Catal* 2018, 8 (9), 8796–8803. <a href="https://doi.org/10.1021/acscatal.8b02446">https://doi.org/10.1021/acscatal.8b02446</a>.
- (22) Safaie, N.; Rawal, B.; Ohno, K.; Ferrier, R. C. Aluminum-Based Initiators from Thiols for Epoxide Polymerizations. *Macromolecules* 2020, 53 (19), 8181–8191. https://doi.org/10.1021/acs.macromol.0c00464.
- (23) Almena, A.; Martín, M. Technoeconomic Analysis of the Production of Epichlorohydrin from Glycerol. *Ind Eng Chem Res* 2016, 55 (12), 3226–3238. <a href="https://doi.org/10.1021/acs.iecr.5b02555">https://doi.org/10.1021/acs.iecr.5b02555</a>.
- (24) Shukla, G.; Ferrier, R. C. The Versatile, Functional Polyether, Polyepichlorohydrin: History, Synthesis, and Applications. *Journal of Polymer Science*. John Wiley and Sons Inc November 15, 2021, pp 2704–2718. <a href="https://doi.org/10.1002/pol.20210514">https://doi.org/10.1002/pol.20210514</a>.
- (25) Obermeier, B.; Wurm, F.; Mangold, C.; Frey, H. Multifunctional Poly(Ethylene Glycol)s. *Angewandte Chemie International Edition*. August 22, 2011, pp 7988–7997. <a href="https://doi.org/10.1002/anie.201100027">https://doi.org/10.1002/anie.201100027</a>.
- (26) Mangold, C.; Dingels, C.; Obermeier, B.; Frey, H.; Wurm, F. PEG-Based Multifunctional Polyethers with Highly Reactive Vinyl-Ether Side Chains for Click-Type Functionalization. *Macromolecules* 2011, 44 (16), 6326–6334. https://doi.org/10.1021/ma200898n.
- (27) Huynh, V. T.; Chen, G.; Souza, P. De; Stenzel, M. H. Thiol-Yne and Thiol-Ene "Click" Chemistry as a Tool for a Variety of Platinum Drug Delivery Carriers, from Statistical Copolymers to Crosslinked Micelles. *Biomacromolecules* 2011, *12* (5), 1738–1751. <a href="https://doi.org/10.1021/bm200135e">https://doi.org/10.1021/bm200135e</a>.
- (28) Hoogenboom, R. Thiol-Yne Chemistry: A Powerful Tool for Creating Highly Functional Materials. *Angewandte Chemie International Edition* 2010, 49 (20), 3415–3417. <a href="https://doi.org/10.1002/anie.201000401">https://doi.org/10.1002/anie.201000401</a>.
- (29) Huynh, V. T.; Chen, G.; Souza, P. De; Stenzel, M. H. Thiol-Yne and Thiol-Ene "Click" Chemistry as a Tool for a Variety of Platinum Drug Delivery Carriers, from Statistical Copolymers to Crosslinked Micelles. *Biomacromolecules* 2011, *12* (5), 1738–1751. https://doi.org/10.1021/bm200135e.
- (30) Herzberger, J.; Leibig, D.; Langhanki, J.; Moers, C.; Opatz, T.; Frey, H. "Clickable PEG" via Anionic Copolymerization of Ethylene Oxide and Glycidyl Propargyl Ether. *Polym Chem* 2017, 8 (12), 1882–1887. https://doi.org/10.1039/c7py00173h.
- (31) Voorter, P. J.; McKay, A.; Dai, J.; Paravagna, O.; Cameron, N. R.; Junkers, T. Solvent-Independent Molecular Weight Determination of Polymers Based on a Truly Universal Calibration. *Angewandte Chemie International Edition* 2022, 61 (5). <a href="https://doi.org/10.1002/anie.202114536">https://doi.org/10.1002/anie.202114536</a>.

- (32) Evans, R.; Dal Poggetto, G.; Nilsson, M.; Morris, G. A. Improving the Interpretation of Small Molecule Diffusion Coefficients. *Anal Chem* 2018, 90 (6), 3987–3994. https://doi.org/10.1021/acs.analchem.7b05032.
- (33) Bakkour, Y.; Darcos, V.; Li, S.; Coudane, J. Diffusion Ordered Spectroscopy (DOSY) as a Powerful Tool for Amphiphilic Block Copolymer Characterization and for Critical Micelle Concentration (CMC) Determination. *Polym Chem* 2012, *3* (8), 2006–2010. <a href="https://doi.org/10.1039/c2py20054f">https://doi.org/10.1039/c2py20054f</a>.
- (34) Lynd, N. A.; Ferrier, R. C.; Beckingham, B. S. Recommendation for Accurate Experimental Determination of Reactivity Ratios in Chain Copolymerization. *Macromolecules* 2019, 52 (6), 2277–2285. https://doi.org/10.1021/acs.macromol.8b01752.

#### **APPENDIX**

## Sample conversion calculation for copolymerization:

= 5.875

Opened <sup>1</sup>H NMR on MNova software, first corrected the baseline and phase. Set the reference for residual signal of CDCl<sub>3</sub> to 7.26. Set integration for peak at  $\delta$  4.21 to 2 corresponding to peak from unreacted PGE. Took integration of peaks corresponding to peak emerging from PPGE at  $\delta$  4.17 (11.13), for polymer backbone at  $\delta$  3.8-3.5 (57.2) and for residual ECH at  $\delta$  3.24 (0.27). (As shown in Figure 37)

PGE conversion = 
$$\frac{\text{PPGE integration}}{\text{PPGE integration} + 2} \times 100 = \frac{11.13}{11.13 + 2} \times 100 = 84.76\%$$

$$ECH \ converted = \frac{backbone \ integration - (PPGE \ integration \times \frac{5}{2})}{5} = \frac{57.2 - (11.13 \times 2.5)}{5}$$

ECH conversion = 
$$\frac{\text{ECH converted}}{\text{ECH converted} + \text{ECH residual integration}} = \frac{5.875}{5.875 + 0.27} = 95.6\%$$

Total conversion = mol% ECH  $\times$  conversion of ECH + mol% PGE  $\times$  conversion of PGE

$$= 0.5 \times 84.76 + 0.5 \times 95.6 = 90.18\%$$

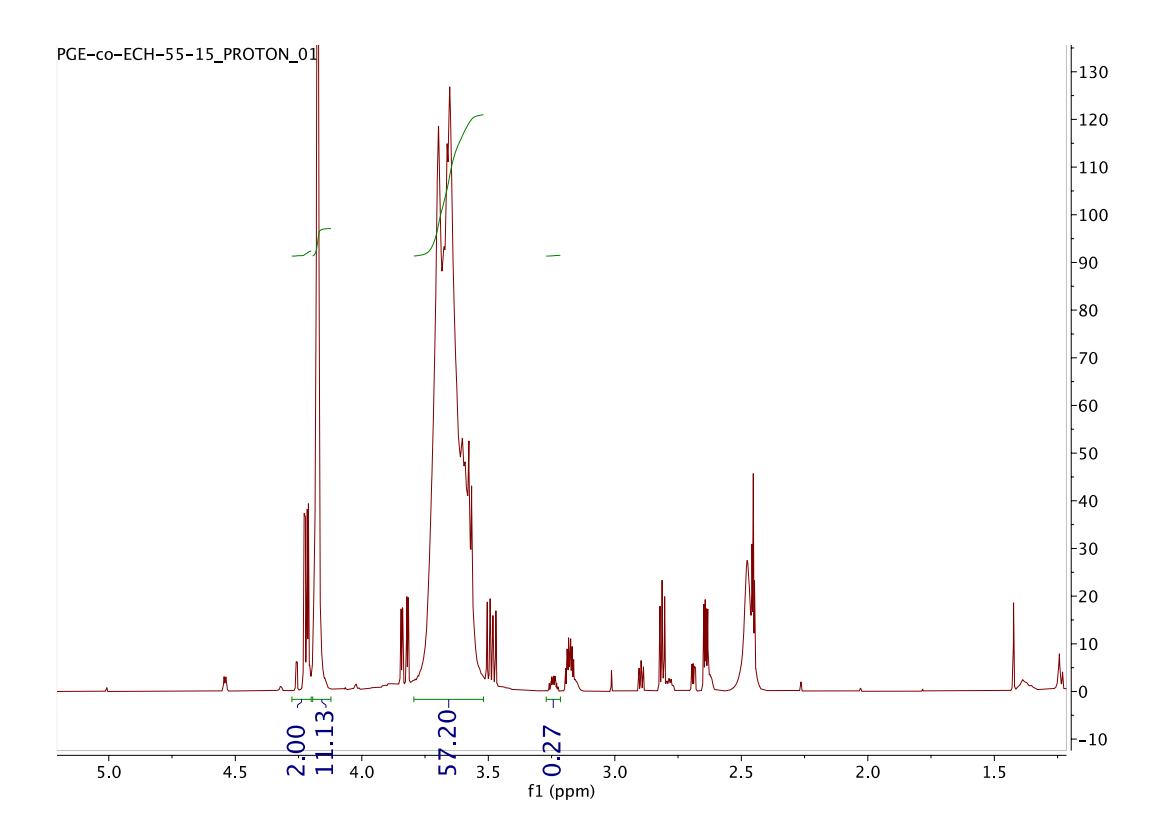


Figure 37: <sup>1</sup>H NMR of P(PGE-*stat*-ECH) showing peak integration used for calculating monomer conversion

#### Sample calculation for determining ECH and PGE composition in copolymer:

Opened ¹H NMR on MNova software, first corrected the baseline and phase. Set the reference for residual signal of CDCl₃ to 7.26. Set integration for peak at δ 4.17 to 2 protons from pendant HC≡CCH₂O− from PGE component. Took integration of peaks corresponding to peak emerging from polymer backbone at δ 3.85-3.4 (6.34). (As shown in Figure 38)

Number of ECH backbone units per 1 PGE units

$$=\frac{\text{backbone integration}-5(\text{\# of H per PGE backbone})}{5(\text{\# of H per ECH backbone})}=\frac{6.34-5}{5}=0.268$$
% ECH = 
$$\frac{\text{Number of ECH backbone units per 1 PGE units}}{\text{Number of ECH backbone units per 1 PGE units}}=\frac{0.268}{0.268+1}=21.13\%$$

% PGE = 100 - %ECH = 100 - 21.23 = 78.87%

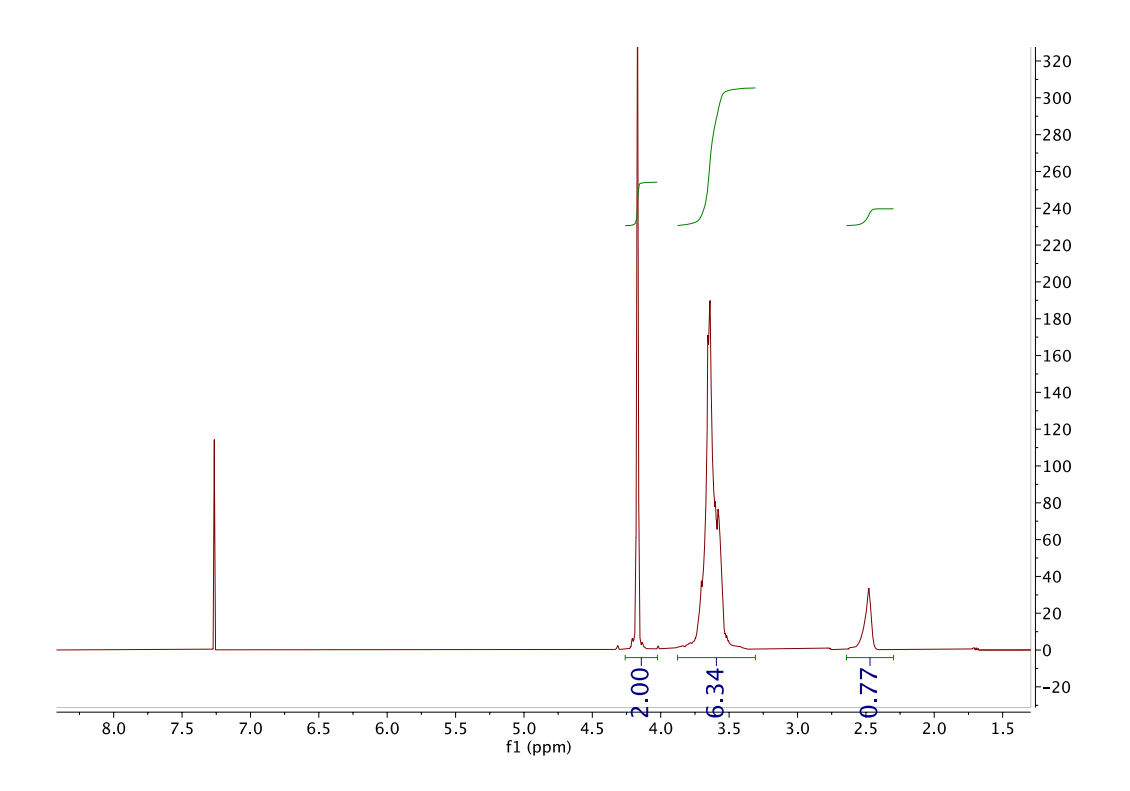


Figure 38: <sup>1</sup>H NMR of sample P(PGE-*stat*-ECH) showing peak integration used for calculating composition of PGE and ECH

# Number average molecular weight determination using end group analysis:

Opened <sup>1</sup>H NMR for a polymer using MNova software, first corrected the baseline and phase. Set the reference for residual signal of methylene dichloride-d2 to 5.32. Set integration for peak at  $\delta$  7.27 to 5 protons corresponding to aromatic benzyl protons from end group. We Choose NMR solvent methylene dichloride-d2, so that the peak corresponding to end group is not overlapping with residual solvent peak. Took integration of peak corresponding to peak emerging from polymer backbone at  $\delta$  3.85-3.4 (953.17). (As shown in Figure *39*)

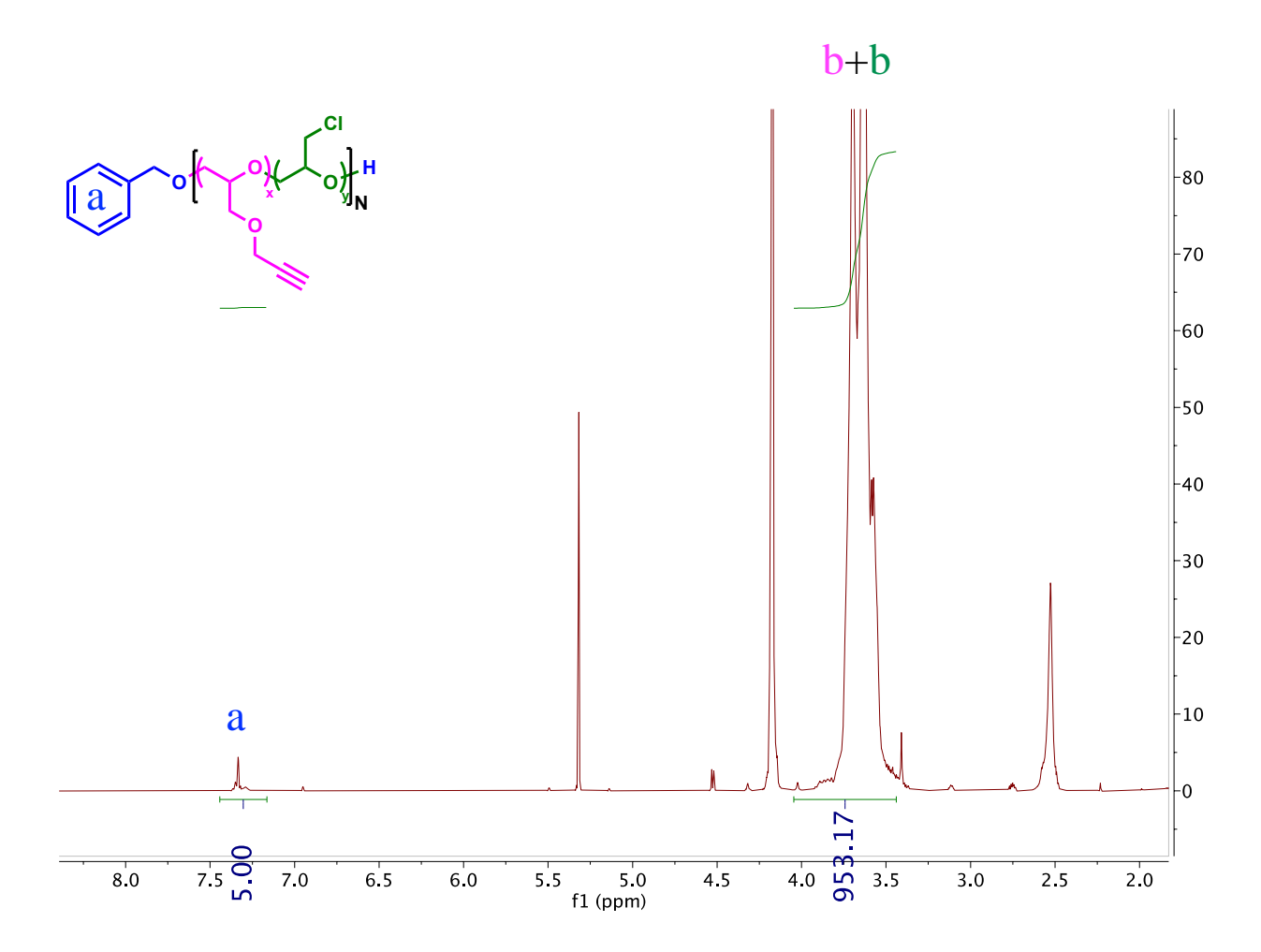


Figure 39: <sup>1</sup>H NMR of sample P(PGE-*stat*-ECH) showing peak integration used for end group analysis

 $\mathbf{M}_n = \text{Formula}$  weight for end groups + xN × PGE repeat unit molar mass

+ yN  $\times$  ECH repeat unit molar mass

Where, 
$$N = \frac{Polymer\ backbone\ integration}{5\ (\#\ of\ protons\ in\ backbone)} = \frac{953.17}{5} \approx 191\ repeat\ units$$

$$\rm M_n = 108 + 0.478 \times 191 \times 112 + 0.522 \times 191 \times 92 = 19506 \ g/mol$$

This is approximately equal to targeted molecular weight of 20000 g/mol.

# Chapter 3. Post polymerization modification to obtain tunable ioncontaining polyether using thiol click chemistry

#### 3.1 Introduction

In chapter 2 we synthesized polyethers using MOB initiators. These polyethers are low-cost and easily synthesized as showcased in earlier chapter. <sup>1-6</sup> Functional polyethers have importance in polymer field to achieve desired material properties. During polymerization epoxide ring opens to form a skeleton of polymer called as polymer backbone while functional groups on epoxide ring remains unreacted and are present as a pendent group. Different Physical and chemical properties of polyethers depends on both polymer backbone and pendent group functionality. For example, polyethylene glycol (PEG) has good water solubility compared to aliphatic polyethers (3 or more carbons in a repeat unit) due to hydrogen bonding capabilities from polar polymer backbone. To compare the effect of pendent group, PEG which is semicrystalline compared with PPO which is amorphous which shows that single methyl pendent group affects crystallinity of the resulting polyether.<sup>7</sup>

PEG based polymers are ubiquitous in our day-to-day life. These polyethers are used to facilitate drug delivery in medicines<sup>8,9</sup>, as emulsifier in cosmetics and surfactants as well as additive in food item. <sup>10</sup>PEG itself is neutral in nature but when modified with tuned functionality these can be used for advanced applications. <sup>11,12</sup> Charged polymers contains ionic groups as a part of their side chains. PEG modified with charged moieties have shown excellent performance properties highwater solubilities, hydrophilicity, excellent electrochemical properties for ion transport, biocompatibility, and surface functionality to enhance antifouling performance. The oxygens from polyether backbone can interact very well with Li ions and hence can be used as solid electrolytes. In Li ion batteries these benign polymers can substitute unsafe and flammable liquid electrolyte

without compromising efficiency of these energy storage devices. <sup>13,14</sup> Antifouling coatings of charged polyethers on the surface of membranes have shown promising results. Increasing surface charges increases the donnan potential and helps to reduce fouling tendency. <sup>15–18</sup> Due to these outstanding characteristics of charged polymer are often used for diverse application in drug delivery and biomaterials <sup>19–21</sup>, coatings <sup>22,23</sup>, ion exchange membranes <sup>24,25</sup> and energy storage devices <sup>26,27</sup>. This thesis research involves synthesis of charged polyethers and their advanced applications using facile post polymerization modifications of precursor polymers.

In this work we have modified polyether synthesized in chapter 2 to introduce charged moieties to obtain a tunable polymer platform. Various (co)polymers of allyl glycidyl ether (AGE), propargyl glycidyl ether (PGE) and epichlorohydrin (ECH) with functional alkene, alkyne, and chloromethyl groups respectively have been modified with the use of orthogonal chemistries. This platform allows for control over parameters such as molecular weight, charge density, monomer sequence, polymer architecture, and counter-ions independently through novel polymer synthesis. Pendent alkene, alkyne and Chloromethyl groups provides handle for post polymerization modification to achieve required material properties through composition control. Each of these groups brings unique characteristics which we will utilize to develop materials for specific application.

Sharpless and co-workers first developed powerful click chemistry reactions in 2001. This radical thiol click chemistry has been established as a versatile tool for the synthesis of functional lipids, peptides, dendrimers, hyperbranched polymers, and polymer networks since then. Pendant alkene or alkyne group can be modified using thiol click chemistry. Thiol—yne chemistry is the radical addition of two equivalents of thiol to a carbon—carbon triple bond. These reactions are superior to other methodologies because of few advantages such as facile synthetic access to both alkenes or alkynes and thiols as well as spatiotemporal control that can be achieved by using a radical

initiator. The high functional group tolerance of thiol-yne chemistry makes this methodology applicable to the synthesis of a wide range of functionalized polymers.<sup>28,29</sup>

Material properties are dependent on presence of different functional groups and its distribution across the polymer chain which we can tailor using charged polyethers to obtain desired characteristics and innovate better technologies in future.

# 3.2 Experimental section

#### 3.2.1 Materials

Precursor polymers (from chapter 2) were used after purification and drying as it is for further modification. Sodium 3-mercapto-1-propane sulfonate (Sigma-Aldrich), methyl imidazole (Sigma-Aldrich), cysteamine hydrochloride (Sigma-Aldrich) were all used as received. Chloroform-d (Cambridge Isotope Laboratories, Inc. 99.8%), deuterium oxide (Cambridge Isotope Laboratories, Inc. 99.9%) and dimethyl sulfoxide-d6 (Cambridge Isotope Laboratories, Inc. 99.5%) were used without any further purification as NMR solvents.

Glovebox was used to carry out all moisture and oxygen sensitive reactions under nitrogen environment. Reactions carried out in dimethyl sulfoxide (DMSO, Sigma-Aldrich ≥99.9%), and ethanol (KOPTEC 200 proof pure ethanol), acetonitrile (ACN), precipitated in ethyl acetate. Free radical initiator 2,2'-Azobis(2-methylpropionitrile) (AIBN, Sigma-Aldrich 98%) was used for polymer modification. Cellulose dialysis membrane (Slide-A-lyzer<sup>TM</sup> Fisher Scientific) with molecular weight cut off (MWCO) of 2k is used for dialysis.

#### 3.2.2 Instrumentation

<sup>1</sup>H NMR, <sup>13</sup>C NMR, and gradient correlation spectroscopy (gCOSY) was performed on Agilent DDR2 500 MHz NMR spectrometer using deuterated solvents at room temperature. The chemical

shifts are reported in parts per million (ppm) and are referenced using the residual <sup>1</sup>H peak from the deuterated solvent.

The gel permeation chromatography (GPC) was performed on the Malvern OMNISEC system with an isocratic pump, degasser, and temperature-controlled column oven operated at 35 °C containing 2 Viscotek 300×8.0 mm columns (T3000 and T4000) with an exclusion limit of 400 kDa. Triple detection with light scattering, viscometer, and refractive index has been used for determining absolute molecular weight of polymers. Calibration was carried out using polystyrene standards (from scientific polymer) in THF (Sigma-Aldrich 99.8%).

Differential scanning calorimetric (DSC) tests were carried out on a TA250 instrument with a heating rate of 10 °C min<sup>-1</sup> under a N<sub>2</sub> atmosphere, and the data from the second heating curve was used for further analysis.

Thermogravimetric Analysis (TGA) was performed using a TGA 500 (TA Instruments, USA). A sample (about 10 mg) was heated to 800 °C with a heating rate of 10 °C /min.

Fourier Transform Infrared (FT-IR) spectra were taken using Shimadzu IRAffinity-1 spectrometer equipped with MIRacle ATR attachment. The spectra were recorded between the wavelength on 500-4000 cm<sup>-1</sup> in absorption mode.

Electrophoretic mobility ( $\zeta$  potential) was measured using Laser doppler micro-electrophoresis with the help of instrument Zetasizer Nano ZS, Malvern. Zeta potential measurement of charged polyether was performed using 10 wt% of polymers in 10 mM KCl as a background electrolyte.

## 3.2.3 Methods

# $Synthesis\ of\ triis obutyla luminum\ adduct\ of (2-dimethylamino) ethoxy-diis obutyla luminum\ (MOB)$

1.0 M tri-isobutylaluminum in hexane (12.7 mL, 12.7mmol) was added to a reaction vial with magnetic stirrer and cooled to −78°C using liquid nitrogen blanket under dry nitrogen environment inside glovebox. To this vial a ligand dimethylaminoethanol (4.7 mmol, 0.5 mL) was added dropwise. The reaction was carried out by continuous stirring until it warms to room temperature overnight. Next day stopped stirring and cooled down the reaction mixture again to −40°C to crystallize the desired product. These crystals were then washed with anhydrous hexanes three times to remove excess reactant and dried under vacuum.

<sup>1</sup>H NMR (CDCl<sub>3</sub>, 500 MHz) δ 0.12 to -0.15 (m, -Al[-CH<sub>2</sub>-CH-(CH<sub>3</sub>)<sub>2</sub>]<sub>2</sub>, and m, -Al[-CH<sub>2</sub>-CH-(CH<sub>3</sub>)<sub>2</sub>]<sub>3</sub>), 0.92 (m, -Al[-CH<sub>2</sub>-CH-(C<u>H</u><sub>3</sub>)<sub>2</sub>]<sub>2</sub>, and m, -Al[-CH<sub>2</sub>-CH-(C<u>H</u><sub>3</sub>)<sub>2</sub>]<sub>3</sub>), 1.82 (m, -Al[-CH<sub>2</sub>-C<u>H</u>-(CH<sub>3</sub>)<sub>2</sub>]<sub>2</sub>, and m, -Al[-CH<sub>2</sub>-CH<sub>2</sub>-(CH<sub>3</sub>)<sub>2</sub>]<sub>3</sub>), 2.59 (s, N-(C<u>H</u><sub>3</sub>)<sub>2</sub>), 2.87 (t, N-C<u>H</u><sub>2</sub>-CH<sub>2</sub>-CH<sub>2</sub>-O), 3.97 (t, N-CH<sub>2</sub>-CH<sub>2</sub>-O) (Figure 40)

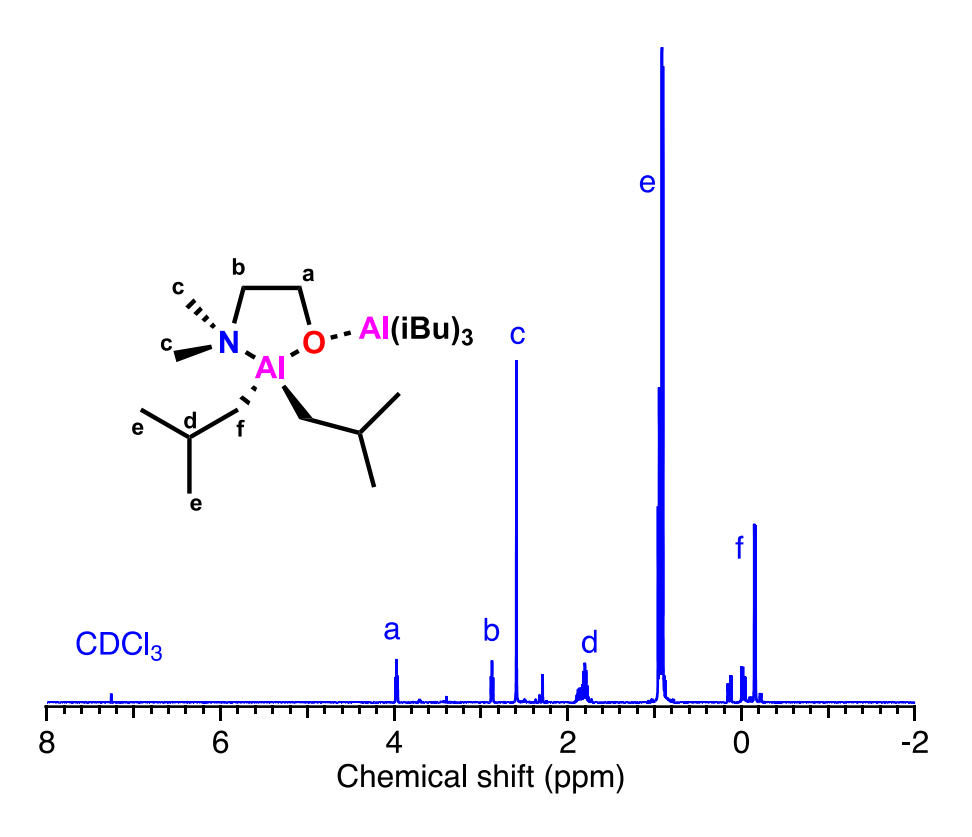


Figure 40: <sup>1</sup>H NMR of MOB in CDCl<sub>3</sub>

#### General procedure for polymerization using MOB system

All polymerizations were performed neat in a septum-capped 20mL reaction vial under inert atmosphere in glovebox. The vials were charged with a stir bar, a monomer(s) and MOB to prepare 2 gm of final polymer weight. MOB quantity was decided depending on targeted molecular weight. The solutions were then heated to the final reaction temperature (50-60 °C, dependent on monomer) and polymerizations were carried out for 48 hours-5 days (until its >90% polymerized). (Figure 41) Reactions were quenched with methanol and dissolved in dichloromethane to remove aluminum. The resulting solution was added dropwise into hexane to precipitate out the desired polymer product. The supernatant was removed, and then again washed the polymer with hexane (or any poor solvent) three times to remove residual catalyst. The polymer was first dried using rotary evaporator and then kept under vacuum overnight to remove excess solvent. Mn was determined using GPC with triple detection system.

Figure 41: General scheme for polymerization of epoxides

#### **Polyanion synthesis:**

Sodium 3-mercapto-1-propane sulfonate (3 equiv for poly(allyl glycidyl ether) PAGE or 5 equiv) was added to a vial containing or poly(propargyl glycidyl ether) (PPGE) (1 equiv alkene or alkyne unit) or poly(propargyl glycidyl ether-stat-epichlorohydrin) P(PGE-stat-ECH) and 2,2'-Azobis(2-methylpropionitrile) (AIBN; 2 wt%) in DMSO solvent. The contents of the vial were degassed with  $N_2$  for 10 min. The mixture was then stirred and heated to 80 °C for 12 hours. (Figure 42, Figure 50 and Figure 58) The mixture was precipitated in ethyl acetate. The reaction mixture was diluted and extensively dialyzed against water. Dialysis is carried out using snakeskin tubing (MWCO = 2 kg/mol, eight cycles) against 3 L of water. Dialyzed solution was then dried in oven to obtain final purified product.

## **Polycation synthesis using cysteamine hydrochloride:**

Cysteamine hydrochloride (3 equiv for poly(allyl glycidyl ether) PAGE or 5 equiv) was added to a vial containing PPGE (1 equiv alkyne unit) or P(PGE-stat-ECH) and 2,2'-Azobis(2-methylpropionitrile) (AIBN; 2 wt%) in DMSO solvent. The contents of the vial were degassed with  $N_2$  for 10 min. The mixture was then stirred and heated to 80 °C for 12 hours. (Figure 67) The mixture was precipitated in ethyl acetate. The reaction mixture was diluted and extensively dialyzed against water. Dialysis is carried out using snakeskin tubing (MWCO = 3.5 kg/mol, eight cycles) against 3 L of water. Dialyzed solution was then dried in oven to obtain final purified product.

#### Polycation synthesis using methyl imidazole attachment:

To modify chloromethyl pendent group on P(PGE-*stat*-ECH) we reacted it with methyl imidazole. Methyl imidazole (3 equiv) was added to a vial containing P(PGE-*stat*-ECH) (1 equiv -Cl) and 2,2'-Azobis(2-methylpropionitrile) (AIBN; 2 wt%) in ACN solvent. The contents of the vial were degassed with N<sub>2</sub> for 10 min. The mixture was then stirred and heated to 80 °C for 12 hours. (Figure 65) The mixture was precipitated in water. The reaction mixture was diluted and extensively dialyzed against water. Dialysis is carried out using snakeskin tubing against 3 L of water. Dialyzed solution was then dried in oven to obtain final purified product.

## 3.3 Result and discussion

Radical thiol click chemistry has been established as a versatile tool for the synthesis of functional polymers. We used this facile chemistry to modify pendant alkene or alkyne groups. These reactions are superior to other methodologies because its highly efficient with spatiotemporal control. We can obtain precisely tailored multifunctional structures with high product yields for versatile functionality. In addition, it is regiospecific and easy to perform.

Thiol click chemistry has been widely used to functionalize polymers due to several advantages such as high yeilds, fast reaction kinetics, simple purification requirements. We first carried out these click reactions on homopolymers to test it out and then applied it to copolymers P(PGE-*stat*-ECH) which is crucial in developing multifunctional polyethers.

#### 3.3.1 Thiol-ene click chemistry reaction using PAGE

Reaction scheme for modification of PAGE using thiol-ene click chemistry to obtain polyanion and polycations is shown in Figure 42. <sup>1</sup>H NMR of PAGE and modified PAGE is shown in Figure 43 and Figure 44.

After reaction, NMR shows no peaks in the alkene region which indicates 100% conversion in click reaction. To further confirm the addition of thiol we performed gradient correlation spectroscopy (gCOSY) was performed for polyanion. This Figure 45 shows <sup>1</sup>H-<sup>1</sup>H correlation spectrum. A cross peak will be observed for protons that have 3-bond scalar coupling. For protons c and e cross peak indicates existence of C—S bond formation.

Figure 42: Reaction scheme for thiol-ene click reaction

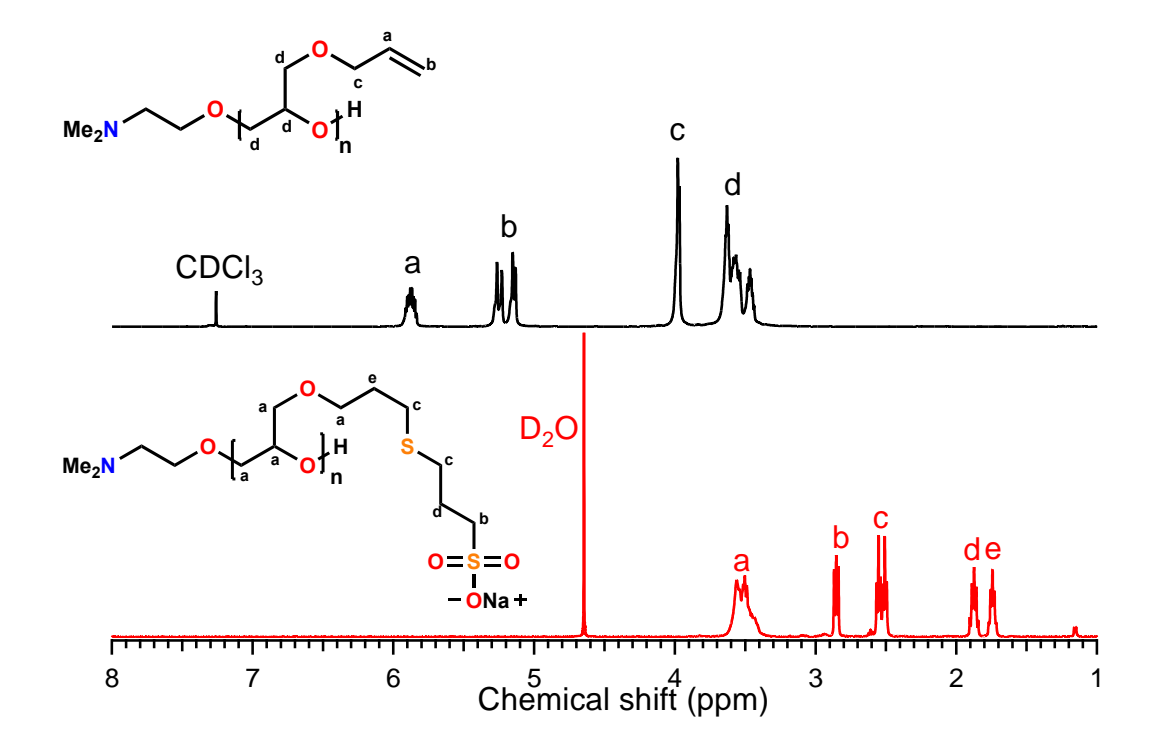


Figure 43: <sup>1</sup>H NMR of PAGE in (CDCl<sub>3</sub>) and polyanionic modified PAGE in (D<sub>2</sub>O)

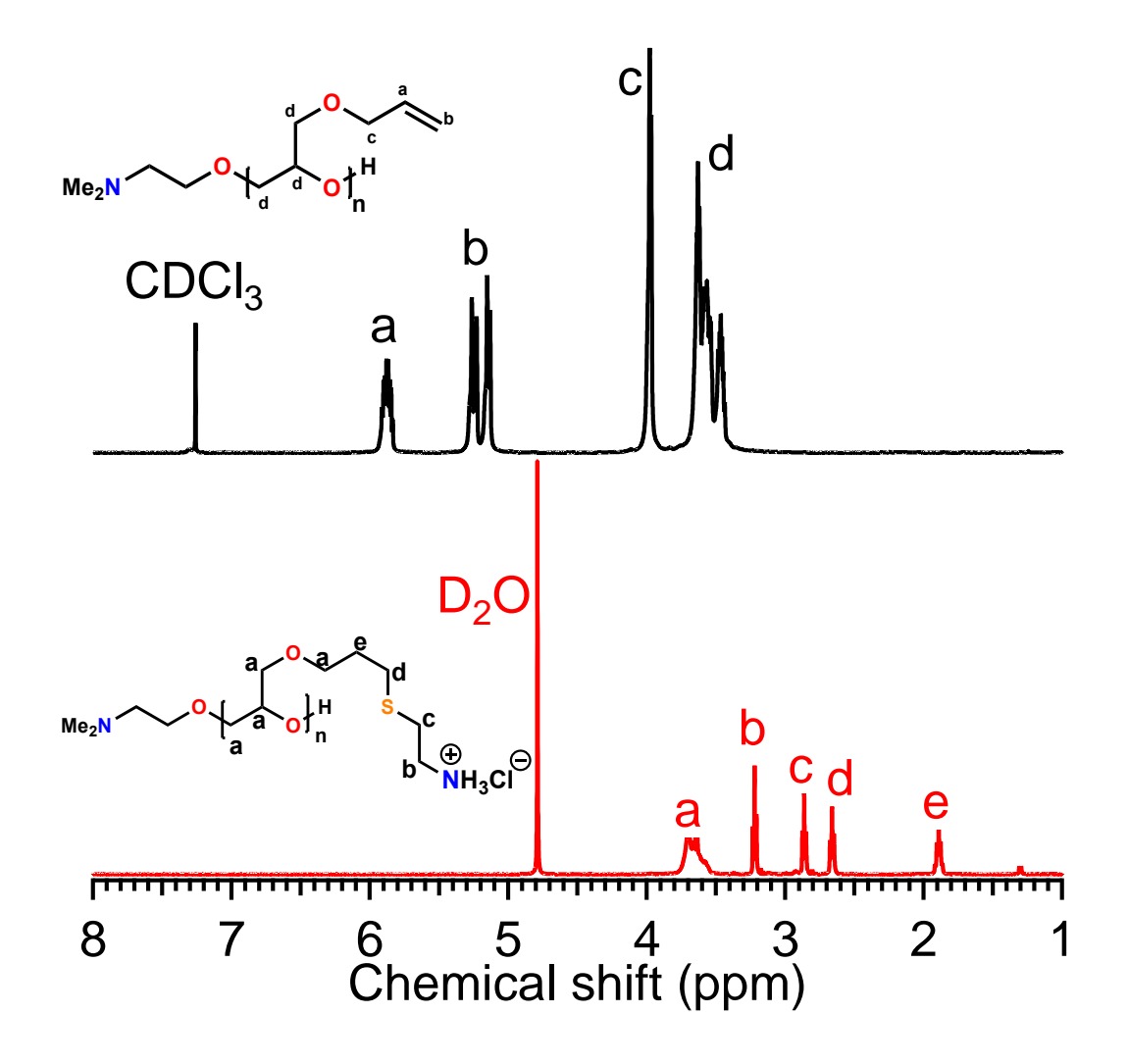


Figure 44: <sup>1</sup>H NMR of PAGE in (CDCl<sub>3</sub>) and polycationic modified PAGE in (D<sub>2</sub>O)

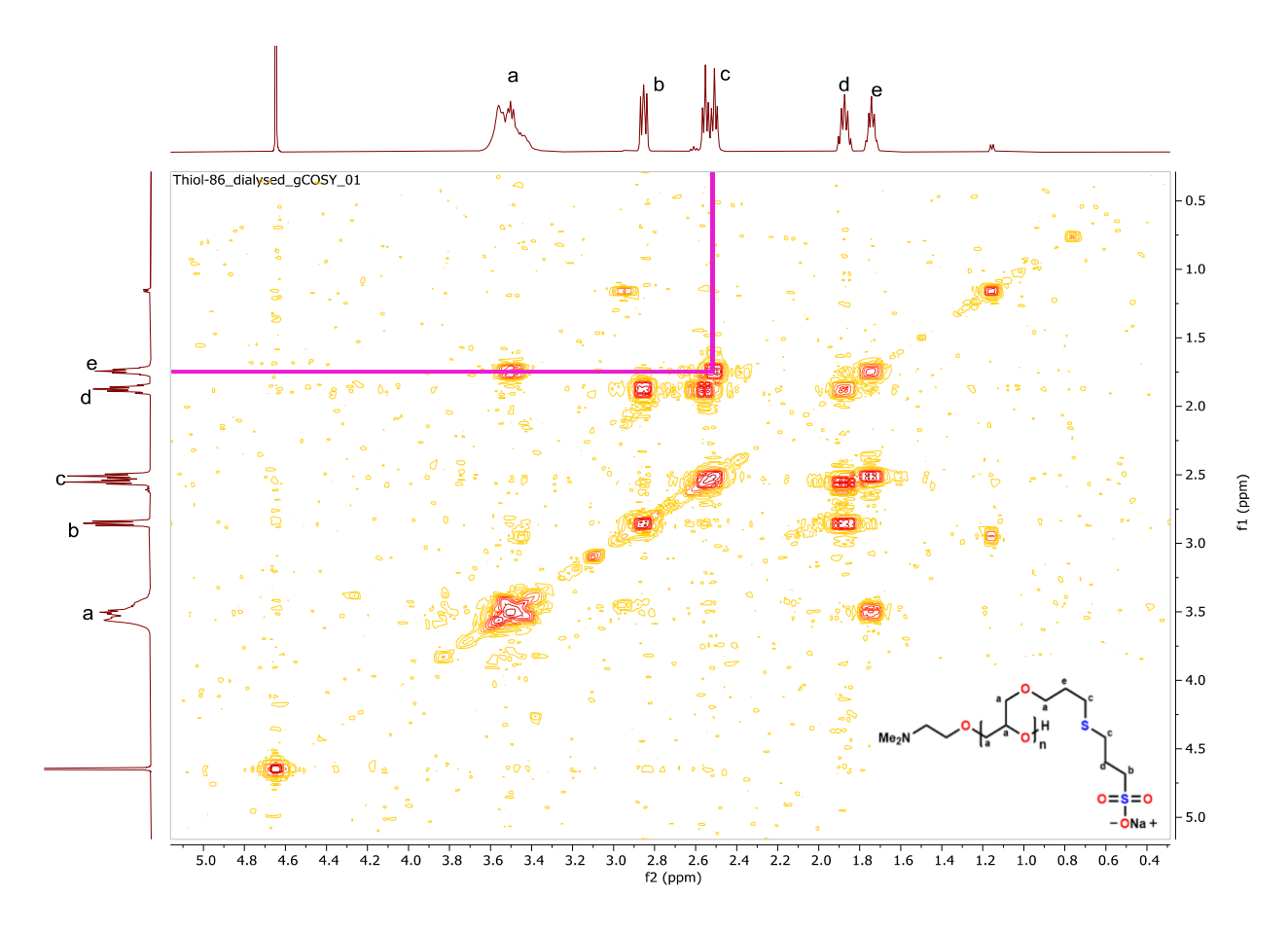


Figure 45: gCOSY of purified anionic thiol clicked PAGE

Thiol-ene click chemistry is well understood and can be explained using mechanism shown in Figure 46. From a thiol molecule thiyl radical gets generated by initiator activated by either heat or light. It adds to the alkene, generating a sp<sup>3</sup> carbon-centered radical in a propagation step. This radical then abstracts a hydrogen atom from another thiol to form the thioether product and regenerates a thiyl radical that propagates a further cycle which is a chain transfer step. Electron-rich alkenes have the highest radical addition rates, while the rate of hydrogen abstraction is limited by the stability of the carbon centered radical. Advantages of this reaction over other methodologies include facile synthetic access to both alkenes and thiols as well as spatiotemporal control that can be achieved by using a radical initiator.<sup>28</sup>

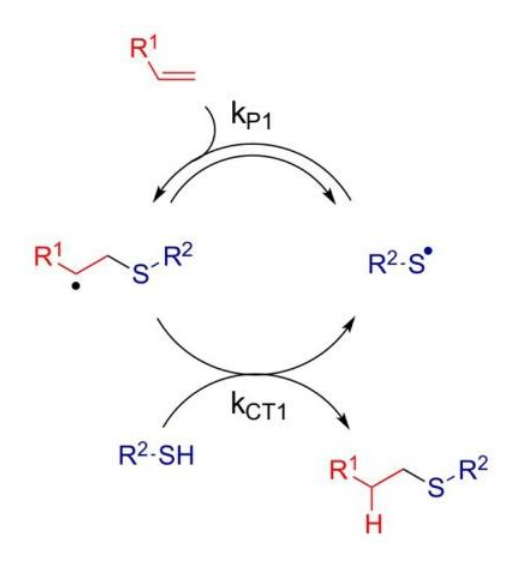


Figure 46: Mechanism of thiol-ene click reaction

#### 3.3.1.1 Result and discussion

Characterization of the PAGE and polyanionic thiol clicked PAGE was done using Differential Scanning Calorimetry (DSC), Gel Permeation Chromatography (GPC), Fourier Transform Infrared spectroscopy (FT-IR), and zeta potential analyzer. DSC plot shows  $T_g = -78$ °C for PAGE. After reaction  $T_g$  was found out to be disappearing from -78 °C.  $T_g$  value of thiol clicked PAGE is expected to increase, because of the aggregate formation due to ionomers and the increased polarity of the sulfone containing side chains. The higher oxidation state of the sulfur atoms induces a stronger dipolar association of the chains and a reduction of the segmental mobility with a consequent increase in the  $T_g$  value.<sup>33</sup> But no well-defined peak was observed for the clicked sample in thermogram obtained from DSC. (Figure 47) As seen in Figure 69 B modified polymer has turned glassy in nature at room temperature after the reaction.

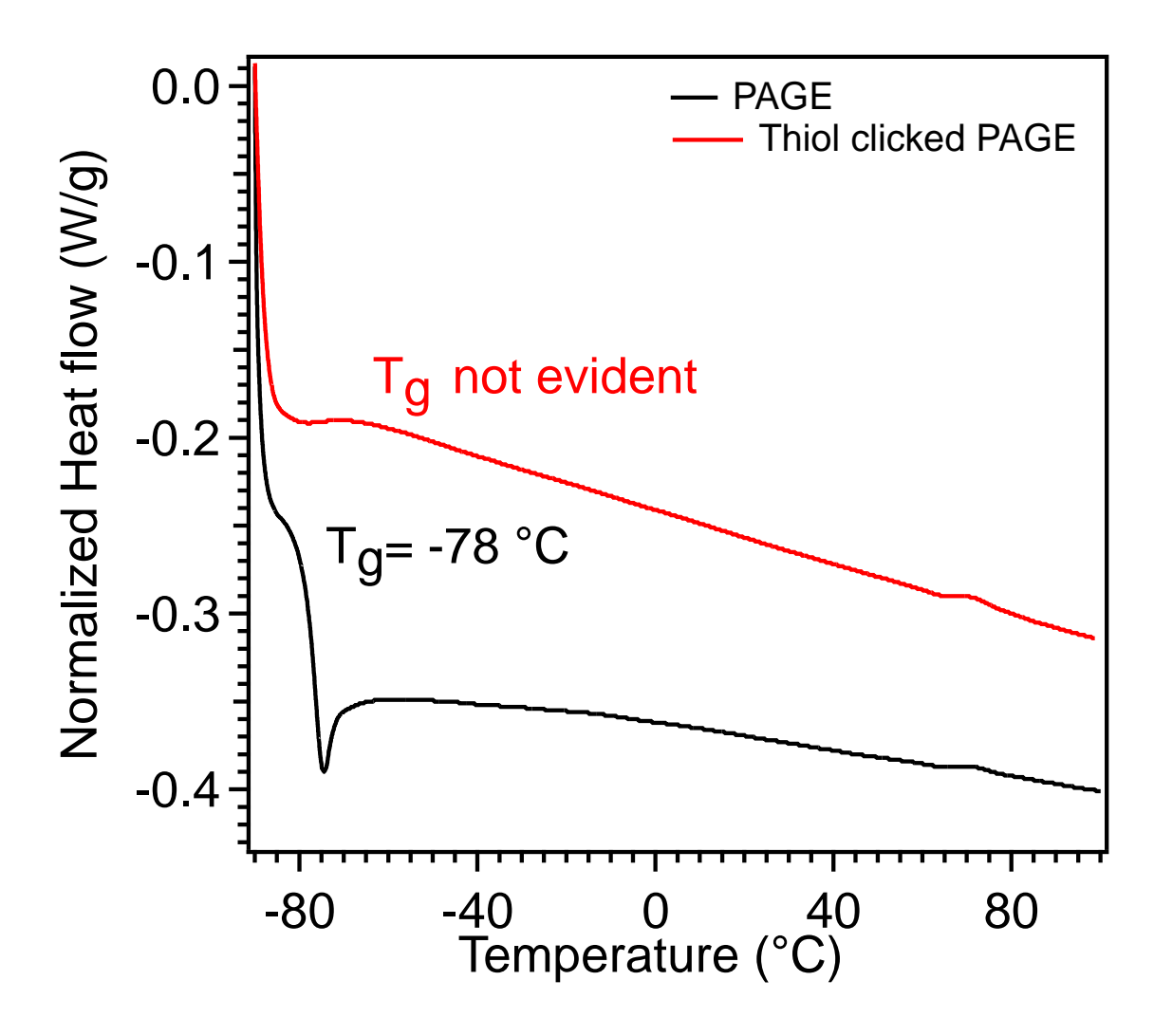


Figure 47: DSC plot for PAGE and thiol clicked PAGE

GPC trace using RI detector for PAGE is given in the appendix. (Figure 70) The  $M_n$  and D was determined to be 40.7 kg/mol and 1.26. After reaction compound is not soluble in THF so  $M_n$  could not be determined using GPC.

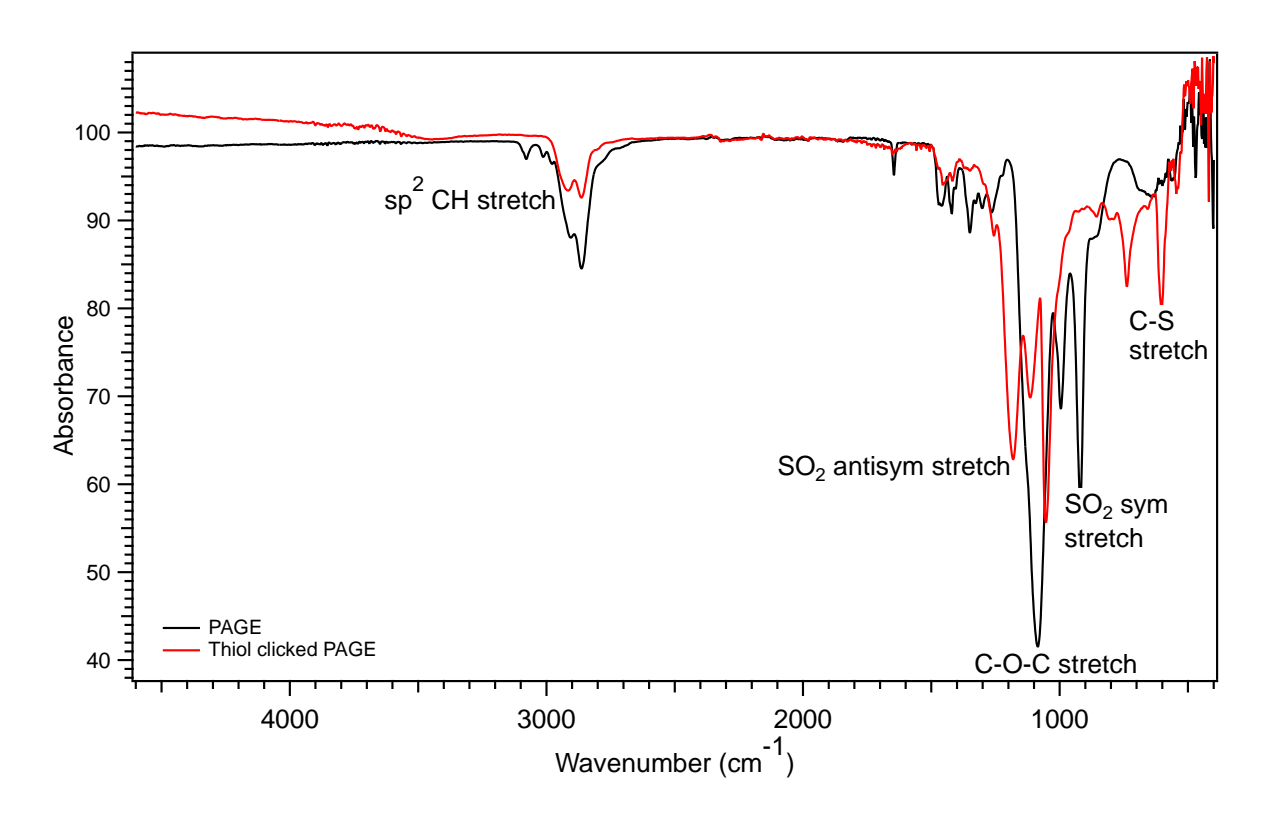


Figure 48: FT-IR spectra of PAGE and thiol-clicked PAGE

As seen in Figure 48 FT-IR of PAGE and thiol clicked PAGE has been compared. After reaction peak corresponds to sp<sup>2</sup> CH stretch around 3100 cm<sup>-1</sup> is disappearing indicating all alkene bonds have been clicked. In addition, peaks corresponding to SO<sub>2</sub> symmetric and antisymmetric stretch is appearing around wavenumbers 1050 cm<sup>-1</sup> and 1200 cm<sup>-1</sup> respectively. Along with C—S stretch at 610 cm<sup>-1</sup> which shows that thiol has been added successfully to the side chain.

The thermal degradation of precursor as well as modified polymer was studied using TGA. For this analysis, a sample (approximately 10 mg) was heated to 600 °C at a heating rate of 10°C/min under N<sub>2</sub> environment. The TGA plot in Figure 49 shows two step weight loss for the PAGE. The first step weight loss is observed around 300-350 °C and is due to cleavage of C-O, C-C and C=C from pendent polymer chain whereas the second step weight loss beyond 350 °C is due to the degradation of polymer backbone. For thiol modified polymer we observed a three-step weight loss. The first step weight loss occurs at 100-240 °C due to the solvent or moisture trapped whereas

second and third step weight loss between beyond 300 °C is attributed to the degradation of pendent functional groups attached to the polymer such as -SO<sub>3</sub>H, C-O, and C-C and polymer backbone degradation. The residual weight for is 50% whereas for the unmodified PAGE it is close to 0 %. The remaining mass percent thiol clicked PAGE due to the organic network formed through the thiol click free radical reaction and due to residual reactants.

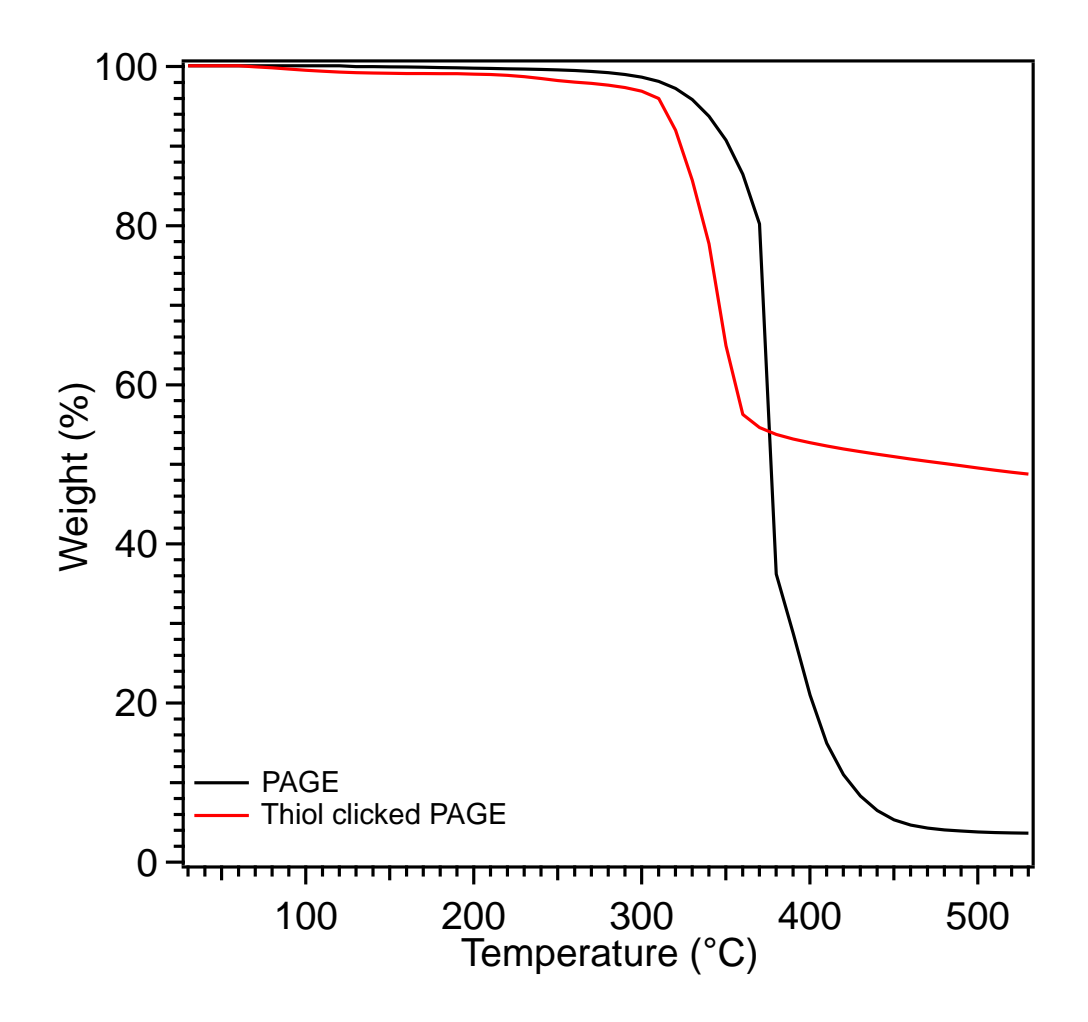


Figure 49: TGA plot for PAGE and modified PAGE

# 3.3.2 Thiol-yne click chemistry reaction using PPGE

Now using thiol click chemistry for alkyne functional polyether which is PPGE we can significantly increase functionalities on side chains. This will be crucial in obtaining control over

charge densities of modified polymers. Reaction scheme for modification of PPGE using thiolyne click chemistry to obtain polyanion is shown in Figure 50.

Figure 50: Reaction scheme of thiol-yne click chemistry

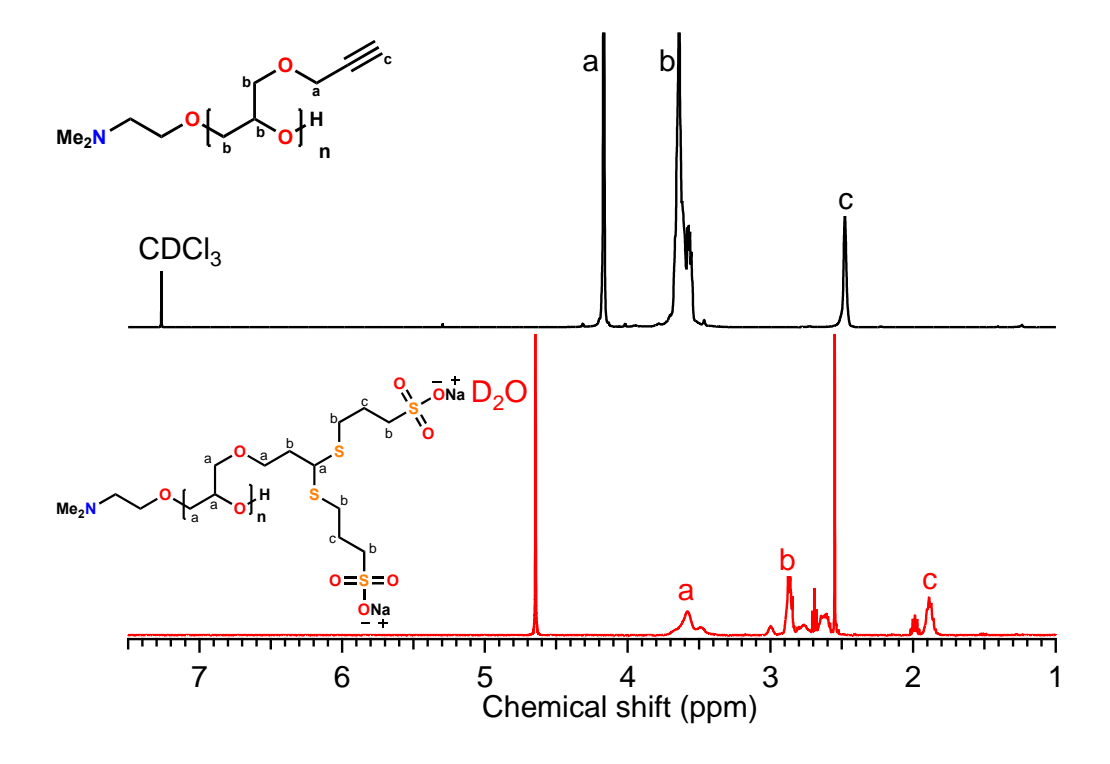


Figure 51: <sup>1</sup>H spectra of PPGE and thiol-clicked PPGE

Figure 51 shows the NMR of PPGE and clicked PPGE. Peak corresponding to alkyne proton has completely disappeared showing 100% conversion into clicked polymer.

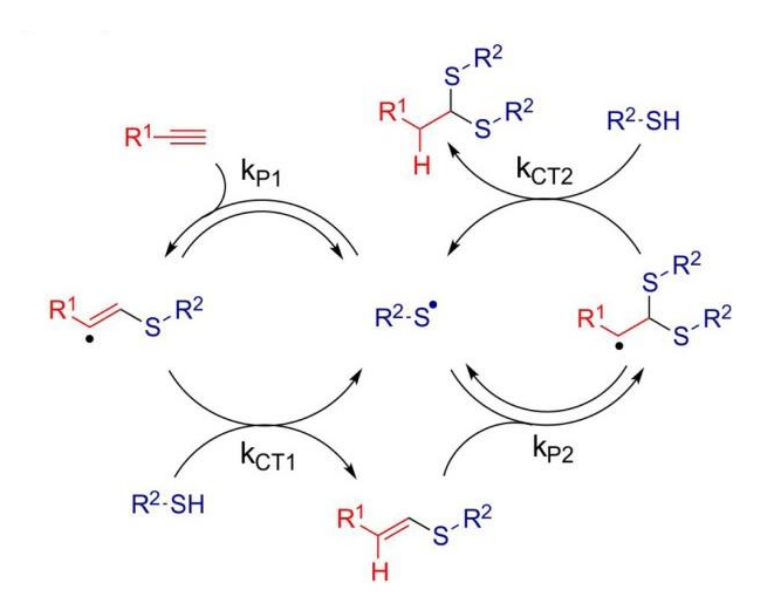


Figure 52: Mechanism of thiol-yne click reaction

Thiol-yne click chemistry follows the identical propagation and chain transfer steps as the thiolene reaction. (Figure 52) The first addition of the thiol to the alkyne forms a vinyl sulfide intermediate that can then react with another thiol to form the bis-adduct. In both reactions, the addition of the thiyl radical is reversible, whereas the hydrogen abstraction is irreversible.

#### 3.3.2.1 Result and discussion

Characterization of the PPGE and polyanionic thiol clicked PPGE was done using Differential Scanning Calorimetry (DSC), Gel Permeation Chromatography (GPC), Fourier Transform Infrared spectroscopy (FT-IR), and zeta potential analyzer. DSC plot shows  $T_g = -36$  °C for PPGE which is consistent with literature value.<sup>30</sup> After reaction  $T_g$  was found out to be increased to 70 °C. This is not a sharp transition as observed in thermogram.  $T_g$  value of thiol clicked PPGE is about 106 °C higher, as a result of the increased polarity of the sulfone containing side chains and ionomer aggregate formation. The higher oxidation state of the sulfur atoms induces a stronger dipolar association of the chains and a reduction of the segmental mobility with a consequent increase in the  $T_g$  value. (Figure 53)

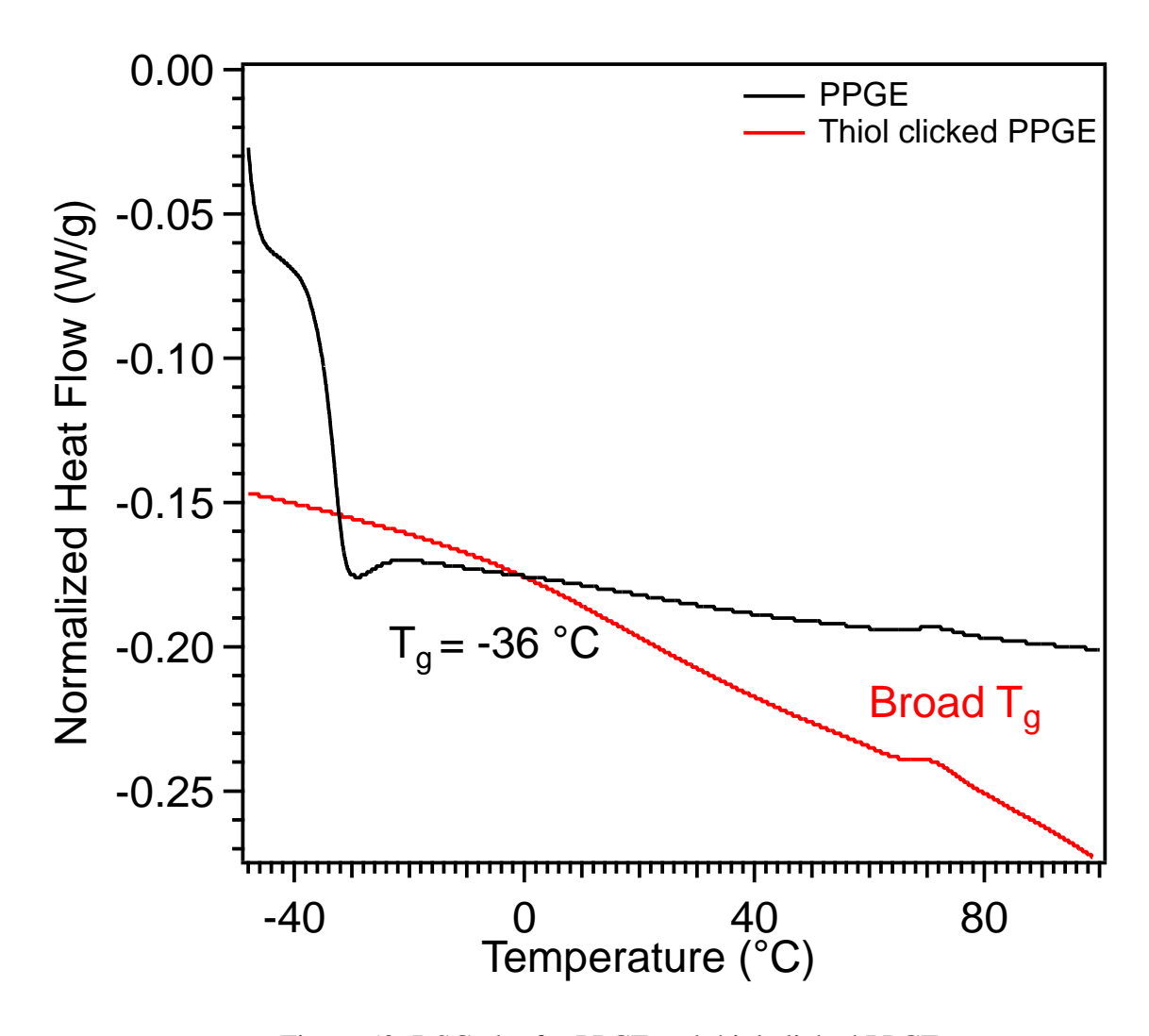


Figure 53: DSC plot for PPGE and thiol clicked PPGE

GPC using RI detector for PPGE is given in the Figure 70. The  $M_n$  and D was determined to be 23 kg/mol and 1.46. After reaction compound is not soluble in THF so  $M_n$  could not be determined using GPC.

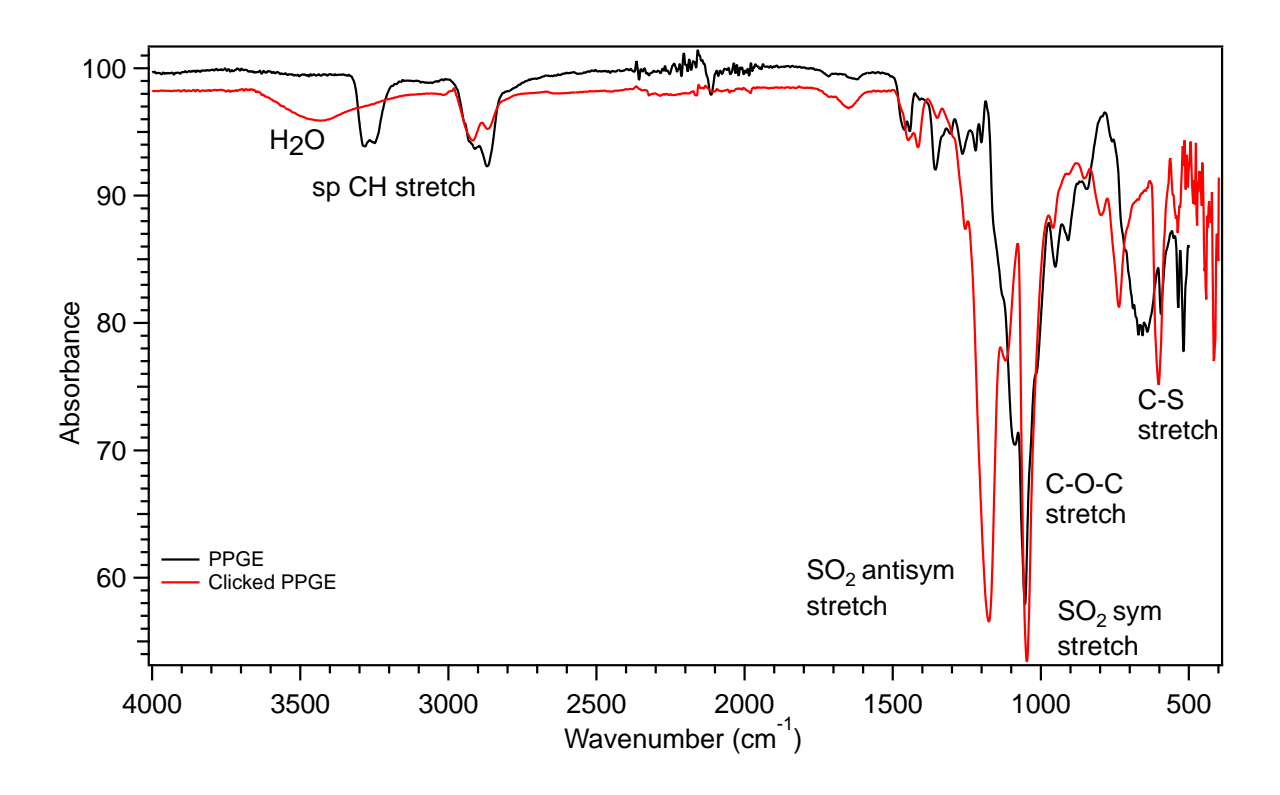


Figure 54: FTIR spectra for PPGE and thiol clicked PPGE

As seen in Figure 54, FT-IR of PPGE and thiol clicked PPGE has been compared. After reaction peak corresponds to sp CH stretch at 3250 cm<sup>-1</sup> is disappearing indicating all alkyne bonds have been clicked. In addition, peaks corresponding to SO<sub>2</sub> symmetric and antisymmetric stretch is appearing at 1050 cm<sup>-1</sup> and 1200 cm<sup>-1</sup> respectively along with C—S stretch at 650 cm<sup>-1</sup> which shows that thiol has been added successfully to the side chain. As a result of charged group purified product is hygroscopic in nature. Peak around 3500 cm<sup>-1</sup> shows presence of water in the purified polymer.

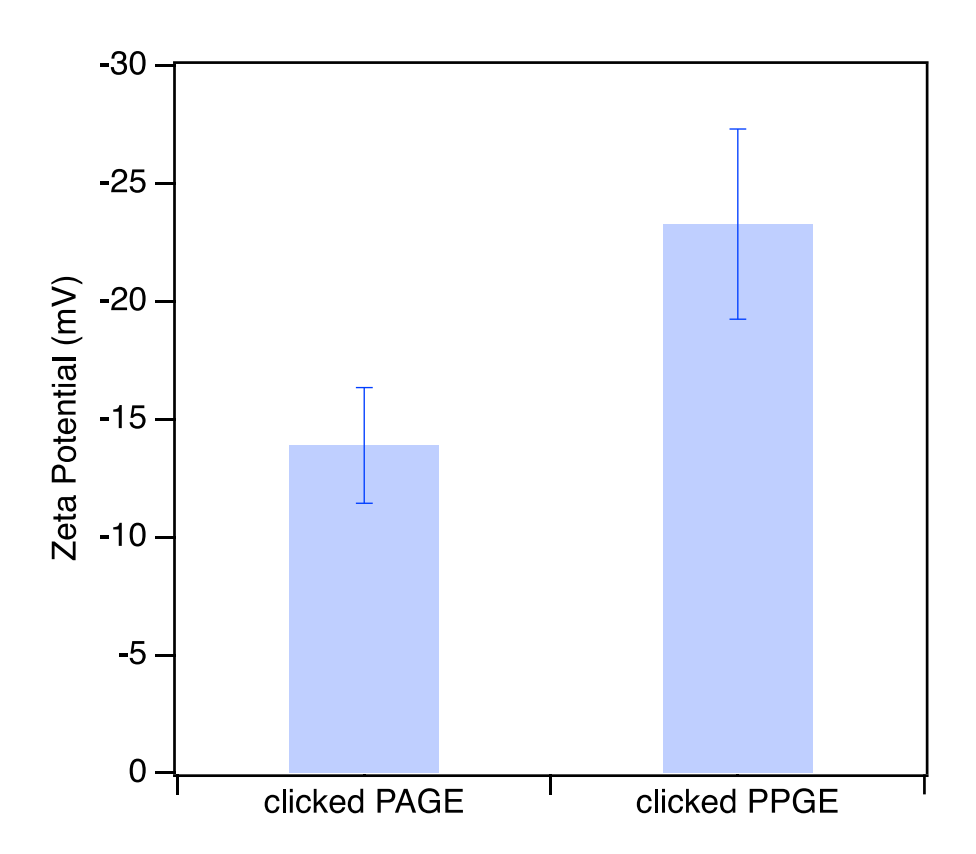


Figure 55: Zeta potential comparison for clicked PAGE and PPGE

Zeta potential measurement of clicked PAGE and PPGE was performed using 10 wt% of polymers in 10 mM KCl as a background electrolyte. For PAGE it was found out to be -13.89±2.45 mV and for PPGE -23.27±4.03 mV. (Figure 55)

As two charged groups have been clicked for PPGE it was expected to have higher zeta potential. As the molecular weights for PAGE and PPGE are different, number of repeat units and hence charged groups is different. If we consider zeta potential per repeat units it is found out to be 0.0389 mV/repeat unit for PAGE and 0.1133 mV/repeat unit for PPGE which is considerably larger than PAGE clicked polymer. Hence with thiol-yne click chemistry we can achieve highly negatively charged coating. We can control number of alkyne repeat units using copolymer of PGE and spacer monomer.

The thermal degradation of precursor as well as modified polymer was studied using TGA. For this analysis, a sample (approximately 10 mg) was heated to 600 °C at a heating rate of 10°C/min under  $N_2$  environment. The TGA shows two step weight loss for the PPGE. (Figure 56) The first step weight loss is observed around 300-350 °C and is due to cleavage of C-O, C-C and C $\equiv$ C from pendent polymer chain whereas the second step weight loss beyond 350 °C is due to the degradation of polymer backbone. For thiol modified polymer we observed a three-step weight loss. The first step weight loss occurs at 100-240 °C due to the solvent or moisture trapped whereas second and third step weight loss between beyond 300 °C is attributed to the degradation of pendent functional groups attached to the polymer such as -SO<sub>3</sub>H, C-O, and C-C and polymer backbone degradation. The residual weight for is 50% whereas for the unmodified PPGE it is close to 30 %. The remaining mass percent thiol clicked PPGE due to the organic network formed through the thiol click free radical reaction and due to residual reactants.

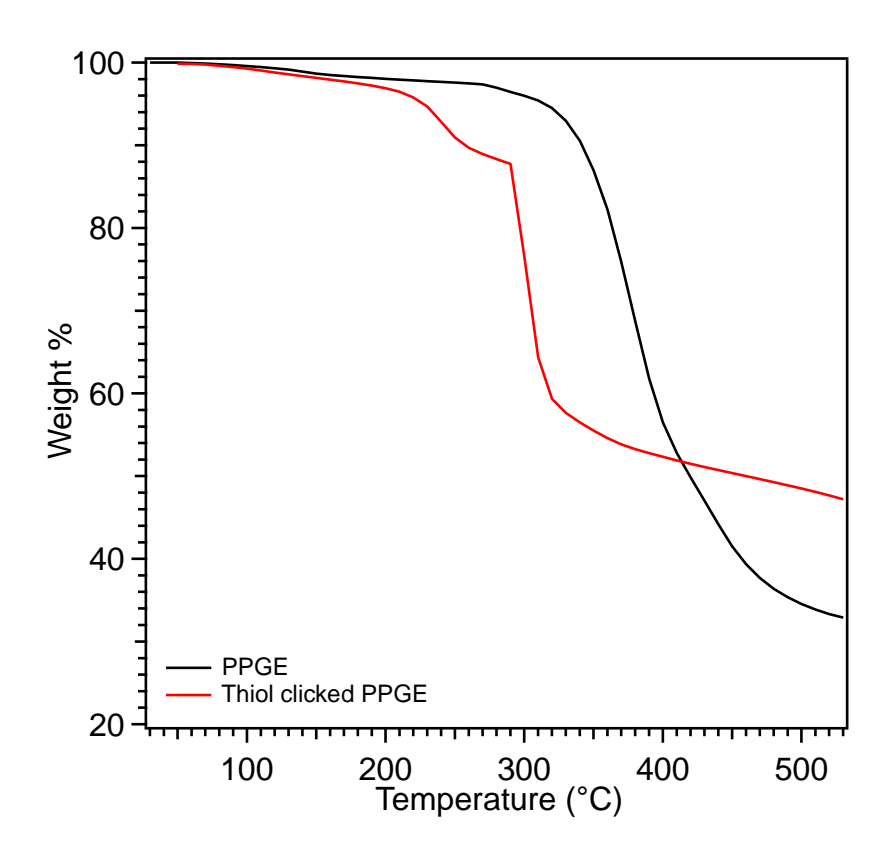


Figure 56: TGA plot for PPGE and modified PPGE

3.3.3 Thiol click chemistry on P(PGE-*stat*-ECH) to obtain control over charge densities Now that thiol click chemistry was successful in modifying homopolymers PAGE and PPGE we wanted to demonstrate control over composition and charge densities and eventually material properties with the help of copolymer modification methodology. To achieve that we performed radical click chemistry using P(PGE-stat-ECH) using charged thiols. The reaction scheme for precursor and modification with sulfonate charged groups S-P(PGE-stat-ECH) are shown in Figure 57 and Figure 58. Thiol-yne reaction conditions used were same as discussed in 3.3.2. Click reaction was successfully performed on various composition and molecular weights of polymer. Here representative results have been presented for 50-50 mol% PGE-ECH copolymer with  $M_n = 20$  kg/mol.

The copolymer was characterized by <sup>1</sup>H and <sup>13</sup>C NMR spectroscopy, revealing spectroscopic peaks consistent with a statistical copolymer structure, as can be seen in Figure 59 A & B respectively. In proton NMR peak corresponding to alkyne proton at 2.54 has disappeared indicating addition of thiol to alkyne end successfully. (Figure 60)

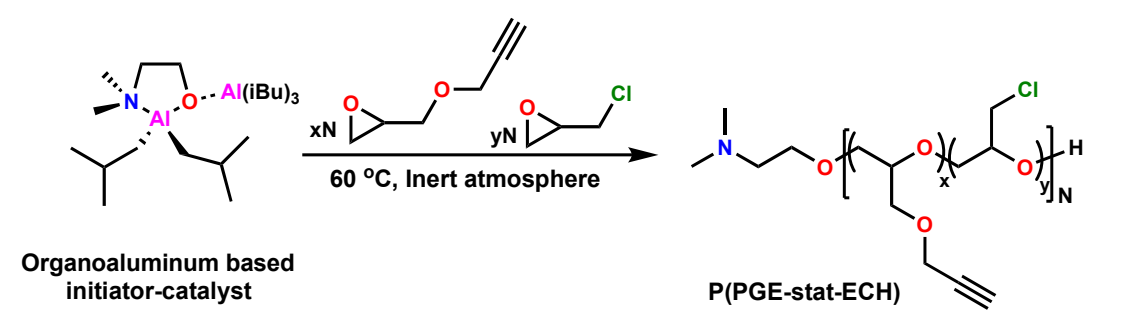


Figure 57: Reaction scheme of precursor P(PGE-stat-ECH) synthesis

Figure 58: Reaction scheme for polyanion synthesis using P(PGE-stat-ECH)

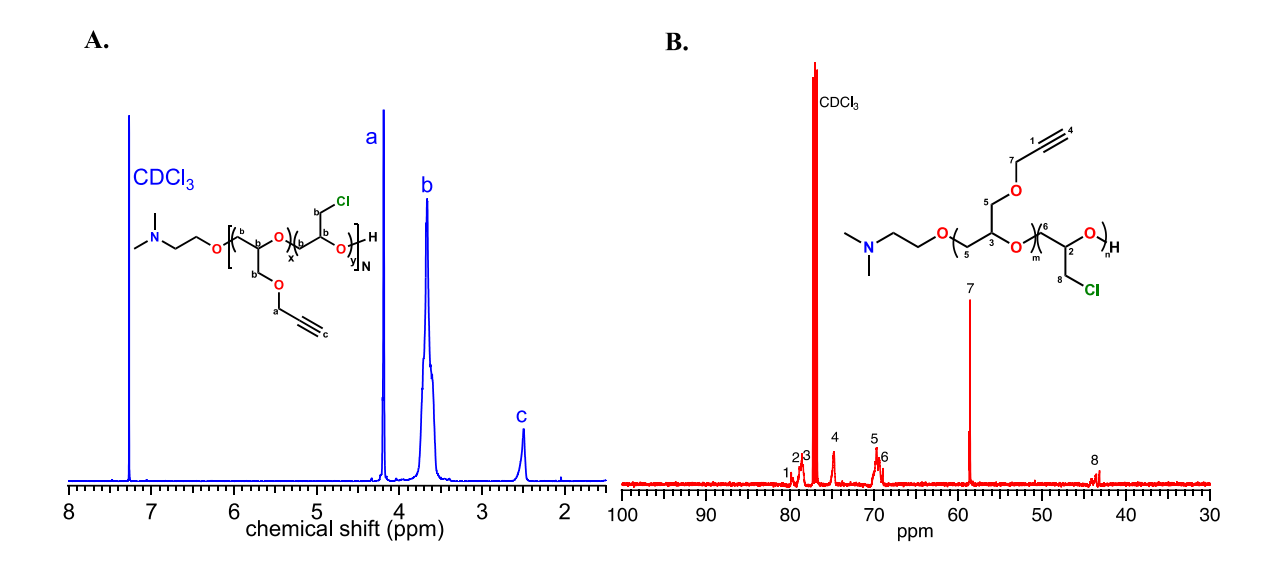


Figure 59: <sup>1</sup>H and <sup>13</sup>C NMR spectra of P(PGE-stat-ECH)

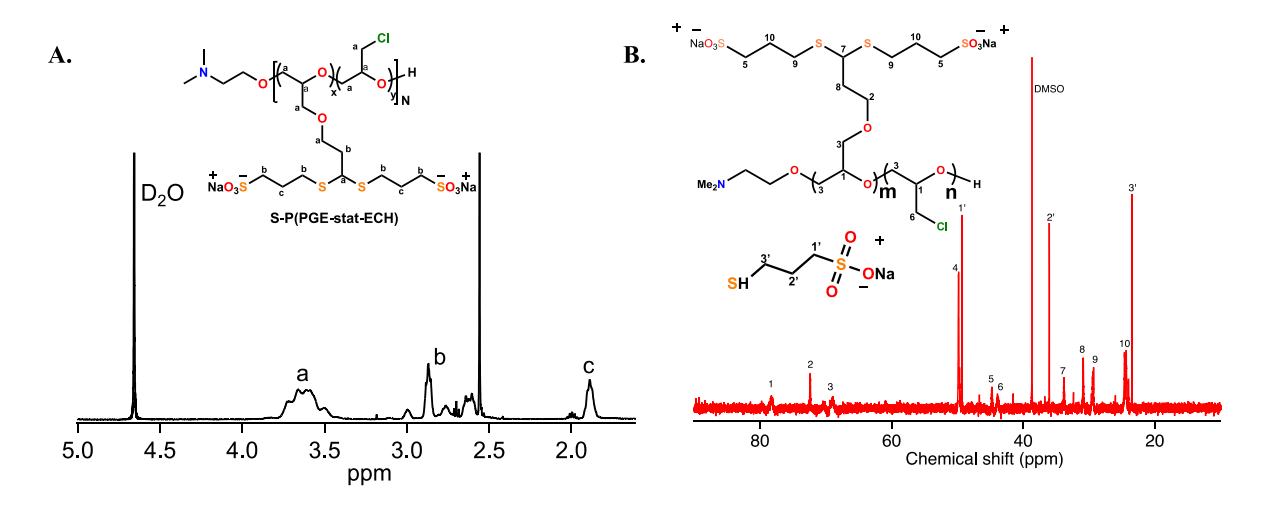


Figure 60: A. <sup>1</sup>H and B. <sup>13</sup>C NMR spectra of S-P(PGE-stat-ECH)

From analysis of the NMR spectrum, the ratio of ECH to PGE was determined to be 50-50%, which is consistent with anticipated ratio. (Sample calculation in chapter 2)

# 3.3.3.1 Result and discussion

FT-IR spectra of P(PGE-*stat*-ECH) and thiol clicked copolymer was taken. (Figure 61) After reaction peak corresponds to sp CH stretch at 3300 cm<sup>-1</sup> is disappearing indicating all alkyne bonds have been clicked. In addition, peaks corresponding to SO<sub>2</sub> symmetric and antisymmetric stretch is appearing at 3050 cm<sup>-1</sup> and 3200 cm<sup>-1</sup> which shows that thiol has been added successfully to the

side chain. Peak around 3500 cm<sup>-1</sup> shows traces of water as purified product was obtained after dialysis using water. C-Cl stretching band is still present at 750 cm<sup>-1</sup> for S-P(PGE-stat-ECH) which confirms orthogonal nature of click chemistry reactions where only alkyne group modifies leaving chloromethyl function group unaltered. This chloromethyl group can be used to introduce further functionality (Will be demonstrated in chapter 4).

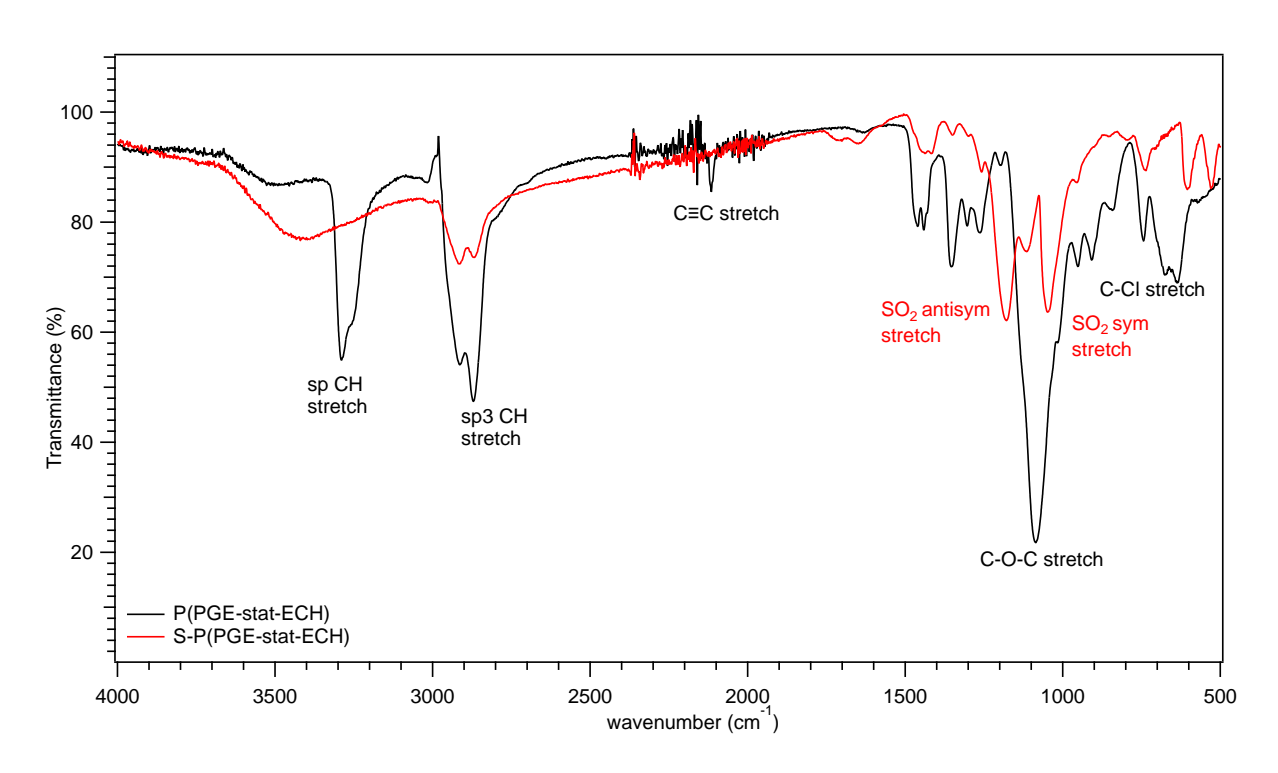


Figure 61: FTIR spectra of P(PGE-stat-ECH) and S- P(PGE-stat-ECH)

The precursor copolymer was further characterized by size-exclusion chromatography (SEC) in THF with triple detection, revealing a molecular weight of 25.5 kg/mol and D = 1.43, which is consistent with the targeted molecular weight of 20 kg/mol. (Figure 62) The relatively high polydispersity is likely due to the difficult ring opening polymerization of the two epoxides. After reaction product is insoluble in THF hence SEC couldn't be performed for modified polymers.

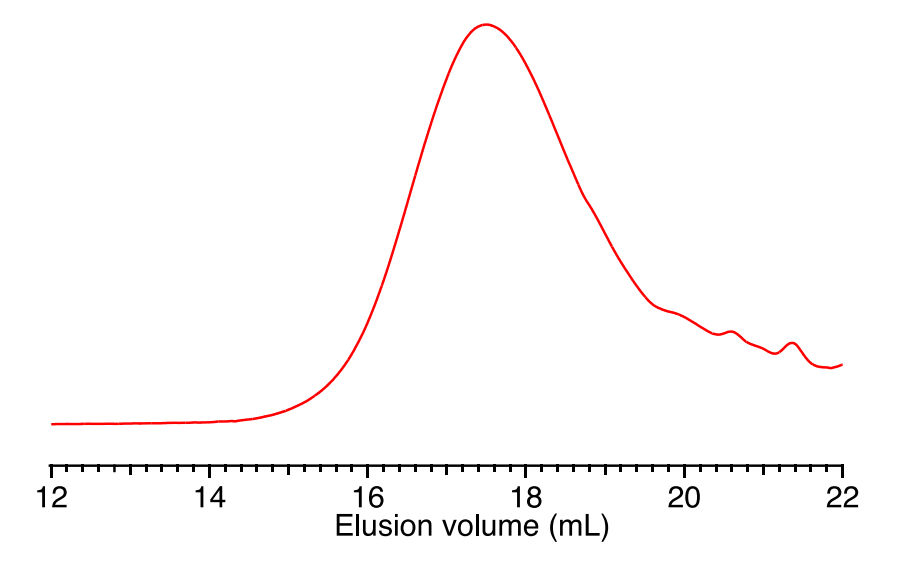


Figure 62: GPC trace of P(PGE-stat-ECH) revealing a molecular weight of 25.5 kg/mol and  $\Phi = 1.43$ 

The thermal properties of the modified polymer and P(PGE-stat-ECH) were characterized with differential scanning calorimetry (DSC) and thermogravimetric analysis (TGA), as shown in Figure 63 and Figure 64. The DSC thermogram (Figure 63) reveals a single Tg at -36 °C for P(PGE-stat-ECH), which is consistent with the statistical nature of the copolymer. After the click reaction, the Tg at -36 °C disappeared, and a broad Tg at 68 °C was evident, consistent with the click reaction of anionic groups. The Tg value S-P(PGE-stat-ECH) is 68 °C, an approximately 106 °C shift from the Tg of P(PGE-stat-ECH). We attributed this shift to the organic network formed through the thiol-yne free radical-polymerization. The higher oxidation state of the sulfur atoms induces a stronger dipolar association of the chains and a reduction of the segmental mobility with a commensurate increase in the Tg value. The thermal degradation behavior of the prepared P(PGE-stat-ECH) and S-P(PGE-stat-ECH) were also examined using TGA. (Figure 64) For this analysis, a sample (approximately 10 mg) was heated to 800 °C at a heating rate of 10 °C /min under N2 environment. The TGA shows three step weight loss for the P(PGE-stat-ECH). The weight loss near 100-150 °C is due to solvent or moisture trapped in the membrane. The second step weight

loss is observed around 300-390 °C and is due to cleavage of C-O, C-C, C≡C and C-Cl from pendant polymer chain whereas the third step weight loss beyond 400 °C is due to the degradation of polymer backbone. For S-P(PGE-*stat*-ECH), we observed a four-step weight loss. The first step weight loss occurs at 100-240 °C due to the solvent or moisture trapped in the membrane matrix whereas second and third step weight loss between 240-540 °C is attributed to the degradation of pendent functional groups attached to the polymer such as -SO<sub>3</sub>H, C-O, C-C and C-Cl. The fourth step weight loss beyond 540 °C is due to the polymer backbone degradation. Finally, the residual weight for S-P(PGE-*stat*-ECH) is 10% whereas for the P(PGE-*stat*-ECH) it is 17.6 %.

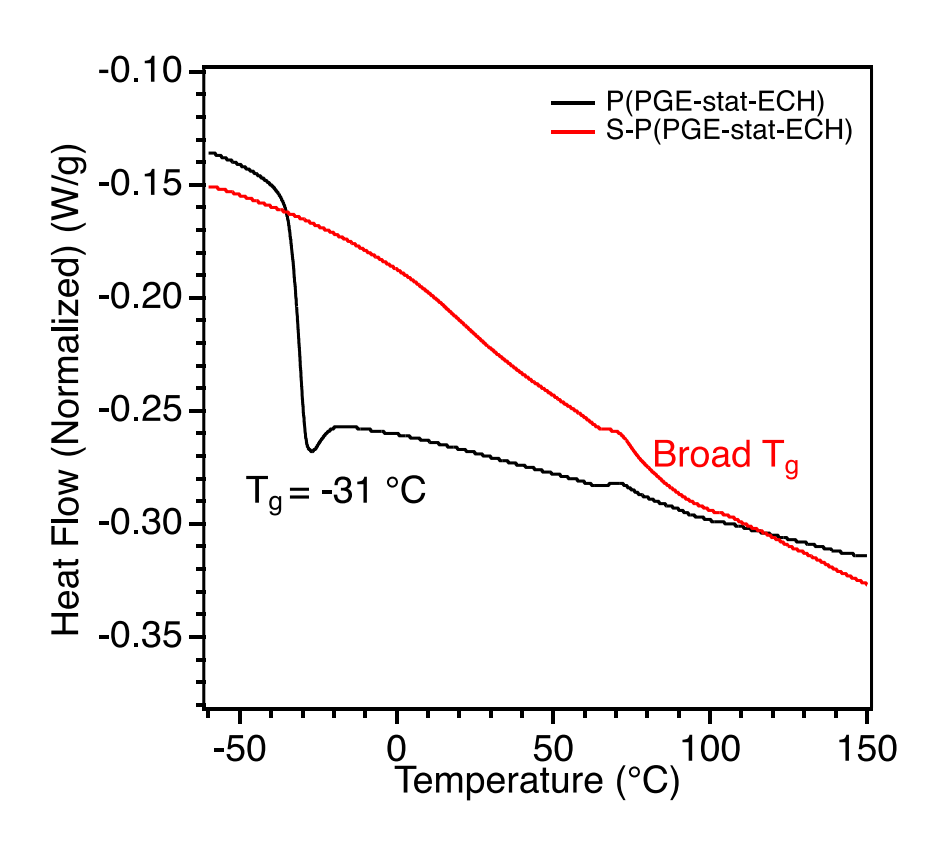


Figure 63: DSC plot for P(PGE-stat-ECH) and S- P(PGE-stat-ECH)

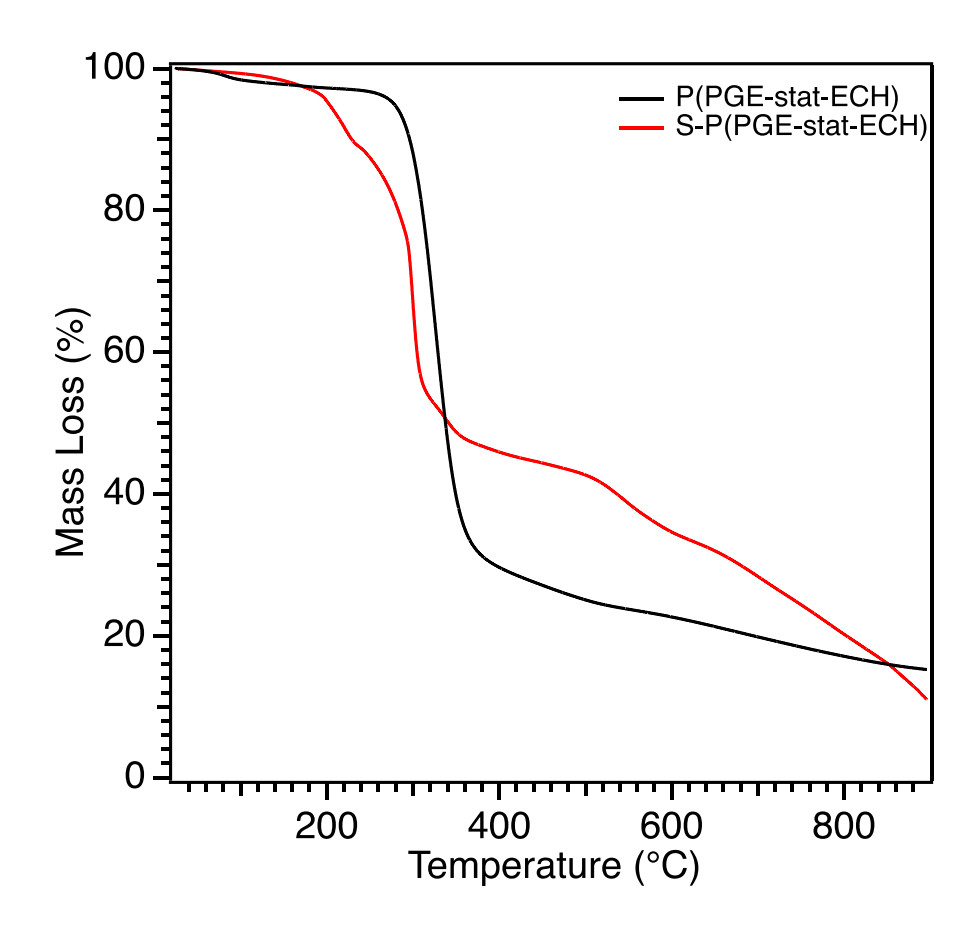


Figure 64: TGA plot for P(PGE-stat-ECH) and S- P(PGE-stat-ECH)

Here we discussed polyanion synthesis with the use of sodium-3-mercaptopropane sulfonate. We also prepared polycation with the use same procedure using cysteamine hydrochloride. A representative NMR and FTIR is given in appenix. (Figure 67 and Figure 68)

3.3.4 Modification of chloromethyl group from P(PGE-*stat*-ECH) with methyl imidazole In earlier sections we demonstrated modification of alkyne moiety. We wanted to test out modification of chloromethyl group without modifying pendent alkyne functional group. This procedure will us access to multiple sites for modification and significantly increasing loading capacities for functionality.

Methyl imidazole (3 equiv) was added to a vial containing P(PGE-*stat*-ECH) (1 equiv -Cl) and in ACN solvent. The contents of the vial were degassed with N<sub>2</sub> for 10 min. The mixture was then stirred and heated to 80 °C for 48 hours. The mixture was precipitated in water. The reaction mixture was diluted and extensively dialyzed against water. Dialysis is carried out using snakeskin tubing against 3 L of water. Dialyzed solution was then dried in oven to obtain final purified product. (Figure 65)

Figure 65: Reaction scheme for modifying P(PGE-*stat*-ECH) into polycation using methyl imidazole

FT-IR spectra of P(PGE-*stat*-ECH) and polycation with methyl imidazole was taken. (Figure 66) After reaction C-Cl stretching band is disappearing at around 700 cm<sup>-1</sup> which confirms the modification. A peak corresponds to sp CH stretch at 3300 cm<sup>-1</sup> and C≡C bond stretch at 2100 cm<sup>-1</sup> are still present indicating presence of alkyne functional groups. Hence, we demonstrated selective modification of both alkyne and chloromethyl groups. In addition, peaks corresponding to NH deformation is appearing at 1600 cm<sup>-1</sup> which shows that imidazole has been added

successfully to the side chain. Peak around 3500 cm<sup>-1</sup> shows traces of water as purified product was obtained after dialysis using water.

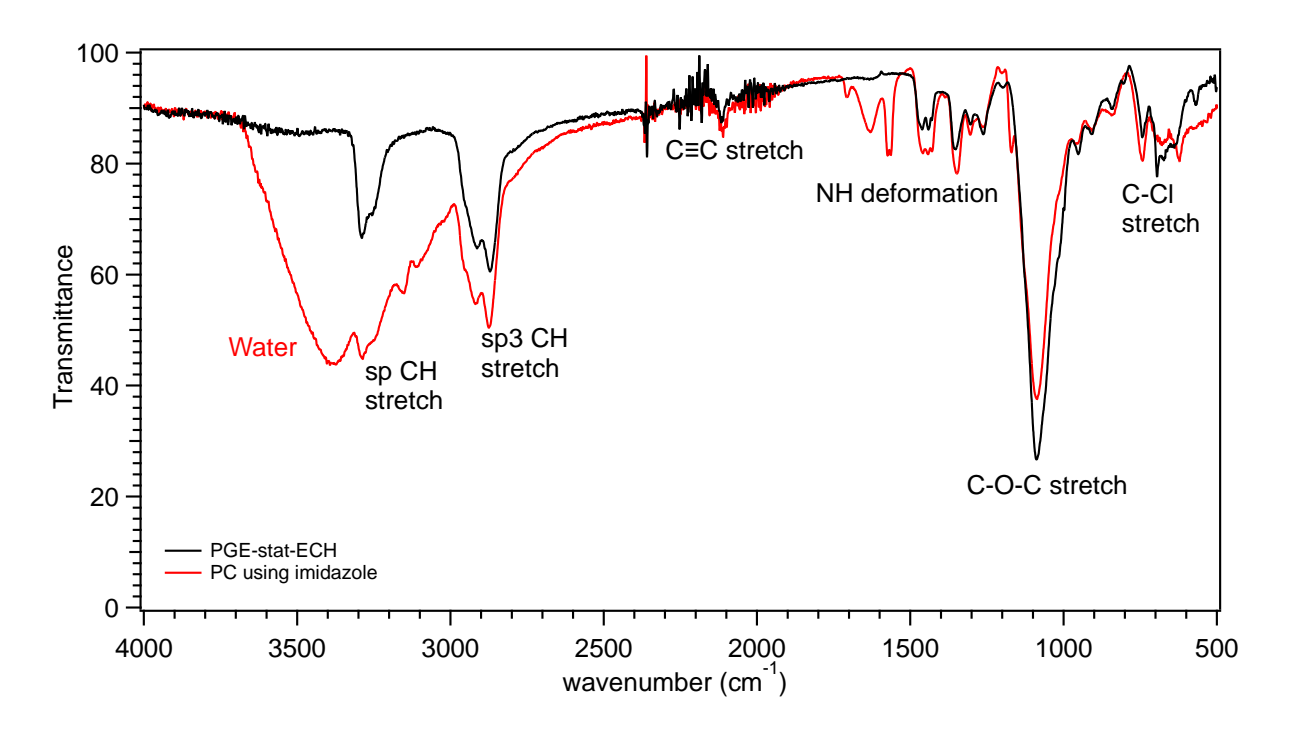


Figure 66: FTIR of P(PGE-stat-ECH) and modified P(PGE-stat-ECH) using methyl imidazole

#### 3.4 Conclusion

In conclusion, we modified precursor polyethers (described in chapter 2) to further introduce charged components in controlled manner. With the use of different charged thiol, we have successfully modified it to obtain polyanion with sulfonate groups (using sodium-3-mercaptopropane sulfonate) as well as polycation with imidazole (Using methyl imidazole) or quaternary amine groups (using cysteamine hydrochloride). Thiol click chemistry proved to be efficient way of modifying alkene and alkyne moieties to obtain desired charged group. With the use of MOB system, we can polymerize functional epoxides with varying composition, functionality, and molecular weight and by using orthogonal chemistries we can modify these precursor polyethers. We demonstrated practical and conceptual tools to control macromolecular architecture in polyethers by post polymerization reactions.

We have utilized this technique to synthesize tunable polymerization platform providing us with good structure–property relationships control for further application. We will demonstrate its use for application to develop amphoteric ion exchange membrane and to study charged polymer self-assembly in chapter 4 and 5.

#### BIBLIOGRAPHY

- (1) Shukla, G.; Ferrier, R. C. The Versatile, Functional Polyether, Polyepichlorohydrin: History, Synthesis, and Applications. *Journal of Polymer Science*. John Wiley and Sons Inc November 15, 2021, pp 2704–2718. https://doi.org/10.1002/pol.20210514.
- (2) Ferrier, R. C.; Imbrogno, J.; Rodriguez, C. G.; Chwatko, M.; Meyer, P. W.; Lynd, N. A. Four-Fold Increase in Epoxide Polymerization Rate with Change of Alkyl-Substitution on Mono-μ-Oxo-Dialuminum Initiators. *Polym Chem* 2017, 8 (31), 4503–4511. https://doi.org/10.1039/c7py00894e.
- (3) Rodriguez, C. G.; Ferrier, R. C.; Helenic, A.; Lynd, N. A. Ring-Opening Polymerization of Epoxides: Facile Pathway to Functional Polyethers via a Versatile Organoaluminum Initiator. *Macromolecules* 2017, 50 (8), 3121–3130. https://doi.org/10.1021/acs.macromol.7b00196.
- (4) Safaie, N.; Smak, J.; DeJonge, D.; Cheng, S.; Zuo, X.; Ohno, K.; Ferrier, R. C. Facile Synthesis of Epoxide-Co-Propylene Sulphide Polymers with Compositional and Architectural Control. *Polym Chem* 2022. https://doi.org/10.1039/d2py00005a.
- (5) Imbrogno, J.; Ferrier, R. C.; Wheatle, B. K.; Rose, M. J.; Lynd, N. A. Decoupling Catalysis and Chain-Growth Functions of Mono(μ-Alkoxo)Bis(Alkylaluminums) in Epoxide Polymerization: Emergence of the N-Al Adduct Catalyst. *ACS Catal* 2018, 8 (9), 8796–8803. https://doi.org/10.1021/acscatal.8b02446.
- (6) Safaie, N.; Rawal, B.; Ohno, K.; Ferrier, R. C. Aluminum-Based Initiators from Thiols for Epoxide Polymerizations. *Macromolecules* 2020, 53 (19), 8181–8191. https://doi.org/10.1021/acs.macromol.0c00464.
- (7) Hamaide, T.; Goux, A.; Llauro, M.-F.; Spitz, R.; Guyot, A.; Hamaide, T.; Goux, A.; Llauro, M.-F.; Spitz, R.; Guyot, A. Stat-Poly(Ethy1ene Oxide-Co-Propylene Oxide) Synthesis, NMR Characterization and Crystallinity Studies. *Correlation with Monte Carlo Simulation*; 1996; Vol. 237.
- (8) Herzberger, J.; Niederer, K.; Pohlit, H.; Seiwert, J.; Worm, M.; Wurm, F. R.; Frey, H. Polymerization of Ethylene Oxide, Propylene Oxide, and Other Alkylene Oxides: Synthesis, Novel Polymer Architectures, and Bioconjugation. *Chemical Reviews*. American Chemical Society December 29, 2016, pp 2170–2243. https://doi.org/10.1021/acs.chemrev.5b00441.
- (9) Pasut, G.; Veronese, F. M. State of the Art in PEGylation: The Great Versatility Achieved after Forty Years of Research. *Journal of Controlled Release*. July 20, 2012, pp 461–472. https://doi.org/10.1016/j.jconrel.2011.10.037.
- (10) Dingels, C.; Schömer, M.; Frey, H. Die Vielen Gesichter Des Poly(Ethylenglykol)s: Von Der Kosmetik Zum Ionenleiter. *Chemie in Unserer Zeit* 2011, 45 (5), 338–349. https://doi.org/10.1002/ciuz.201100551.
- (11) Mangold, C.; Dingels, C.; Obermeier, B.; Frey, H.; Wurm, F. PEG-Based Multifunctional Polyethers with Highly Reactive Vinyl-Ether Side Chains for Click-Type Functionalization. *Macromolecules* 2011, *44* (16), 6326–6334. https://doi.org/10.1021/ma200898n.

- (12) Obermeier, B.; Wurm, F.; Mangold, C.; Frey, H. Multifunctional Poly(Ethylene Glycol)s. *Angewandte Chemie International Edition*. August 22, 2011, pp 7988–7997. https://doi.org/10.1002/anie.201100027.
- (13) Hu, H.; Yuan, W.; Lu, L.; Zhao, H.; Jia, Z.; Baker, G. L. Low Glass Transition Temperature Polymer Electrolyte Prepared from Ionic Liquid Grafted Polyethylene Oxide. *J Polym Sci A Polym Chem* 2014, 52 (15), 2104–2110. https://doi.org/10.1002/pola.27217.
- (14) Viviani, M.; Meereboer, N. L.; Saraswati, N. L. P. A.; Loos, K.; Portale, G. Lithium and Magnesium Polymeric Electrolytes Prepared Using Poly(Glycidyl Ether)-Based Polymers with Short Grafted Chains. *Polym Chem* 2020, *11* (12), 2070–2079. https://doi.org/10.1039/c9py01735f.
- (15) Sarkar, A.; Carver, P. I.; Zhang, T.; Merrington, A.; Bruza, K. J.; Rousseau, J. L.; Keinath, S. E.; Dvornic, P. R. Dendrimer-Based Coatings for Surface Modification of Polyamide Reverse Osmosis Membranes. *J Memb Sci* 2010, 349 (1–2), 421–428. https://doi.org/10.1016/j.memsci.2009.12.005.
- (16) Hatakeyama, E. S.; Ju, H.; Gabriel, C. J.; Lohr, J. L.; Bara, J. E.; Noble, R. D.; Freeman, B. D.; Gin, D. L. New Protein-Resistant Coatings for Water Filtration Membranes Based on Quaternary Ammonium and Phosphonium Polymers. *J Memb Sci* 2009, *330* (1–2), 104–116. https://doi.org/10.1016/j.memsci.2008.12.049.
- (17) La, Y. H.; McCloskey, B. D.; Sooriyakumaran, R.; Vora, A.; Freeman, B.; Nassar, M.; Hedrick, J.; Nelson, A.; Allen, R. Bifunctional Hydrogel Coatings for Water Purification Membranes: Improved Fouling Resistance and Antimicrobial Activity. *J Memb Sci* 2011, 372 (1–2), 285–291. https://doi.org/10.1016/j.memsci.2011.02.005.
- (18) Sagle, A. C.; Van Wagner, E. M.; Ju, H.; McCloskey, B. D.; Freeman, B. D.; Sharma, M. M. PEG-Coated Reverse Osmosis Membranes: Desalination Properties and Fouling Resistance. *J Memb Sci* 2009, 340 (1–2), 92–108. https://doi.org/10.1016/j.memsci.2009.05.013.
- (19) Love, B. Polymeric Biomaterials. In *Biomaterials*; Elsevier, 2017; pp 205–238. https://doi.org/10.1016/B978-0-12-809478-5.00009-2.
- (20) Pasut, G.; Veronese, F. M. State of the Art in PEGylation: The Great Versatility Achieved after Forty Years of Research. *Journal of Controlled Release*. July 20, 2012, pp 461–472. https://doi.org/10.1016/j.jconrel.2011.10.037.
- (21) Thomas, A.; Müller, S. S.; Frey, H. Beyond Poly(Ethylene Glycol): Linear Polyglycerol as a Multifunctional Polyether for Biomedical and Pharmaceutical Applications. *Biomacromolecules*. American Chemical Society June 9, 2014, pp 1935–1954. https://doi.org/10.1021/bm5002608.
- (22) Bruening, M. L.; Dotzauer, D. M.; Jain, P.; Ouyang, L.; Baker, G. L. Creation of Functional Membranes Using Polyelectrolyte Multilayers and Polymer Brushes. *Langmuir* 2008, 24 (15), 7663–7673. https://doi.org/10.1021/la800179z.

- (23) Nayak, K.; Kumar, A.; Tripathi, B. P. Molecular Grafting and Zwitterionization Based Antifouling and Underwater Superoleophobic PVDF Membranes for Oil/Water Separation. *J Memb Sci* 2022, 643. https://doi.org/10.1016/j.memsci.2021.120038.
- (24) Luo, S.; Stevens, K. A.; Park, J. S.; Moon, J. D.; Liu, Q.; Freeman, B. D.; Guo, R. Highly CO2-Selective Gas Separation Membranes Based on Segmented Copolymers of Poly(Ethylene Oxide) Reinforced with Pentiptycene-Containing Polyimide Hard Segments. *ACS Appl Mater Interfaces* 2016, 8 (3), 2306–2317. https://doi.org/10.1021/acsami.5b11355.
- (25) Rodriguez, C. G.; Chwatko, M.; Park, J.; Bentley, C. L.; Freeman, B. D.; Lynd, N. A. Compositionally Controlled Polyether Membranes via Mono(μ-Alkoxo)Bis(Alkylaluminum)-Initiated Chain-Growth Network Epoxide Polymerization: Synthesis and Transport Properties. *Macromolecules* 2020, *53* (4), 1191–1198. https://doi.org/10.1021/acs.macromol.9b02318.
- (26) Xue, Z.; He, D.; Xie, X. Poly(Ethylene Oxide)-Based Electrolytes for Lithium-Ion Batteries. *Journal of Materials Chemistry A*. Royal Society of Chemistry July 17, 2015, pp 19218–19253. https://doi.org/10.1039/c5ta03471j.
- (27) Vallbe, A.; Besner, S.; Prud'homme, J. Comparative Study Of Poly(Ethylene Oxide) Electrolytes Made With Lin(Cf, So,), Licf, So, And Liclo,: Thermal Properties And Conductivity Behaviour; Vol. 37.
- (28)Sprafke, J. K.; Spruell, J. M.; Mattson, K. M.; Montarnal, D.; McGrath, A. J.; Pötzsch, R.; Miyajima, D.; Hu, J.; Latimer, A. A.; Voit, B. I.; Aida, T.; Hawker, C. J. Revisiting Thiol-Yne Chemistry: Selective and Efficient Monoaddition for Block and Graft Copolymer Formation. JPolym Sci $\boldsymbol{A}$ Polym Chem 2015, 53 (2),319–326. https://doi.org/10.1002/pola.27345.
- (29) Krannig, K. S.; Huang, J.; Heise, A.; Schlaad, H. Photochemical Thiol-Yne Functionalization of Polypeptide Scaffolds. *Polym Chem* 2013, *4* (14), 3981–3986. https://doi.org/10.1039/c3py00428g.
- (30) Krimalowski, A.; Rosenbach, D.; Erabhoina, H.; Thelakkat, M. Versatile Solid Polymer Electrolytes from Clickable Poly(Glycidyl Propargyl Ether) for Lithium Metal Batteries. *J Energy Storage* 2023, 65. https://doi.org/10.1016/j.est.2023.107348.

Figure 67: Reaction scheme for polycation preparation using cysteamine hydrochloride

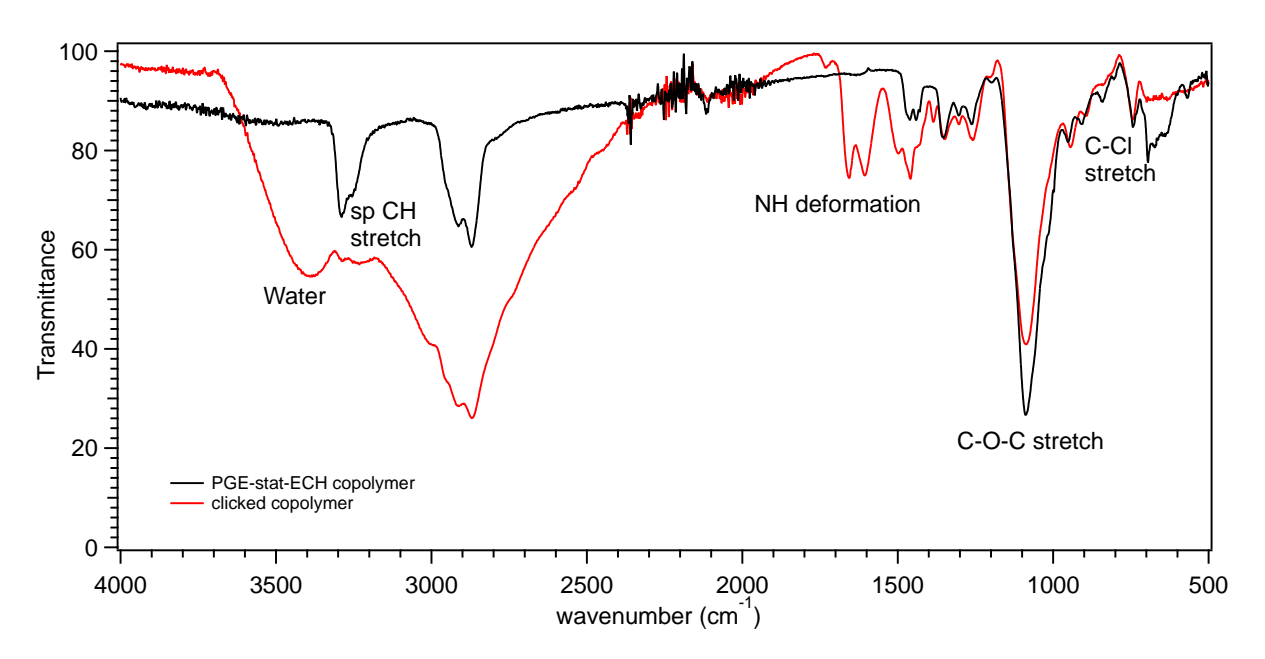


Figure 68: FTIR of P(PGE-stat-ECH) and clicked P(PGE-stat-ECH) using cysteamine hydrochloride

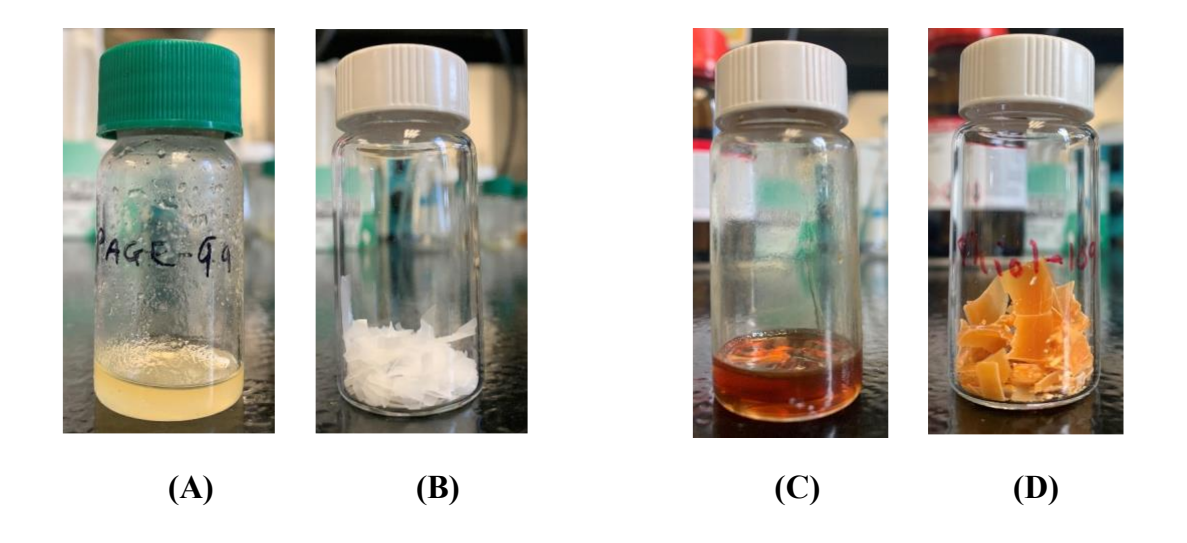


Figure 69: Visual picture of A. PAGE B. Polyanionic PAGE C. PPGE D. Polyanionic PPGE

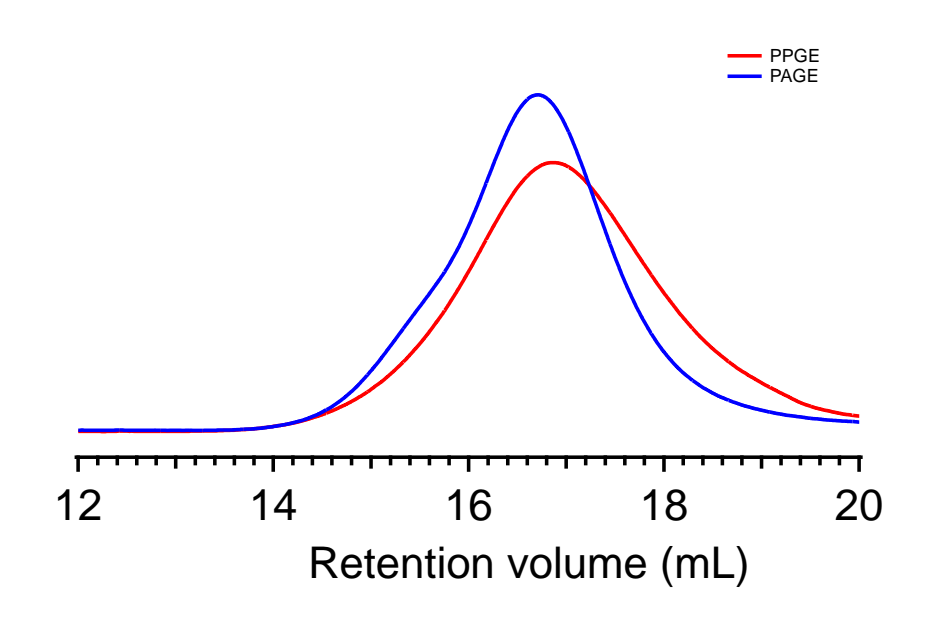


Figure 70: GPC traces of PAGE and PPGE

Chapter 4. Poly(vinylidene difluoride-co-hexafluoropropylene) grafted with novel polyether amphoteric ion exchange membranes for redox flow batteries

#### Abstract

Vanadium Redox Flow Batteries (VRFBs) are promising candidates for large scale energy storage due to their high energy efficiency. Nafion ion exchange membranes have been used in VRFB applications owing to their good ionic conductivity and excellent chemical and mechanical stability, but Nafion's high cost, excessive swelling and low ion selectivity limits its use for commercialization. Amphoteric ion-exchange membranes have potential for preventing vanadium ion penetration, thus increasing ion selectivity. In our current work, we have synthesized an economical crosslinked network to make amphoteric ion exchange membranes. Membranes were synthesized by grafting of epichlorohydrin and propargyl glycidyl ether-based charged copolymer (S-PPGE-ECH) to the PVDF-co-HFP membrane matrix. We varied the copolymer composition in the matrix to study its effect on ionic conductivity. All membranes were characterized using NMR and FTIR spectroscopy to confirm the presence of sulfonate and quaternary ammonium charged groups. Gradual increase of copolymer content decreases the contact angle from 83° (1% of S-PPGE-ECH) up to 73° (10% of S-PPGE-ECH), indicating improvement in the hydrophilicity of membrane surfaces with addition of the copolymer. This increase in hydrophilicity resulted in a commensurate increase in swelling ratio from 17.5% to 27.0%, which is comparable to 18.6% for Nafion117. We further saw a commensurate increase in ionic conductivity with an increase in copolymer content up to 4.00 mS/cm. Cation exchange capacity also increased steadily with increasing copolymer content while anion exchange capacity increased only slightly. The increase in exchange capacity was attributed to the presence of -NR<sub>3</sub> and-SO<sub>3</sub>H groups in the membranes.

In this work, we demonstrated control over ionic conductivities by tuning copolymer content without compromising thermal and mechanical stability of the membrane.

#### 4.1 Introduction

Vanadium-based redox flow batteries (VRFBs) were successfully developed by the Skyllas-Kazacos research group in the 1980s. 1-4 Since then, VRFBs are emerging as a popular option for large scale energy storage. This popularity is growing as researchers explore the use of renewable energy sources to fulfill our electricity demands. Unfortunately, in the journey towards complete dependence on renewable energy sources, there is an obstacle due to the intermittent nature of wind and solar energy sources; specifically, existing electric grid systems are not equipped to handle the resulting large fluctuations in energy production. Hence, large-scale electrical storage systems are required for the smooth operation of electrical grid system using renewable sources.<sup>5</sup> As a large-scale energy storage solution, VRFBs are popular due to their modular setup, long performance lifetime, versatile operating conditions including wide temperature ranges both indoors as well as outdoors, and avoidance of flammable solvents.<sup>6</sup> Additionally, VRFBs utilize oxovanadium species as both anolyte and catholyte, which minimizes catastrophic impacts associated with membrane crossover (e.g., total system failure). Despite the limited risk of degradation caused by membrane crossover, excessive permeability of oxovanadium through the ion exchange membrane can result in comproportionation (or self-discharge), and thus, significantly diminish the coulombic efficiency (CE) of a VRFB.

Semipermeable ion exchange membranes (IEM) are crucial components of VRFBs.

For efficient operation of a VRFB, the IEM must have good proton conductivity, low water uptake and swelling ratio, as well as good chemical and thermal stability with minimal vanadium ion transfer.<sup>7–10</sup> Numerous fluorocarbon- and hydrocarbon-based polymer membranes have been

previously developed.<sup>7,11–18</sup> Among these, fluorocarbon-based Nafion is the most widely used cation exchange membrane (CEM) for VRFB applications due to its good perm-selectivity, proton conductivity as well as excellent chemical stability. Unfortunately, its commercial applicability is limited due to high cost, excessive swelling, and fast crossover of vanadium ions.<sup>3,7,19</sup> To address these issues, a variety of anion exchange membranes (AEMs) have been developed. AEMs have fixed cationic groups which prevents positively charged vanadium ions from permeating and leading to ultra-low vanadium crossover.<sup>20</sup> Due to the donnan exclusion effect, quaternary ammonium groups in an AEM can prevent cations, such as oxovanadium ions, from passing through the membrane. In this way, AEMs can be synthesized to provide extremely low vanadium ion permeability and high CE. Unfortunately, many AEMs suffer from poor redox stability and low ionic conductivity, which leads to low voltage efficiency (VE) and high rate of capacity loss. Amphoteric ion exchange membranes (AIEMs) combine properties of CEMs and AEMs by having two types of functional groups providing both cationic and anionic properties in one single membrane. Performance properties of AIEMs, such as permeability and conductivity, depend on the extent of functionality present in it which is often achieved by complex preparation techniques. Commonly used techniques to obtain AIEM include irradiation grafting or solution phase inversion methods which both have an associated high cost. 7,18,21-25 There is a need to develop simple methods to fabricate AIEMs using inexpensive starting material(s) and with a balance of functional groups. Many researchers have been exploring cheaper alternatives to address these issues using partially fluorinated polymers. These polymers provide good mechanical stability while maintaining performance properties at reduced cost. 18,21,23,24,26

In this work, a novel AIEM is prepared from a partially fluorinated membrane matrix using PVDF-co-HFP grafted with a functional polyether of epichlorohydrin (ECH) and propargyl glycidyl ether

(PGE) to serve as low-cost alternative to Nafion. The polyether synthesis described here follows green chemistry principles, especially with respect to atom economy, as we polymerize up to 99% of the starting materials using solvent-free reaction conditions. Additionally, the starting epoxides are derived from renewable feedstocks like glycerol. We use MOB catalyst-initiator system for polymerization, significantly reducing the reaction times while enabling the use of moderate or ambient reaction temperatures. By adjusting molecular weight as well as composition of ECH and PGE in the matrix we can obtain good balance of cationic and anionic species. The resulting homogeneous polymer membrane was tested for physicochemical, surface, and electrochemical properties. This novel AIEM with promising thermal, mechanical, and electrochemical properties with low cost have a potential candidacy to use in VRFB system.

### 4.2 Experimental section

#### 4.2.1 Materials

Propargyl alcohol (Sigma-Aldrich, 99%), sodium hydroxide pellets (Fisher Chemical), epichlorohydrin (Sigma-Aldrich, 99%), triisobutylaluminum (AlMe3, 2.0 M in hexanes, Sigma-Aldrich), dimethylethanolamine (Sigma-Aldrich, >98%), sodium-3-mercapto-1-propane sulfonate (Sigma-Aldrich), 1-vinyl imidazole (Sigma-Aldrich) and 2,2'-Azobis(2-methylpropionitrile (AIBN, Sigma-Aldrich, 98%) were all used as received. CDCl₃ (Cambridge Isotope Laboratories, Inc. 99.8%) and deuterium oxide (Cambridge Isotope Laboratories, Inc. 99.9%) were used without any further purification. Methanol (MeOH, Fisher, Certified ACS), hexane (Fisher, Certified ACS), and dichloromethane (DCM, Fisher, Certified ACS) were used for polymer cleaning. Reactions were carried out in dimethyl sulfoxide (DMSO, Sigma-Aldrich ≥99.9%), and dimethyl acetamide (DMAc) (Fischer Chemicals, ACS certified), precipitated in ethyl acetate (Fischer Chemicals, ACS certified). All air and moisture sensitive reactions were carried out under a dry

nitrogen atmosphere inside a glovebox. Cellulose dialysis membrane (Slide-A-lyzer™ Fisher Scientific) with molecular weight cut off (MWCO) of 2 kg/mol is used for dialysis.

#### 4.2.2 Instrumentation

#### **NMR Spectroscopy**

<sup>1</sup>H NMR spectroscopy was performed to confirm copolymer formation on an Agilent DDR2 500 MHz NMR spectrometer using deuterated solvents at room temperature. The chemical shifts are reported in parts per million (ppm) and are referenced using the residual <sup>1</sup>H peak from the deuterated solvent.

#### Fourier Transform Infrared (FTIR) Spectroscopy

Fourier Transform Infrared (FTIR) spectra were taken using Shimadzu IRAffinity-1 spectrometer equipped with MIRacle ATR attachment. The spectra were recorded between the wavelength on 500-4000 cm<sup>-1</sup> in absorption mode.

#### **Gel Permeation Chromatography (GPC)**

Gel permeation chromatography (GPC) was carried out on the Malvern OMNISEC system with an isocratic pump, degasser, and temperature-controlled column oven held at 35 °C containing 2 Viscotek 300×8.0 mm columns (T3000 and T4000) with an exclusion limit of 400 kDa. Absolute molecular weight was determined using triple detection method with light scattering, viscometer, and refractive index. Polystyrene standards solutions (from scientific polymer) in THF (Sigma-Aldrich 99.8%) were prepared for calibration.

#### **Differential Scanning Calorimetry (DSC)**

Differential scanning calorimetric (DSC) tests were conducted on a TA250 instrument with a heating rate of 10 °C min<sup>-1</sup> under a N<sub>2</sub> atmosphere, and the data from the second heating curve was used for further analysis.

#### Thermogravimetric Analysis (TGA)

Thermogravimetric Analysis (TGA) was performed using a TGA 500 (TA Instruments, USA). A sample (about 10 mg) was heated to 800 °C with a heating rate of 10°C /min.

# **Scanning Electron Microscopy (SEM)**

Scanning Electron Microscopic inspection was performed using a JEOL 6610LV (JEOL Ltd. Tokyo, Japan)

### **Contact Angle Goniometry**

Water contact angles were measured on a goniometer (Krüss DSA30). All contact angle measurements were performed on non-functionalized and post-functionalized surfaces. The apparent contact angles were measured using the sessile drop method with deionized water (droplet volume of  $2\,\mu L$ ). For each surface, three measurements were taken at different positions to estimate the standard deviation.

#### Water Uptake

Water uptake (WU) of the AIEM reveals the trapped water content in membrane matrix and can be estimated by weight difference of wet membrane ( $W_{wet}$ ) and completely vacuum dried membrane ( $W_{dry}$ ) using following equation.

$$WU = \frac{W_{wet} - W_{dry}}{W_{dry}} \times 100 \tag{1}$$

Measuring error of WU is  $\pm 1.0\%$ .

#### **Swelling ratio**

The swelling ratio (SR) acquaints the membrane's dimensional changes and can be determined by treating the membrane samples in water at 65 °C for 12h, using equation 2.

$$SR = \frac{L_{wet} - L_{dry}}{L_{dry}} \times 100 \tag{2}$$

Average size of wet and dry membrane ( $L_{wet}$  and  $L_{dry}$ , respectively) may be defined as  $L_{wet} = (L_{wet1} L_{wet2})^{1/2}$  and  $L_{dry} = (L_{dry1} L_{dry2})^{1/2}$ . Measuring error of SR is  $\pm 1.0\%$ .

# Ion exchange capacity- Cation Exchange Capacity (CEC) and Anion Exchange Capacity (AEC) calculation

The ion-exchange capacities - CEC and AEC of membranes were determined with the use of direct titration and back titration respectively.

For CEC measurements, the dry membranes were immersed in a 1M NaCl solution for 24 h to allow exchange of H<sup>+</sup> ions with Na<sup>+</sup> ions. Using simple titration with a 0.01 M NaOH solution we then quantified the H<sup>+</sup> ions concentration from the solution. (equation 3)

$$CEC = \frac{c_{NaOH}v_{NaOH}}{w_{dry}} \tag{3}$$

For determining AEC, the dry membranes were immersed in a standard 0.05 HCl solution overnight. Then we titrated this solution against 0.05M NaOH to quantified AEC using equation 4.<sup>27–29</sup>

$$AEC = \frac{C_{HCl}V_{HCl} - C_{NaOH}V_{NaOH}}{W_{drv}} \tag{4}$$

Where C and V denote the concentration and volume of HCl or NaOH. Measuring error of IEC is  $\pm 0.01$  meq/g.

#### Ionic conductivity of the AIEM

The ionic conductivity for different prepared AIEM samples was measured by electrochemical impedance spectroscopy using Biologic VSP potentiostat. The potential was set to open circuit, and an alternating potential of 20 mV amplitude was scanned from 20 Hz to 1 MHz frequency. The cell resistance was found as the high-frequency limit of the real part of the impedance. The membranes were soaked overnight in 1M NaOH and rinsed with DI water prior to measurement. The membranes with area 0.13 cm<sup>2</sup> were loaded in a Biologic Controlled

Environment Sample Holder (CESH), consisting of two parallel anodized aluminum plates, a fixed bottom disc of 47 mm diameter on which a gold electrode (1/4 inch) is installed, and an upper metallic plate, moveable vertically versus the bottom plate.

# Representative calculation of membrane electrical conductivity, $\kappa_m$

The membrane resistance ( $R_m$ ) was determined from electrochemical impedance spectroscopy, as the high-frequency x-axis intercept of Nyquist impedance plots, and membrane conductivity ( $\kappa_m$ ) was estimated by the following equation.

$$\kappa_m(S/cm) = \frac{L(cm)}{R_m(\Omega) \times A(cm^2)}$$
 (5)

#### 4.3 Result and discussion

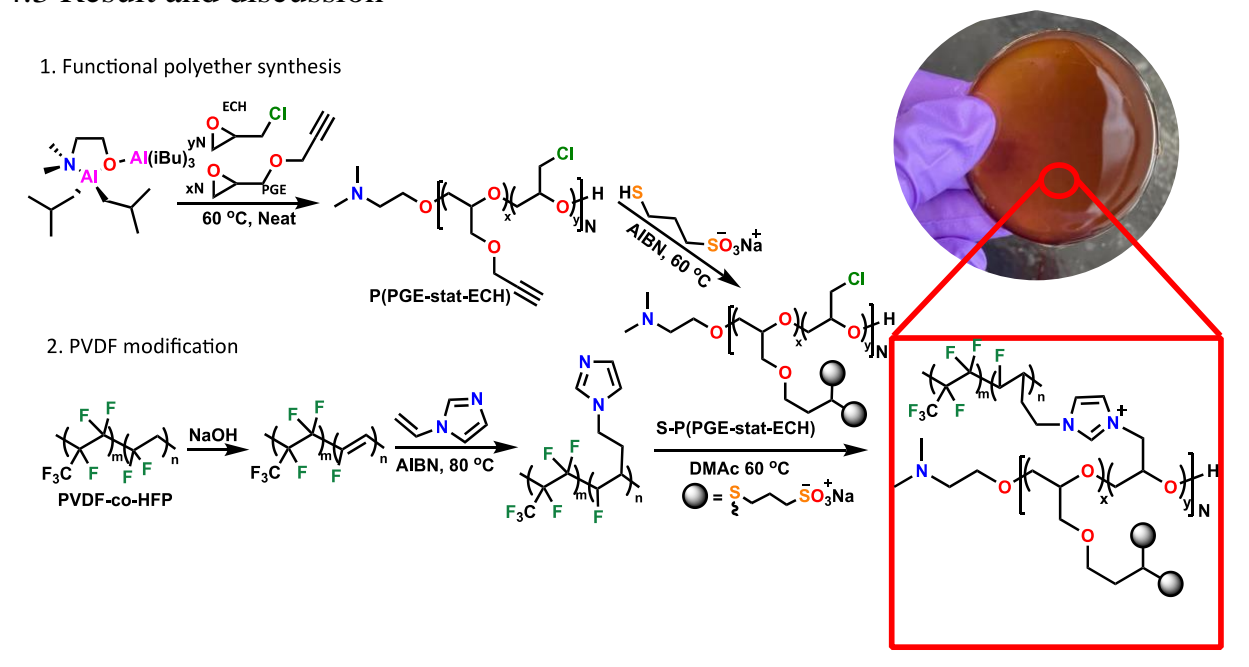


Figure 71: Synthetic scheme of novel charged polyether (1) and modification of PVDF (2) along with picture of final membrane.

Semi-permeable membranes, either ion exchange or non-ionic porous membranes, constitute an integral part of VRFBs. To ensure smooth operation of VRFB, the membrane should have good ionic exchange capacity, high ionic conductivity, low water uptake, low swelling ratio, low area electrical resistance and low vanadium and other polyhalide ions permeability, good chemical, and

thermal stability as well as low cost. Recent work has outlined the effective modification of PVDF-based membranes with functional groups. We hypothesized that we could adapt these modification schemes to graft functional polymers with controlled composition onto the PVDF backbone to make an amphoteric membrane for VFRB applications. The synthetic scheme we employed is highlighted in Figure 71. This approach requires the synthesis of polymers with orthogonally addressable chemistries to enable (1) grafting to the PVDF backbone and incorporation of the cationic moiety, and (2) covalent incorporation of the anionic moiety. We first set out to synthesize such a polymer through our recently developed aluminum-based epoxide polymerization platform. <sup>30–32</sup>

Copolymers with orthogonally addressable chemical functional groups were synthesized with controlled molecular weight and composition to tune transport properties. Polyether copolymers were synthesized from two epoxide monomers, propargyl glycidyl ether (PGE) and epichlorohydrin (ECH), which were chosen due to their functional pendant groups. Specifically, PGE contains a pendant alkyne which can be modified through thiol-yne click chemistry by up to two thiol containing ligands, while ECH has a chloromethyl group that can react with amines. 33-35 Ultimately two sulfonate groups will be attached to PGE, while ECH will be used to graft to a modified PVDF membrane. It should be noted that polymerizations involving PGE are notoriously difficult, 30,34,35 and the targeted copolymer has not been synthesized before as far as the authors are aware. Polymerizations were performed in a septum-capped reaction vial charged with a stir bar, an aluminum-based initiator, 30-32,36,37 (Figure 78) and a 1:1 molar ratio of PGE and ECH. The solution was then heated at 60 °C for 48 hrs. After completion of the polymerization, the reaction mixture was quenched with methanol and dissolved in DCM to remove any unreacted aluminum. The resulting solution was then washed with hexane to precipitate the desired polymer product.

The supernatant was removed, and the polymer was dried *in vacuo*. The copolymer was characterized by  $^{1}$ H and  $^{13}$ C NMR spectroscopy, revealing spectroscopic peaks consistent with a statistical copolymer structure, as can be seen in Figure 72 A and Figure 79, respectively. From analysis of the NMR spectrum, the ratio of ECH to PGE was determined to be 50-50%, which is consistent with anticipated ratio. The precursor copolymer was further characterized by size-exclusion chromatography (SEC) with triple detection, revealing a molecular weight of 25.5 kg/mol and D = 1.43, which is consistent with the targeted molecular weight of 20 kg/mol (Figure 72B). The relatively high polydispersity is likely due to the difficult ring opening polymerization of the two epoxides. Finally, we performed differential scanning calorimetry which revealed a single  $T_g$  at -31  $^{\circ}$ C consistent with a 50-50% statistical copolymer of these two epoxides.

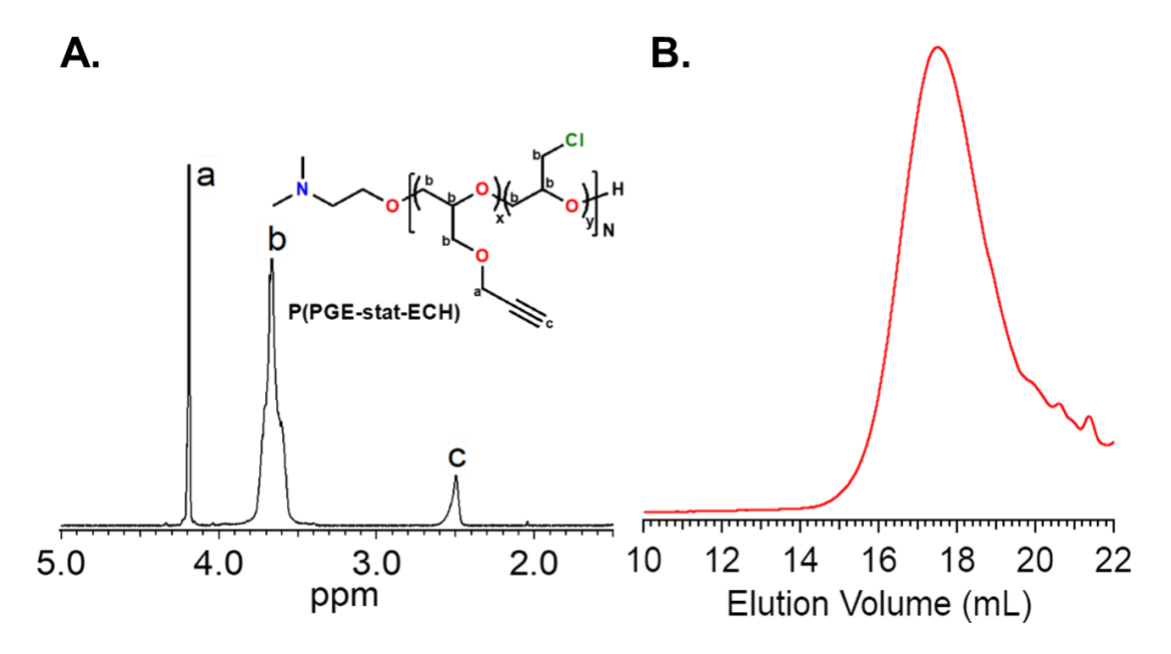


Figure 72: A.  $^{1}$ H NMR spectrum of P(PGE-*stat*-ECH). The peaks are consistent with anticipated structure, which is further confirmed by the  $^{13}$ C NMR spectrum (in appendix). B. RI trace of the synthesized polymer with  $M_n = 25.5$  kg/mol and D = 1.43, consistent with the targeted molecular weight

The precursor copolymer P(PGE-stat-ECH) was modified with negatively charged sulfonate groups through click chemistry.<sup>38–40</sup> After successfully synthesizing the pre-cursor polymer, we

sought to selectively modify the alkyne groups, while leaving the chloromethyl groups untouched. Here, sodium 3-mercapto-1-propane sulfonate (5 equivalents) was added to a vial containing P(PGE-stat-ECH) (1 equivalents alkyne unit) and 2,2'-azobis(2-methylpropionitrile) (AIBN; 2 wt%) in DMSO solvent. The contents of the vial were degassed with N2 for 10 min. The mixture was then stirred and heated to 80 °C for 12 hours. Following the reaction, the mixture was precipitated in ethyl acetate, diluted, and dialyzed against 3 L of water using cellulose dialysis membrane (Slide-A-lyzer<sup>TM</sup> Fisher Scientific) with MWCO of 2 kg/mol. The dialyzed solution was then dried in the oven to obtain final purified product. The final product appeared glassy as compared with the liquid-at-room temperature precursor polymer, because of the increased polarity of the sulfone containing side chains indicating successful attachment of the charge containing ligands.

The thermal properties of the modified polymer and P(PGE-stat-ECH) were characterized with differential scanning calorimetry (DSC) and thermogravimetric analysis (TGA), as shown in Figure 73. The DSC thermogram (Figure 73A) reveals a single Tg at -36 °C for P(PGE-stat-ECH), which is consistent with the statistical nature of the copolymer. After the click reaction, the Tg at -36 °C disappeared, and a broad Tg at 68 °C was evident, consistent with the click reaction of cationic groups. The Tg value of thiol clicked PPGE is 68 °C, an approximately 106 °C shift from the Tg of P(PGE-stat-ECH). We attributed this shift to the organic network formed through the thiol-yne free radical-polymerization. The higher oxidation state of the sulfur atoms induces a stronger dipolar association of the chains and a reduction of the segmental mobility with a commensurate increase in the Tg value. The thermal degradation behavior of the prepared P(PGE-stat-ECH) and S-P(PGE-stat-ECH) were also examined using TGA (Figure 73B). For this analysis, a sample (approximately 10 mg) was heated to 800 °C at a heating rate of 10°C /min

under N<sub>2</sub> environment. The TGA shows three step weight loss for the P(PGE-stat-ECH). The weight loss near 100-150 °C is due to solvent or moisture trapped in the membrane. The second step weight loss is observed around 300-390 °C and is due to cleavage of C-O, C-C, C≡C and C-Cl from pendant polymer chain whereas the third step weight loss beyond 400 °C is due to the degradation of polymer backbone. For S-P(PGE-stat-ECH), we observed a four-step weight loss. The first step weight loss occurs at 100-240 °C due to the solvent or moisture trapped in the membrane matrix whereas second and third step weight loss between 240-540 °C is attributed to the degradation of pendent functional groups attached to the polymer such as -SO<sub>3</sub>H, C-O, C-C and C-Cl. The fourth step weight loss beyond 540 °C is due to the polymer backbone degradation. Finally, the residual weight for S-P(PGE-stat-ECH) is 10% whereas for the P(PGE-stat-ECH) it is 17.6 %. The remaining mass percent for P(PGE-stat-ECH) is slightly more compared to the S-P(PGE-stat-ECH) due to the organic network formed through the thiol-yne free radical reaction. The chemical composition of modified and precursor polymers was characterized through NMR and FTIR spectroscopy. Figure 74 A and Figure 80 shows the <sup>1</sup>H NMR and <sup>13</sup>C NMR spectrum of S-P(PGE-stat-ECH). New peaks are evident at (3.9-3.6), (3.2-2.7), and (2.04) ppm, which are consistent with the successful functionalization of the copolymer. Precisely, thiol-yne click chemistry follows the propagation and chain transfer steps. The first addition of thiol to the alkyne forms a vinyl sulfide intermediate that can then react with another thiol to form the bis-adduct. In both reactions, the addition of the thiyl radical is reversible, whereas the hydrogen abstraction is irreversible. After the thiol-yne click reaction, the peak in the copolymer spectra around 2.5 ppm corresponding to the proton in the terminal alkyne group completely disappeared, which suggests the attachments of sulfonic acid group onto the copolymer. The extra peaks located at 2.9 and 1.9

ppm confirm the formation of S-PPGE-ECH. Additionally, after the reaction, the polymer is no longer soluble in THF, again consistent with successful modification.

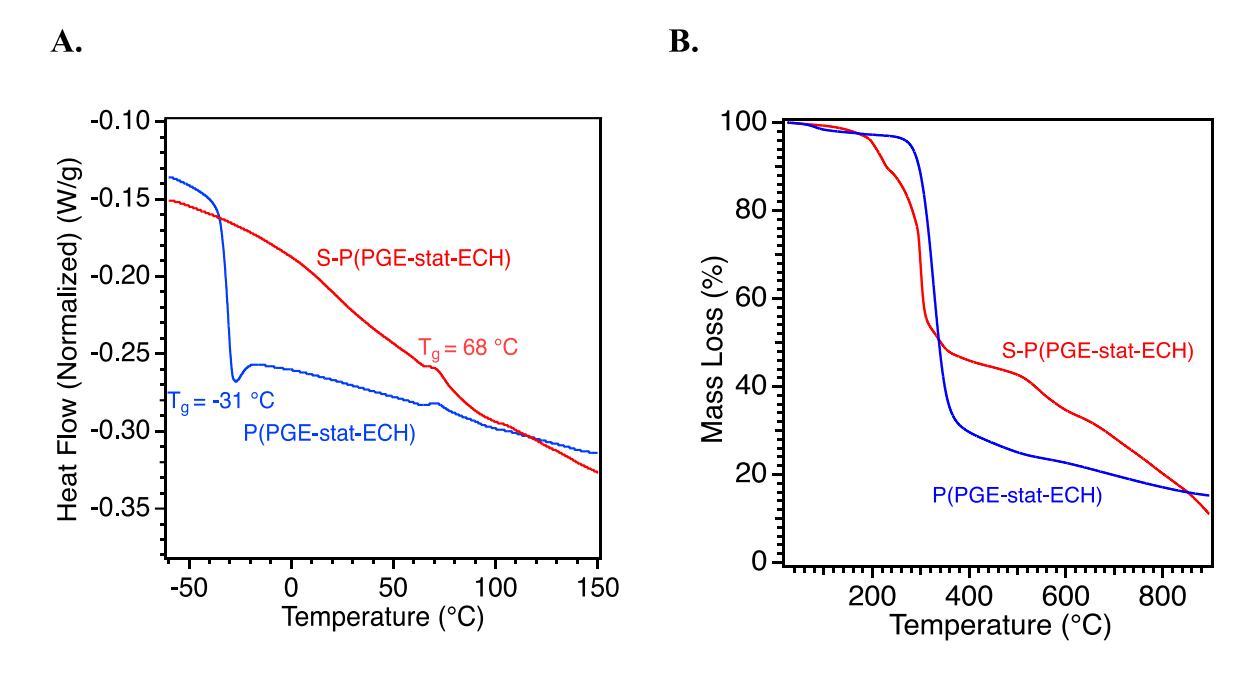


Figure 73: A. DSC traces for precursor polymer (blue) and modified polymer). The precursor polymer shows a T<sub>g</sub> consistent with the glass transition of a statistical copolymer of PGE-stat-ECH, while the modified polymer shows a broad T<sub>g</sub> owing to the pendant modification. B. TGA of the precursor polymer (blue) and charged polymer (red). The precursor polymer displays three weight loss steps related to trapped solvent, pendant group scission, backbone scission, while the modified polymer shows additional weight loss steps due to the incorporated ions and pendant groups.

While it is well-documented in literature that a thiol under the click conditions is not enough to replace the chloromethyl group, we further characterized the modified and pre-cursor polymer with FTIR spectroscopy. Prior to the click reaction, a clear CH stretch peak at 3296 cm<sup>-1</sup> and 2112 cm<sup>-1</sup> can be seen, which confirms the presence of the alkyne of the unmodified polyether. After the click reaction, these peaks disappear, consistent with the alkyne peak being reacted away. In addition, peaks corresponding to SO<sub>2</sub> symmetric and antisymmetric stretches appear at wavenumbers 1136 cm<sup>-1</sup> and 1300 cm<sup>-1</sup> respectively, which shows that thiol has been added successfully to the side chain. The peak around 3500 cm<sup>-1</sup> shows presence of water, as purified product was obtained after dialysis using water and it is not completely removed. The sharp band

around 750 cm<sup>-1</sup> for both P(PGE-stat-ECH) and S-P(PGE-stat-ECH) is consistent with C-Cl

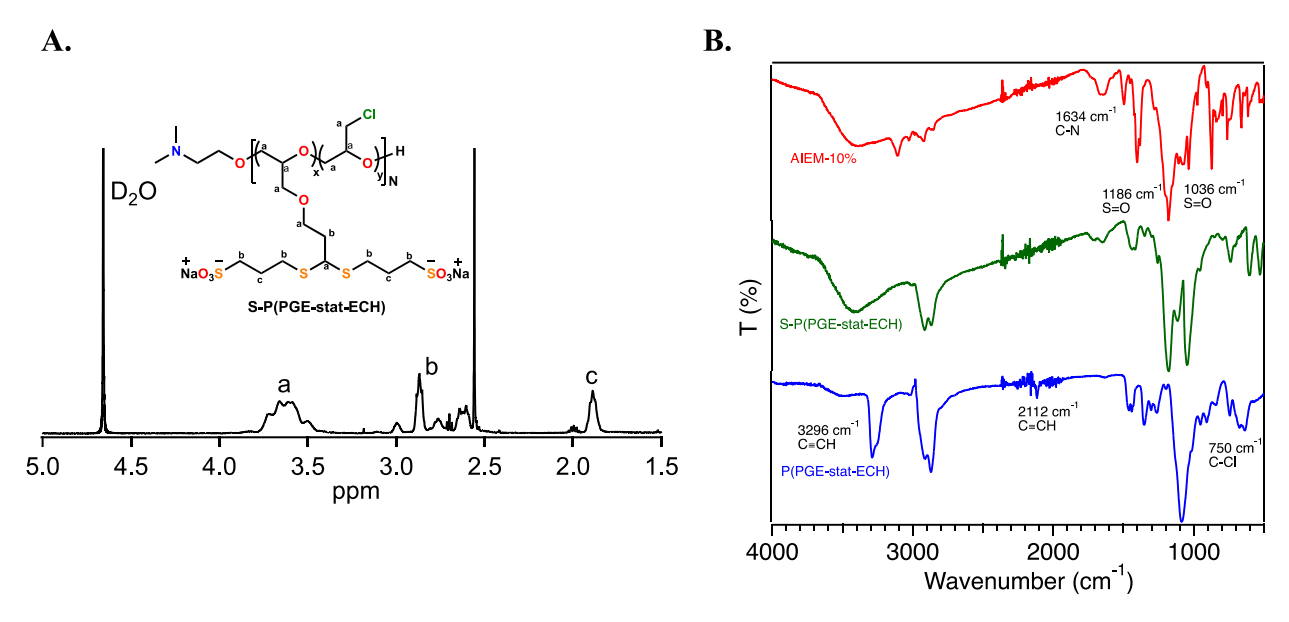


Figure 74: A. <sup>1</sup>H NMR spectrum of S-P(PGE-*stat*-ECH). The peaks are consistent with anticipated structure. B. FTIR Spectra of precursor polymer (blue, bottom), modified polymer (green, middle) and final AIEM-10% (red, top).

stretching, indicating that the chloromethyl unit remains intact for further functionalization. (Figure 74 B)

After confirming the compositional structure of the functional polyethers, we set out to modify PVDF-co-HFP to create an amphoteric membrane. A modified PVDF-co-HFP was used as the base for the VFRB membrane due to its chemical, thermal, and mechanical stability. We set out to modify PVDF-co-HFP with a double bond as reported in the literature. This double bond provides the necessary chemical handle to graft S-P(PGE-*stat*-ECH). To create the double bond in PVDF-co-HFP, we first dissolved the polymer in DMAc followed by the addition of a saturated NaOH solution in IPA (*cf.*, Figure 71, reaction 2). The PVDF-co-HFP solution turned from a transparent to a dark-brown solution after 7 hours, indicating the successful incorporation of the double bond. The obtained reaction mixture was precipitated into DI water, collected, and dried in a vacuum oven at 60 °C to obtain the polymer named DPVDF-co-HFP. FTIR spectroscopy of this

polymer revealed the evolution of spectroscopic peaks at 1620 cm<sup>-1</sup>, consistent with the presence of the double bond in the backbone. (Figure 83) Furthermore, the resulting spectra matched examples found in the literature. The thermograms for PVDF-co-HFP and DPVDF-co-HFP reveal a T<sub>m</sub> at 143 °C (Figure 81), consistent with literature.<sup>44</sup>

Next, DPVDF-co-HFP was further modified with vinyl imidazole. <sup>45,46</sup> The vinyl group of the vinyl imidazole reacted with the double bond in the backbone of the DPVDF-co-HFP, providing a grafting site for the chloromethyl group in the S-P(PGE-stat-ECH) polymer as well as providing a positive charge through quaternization of the amine in the imidazole. To perform the modification, DPVDF-co-HFP (1g) was dissolved in DMAc (10 mL) and to this solution AIBN and 1 mL of vinyl imidazole was added and the resulting solution was heated to 90 °C for 24 hours. Finally, a solution of S-P(PGE-stat-ECH) in DMSO (2 mL) was prepared from 1 to 10 wt%. This solution was added to the imidazole modified DPVDF-co-HFP in DMAc and heated again to 90 °C for 24 hours. The final reaction mixture was cast on a glass plate and held at 60 °C for 24 hours in a vacuum oven to form a flat, contiguous membrane. The dried membrane was then washed repeatedly in water to remove any excess chemicals. The resulting membrane was a robust free-standing film approximately 150 μm in thickness. An example of a final membrane can be seen in Figure 71.

FTIR spectroscopy was performed on the functionalized polyethers as well as on the modified membranes. FTIR spectra of S-P(PGE-*stat*-ECH) along with final AIEM spectra is shown in Figure 74 B. The FTIR spectrum of the final AIEM shows the presence of a C-N stretch around 1630 cm<sup>-1</sup>, which confirms the presence of the imidazole group, while peaks at 716 cm<sup>-1</sup> and 760 cm<sup>-1</sup> correspond to stretching due to the presence of C-F in a DPVDF. The peak around 750 cm<sup>-1</sup>, corresponding to the chloromethyl group, has disappeared, indicating the successful modification

of the DPVDF with S-P(PGE-stat-ECH). Furthermore, the presence of peaks at 1186 and 1036 cm<sup>-1</sup> confirms the incorporation of sulfonate groups in the membrane. Taken together, the FTIR spectra suggests the successful click reaction of the pre-cursor polyether as well as the modification of DPVDF with the functionalized polyether.

The thermal properties of the modified membranes were characterized by DSC and TGA. DSC reveals a Tg shift to lower temperature and a suppression of the melting transition with increasing wt% of polyether; this is consistent with functionalization of the copolymer disrupting organization of the PVDF chains (in Figure 81). The thermal stability of prepared AIEMs was studied by TGA, similar to the copolymer degradation study described above (in Figure 82). The pristine DPVDF reveals a two-step weight loss, whereas different modified AIEM membranes reveal three-step weight loss. For DPVDF, the first step weight loss occurs at 300-400 °C due to the C-C and C-F bond cleavage, whereas the second step beyond 400 °C is due to polymer backbone degradation. In AIEM first step weight loss 100-150 °C is due to trapped moisture in the membrane matrix. The second step weight loss above 200 °C is attributed to the degradation of functional groups 'SO<sub>3</sub>H and 'N(CH<sub>3</sub>)<sub>3</sub>. The weight loss above the 600 °C is due to the polymer backbone degradation. High weight loss in the AIEM compared to DPVDF confirms the hydrophilic nature of AIEM.

The water contact angle (WCA) on the unmodified and modified membranes was characterized using goniometry. The hydrophilicity of the surface has an immense impact on separations involving water. Specifically, a very low WCA is highly desirable to ensure good surface wetting.<sup>47</sup> The measured contact angles are reported in Figure 75 A. As expected, the unmodified membrane shows a relatively high contact angle of 90°, consistent with a hydrophobic surface. Upon modification with the functionalized polyether, we see a limited change in WCA. At 1%,

the WCA is 83°, followed by 87° at 5% and 73° at 10%. While there is a decrease in WCA from 0% to 10% copolymer, the surface would still be considered relatively hydrophobic. We anticipated that functionalization with a charged copolymer would significantly increase the hydrophilicity of the surface, but this does not seem to be the case. As we will show later, while the surface hydrophilicity remains largely unchanged, there is a 5-fold increase in water uptake, suggesting that the PVDF has been successfully modified with hydrophilic polymer. This type of behavior is consistent with the behavior of other fluorinated membranes with grafted or pendant charged chains like Nafion 117, which shows a WCA of around 89.6° but high water uptake of 33%.48

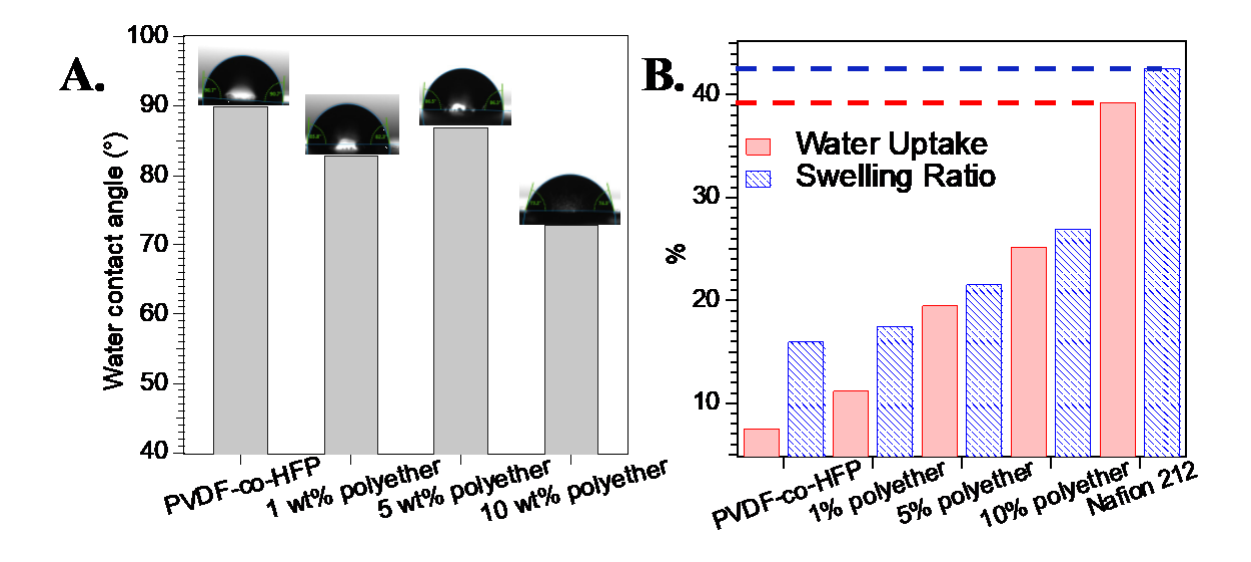


Figure 75: A. Contact angle measurements as a function of copolymer content. B. Water uptake red, left axis and swelling ratio blue, right axis as a function of copolymer content.

Water uptake and swelling ratio of membranes were characterized using method described in experimental section. Since water is critical for the formation of charge carriers, water uptake (WU) and swelling ratio (SR) significantly impact the ion transport in ion exchange membranes, and therefore, have been identified as one of the most important considerations for the AIEM which impact the suitability of a membrane for electrochemical applications. Figure 75 B shows

the water uptake and swelling ratio of the DPVDF and S-P(PGE-stat-ECH) membranes. Membranes absorb water depending on the hydrophilicity of the backbone polymer and the nature of the ionic groups attached to the polymer chains. As the charged polymer content increases, a commensurate increase in WU and SR are seen. Specifically, WU increases from 11.2% to 25.2%, while SR increases from 17.5 to 27. Therefore, a relatively small amount of functional copolymer more than doubles the WU. While this is favorable for ionic conductivity, it does come with unwanted swelling of the membrane. Compared to Nafion 212 these membranes showed significant reduction in WU as well as SR. Compared to other VRFB membranes, we see a middle of the road WU and SR of our membranes compared to the literature results. We anticipate that WU could be further improved through increased functional polymer grafting by incubating higher concentrations of polymer with the vinyl imidazole modified membrane. Furthermore, SR could be improved through a separate crosslinking step to mitigate potential swelling. These membranes are currently not optimized but have promising water interaction features.

Scanning electron microscopy (SEM) was performed to determine the membrane morphology. Figure 76 contains a representative SEM image of the AIEM with 10% copolymer. The surface of AIEM was found to be homogenous and densely-packed with no obvious micro-pores or dents. Furthermore, to confirm the presence of all the elements in the final membrane, EDS analysis was performed. The elemental mapping result is also shown in Figure 76 B. The results show the uniform and homogenous distribution of C (63.9%), O (7.5%) (due to the polyether backbone of copolymer), F (10.8%) (due to the PVDF-co-HFP backbone attached to the copolymer), N (12.7%) and S (4.5%) (due to the 1-vinylimidazole and propyl sulphonic acid) in the membrane matrix. This result confirms that the desired membrane was successfully synthesized with uniform distribution of the copolymer in the membranes.

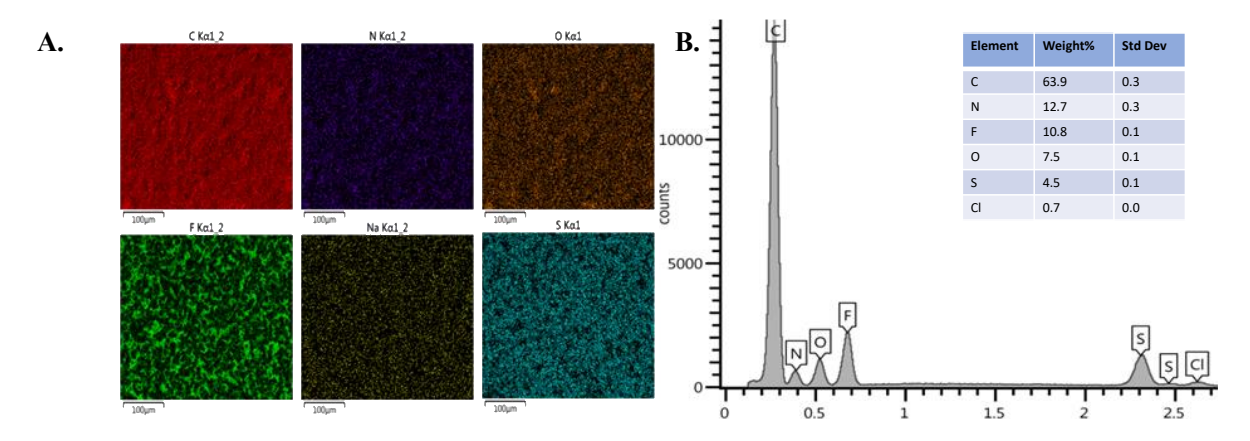


Figure 76: A. SEM image of the synthesized membrane with EDS analysis showing the position of the various elements. B. EDS analysis of the membranes with the percentages of the elements present. The elements and their respective ratios are consistent with the anticipated chemical make-up of the membrane

#### **Membrane Electrochemical Properties**

We characterized the ion exchange capacity (IEC) of the membranes. The IEC measures the density of exchangeable charged groups responsible for the ionic conduction. In case of AIEM, IEC depends on concentration of fixed charged functional moieties in the membrane phase. Thus, the AIEM is expected to exhibit cation- (H<sup>+</sup>), and anion-exchange capacity (OH<sup>-</sup>). For P-1%, P-5% and P-10% the CEC is 1.26, 1.40 and 1.65 meq/g, whereas the AEC is 0.84, 0.86 and 0.89 meq/g respectively. (Shown in Figure 77 A) The continuous increase in AEC and CEC is attributed to the presence of -NR<sub>3</sub> and-SO<sub>3</sub>H groups in the membranes. The IEC was comparable or better than many other membranes found in literature. For instance, at higher copolymer concentration, the CEC exhibited by AIEM rivaled that of commercial Nafion membranes, likely due to the double sulfonate groups per PGE monomer. Similarly, AIEM membrane outperformed few literature reported membranes in CEC.<sup>7,21</sup> Therefore, our membranes have very favorable IEC, making them promising as VRFB membranes.

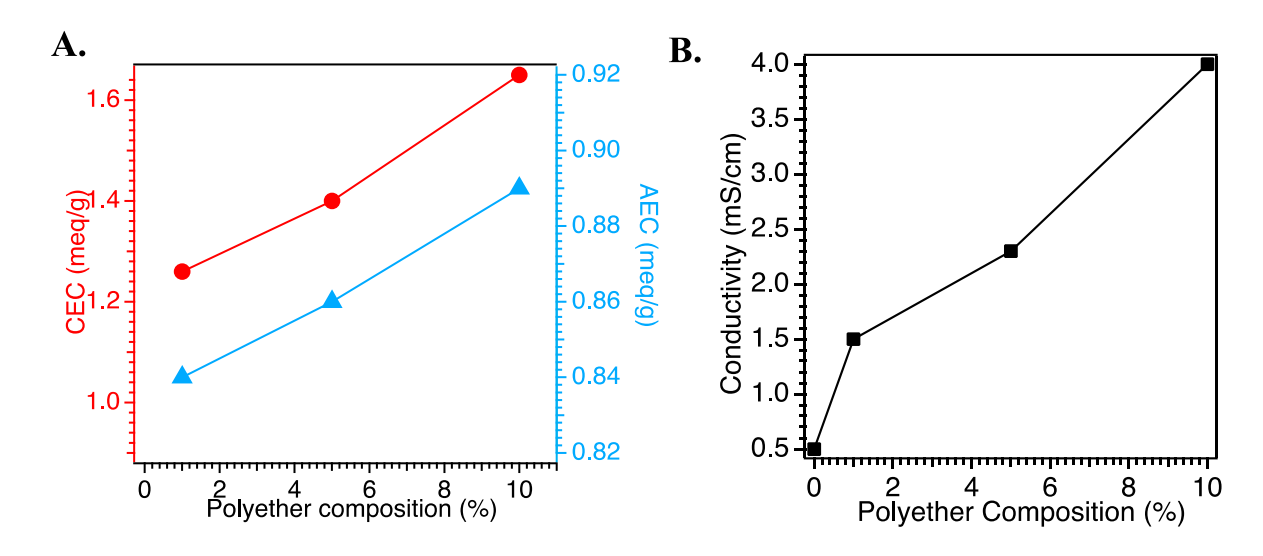


Figure 77: A. IEC B. Conductivity as a function of copolymer content. Generally, as copolymer content increases, conductivity, water uptake, and swelling ratio increase while contact angle decreases.

Table 2: Summary of membrane properties

Entry	Sample	CEC	AEC	Thickness	WU	SR
1	P-1%	1.26	0.84	150	11.2	17.49
2	P-5%	1.40	0.86	146	19.5	21.56
3	P-10%	1.65	0.89	151	25.2	26.96
a rea	 action condition: prist	ine membrane wa	as prepared o	on using 14 mg o	f MOB	

We characterized the ionic conductivity of the membranes. Membrane conductivity ( $\kappa_m$ ) depends on the molality of dissociable functional groups and is one of the most significant factors for defining the performance of AIEMs. The membrane resistance ( $R_m$ ) was determined from electrochemical impedance spectroscopy, as the high-frequency x-axis intercept of Nyquist impedance plots. (Figure 84) For P-1%, P-5% and P-10% membrane ionic conductivity was found to be 1.5 x  $10^{-3}$  S/cm, 2.3 x  $10^{-3}$  S/cm and 4.0 x  $10^{-3}$  S/cm respectively (Figure 77 B). The ionic conductivity of prepared membrane increases due to the grafting of quaternary ammonium

moieties via side chain with -SO<sub>3</sub>H groups. This functional group moiety concentration increases with increasing the S-P(PGE-*stat*-ECH) content in the membrane. Ultimately, we see a 5-fold increase in ionic conductivity from 0.5 mS/cm for the unmodified membranes to 4.0 mS/cm for the 10% polyether. While this is low compared to Nafion, it is comparable to other PVDF-based membranes. We hypothesize that we can further increase the ionic conductivity through compositional control over the polyethers.

#### 4.4 Conclusion

In this work, we synthesized and characterized novel graft polymer membranes for electrochemical applications. By utilizing our robust epoxide polymerization method, we successfully synthesized polyether copolymers containing orthogonally addressable functional groups that we modified with charged moieties. We grafted these polymers to modified PVDF-co-HFP to create AIEMs which were thermally and mechanically stable. The membrane properties were modified by tuning copolymer content. We found a significant increase in water uptake, ionic conductivity, and IEC capacity with increased copolymer content, without a significant effect on stability. These properties compared favorably with other membranes found in the literature and we anticipate that through optimization we can further enhance membrane performance.

#### BIBLIOGRAPHY

- (1) Sum, E.; Skyllas-Kazacos, M. A Study of the V(II)/V(III) Redox Couple for Redox Flow Cell Applications; 1985; Vol. 15.
- (2) Sum, E.; Rychcik, M.; Skyllas-Kazacos, M. Investigation of the V(V)/V(IV) System for Use in the Positive Half-Cell of a Redox Battery; 1985; Vol. 16.
- (3) Skyllas-Kazacos, M.; Chakrabarti, M. H.; Hajimolana, S. A.; Mjalli, F. S.; Saleem, M. Progress in Flow Battery Research and Development. *J Electrochem Soc* 2011, *158* (8), R55. https://doi.org/10.1149/1.3599565.
- (4) Rahman, F.; Skyllas-Kazacos, M. Vanadium Redox Battery: Positive Half-Cell Electrolyte Studies. *J Power Sources* 2009, *189* (2), 1212–1219. https://doi.org/10.1016/j.jpowsour.2008.12.113.
- (5) Gür, T. M. Review of Electrical Energy Storage Technologies, Materials and Systems: Challenges and Prospects for Large-Scale Grid Storage. *Energy and Environmental Science*. Royal Society of Chemistry October 1, 2018, pp 2696–2767. <a href="https://doi.org/10.1039/c8ee01419a">https://doi.org/10.1039/c8ee01419a</a>.
- (6) Shibata, A.; Sato, K. Development of Vanadium Redox Flow Battery for Electricity Storage. *Power Engineering Journal* 1999, 13 (3), 130–135. <a href="https://doi.org/10.1049/pe:19990305">https://doi.org/10.1049/pe:19990305</a>.
- (7) Shi, Y.; Eze, C.; Xiong, B.; He, W.; Zhang, H.; Lim, T. M.; Ukil, A.; Zhao, J. Recent Development of Membrane for Vanadium Redox Flow Battery Applications: A Review. *Applied Energy*. Elsevier Ltd March 15, 2019, pp 202–224. <a href="https://doi.org/10.1016/j.apenergy.2018.12.087">https://doi.org/10.1016/j.apenergy.2018.12.087</a>.
- (8) Li, X.; Zhang, H.; Mai, Z.; Zhang, H.; Vankelecom, I. Ion Exchange Membranes for Vanadium Redox Flow Battery (VRB) Applications. *Energy and Environmental Science*. April 2011, pp 1147–1160. <a href="https://doi.org/10.1039/c0ee00770f">https://doi.org/10.1039/c0ee00770f</a>.
- (9) Prifti, H.; Parasuraman, A.; Winardi, S.; Lim, T. M.; Skyllas-Kazacos, M. Membranes for Redox Flow Battery Applications. *Membranes*. MDPI AG 2012, pp 275–306. <a href="https://doi.org/10.3390/membranes2020275">https://doi.org/10.3390/membranes2020275</a>.
- (10) Schwenzer, B.; Zhang, J.; Kim, S.; Li, L.; Liu, J.; Yang, Z. Membrane Development for Vanadium Redox Flow Batteries. *ChemSusChem*. Wiley-VCH Verlag October 17, 2011, pp 1388–1406. <a href="https://doi.org/10.1002/cssc.201100068">https://doi.org/10.1002/cssc.201100068</a>.
- (11) Zhang, D.; Xu, Z.; Zhang, X.; Zhao, L.; Zhao, Y.; Wang, S.; Liu, W.; Che, X.; Yang, J.; Liu, J.; Yan, C. Oriented Proton-Conductive Nanochannels Boosting a Highly Conductive Proton-Exchange Membrane for a Vanadium Redox Flow Battery. ACS Appl Mater Interfaces 2021, 13 (3), 4051–4061. <a href="https://doi.org/10.1021/acsami.0c20847">https://doi.org/10.1021/acsami.0c20847</a>.

- (12) Yuan, Z.; Zhang, H.; Li, X. Ion Conducting Membranes for Aqueous Flow Battery Systems. *Chemical Communications* 2018, 54 (55), 7570–7588. <a href="https://doi.org/10.1039/C8CC03058H">https://doi.org/10.1039/C8CC03058H</a>.
- (13) Zhang, Q.; Wang, Q.; Huang, S.; Jiang, Y.; Chen, Z. Preparation and Electrochemical Study of PVDF-HFP/LATP/g-C3N4 Composite Polymer Electrolyte Membrane. *Inorg Chem Commun* 2021, *131*. <a href="https://doi.org/10.1016/j.inoche.2021.108793">https://doi.org/10.1016/j.inoche.2021.108793</a>.
- (14) Li, Z.; Xi, J.; Zhou, H.; Liu, L.; Wu, Z.; Qiu, X.; Chen, L. Preparation and Characterization of Sulfonated Poly(Ether Ether Ketone)/Poly(Vinylidene Fluoride) Blend Membrane for Vanadium Redox Flow Battery Application. *J Power Sources* 2013, 237, 132–140. <a href="https://doi.org/10.1016/j.jpowsour.2013.03.016">https://doi.org/10.1016/j.jpowsour.2013.03.016</a>.
- (15) Cao, J.; Yuan, Z.; Li, X.; Xu, W.; Zhang, H. Hydrophilic Poly(Vinylidene Fluoride) Porous Membrane with Well Connected Ion Transport Networks for Vanadium Flow Battery. *J Power Sources* 2015, 298, 228–235. <a href="https://doi.org/10.1016/j.jpowsour.2015.08.067">https://doi.org/10.1016/j.jpowsour.2015.08.067</a>.
- (16) Zhou, Y.; Qiu, P.; Ma, Y.; Zhang, X.; Xu, D.; Lin, J.; Tang, Y.; Wang, F.; He, X.; Zhou, Z.; Sun, N.; Sun, D. BaTiO3/PVDF-g-PSSA Composite Proton Exchange Membranes for Vanadium Redox Flow Battery. In *Ceramics International*; Elsevier Ltd, 2015; Vol. 41, pp S758–S762. <a href="https://doi.org/10.1016/j.ceramint.2015.03.131">https://doi.org/10.1016/j.ceramint.2015.03.131</a>.
- (17) Tian, B.; Wang, X. Y.; Zhang, L. N.; Shi, F. N.; Zhang, Y.; Li, S. X. Preparation of PVDF Anionic Exchange Membrane by Chemical Grafting of GMA onto PVDF Macromolecule. *Solid State Ion* 2016, 293, 56–63. https://doi.org/10.1016/j.ssi.2016.06.006.
- (18) Qiu, J.; Zhang, J.; Chen, J.; Peng, J.; Xu, L.; Zhai, M.; Li, J.; Wei, G. Amphoteric Ion Exchange Membrane Synthesized by Radiation-Induced Graft Copolymerization of Styrene and Dimethylaminoethyl Methacrylate into PVDF Film for Vanadium Redox Flow Battery Applications. *J. Memb. Sci.* 2009, 334 (1–2), 9–15. <a href="https://doi.org/10.1016/j.memsci.2009.02.009">https://doi.org/10.1016/j.memsci.2009.02.009</a>.
- (19) Kreuer, K. D. Ion Conducting Membranes for Fuel Cells and Other Electrochemical Devices. *Chemistry of Materials*. January 14, 2014, pp 361–380. <a href="https://doi.org/10.1021/cm402742u">https://doi.org/10.1021/cm402742u</a>.
- (20) Varcoe, J. R.; Atanassov, P.; Dekel, D. R.; Herring, A. M.; Hickner, M. A.; Kohl, P. A.; Kucernak, A. R.; Mustain, W. E.; Nijmeijer, K.; Scott, K.; Xu, T.; Zhuang, L. Anion-Exchange Membranes in Electrochemical Energy Systems. *Energy and Environmental Science*. Royal Society of Chemistry October 1, 2014, pp 3135–3191. https://doi.org/10.1039/c4ee01303d.
- (21) Yuan, J.; Yu, C.; Peng, J.; Wang, Y.; Ma, J.; Qiu, J.; Li, J.; Zhai, M. Facile Synthesis of Amphoteric Ion Exchange Membrane by Radiation Grafting of Sodium Styrene Sulfonate and N,N-Dimethylaminoethyl Methacrylate for Vanadium Redox Flow Battery. *J Polym Sci A Polym Chem* 2013, *51* (24), 5194–5202. <a href="https://doi.org/10.1002/pola.26949">https://doi.org/10.1002/pola.26949</a>.

- (22) Liu, L.; Wang, C.; He, Z.; Das, R.; Dong, B.; Xie, X.; Guo, Z. An Overview of Amphoteric Ion Exchange Membranes for Vanadium Redox Flow Batteries. *Journal of Materials Science and Technology*. Chinese Society of Metals April 10, 2021, pp 212–227. <a href="https://doi.org/10.1016/j.jmst.2020.08.032">https://doi.org/10.1016/j.jmst.2020.08.032</a>.
- (23) Hu, G.; Wang, Y.; Ma, J.; Qiu, J.; Peng, J.; Li, J.; Zhai, M. A Novel Amphoteric Ion Exchange Membrane Synthesized by Radiation-Induced Grafting α-Methylstyrene and N,N-Dimethylaminoethyl Methacrylate for Vanadium Redox Flow Battery Application. J Memb Sci 2012, 407–408, 184–192. https://doi.org/10.1016/j.memsci.2012.03.042.
- (24) Qiu, J.; Zhao, L.; Zhai, M.; Ni, J.; Zhou, H.; Peng, J.; Li, J.; Wei, G. Pre-Irradiation Grafting of Styrene and Maleic Anhydride onto PVDF Membrane and Subsequent Sulfonation for Application in Vanadium Redox Batteries. *J Power Sources* 2008, *177* (2), 617–623. <a href="https://doi.org/10.1016/j.jpowsour.2007.11.089">https://doi.org/10.1016/j.jpowsour.2007.11.089</a>.
- (25) Kondratenko, M. S.; Karpushkin, E. A.; Gvozdik, N. A.; Gallyamov, M. O.; Stevenson, K. J.; Sergeyev, V. G. Influence of Aminosilane Precursor Concentration on Physicochemical Properties of Composite Nafion Membranes for Vanadium Redox Flow Battery Applications. *J. Power Sources* 2017, 340, 32–39. <a href="https://doi.org/10.1016/j.jpowsour.2016.11.045">https://doi.org/10.1016/j.jpowsour.2016.11.045</a>.
- (26) Parasuraman, A.; Lim, T. M.; Menictas, C.; Skyllas-Kazacos, M. Review of Material Research and Development for Vanadium Redox Flow Battery Applications. *Electrochimica Acta*. 2013, pp 27–40. <a href="https://doi.org/10.1016/j.electacta.2012.09.067">https://doi.org/10.1016/j.electacta.2012.09.067</a>.
- (27) Xu, J.; Dong, S.; Li, P.; Li, W.; Tian, F.; Wang, J.; Cheng, Q.; Yue, Z.; Yang, H. Novel Ether-Free Sulfonated Poly(Biphenyl) Tethered with Tertiary Amine Groups as Highly Stable Amphoteric Ionic Exchange Membranes for Vanadium Redox Flow Battery. *Chemical Engineering Journal* 2021, 424. <a href="https://doi.org/10.1016/j.cej.2021.130314">https://doi.org/10.1016/j.cej.2021.130314</a>.
- (28) Liao, J.; Chen, Q.; Pan, N.; Yu, X.; Gao, X.; Shen, J.; Gao, C. Amphoteric Blend Ion-Exchange Membranes for Separating Monovalent and Bivalent Anions in Electrodialysis. *Sep Purif Technol* 2020, 242. <a href="https://doi.org/10.1016/j.seppur.2020.116793">https://doi.org/10.1016/j.seppur.2020.116793</a>.
- (29) Neitzel, A. E.; Fang, Y. N.; Yu, B.; Rumyantsev, A. M.; De Pablo, J. J.; Tirrell, M. V. Polyelectrolyte Complex Coacervation across a Broad Range of Charge Densities. *Macromolecules* 2021, 54 (14), 6878–6890. <a href="https://doi.org/10.1021/acs.macromol.1c00703">https://doi.org/10.1021/acs.macromol.1c00703</a>.
- (30) Ferrier, R. C.; Imbrogno, J.; Rodriguez, C. G.; Chwatko, M.; Meyer, P. W.; Lynd, N. A. Four-Fold Increase in Epoxide Polymerization Rate with Change of Alkyl-Substitution on Mono-μ-Oxo-Dialuminum Initiators. *Polym Chem* 2017, 8 (31), 4503–4511. <a href="https://doi.org/10.1039/c7py00894e">https://doi.org/10.1039/c7py00894e</a>.
- (31) Rodriguez, C. G.; Ferrier, R. C.; Helenic, A.; Lynd, N. A. Ring-Opening Polymerization of Epoxides: Facile Pathway to Functional Polyethers via a Versatile Organoaluminum

- Initiator. *Macromolecules* 2017, 50 (8), 3121–3130. <a href="https://doi.org/10.1021/acs.macromol.7b00196">https://doi.org/10.1021/acs.macromol.7b00196</a>.
- (32) Imbrogno, J.; Ferrier, R. C.; Wheatle, B. K.; Rose, M. J.; Lynd, N. A. Decoupling Catalysis and Chain-Growth Functions of Mono(μ-Alkoxo)Bis(Alkylaluminums) in Epoxide Polymerization: Emergence of the N-Al Adduct Catalyst. *ACS Catal* 2018, 8 (9), 8796–8803. <a href="https://doi.org/10.1021/acscatal.8b02446">https://doi.org/10.1021/acscatal.8b02446</a>.
- (33) Shukla, G.; Ferrier, R. C. The Versatile, Functional Polyether, Polyepichlorohydrin: History, Synthesis, and Applications. *Journal of Polymer Science*. John Wiley and Sons Inc November 15, 2021, pp 2704–2718. <a href="https://doi.org/10.1002/pol.20210514">https://doi.org/10.1002/pol.20210514</a>.
- (34) Krimalowski, A.; Thelakkat, M. Sequential Co-Click Reactions with Poly(Glycidyl Propargyl Ether) toward Single-Ion Conducting Electrolytes. *Macromolecules* 2019. https://doi.org/10.1021/acs.macromol.9b00206.
- (35) Herzberger, J.; Leibig, D.; Langhanki, J.; Moers, C.; Opatz, T.; Frey, H. "Clickable PEG" via Anionic Copolymerization of Ethylene Oxide and Glycidyl Propargyl Ether. *Polym Chem* 2017, 8 (12), 1882–1887. https://doi.org/10.1039/c7py00173h.
- (36) Safaie, N.; Rawal, B.; Ohno, K.; Ferrier, R. C. Aluminum-Based Initiators from Thiols for Epoxide Polymerizations. *Macromolecules* 2020, 53 (19), 8181–8191. <a href="https://doi.org/10.1021/acs.macromol.0c00464">https://doi.org/10.1021/acs.macromol.0c00464</a>.
- (37) Safaie, N.; Smak, J.; DeJonge, D.; Cheng, S.; Zuo, X.; Ohno, K.; Ferrier, R. C. Facile Synthesis of Epoxide-Co-Propylene Sulphide Polymers with Compositional and Architectural Control. *Polym Chem* 2022. https://doi.org/10.1039/d2py00005a.
- (38) Hoogenboom, R. Thiol-Yne Chemistry: A Powerful Tool for Creating Highly Functional Materials. *Angewandte Chemie International Edition* 2010, 49 (20), 3415–3417. <a href="https://doi.org/10.1002/anie.201000401">https://doi.org/10.1002/anie.201000401</a>.
- (39) Lowe, A. B. Thiol-Yne 'Click'/Coupling Chemistry and Recent Applications in Polymer and Materials Synthesis and Modification. *Polymer*. Elsevier Ltd October 23, 2014, pp 5517–5549. <a href="https://doi.org/10.1016/j.polymer.2014.08.015">https://doi.org/10.1016/j.polymer.2014.08.015</a>.
- (40) Kempe, K.; Krieg, A.; Becer, C. R.; Schubert, U. S. "Clicking" on/with Polymers: A Rapidly Expanding Field for the Straightforward Preparation of Novel Macromolecular Architectures. *Chem Soc Rev* 2012, *41* (1), 176–191. <a href="https://doi.org/10.1039/c1cs15107j">https://doi.org/10.1039/c1cs15107j</a>.
- (41) Rajput, A.; Sharma, J.; Raj, S. K.; Kulshrestha, V. Dehydrofluorinated Poly(Vinylidene Fluoride-Co-Hexafluoropropylene) Based Crosslinked Cation Exchange Membrane for Brackish Water Desalination via Electrodialysis. *Colloids Surf A Physicochem Eng Asp* 2021, 630. https://doi.org/10.1016/j.colsurfa.2021.127576.

- (42) Sharma, P. P.; Yadav, V.; Rajput, A.; Kulshrestha, V. Acid Resistant PVDF Based Copolymer Alkaline Anion Exchange Membrane for Acid Recovery and Electrodialytic Water Desalination. *J Memb Sci* 2018, 563, 561–570. <a href="https://doi.org/10.1016/j.memsci.2018.06.016">https://doi.org/10.1016/j.memsci.2018.06.016</a>.
- (43) Singh, A. K.; Kumar, S.; Bhushan, M.; Shahi, V. K. High Performance Cross-Linked Dehydro-Halogenated Poly (Vinylidene Fluoride-Co-Hexafluoro Propylene) Based Anion-Exchange Membrane for Water Desalination by Electrodialysis. *Sep Purif Technol* 2020, 234. <a href="https://doi.org/10.1016/j.seppur.2019.116078">https://doi.org/10.1016/j.seppur.2019.116078</a>.
- (44) Francisco Malmonge, L.; Antonio Malmonge, J.; Katsumi Sakamoto, W. *Study of Pyroelectric Activity of PZT/PVDF-HFP Composite*; 2003; Vol. 6.
- (45) Green, M. D.; Allen, M. H.; Dennis, J. M.; Cruz, D. S. D. La; Gao, R.; Winey, K. I.; Long, T. E. Tailoring Macromolecular Architecture with Imidazole Functionality: A Perspective for Controlled Polymerization Processes. In *European Polymer Journal*; 2011; Vol. 47, pp 486–496. <a href="https://doi.org/10.1016/j.eurpolymj.2010.09.035">https://doi.org/10.1016/j.eurpolymj.2010.09.035</a>.
- (46) Stumphauser, T.; Kasza, G.; Domján, A.; Wacha, A.; Varga, Z.; Thomann, Y.; Thomann, R.; Pásztói, B.; Trötschler, T. M.; Kerscher, B.; Mülhaupt, R.; Iván, B. Nanoconfined Crosslinked Poly(Ionic Liquid)s with Unprecedented Selective Swelling Properties Obtained by Alkylation in Nanophase-Separated Poly(1-Vinylimidazole)-l-Poly(Tetrahydrofuran) Conetworks. *Polymers (Basel)* 2020, *12* (10), 1–20. <a href="https://doi.org/10.3390/polym12102292">https://doi.org/10.3390/polym12102292</a>.
- (47) Ismail, M. F.; Islam, M. A.; Khorshidi, B.; Tehrani-Bagha, A.; Sadrzadeh, M. Surface Characterization of Thin-Film Composite Membranes Using Contact Angle Technique: Review of Quantification Strategies and Applications. *Advances in Colloid and Interface Science*. Elsevier B.V. January 1, 2022. <a href="https://doi.org/10.1016/j.cis.2021.102524">https://doi.org/10.1016/j.cis.2021.102524</a>.
- (48) Lin, C. H.; Yang, M. C.; Wei, H. J. Amino-Silica Modified Nafion Membrane for Vanadium Redox Flow Battery. *J Power Sources* 2015, 282, 562–571. https://doi.org/10.1016/j.jpowsour.2015.02.102.

**NMR** 

## Synthesis of aluminum-based initiator-catalyst

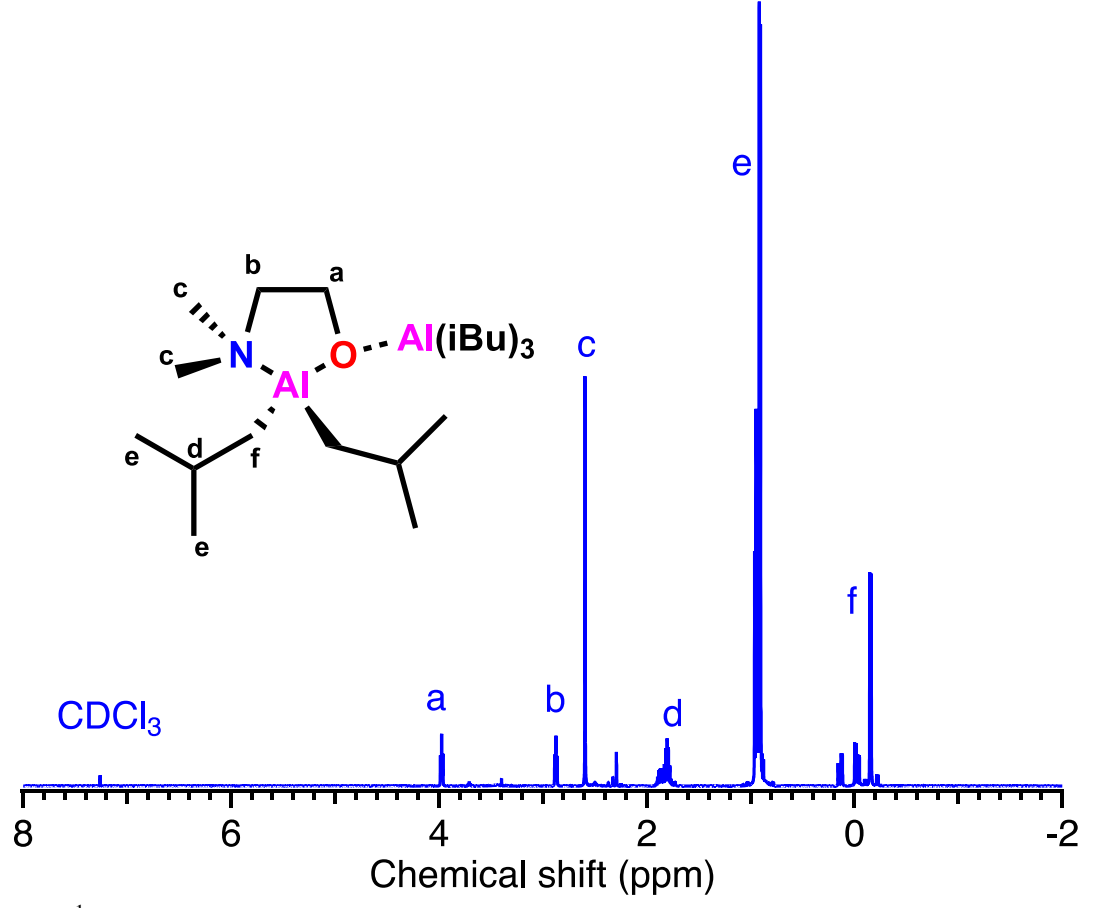


Figure 78: <sup>1</sup>H NMR in CDCl<sub>3</sub> of organo-aluminum catalyst-initiator used for polymerization

## Carbon NMR of P(PGE-stat-ECH)

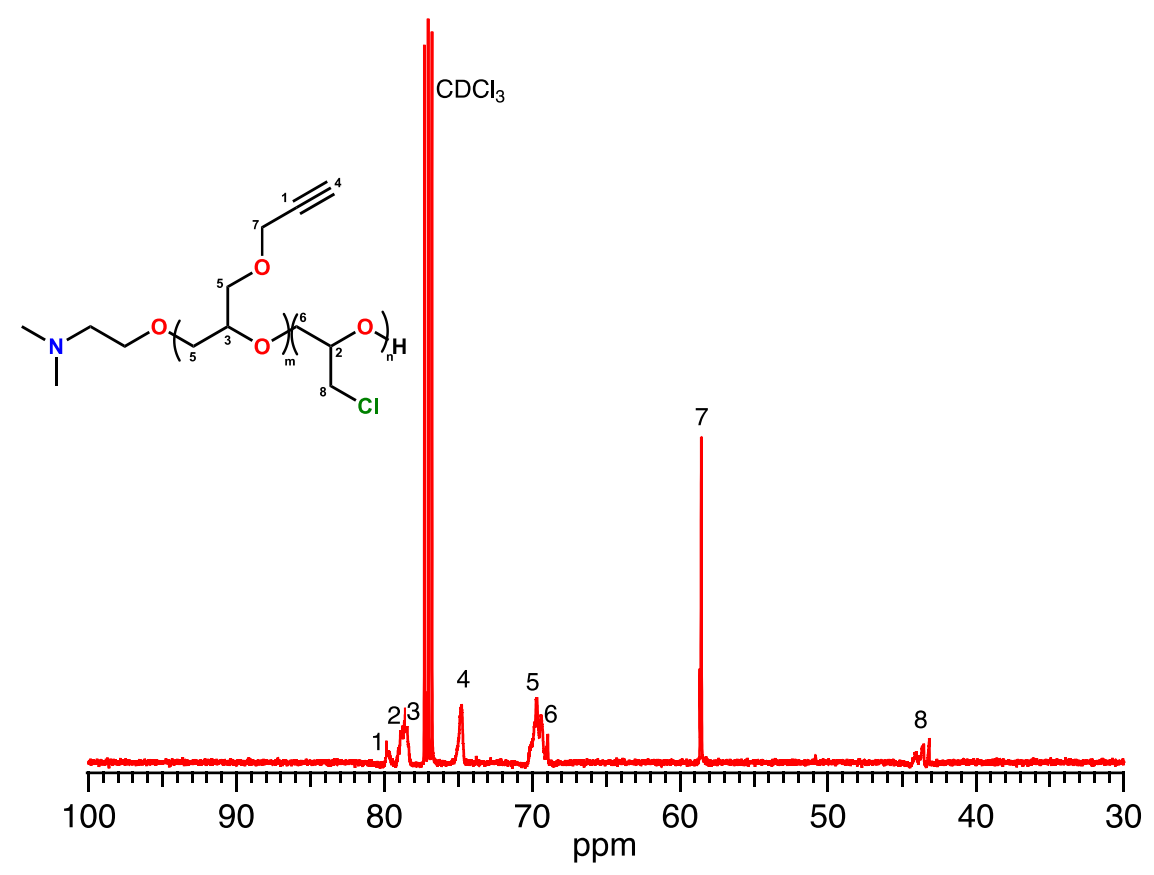


Figure 79: <sup>13</sup>C NMR of P(PGE-stat-ECH) in CDCl<sub>3</sub>

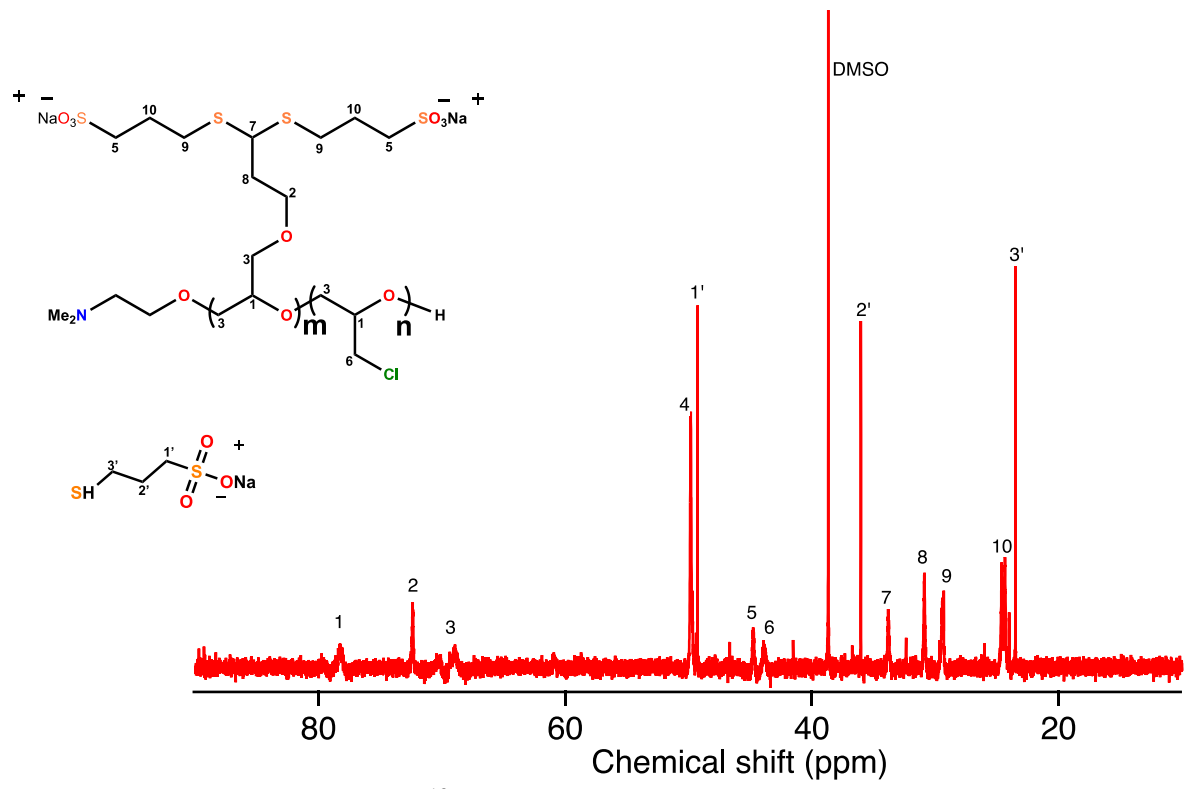


Figure 80: <sup>13</sup>C NMR of S-P(PGE-stat-ECH) in CDCl<sub>3</sub>

## **DSC**

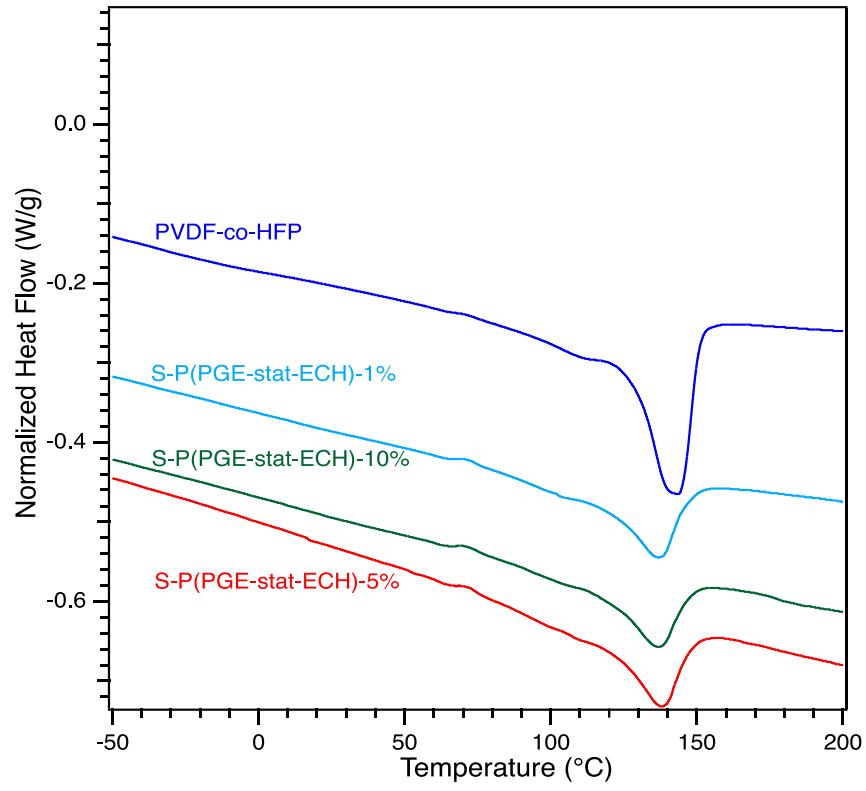


Figure 81: DSC traces from second heating cycle for unmodified and modified membrane

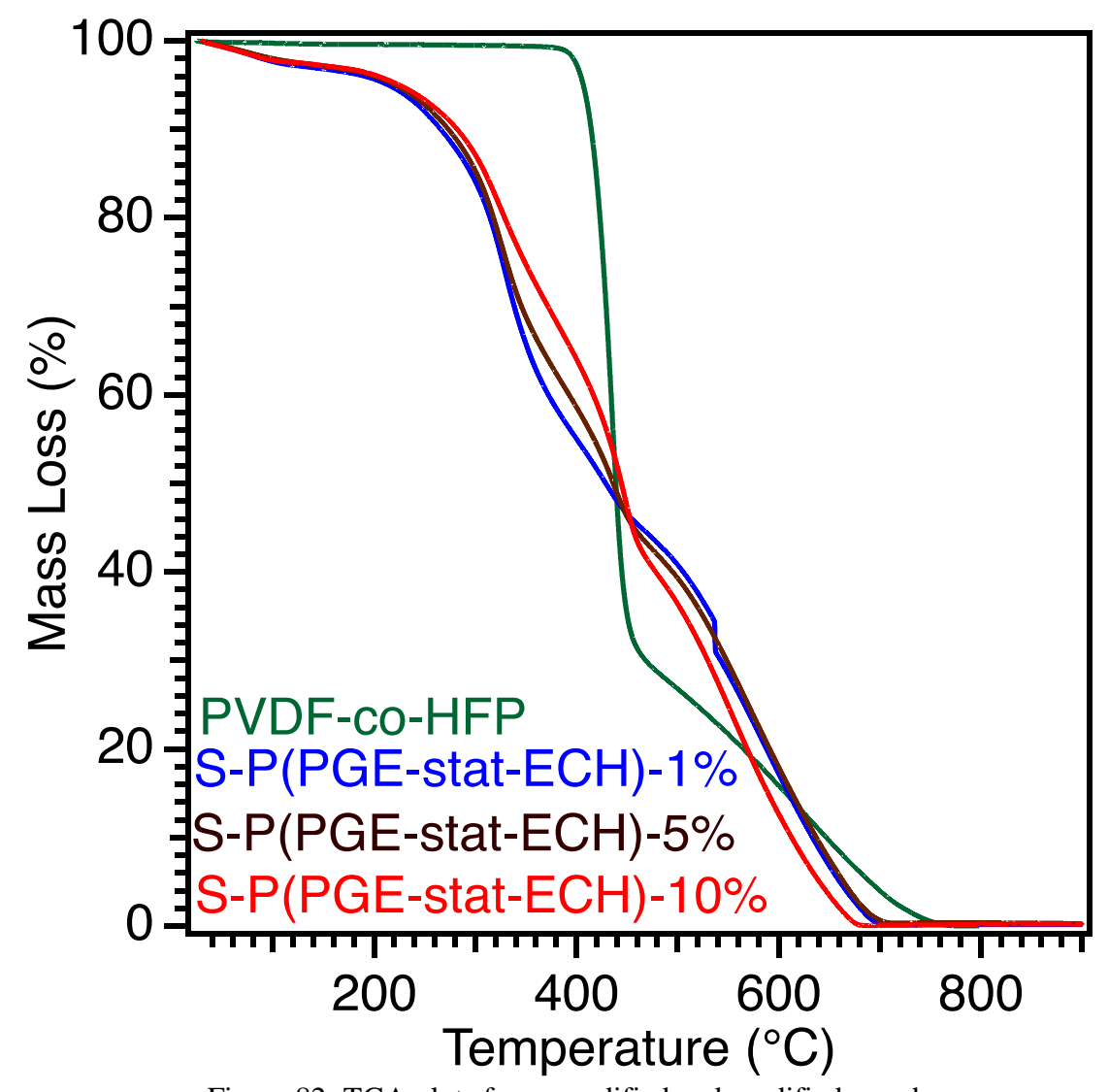


Figure 82: TGA plots for unmodified and modified membrane

## FTIR

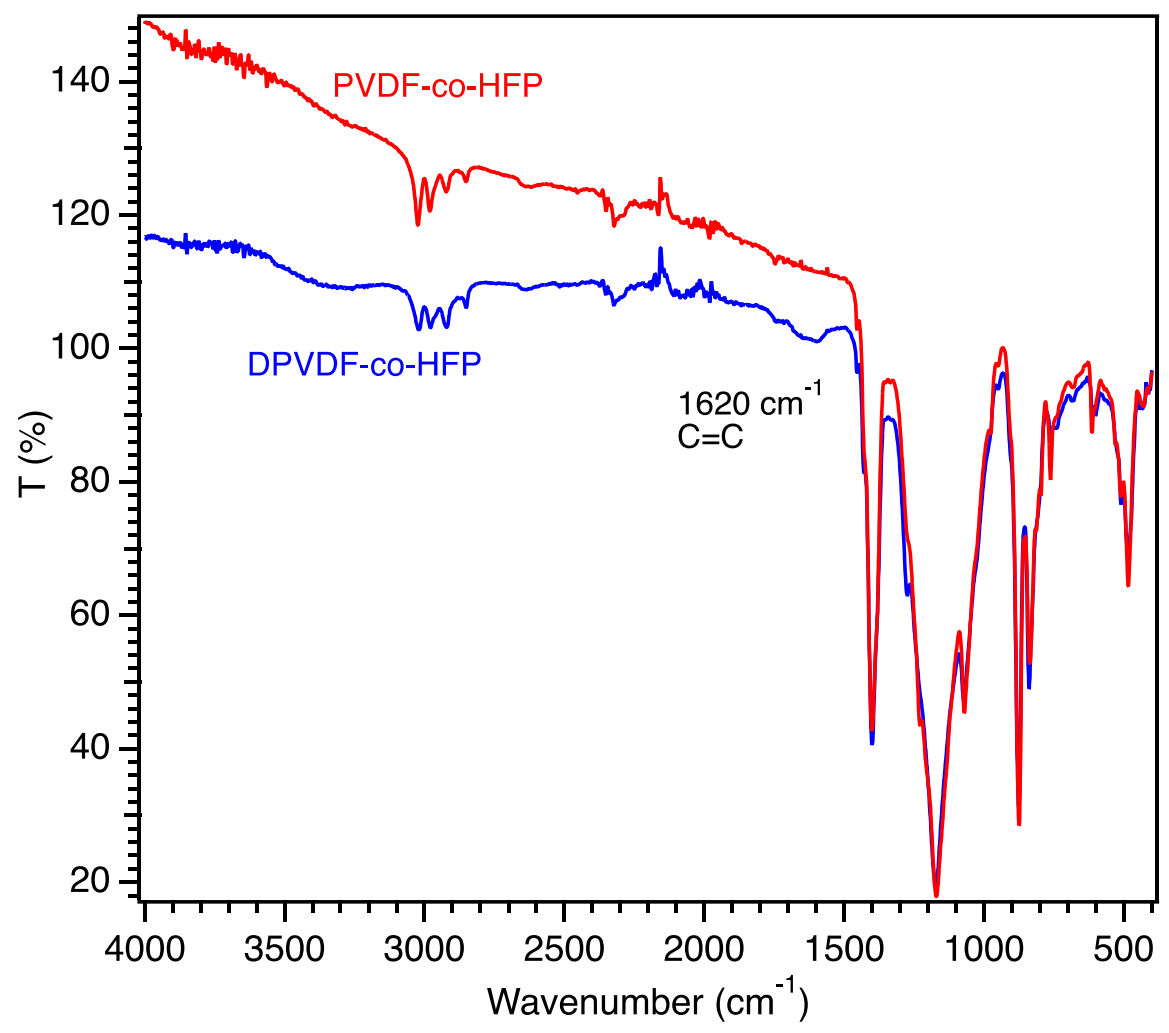


Figure 83: FTIR showing successful modification of PVDF to DPVDF

## EIS study: Nyquist plot

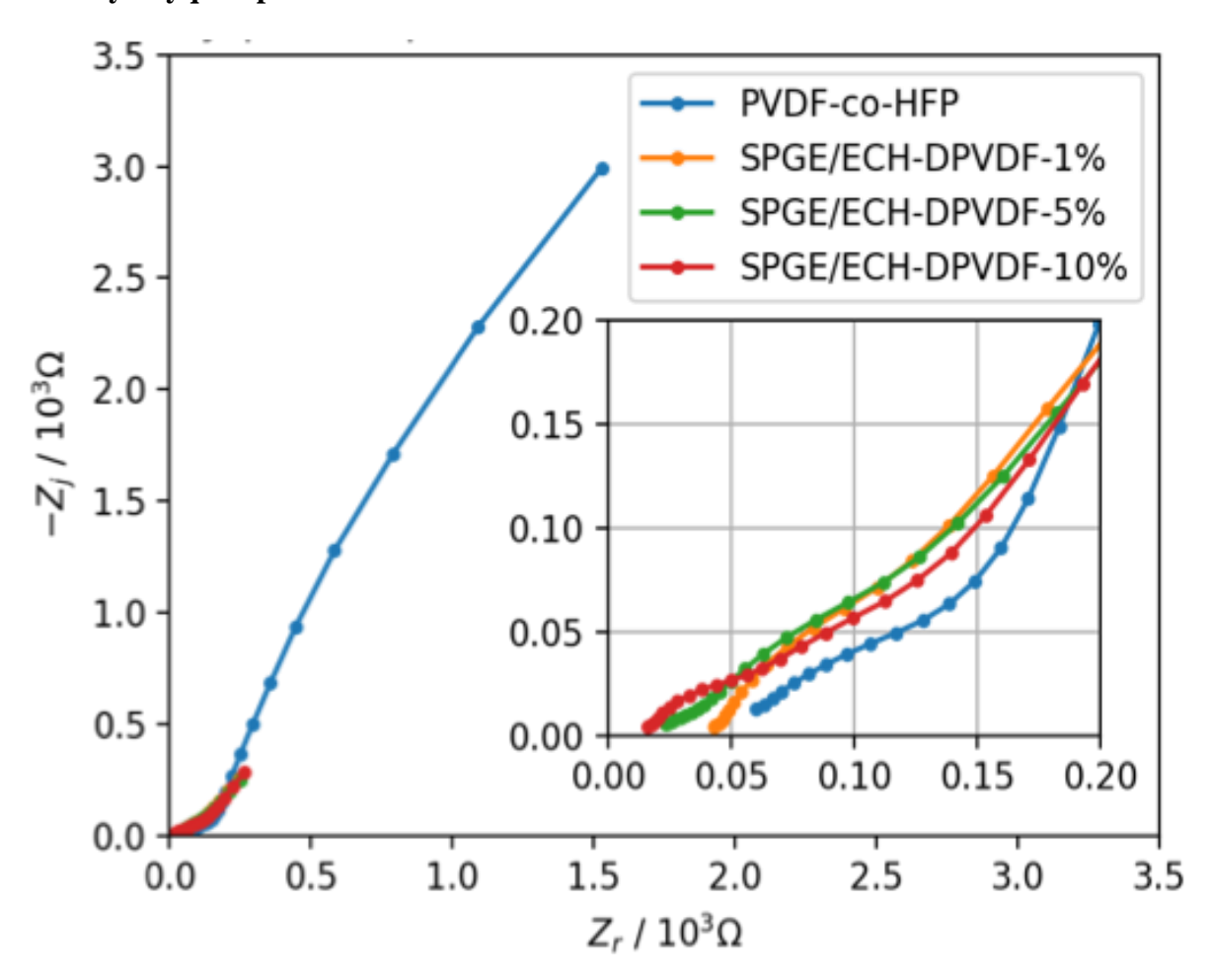


Figure 84: Nyquist plot for unmodified and modified membrane by EIS study

## Chapter 5. Design of tunable polyelectrolytes to study and control its self-assembly behavior

#### 5.1 Introduction

Complex coacervation phenomena occurs when homogeneous colloidal solution spontaneously separates into two separate liquid phases. In case of macromolecules like polyelectrolytes the dense phase which is polymer rich is known as coacervate. This will be in equilibrium with dilute phase which is polymer poor phase. This phenomenon is often driven by interactions between pair of oppositely charged macroions and their self-assembly. Coacervation results from a subtle balance of electrostatic interaction, hydrophobic associations, hydrogen bonds, van der Waals forces, and other weak interactions. Coacervation phenomena has been employed widely for extraction and enrichment of compounds from solvents due to its advantages. This methodology requires less use of organic solvents, simple to use, involves time/energy/cost-saving procedures, it can be easily controlled. This self-assembly behavior has been used for a wide range of applications such as underwater adhesives, drug delivery, food processing, and even for oil recovery. (Figure 85)

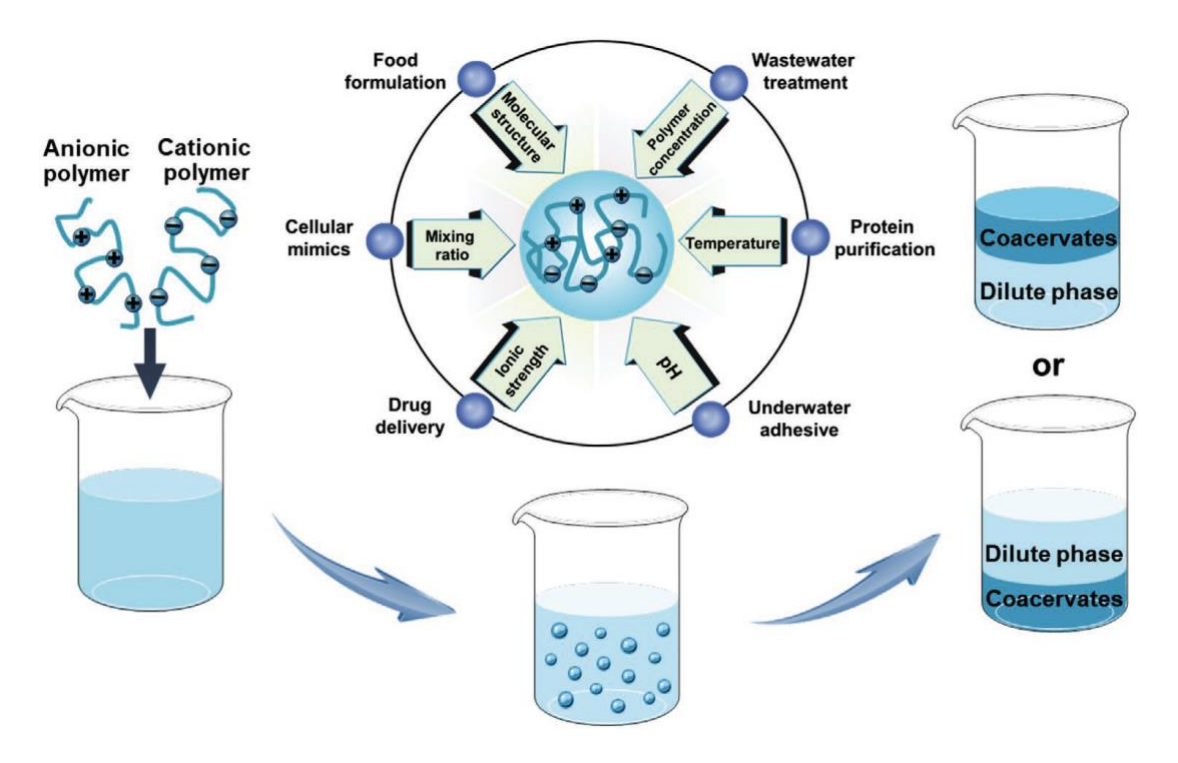


Figure 85: Schematic representation of applications and various parameters on the formation of coacervates<sup>1</sup>

Predicting the phase separation behavior is crucial to successful incorporation of polyelectrolytes for advanced applications. The thermodynamics of polyelectrolyte assembly has historically been described by simple Voorn-Overbeek theory.<sup>6</sup> This theory combines Flory–Huggins theory for the entropy term and the Debye–Hückel theory for electrical interaction term. It determines coacervation formation based on charge density and molecular weight (when  $\sigma^3 r \ge 0.53 \sigma$ , charge density and r, polymer molecular weight). However, Voorn-Overbeek, while convenient, is not applicable for many of the studies it is used to describe and only provides a qualitative picture of the strengths of the interactions. More recent theoretical work describes the thermodynamics of complex coacervation quantitatively to predict phase behavior and interaction strength.<sup>7-10</sup> This new theoretical work has resulted in more accurate matching between experimental and simulation thermodynamic data. However, the matching between experiment and simulation is still qualitative. We hypothesize that this mismatch between experiment and simulation is due to the

disparate chemical nature of the polyelectrolytes that have been studied and, therefore, a holistic approach to polyelectrolyte design is necessary to unify theory and experiment.

In this work, we propose to utilize a single, tunable, polymer platform to study and control the self-assembly of polyelectrolyte materials. The entire polyelectrolyte structure plays a role in the self-assembly of these polymers; the charge density, 11-13 monomer sequence, 7,9 polymer architecture,<sup>8</sup> molecular weight,<sup>14,15</sup> backbone,<sup>10,16</sup> charged moiety,<sup>17–19</sup> and counter-ion,<sup>10</sup> all affect the interactions between charged polymers. Unfortunately, the polyelectrolytes examined in the literature are chemically disparate due to limitations in polymer synthesis. So, while each of these parameters have been explored to some degree, they have not been investigated in the context of one single unified polymer platform.<sup>6,16,20</sup> Therefore, to improve current work in this field, we have utilized a single synthetic platform that can tune each parameter independently to understand and control polyelectrolyte self-assembly. MOB initiators give controlled molecular weight without any chain transfer for a range of functional epoxides. With this polyether synthesis process, we can achieve accurately controlled molecular weights without any chain transfer and controlled chain-end functionality. Even tailored architecture is possible using combinations of spacer monomer and multi-site initiator. <sup>21–26</sup> As demonstrated in chapter 3 various (co)polymers of allyl glycidyl ether (AGE), propargyl glycidyl ether (PGE) and epichlorohydrin (ECH) with functional alkene, alkyne, and chloromethyl groups respectively have been modified with the use of thiol-click chemistry.<sup>27,28</sup> In this work, we will use PAGE modified polyelectrolytes to study complex coacervation phenomena. Previous work has used allyl glycidyl ether (AGE) with a functional alkene to 'click' charged groups, but the molecular weights were limited and copolymers of PGE and ECH were inaccessible due to shortcomings of traditional anionic ring opening polymerization.<sup>29–31</sup> This platform has advantages as it allows control over parameters

such as molecular weight, charge density, monomer sequence, polymer architecture, and counterions independently through novel polymer synthesis. Using different functional thiols polyanion and polycations can be synthesized using different counterions.

The impact of this research stems from the fundamental insights into polyelectrolyte assembly, which will help fill in the gaps in the theory as well as provide new chemistries to be utilized in advanced applications. We expect the broader impacts of this research to encompass innovation in polyelectrolyte design and application.

#### 5.2 Experimental section

#### 5.2.1 Materials

Allyl glycidyl ether (Sigma-Aldrich, ≥99%), triisobutylaluminum (1.0 M in hexanes, Sigma-Aldrich), dimethyl ethanolamine (Sigma-Aldrich, >98%), sodium 3-mercapto-1-propane sulfonate (Sigma-Aldrich), cysteamine hydrochloride (Sigma-Aldrich), were all used as received. Chloroform-d (Cambridge Isotope Laboratories, Inc. 99.8%) and deuterium oxide (Cambridge Isotope Laboratories, Inc. 99.9%) were used without purification as NMR solvents.

Methanol (MeOH, Fisher, Certified ACS), hexane (Fisher, Certified ACS) and dichloromethane (DCM, Fisher, Certified ACS) were used for washing polymers. Reactions carried out in and ethanol (KOPTEC 200 proof pure ethanol) and water and precipitated in water. Free radical initiator 2,2'-Azobis(2-methylpropionitrile) (AIBN, Sigma-Aldrich 98%) was used for polymer modification. Glovebox was used to carry out all moisture and oxygen sensitive reactions under nitrogen environment. Regenerated cellulose dialysis tubing (Fisherbrand) with molecular weight cut off (MWCO) of 6-8k is used for dialysis.

Sodium chloride (NaCl) and lithium chloride (LiCl) salts were used to study their effect on complex coacervation. All samples were prepared in milli-Q water (resistivity of 17.5 M $\Omega$  cm, Thermo-scientific)

#### 5.2.2 Instrumentation

<sup>1</sup>H NMR spectroscopy was performed on Agilent DDR2 500 MHz NMR spectrometer using deuterated solvents at room temperature. The chemical shifts are reported in parts per million (ppm) and are referenced using the residual <sup>1</sup>H peak from the deuterated solvent.

Differential scanning calorimetric (DSC) tests were carried out on a TA250 instrument with a heating rate of 10  $^{\circ}$ C min<sup>-1</sup> under a N<sub>2</sub> atmosphere, and the data from the second heating curve was used for further analysis.

Absorbance was measured using on rapid scanning monochromator with fixed high voltage using 3 scans with scan rate of 1 scan/sec and for wavelength range between 450 nm to 550 nm (For plotting absorbance at 500 nm was used).

#### 5.2.3 Methods

# Synthesis of triisobutylaluminum adduct of (2-dimethylamino)ethoxy-diisobutylaluminum (MOB)

1.0 M tri-isobutylaluminum in hexane (12.7 mL, 12.7mmol) was added to a reaction vial with magnetic stirrer and cooled to −78 °C using liquid nitrogen blanket under dry nitrogen environment inside glovebox. To this vial a ligand dimethylaminoethanol (4.7 mmol, 0.5 mL) was added dropwise. The reaction was carried out by continuous stirring until it warms to room temperature overnight. Next day stopped stirring and cooled down the reaction mixture again to −40°C to crystallize the desired product. These crystals were then washed with anhydrous hexanes three times to remove excess reactant and dried under vacuum.

<sup>1</sup>H NMR (CDCl<sub>3</sub>, 500 MHz) δ 0.12 to -0.15 (m, -Al[-C $\underline{H}_2$ -CH-(CH<sub>3</sub>)<sub>2</sub>]<sub>2</sub>, and m, -Al[-C $\underline{H}_2$ -CH-(CH<sub>3</sub>)<sub>2</sub>]<sub>3</sub>), 0.92 (m, -Al[-CH<sub>2</sub>-CH-(C $\underline{H}_3$ )<sub>2</sub>]<sub>2</sub>, and m, -Al[-CH<sub>2</sub>-CH-(C $\underline{H}_3$ )<sub>2</sub>]<sub>3</sub>), 1.82 (m, -Al[-CH<sub>2</sub>-C $\underline{H}$ -(CH<sub>3</sub>)<sub>2</sub>]<sub>2</sub>, and m, -Al[-CH<sub>2</sub>-CH<sub>2</sub>-(CH<sub>3</sub>)<sub>2</sub>]<sub>3</sub>), 2.59 (s, N-(C $\underline{H}_3$ )<sub>2</sub>), 2.87 (t, N-C $\underline{H}_2$ -CH<sub>2</sub>-CH<sub>2</sub>-O), 3.97 (t, N-CH<sub>2</sub>-C $\underline{H}_2$ -O) (Figure 86)

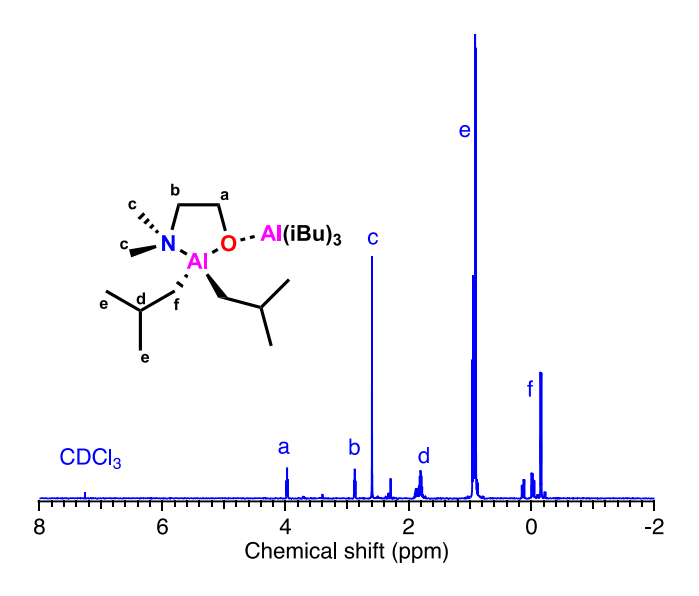


Figure 86: <sup>1</sup>H NMR of MOB in CDCl<sub>3</sub>

#### General procedure for polymerization using organo-aluminum catalyst-initiator system

All polymerizations were performed neat in a septum-capped 20 mL reaction vial under inert atmosphere in glovebox. The vials were charged with a stir bar, allyl glycidyl ether and organoaluminium based the initiator called Mono(μ-oxo)bis(alkyl aluminium) (MOB) to prepare 2 gm of final polymer weight. Initiator-catalyst amount was decided depending on targeted molecular weight. The solutions were then heated to the final reaction temperature of 50 °C and polymerizations were carried out for 48 hours (or until its >90% polymerized). Reactions were quenched with methanol and dissolved in dichloromethane to remove aluminum. The resulting solution was added dropwise into hexane to precipitate out the desired polymer product. The supernatant was removed, and then again washed the polymer with hexane (or any poor solvent)

for three times to remove residual catalyst. The polymer was first dried using rotary evaporator and then kept under vacuum overnight to remove excess solvent.

#### Polyanion (PA) synthesis using sodium 3-mercapto-1-propane sulfonate

Sodium 3-mercapto-1-propane sulfonate (3 equiv) was added to a vial containing poly(allyl glycidyl ether) (PAGE) (1 equiv alkene unit) and 2,2'-Azobis(2-methylpropionitrile) (AIBN; 2 wt%) in ethanol to water ratio of 3:2. The contents of the vial were degassed with  $N_2$  for 10 min. The mixture was then stirred and heated to 80 °C for 12 hours. The mixture was precipitated in DI water. The reaction mixture was diluted and extensively dialyzed against DI water. Dialysis is carried out using dialysis tubing (MWCO = 6-8 kg/mol, 3 cycles) against 1 L of water. Dialyzed solution was then dried in oven to obtain final purified product.

#### Polycation (PC) synthesis using cysteamine hydrochloride

Cysteamine hydrochloride (3 equiv) was added to a vial containing poly(allyl glycidyl ether) (PAGE) (1 equiv alkyne unit) and 2,2'-Azobis(2-methylpropionitrile) (AIBN; 2 wt%) in ethanol to water ratio of 60:40. The contents of the vial were degassed with N<sub>2</sub> for 10 min. The mixture was then stirred and heated to 80 °C for 12 hours. The mixture was precipitated in DI water. The reaction mixture was diluted and extensively dialyzed against DI water. Dialysis is carried out using dialysis tubing (MWCO = 6-8 kg/mol, 3 cycles) against 1 L of water. Dialyzed solution was then dried in oven to obtain final purified product.

#### Preparation of samples for absorbance measurements

Stock solutions of polyanion (PA) and polycation (PC) was prepared in milli-Q water with concentrations of 10mM with respect to the charged repeat units. Stock solutions of NaCl and LiCl were prepared in advance with varying concentrations from 0.5-4 M using millipore water.

The pH was adjusted to 7 using acidic (hydrochloric acid) and basic (sodium hydroxide) buffer solutions.

For complex coacervation study, freshly prepared samples were used with desired PA, PC and salt solution with total volume of 1000  $\mu$ L. The solution was homogenized completely and pipetted into the cuvette for absorbance testing. Coacervation formation was inspected with the help of turbidity measurements. The absorbance was measured for wavelength range of 450-550 nm and at temperature of 25 °C.

$$Turbidity = absorbance = -\ln\left(\frac{I}{I_0}\right)$$

Where I<sub>0</sub> is the incident light intensity, and I is the intensity of light passed through the sample.<sup>32</sup>

#### 5.3 Results and discussions

#### 5.3.1 Synthesis of polyanion and polycation

Precursor PAGE was synthesized using MOB system with targeted molecular weights of 10 kg/mol and 20 kg/mol. These precursors were then modified into PA and PC using thiol-ene click chemistry.<sup>31</sup> (Discussed in detail in chapter 3)

The precursor polymer was kept the same for PA and PC preparation and testing to ensure same number of repeat units hence same number of charged units for coacervation formation. This will eliminate effect due to chain length variation in PA and PC. The reaction scheme for precursor polymer synthesis and post-polymerization modification is given in Figure 87.

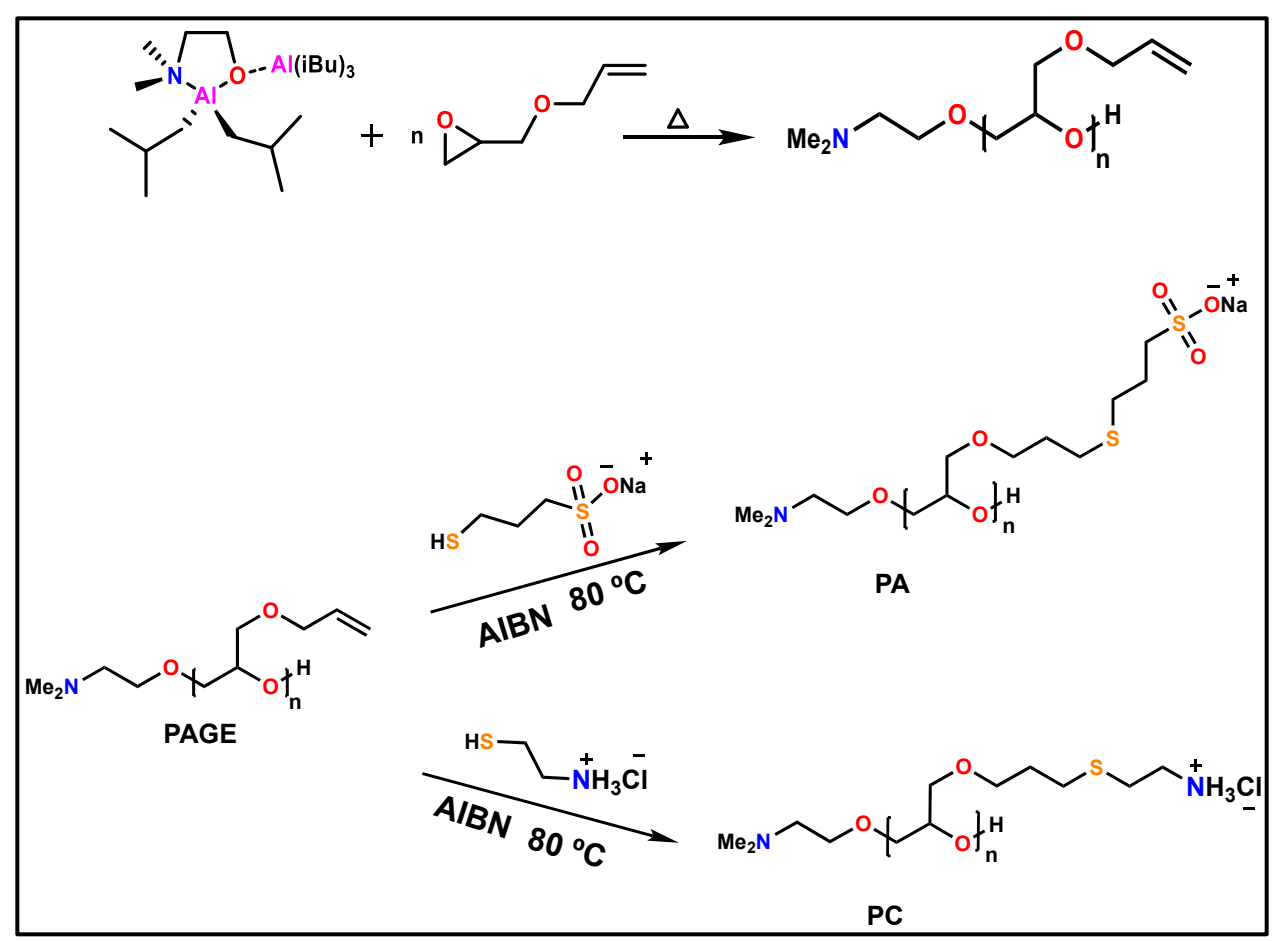


Figure 87: Reaction scheme for synthesizing polyelectrolytes

### 5.3.2 Characterization of polyanion and polycation

Precursor PAGE and thiol clicked PAGE was characterized using <sup>1</sup>H NMR spectroscopy.

The labelled spectra for 10 kg/mol polymers are shown in Figure 88. Similar results were obtained for 20 kg/mol polymers as well.

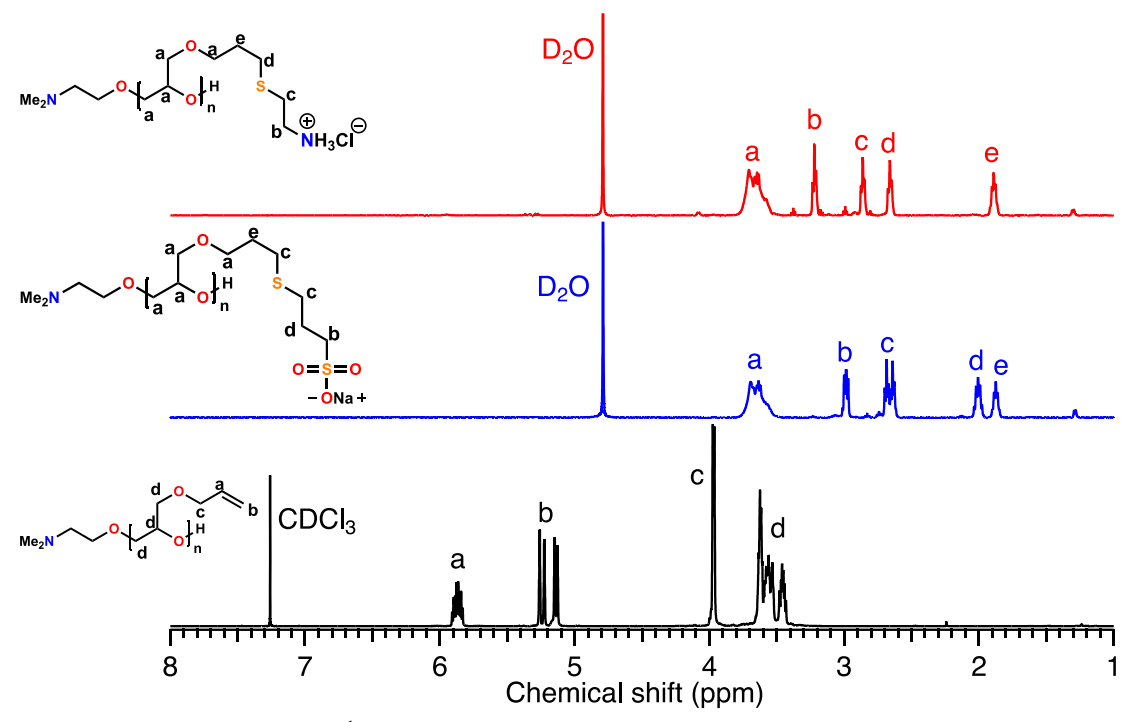


Figure 88: <sup>1</sup>H NMR spectra in CDCl<sub>3</sub> for PAGE, PA, and PC

These novel polyethers were then characterized using DSC thermograms to determine the glass transition temperature ( $T_g$ ). The data from the second heating curve was used for the analysis. Summary of results from DSC is given in following Table 3. This further confirms the successful modification of PAGE. With increase charged pendent groups the chain mobility is restricted which is reflected through  $T_g$  values. All the DSC traces are given in appendix Figure 92 and Figure 97.

Table 3: Summary of  $T_{\rm g}$  values for PAGE and polyelectrolytes from DSC data

Polymer	T <sub>g</sub> (°C)	
PAGE 10k	-74.45	
PAGE 20k	-74.26	
Thiol PA 10k	176.16	
Thiol PC 10k	24.39	
Thiol PA 20k	191.64	
Thiol PC 20k	27.29	

#### 5.3.3 Polyelectrolyte self-assembly studies

PAGE successfully. The self-assembly of the synthesized polyelectrolytes was characterized through turbidity measurements to determine phase transition conditions. When coacervates form, the solution becomes turbid or cloudy. The turbidity can be quantified as the change in transmission of light through the solution.<sup>32</sup> The binodal curve, that is the curve that separates the two-phase region from the single-phase region, can be identified through the turbidity change as a function of different parameters such as the polymer and salt concentration in the phases. The phase behavior for our synthesized polyelectrolyte will be correlated with molecular weight. The pKa values for these novel polymers are unknown which determines charge stoichiometry of these polymers and an important parameter which affects coacervation phenomena. So, to first start with complex coacervation study, we wanted to perform a preliminary test where we varied PA composition without NaCl addition and with 0.5 and 1 M NaCl addition for 10 kg/mol polymers. Coacervation results from a subtle balance of electrostatic interaction, hydrophobic associations, hydrogen bonds, van der Waals forces, and other weak interactions. It was believed that at equal concentrations of PA and PC we will have fully charged polyelectrolytes formation and hence maximum coacervation. As these are weak polyelectrolytes with only difference in charged pendent group, we observed a peak for absorbance at equal composition of PA and PC regardless of presence of NaCl. (Figure 89) This suggest that maximum coacervate formation happens when there is equal percentage of negatively and positively charged specifies. This will allow maximum polyelectrolyte interaction and the solution becomes turbid which can be seen even through naked eyes. (Figure 89)

As demonstrated in earlier sections, we obtained PA and PC starting from 10 kg/mol and 20 kg/mol

Now if we compare plots for no salt vs 0.5 or 1 M, the maximum coacervation happens at 50/50 ratio of PA/PC for all the cases. But the range of PA/PC composition where coacervation has been observed broadens. This type of effect has been reported by S. L. Perry, et. al. as well which is likely due to charge screening effects of NaCl arising due to its interaction with charged moieties causing imbalance of charges.<sup>32</sup>

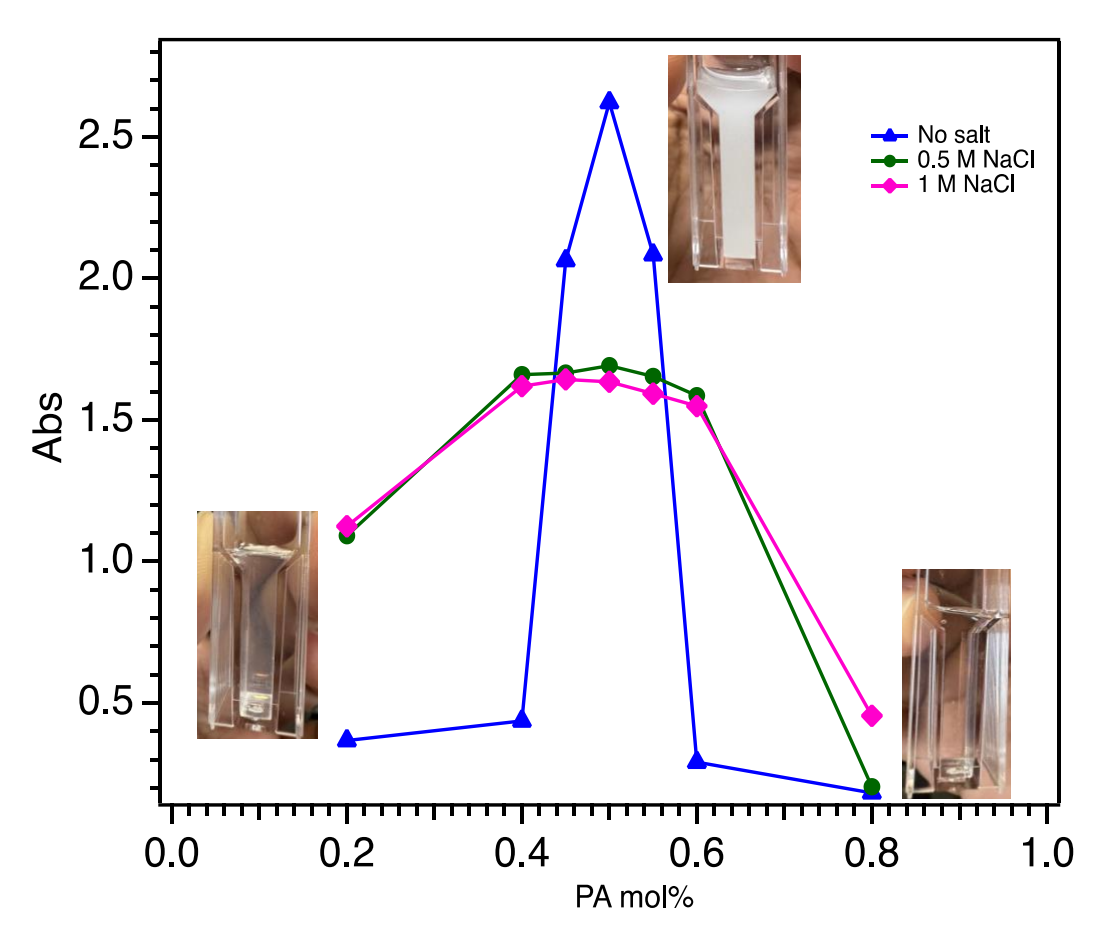


Figure 89: Plot of absorbance as a function of PA composition (for 10 kg/mol polymers)

Similar broadening effect was observed in case of LiCl salt addition as well. (Figure 90 A & B)

As polyether backbone chain is prone to have interactions with Li ions, which explains coacervation behavior over wide range of PA/PC composition for LiCl compared with NaCl.

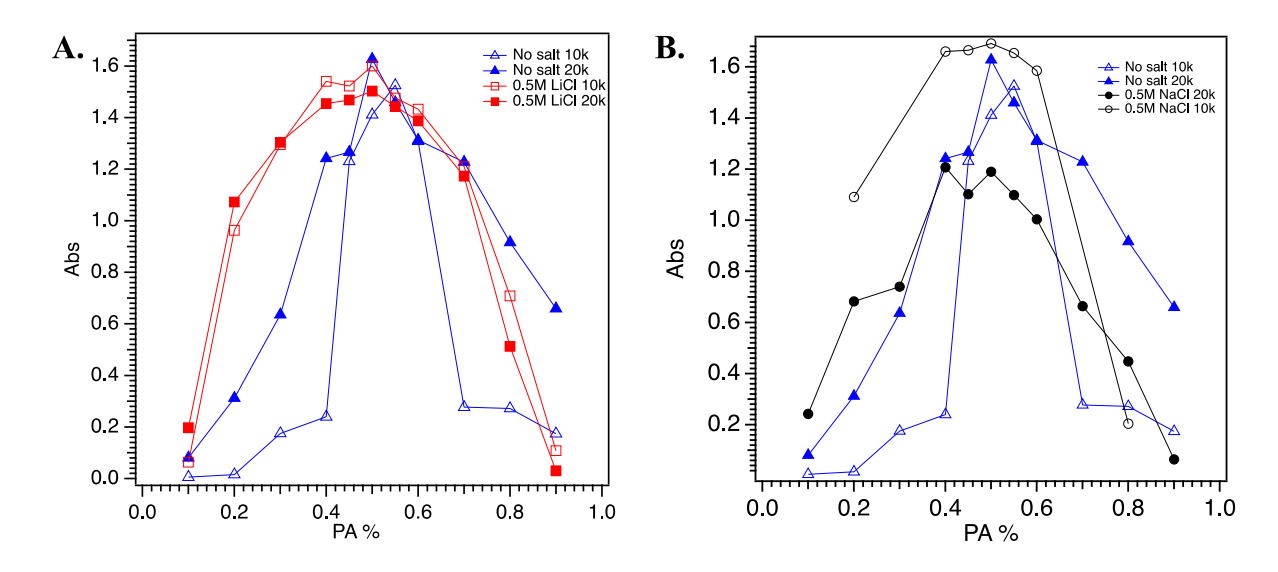


Figure 90: Plot of absorbance as a function of PA composition A. comparison of no salt vs LiCl B. comparison of no salt with NaCl

We observed a peak for 50/50 PA/PC composition for all the cases, so regardless of type of salt and molecular weights we observed similar behavior. Hence, we kept this maximum coacervation composition constant for next study.

Further we were interested in studying coacervation behavior as a function of NaCl and LiCl concentration. NaCl and LiCl were chosen to study effect of monovalent salts with same anionic counterpart and different cationic groups. According to literature, <sup>33–36</sup> with small addition of salt coacervation enhances but with subsequent increase in salt concentration polyelectrolyte interactions becomes difficult and we won't observe phase separation phenomena after a particular point. This concentration is known as critical salt concentration. Hofmeister series can explain strength of polymer-salt interaction. Kosmotrope are the ions which tends to enhance phase separation which results in increase in critical salt concentration. On the other hand, chaotropic ions reduces coacervation by increasing polymer-salt interaction with increase in salt concentration.<sup>32</sup> We have same anionic group in case of NaCl and LiCl salts. As we can see in the Figure 91 for both NaCl and LiCl we observe similar turbidity behavior. Which suggests effect of

cationic salt species is negligible. According to Hofmeister series, Na<sup>+</sup> and Li<sup>+</sup> have similar polymer-salt interactions which explains this behavior.<sup>37</sup>

Now let us consider effect of molecular weight irrespective of type of salt, we observed for higher molecular weight polyelectrolytes (20 kg/mol) coacervation persist even after 4 M salt addition contrast to low molecular weight polyelectrolytes (10 kg/mol) for which critical salt concentration is around 4 M. We can conclude that high molecular weight polyelectrolytes favor coacervate formation.

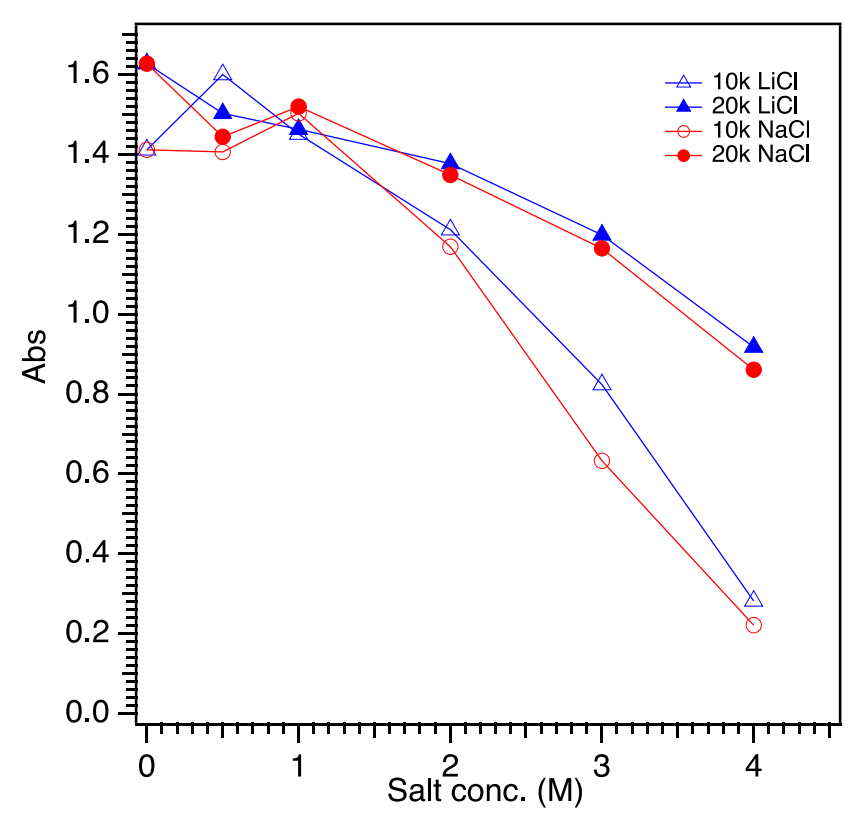


Figure 91: Absorbance measurement as function of increasing salt content (both NaCl and LiCl) keeping PA/PC ratio 50/50

#### 5.4 Conclusion

We have demonstrated a preliminary study to investigate polyelectrolyte self-assembly with the use of simple polyether PAGE. For this system, the maximum coacervation was observed at 50/50 ratio of polyanions and polycations consistent with literature. With addition of salts, we observed broadening in the range of PA/PC composition where coacervation happens which is likely due to charge screening effects of NaCl arising due to its interaction with charged moieties causing imbalance of charges. MOB system allows us to create polyelectrolytes with a multitude of chemical functionalities to investigate how charge, hydrophobicity, molecular weight, architecture, and specific interactions affect complexation. The work presented here will unite previous studies on polyelectrolyte self-assembly using a single, robust, polymerization platform, innovate through interaction design, and inform future theoretical considerations for polyelectrolyte self-assembly. Therefore, fundamental understanding of effect of each of these parameters on self- assembly will help us design these materials better for advanced application in future.

In summary, while the parameters that affect polyelectrolyte self-assembly have been studied before, the complete theoretical picture remains unclear thus the fundamental question of what controls self-assembly needs to be explored. These lingering questions are perhaps a result of the several disparate polymer systems that have been employed to study this phenomenon leading to inconsistencies that affect theory development. Therefore, a holistic approach to polyelectrolyte design that allows for precise tuning of structure and chemistry is necessary to further advance our understanding of polyelectrolyte assembly. This approach ensures that each parameter that affects polymer self-assembly can be decoupled and probed individually. Here, we promote polyether based unifying platform for polyelectrolyte design. This platform will be useful in

connecting the dots from theoretical correlation as well as experimental viewpoint.

## BIBLIOGRAPHY

- (1) Zhou, L.; Shi, H.; Li, Z.; He, C. Recent Advances in Complex Coacervation Design from Macromolecular Assemblies and Emerging Applications. *Macromolecular Rapid Communications*. Wiley-VCH Verlag November 1, 2020. <a href="https://doi.org/10.1002/marc.202000149">https://doi.org/10.1002/marc.202000149</a>.
- (2) Dompé, M.; Cedano-Serrano, F. J.; Vahdati, M.; Sidoli, U.; Heckert, O.; Synytska, A.; Hourdet, D.; Creton, C.; van der Gucht, J.; Kodger, T.; Kamperman, M. Tuning the Interactions in Multiresponsive Complex Coacervate-Based Underwater Adhesives. *Int J Mol Sci* 2020, *21* (1). <a href="https://doi.org/10.3390/ijms21010100">https://doi.org/10.3390/ijms21010100</a>.
- (3) Devi, N.; Sarmah, M.; Khatun, B.; Maji, T. K. Encapsulation of Active Ingredients in Polysaccharide–Protein Complex Coacervates. *Advances in Colloid and Interface Science*. Elsevier B.V. January 1, 2017, pp 136–145. <a href="https://doi.org/10.1016/j.cis.2016.05.009">https://doi.org/10.1016/j.cis.2016.05.009</a>.
- (4) Timilsena, Y. P.; Wang, B.; Adhikari, R.; Adhikari, B. Preparation and Characterization of Chia Seed Protein Isolate-Chia Seed Gum Complex Coacervates. *Food Hydrocoll* 2015, *52*, 554–563. https://doi.org/10.1016/j.foodhyd.2015.07.033.
- (5) Hu, M.; Guo, J.; Yu, Y.; Cao, L.; Xu, Y. Research Advances of Microencapsulation and Its Prospects in the Petroleum Industry. *Materials* 2017, *10* (4). <a href="https://doi.org/10.3390/ma10040369">https://doi.org/10.3390/ma10040369</a>.
- (6) Lytle, T. K.; Chang, L. W.; Markiewicz, N.; Perry, S. L.; Sing, C. E. Designing Electrostatic Interactions via Polyelectrolyte Monomer Sequence. *ACS Cent Sci* 2019, *5* (4), 709–718. https://doi.org/10.1021/acscentsci.9b00087.
- (7) Chang, L. W.; Lytle, T. K.; Radhakrishna, M.; Madinya, J. J.; Vélez, J.; Sing, C. E.; Perry, S. L. Sequence and Entropy-Based Control of Complex Coacervates. *Nat Commun* 2017, 8 (1). https://doi.org/10.1038/s41467-017-01249-1.
- (8) Johnston, B. M.; Johnston, C. W.; Letteri, R. A.; Lytle, T. K.; Sing, C. E.; Emrick, T.; Perry, S. L. The Effect of Comb Architecture on Complex Coacervation. *Org Biomol Chem* 2017, *15* (36), 7630–7642. <a href="https://doi.org/10.1039/c7ob01314k">https://doi.org/10.1039/c7ob01314k</a>.
- (9) Lytle, T. K.; Chang, L. W.; Markiewicz, N.; Perry, S. L.; Sing, C. E. Designing Electrostatic Interactions via Polyelectrolyte Monomer Sequence. *ACS Cent Sci* 2019, *5* (4), 709–718. <a href="https://doi.org/10.1021/acscentsci.9b00087">https://doi.org/10.1021/acscentsci.9b00087</a>.
- (10) Lytle, T. K.; Sing, C. E. Tuning Chain Interaction Entropy in Complex Coacervation Using Polymer Stiffness, Architecture, and Salt Valency. *Mol Syst Des Eng* 2018, *3* (1), 183–196. <a href="https://doi.org/10.1039/c7me00108h">https://doi.org/10.1039/c7me00108h</a>.

- (11) Hamad, F. G.; Chen, Q.; Colby, R. H. Linear Viscoelasticity and Swelling of Polyelectrolyte Complex Coacervates. *Macromolecules* 2018, *51* (15), 5547–5555. <a href="https://doi.org/10.1021/acs.macromol.8b00401">https://doi.org/10.1021/acs.macromol.8b00401</a>.
- (12) Huang, J.; Morin, F. J.; Laaser, J. E. Charge-Density-Dominated Phase Behavior and Viscoelasticity of Polyelectrolyte Complex Coacervates. *Macromolecules* 2019, 52 (13), 4957–4967. https://doi.org/10.1021/acs.macromol.9b00036.
- (13) Obermeyer, A. C.; Mills, C. E.; Dong, X. H.; Flores, R. J.; Olsen, B. D. Complex Coacervation of Supercharged Proteins with Polyelectrolytes. *Soft Matter* 2016, *12* (15), 3570–3581. <a href="https://doi.org/10.1039/c6sm00002a">https://doi.org/10.1039/c6sm00002a</a>.
- (14) Spruijt, E.; Westphal, A. H.; Borst, J. W.; Cohen Stuart, M. A.; Van Der Gucht, J. Binodal Compositions of Polyelectrolyte Complexes. *Macromolecules* 2010, *43* (15), 6476–6484. <a href="https://doi.org/10.1021/ma101031t">https://doi.org/10.1021/ma101031t</a>.
- (15) Souza, H. K. S.; Gončalves, M. D. P.; Gómez, J. Effect of Chitosan Degradation on Its Interaction with β-Lactoglobulin. *Biomacromolecules* 2011, *12* (4), 1015–1023. https://doi.org/10.1021/bm101356g.
- (16) Liu, Y.; Santa Chalarca, C. F.; Carmean, R. N.; Olson, R. A.; Madinya, J.; Sumerlin, B. S.; Sing, C. E.; Emrick, T.; Perry, S. L. Effect of Polymer Chemistry on the Linear Viscoelasticity of Complex Coacervates. *Macromolecules* 2020, *53* (18), 7851–7864. <a href="https://doi.org/10.1021/acs.macromol.0c00758">https://doi.org/10.1021/acs.macromol.0c00758</a>.
- (17) Sadman, K.; Wang, Q.; Chen, Y.; Keshavarz, B.; Jiang, Z.; Shull, K. *Influence of Hydrophobicity on Polyelectrolyte Complexation*.
- (18) Heo, T. Y.; Kim, I.; Chen, L.; Lee, E.; Lee, S.; Choi, S. H. Effect of Ionic Group on the Complex Coacervate Core Micelle Structure. *Polymers (Basel)* 2019, *11* (3). <a href="https://doi.org/10.3390/polym11030455">https://doi.org/10.3390/polym11030455</a>.
- (19) Lou, J.; Friedowitz, S.; Qin, J.; Xia, Y. Tunable Coacervation of Well-Defined Homologous Polyanions and Polycations by Local Polarity. *ACS Cent Sci* 2019, 5 (3), 549–557. <a href="https://doi.org/10.1021/acscentsci.8b00964">https://doi.org/10.1021/acscentsci.8b00964</a>.
- (20) Sing, C. E.; Perry, S. L. Recent Progress in the Science of Complex Coacervation. *Soft Matter* 2020, *16* (12), 2885–2914. <a href="https://doi.org/10.1039/d0sm00001a">https://doi.org/10.1039/d0sm00001a</a>.
- (21) Safaie, N.; Rawal, B.; Ohno, K.; Ferrier, R. C. Aluminum-Based Initiators from Thiols for Epoxide Polymerizations. *Macromolecules* 2020, 53 (19), 8181–8191. https://doi.org/10.1021/acs.macromol.0c00464.
- (22) Imbrogno, J.; Ferrier, R. C.; Wheatle, B. K.; Rose, M. J.; Lynd, N. A. Decoupling Catalysis and Chain-Growth Functions of Mono(μ-Alkoxo)Bis(Alkylaluminums) in Epoxide

- Polymerization: Emergence of the N-Al Adduct Catalyst. *ACS Catal* 2018, 8 (9), 8796–8803. <a href="https://doi.org/10.1021/acscatal.8b02446">https://doi.org/10.1021/acscatal.8b02446</a>.
- (23) Safaie, N.; Smak, J.; DeJonge, D.; Cheng, S.; Zuo, X.; Ohno, K.; Ferrier, R. C. Facile Synthesis of Epoxide-Co-Propylene Sulphide Polymers with Compositional and Architectural Control. *Polym Chem* 2022. https://doi.org/10.1039/d2py00005a.
- (24) Rodriguez, C. G.; Ferrier, R. C.; Helenic, A.; Lynd, N. A. Ring-Opening Polymerization of Epoxides: Facile Pathway to Functional Polyethers via a Versatile Organoaluminum Initiator. *Macromolecules* 2017, 50 (8), 3121–3130. <a href="https://doi.org/10.1021/acs.macromol.7b00196">https://doi.org/10.1021/acs.macromol.7b00196</a>.
- (25) Ferrier, R. C.; Imbrogno, J.; Rodriguez, C. G.; Chwatko, M.; Meyer, P. W.; Lynd, N. A. Four-Fold Increase in Epoxide Polymerization Rate with Change of Alkyl-Substitution on Mono-μ-Oxo-Dialuminum Initiators. *Polym Chem* 2017, 8 (31), 4503–4511. <a href="https://doi.org/10.1039/c7py00894e">https://doi.org/10.1039/c7py00894e</a>.
- (26) Shukla, G.; Ferrier, R. C. The Versatile, Functional Polyether, Polyepichlorohydrin: History, Synthesis, and Applications. *Journal of Polymer Science*. John Wiley and Sons Inc November 15, 2021, pp 2704–2718. <a href="https://doi.org/10.1002/pol.20210514">https://doi.org/10.1002/pol.20210514</a>.
- (27) Krannig, K. S.; Huang, J.; Heise, A.; Schlaad, H. Photochemical Thiol-Yne Functionalization of Polypeptide Scaffolds. *Polym Chem* 2013, *4* (14), 3981–3986. <a href="https://doi.org/10.1039/c3py00428g">https://doi.org/10.1039/c3py00428g</a>.
- (28)Sprafke, J. K.; Spruell, J. M.; Mattson, K. M.; Montarnal, D.; McGrath, A. J.; Pötzsch, R.; Miyajima, D.; Hu, J.; Latimer, A. A.; Voit, B. I.; Aida, T.; Hawker, C. J. Revisiting Thiol-Yne Chemistry: Selective and Efficient Monoaddition for Block and Graft Copolymer Formation. Polym Sci $\boldsymbol{A}$ Polym Chem 2015, 53 319–326. J(2),https://doi.org/10.1002/pola.27345.
- (29) Krogstad, D. V.; Lynd, N. A.; Miyajima, D.; Gopez, J.; Hawker, C. J.; Kramer, E. J.; Tirrell, M. V. Structural Evolution of Polyelectrolyte Complex Core Micelles and Ordered-Phase Bulk Materials. *Macromolecules* 2014, 47 (22), 8026–8032. <a href="https://doi.org/10.1021/ma5017852">https://doi.org/10.1021/ma5017852</a>.
- (30) Hunt, J. N.; Feldman, K. E.; Lynd, N. A.; Deek, J.; Campos, L. M.; Spruell, J. M.; Hernandez, B. M.; Kramer, E. J.; Hawker, C. J. Tunable, High Modulus Hydrogels Driven by Ionic Coacervation. *Advanced Materials* 2011, *23* (20), 2327–2331. <a href="https://doi.org/10.1002/adma.201004230">https://doi.org/10.1002/adma.201004230</a>.
- (31) Kim, J. M.; Heo, T. Y.; Choi, S. H. Structure and Relaxation Dynamics for Complex Coacervate Hydrogels Formed by ABA Triblock Copolymers. *Macromolecules* 2020, *53* (21), 9234–9243. https://doi.org/10.1021/acs.macromol.0c01600.

- (32) Perry, S. L.; Li, Y.; Priftis, D.; Leon, L.; Tirrell, M. The Effect of Salt on the Complex Coacervation of Vinyl Polyelectrolytes. *Polymers (Basel)* 2014, 6 (6), 1756–1772. https://doi.org/10.3390/polym6061756.
- (33) Chollakup, R.; Smitthipong, W.; Eisenbach, C. D.; Tirrell, M. Phase Behavior and Coacervation of Aqueous Poly(Acrylic Acid)-Poly(Allylamine) Solutions. *Macromolecules* 2010, *43* (5), 2518–2528. <a href="https://doi.org/10.1021/ma902144k">https://doi.org/10.1021/ma902144k</a>.
- (34) Chollakup, R.; Beck, J. B.; Dirnberger, K.; Tirrell, M.; Eisenbach, C. D. Polyelectrolyte Molecular Weight and Salt Effects on the Phase Behavior and Coacervation of Aqueous Solutions of Poly(Acrylic Acid) Sodium Salt and Poly(Allylamine) Hydrochloride. *Macromolecules* 2013, 46 (6), 2376–2390. <a href="https://doi.org/10.1021/ma202172q">https://doi.org/10.1021/ma202172q</a>.
- (35) Priftis, D.; Tirrell, M. Phase Behaviour and Complex Coacervation of Aqueous Polypeptide Solutions. *Soft Matter* 2012, 8 (36), 9396–9405. https://doi.org/10.1039/c2sm25604e.
- (36) Priftis, D.; Megley, K.; Laugel, N.; Tirrell, M. Complex Coacervation of Poly(Ethylene-Imine)/Polypeptide Aqueous Solutions: Thermodynamic and Rheological Characterization. *J Colloid Interface Sci* 2013, 398, 39–50. https://doi.org/10.1016/j.jcis.2013.01.055.
- (37) Kang, B.; Tang, H.; Zhao, Z.; Song, S. Hofmeister Series: Insights of Ion Specificity from Amphiphilic Assembly and Interface Property. *ACS Omega*. American Chemical Society March 31, 2020, pp 6229–6239. <a href="https://doi.org/10.1021/acsomega.0c00237">https://doi.org/10.1021/acsomega.0c00237</a>.

## APPENDIX

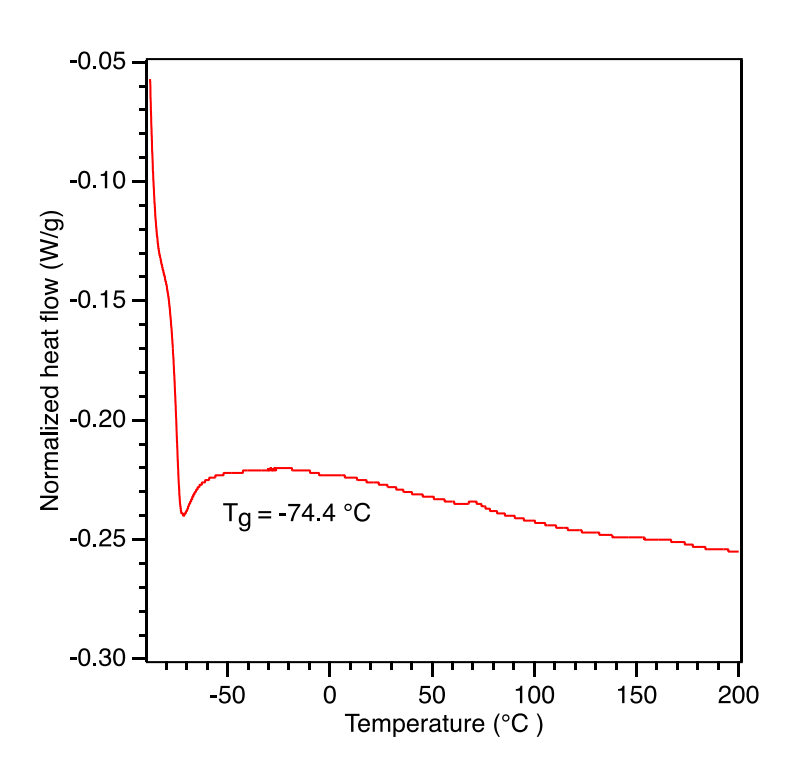


Figure 92: DSC data for PAGE-10 kg/mol

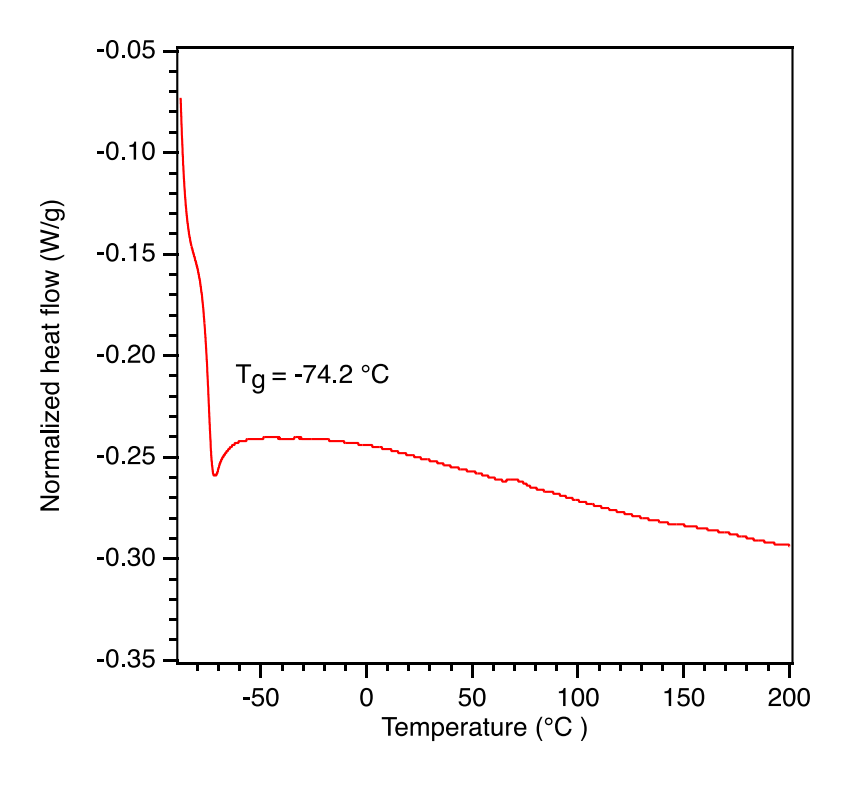


Figure 93: DSC data for PAGE-20 kg/mol

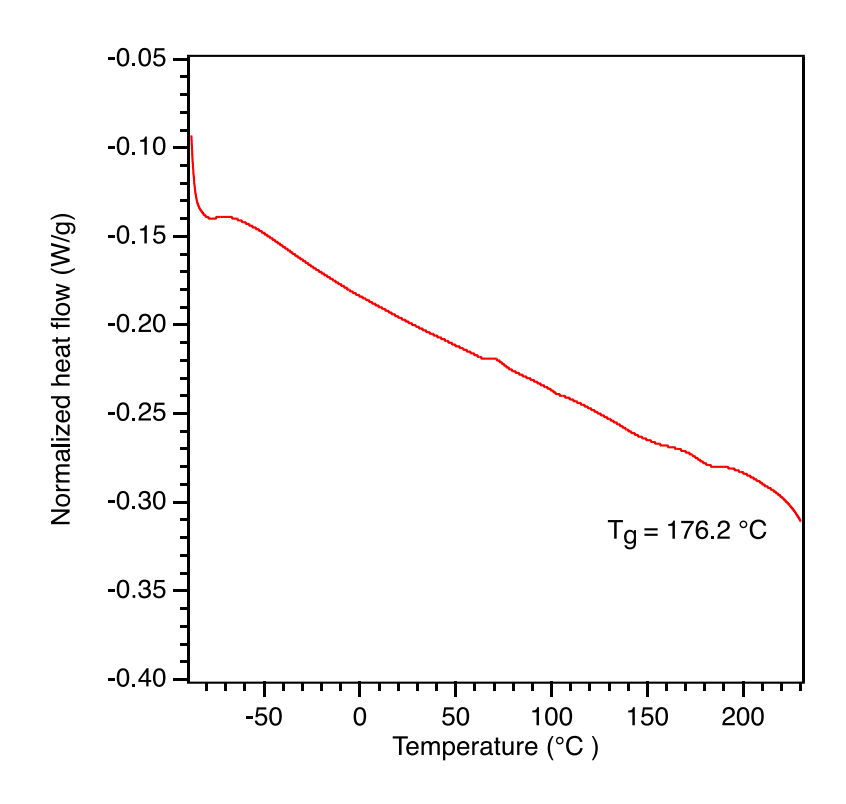


Figure 94: DSC data for Polyanion obtained from PAGE-10 kg/mol

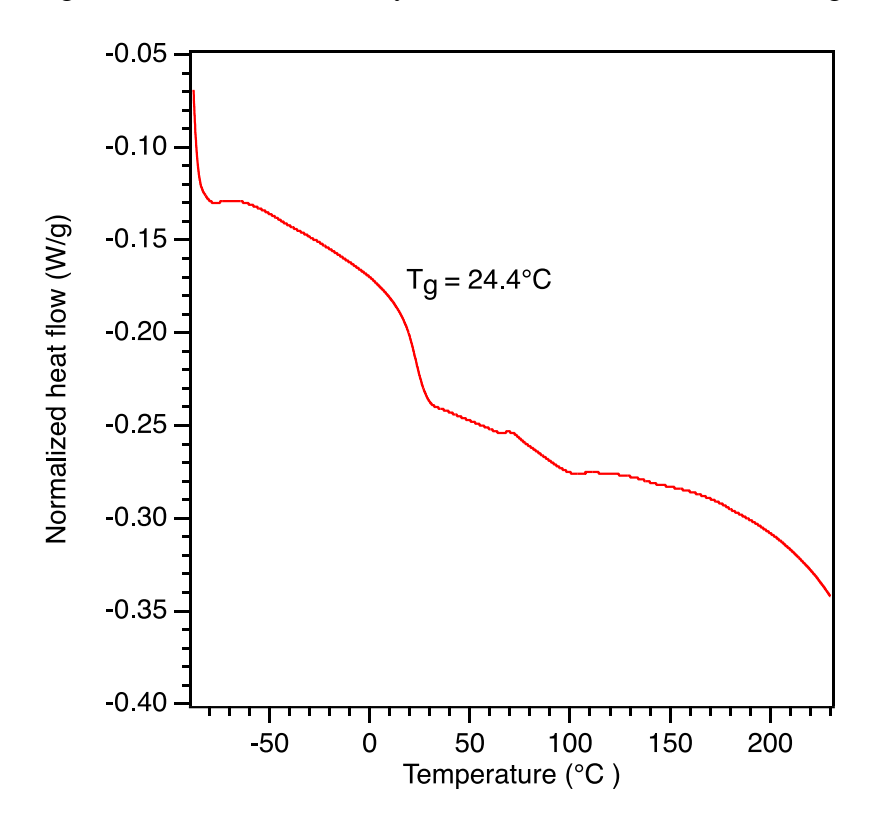


Figure 95: DSC data for Polycation obtained from PAGE-10 kg/mol

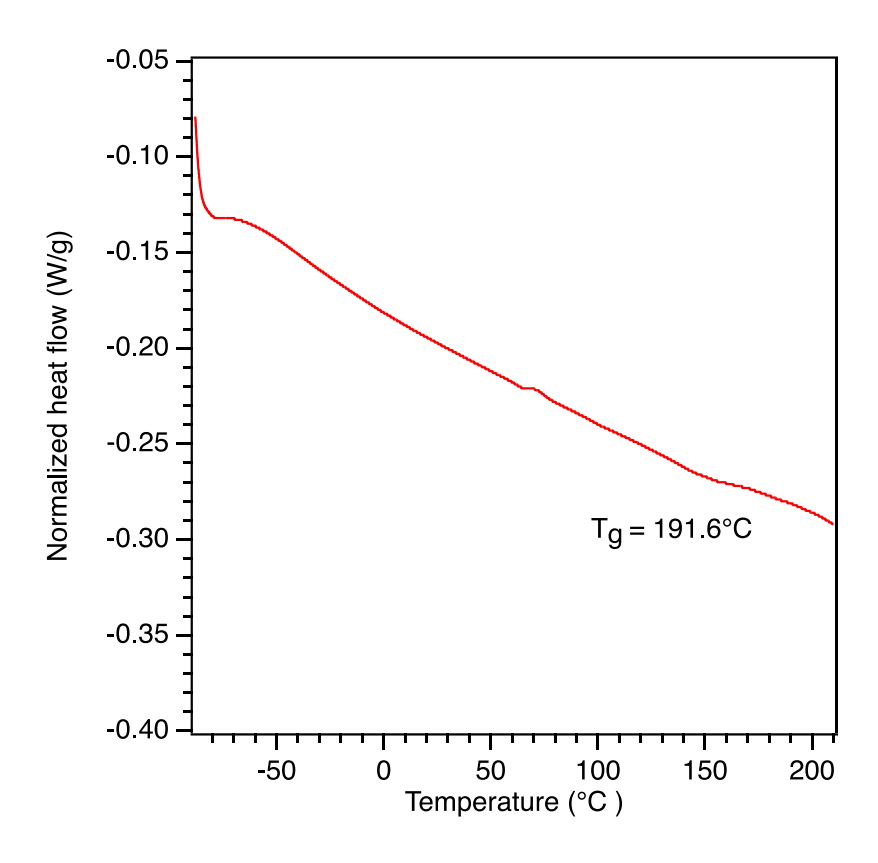


Figure 96: DSC data for Polyanion obtained from PAGE-20 kg/mol

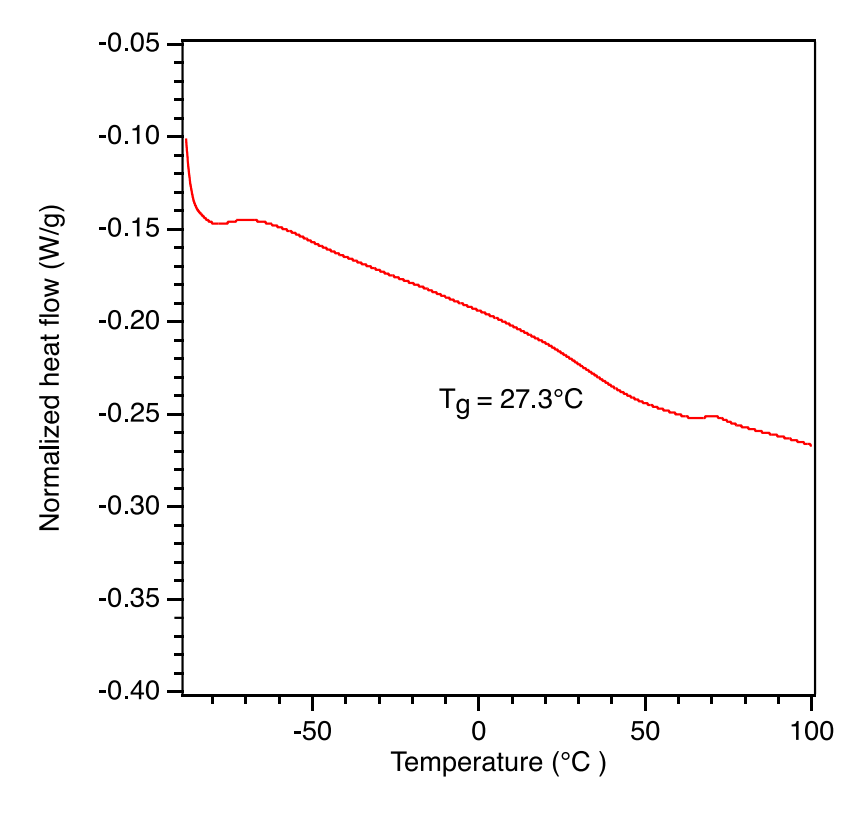


Figure 97: DSC data for Polycation obtained from PAGE-20 kg/mol

## Chapter 6. Conclusions and future work

Epoxides are a prime candidate for synthesizing functional polymeric materials due to as they are cost effective and ring strain enables polymerization feasible. There are array of functional epoxides available for polymerization and with the use of facile polymerization technique using mono(μ-alkoxo)bis(alkylaluminum) (MOB) system these epoxides have been effortlessly polymerized. In addition, the advantage of this system includes controlled molecular weight without any chain transfer for a range of functional epoxides.

In chapter 2, we demonstrated (co)polymerization of traditionally difficult epoxides polymerizations with the use of MOB system. We obtained multifunctional polyether via polymerization of two functional epoxides epichlorohydrin (ECH) and propargyl glycidyl ether (PGE) without requiring any protective chemistry for chloromethyl and alkyne functional group respectively. These types of copolymers have not been reported in literature previously. We achieved relatively higher molecular weight (upto 100 kg/mol) and good polydispersities. Conventionally researchers have used post polymerization modification methodologies to introduce these functionalities in polyethers. With the help of this techniques, we can eliminate the extra step for obtaining desired material properties. Since this is novel polymer, we studied the polymerization kinetics for copolymerization of PGE and ECH using in *situ* <sup>1</sup>H NMR spectroscopy. We calculated reactivity ratios and determined architecture of the copolymer to be a gradient statistical copolymer with more favorable addition of ECH over PGE. The benefit of having pendant alkene, alkyne or chloride is that we can further modify these polymers advanced applications.

In chapter 3, we showed that pendent functionality can be modified using orthogonal chemistries. Specifically, this thesis work involved post polymerization modification of polyethers to obtain

charged polymers. We modified precursor polyethers (described in chapter 2) to further introduce charged components in controlled manner. To accomplish this goal, first we employed thiol click chemistry reactions to modify alkene and alkyne pendent groups. With the use of different charged thiol, we have successfully modified homopolymers poly(allyl glycidyl ether) and poly(propargyl glycidyl ether) to obtain polyanion with sulfonate groups (using sodium-3-mercaptopropane sulfonate) as well as quaternary amine groups (using cysteamine hydrochloride). Simplistic thiol click chemistry proved to be efficient in achieving good control over charged moieties. To modify chloride from copolymer we carried out simple substitution reaction with methyl imidazole to obtain polycations. With the use of MOB system, we polymerized functional epoxides with varying composition, functionality, and molecular weight and by using orthogonal chemistries we can modified these precursor polyethers.

Next, we have utilized this platform to synthesize novel amphoteric ion exchange membranes (AIEMs). In this work, we developed a novel membrane by grafting charged polyether to PVDF-co-HFP matrix for electrochemical applications. We utilized sulfonate clicked copolymer of PGE and ECH which is (S-P(PGE-stat-ECH)) to graft onto PVDF-co-HFP using lingering chloromethyl as a grafting tool. These AIEMs demonstrated good thermal and mechanical stability. By tuning charged polyether content, membrane properties were optimized. We found a significant increase in water uptake, ionic conductivity, and IEC capacity with increased copolymer content, without a significant effect on stability. These properties compared favorably with other membranes found in the literature.

Furthermore, in chapter 5, we have utilized this charged polyether platform to study polyelectrolyte self-assembly. We performed some preliminary study using PAGE polymer system. We modified PAGE using thiol click chemistry and obtained polyanions (with sulfonates) and polycations (with

quaternary ammonium) to study effect of charge and molecular weight on self-assembly. Coacervation phenomenon was studied using turbidity measurements from UV-vis spectrophotometer. The absorbance spectra were used to correlate turbidity and extent of coacervation. We studied effect of NaCl and LiCl salt on polyelectrolyte self-assembly as well. The polymerization methodology using MOB system allows us to create polyelectrolytes with a multitude of chemical functionalities to investigate how charge, molecular weight, architecture, monomer sequence, hydrophobicity affect complexation. The work presented here will unite previous studies on polyelectrolyte self-assembly through the use of a single, robust, polymerization platform, innovate through interaction design, and inform future theoretical considerations for polyelectrolyte self-assembly. Therefore, fundamental understanding of effect of each of these parameters on self- assembly will help us design these materials better for advanced application in future.

Future directions for this thesis research involve development of multifunctional polyethers using variety of charged thiols and utilize it for engineering applications. We have developed tunable polymerization platform providing us with good structure—property relationships control for future applications.

Firstly, for AIEMs we anticipate that through optimization of functional groups by tuning charged component we can further enhance membrane performance. This membrane has a potential for use in electrochemical applications. Specifically, we want to study its cell performance in vanadium redox flow battery and quantify effect of amphoteric nature on vanadium ion permeability.

Next, we are equipped with this versatile platform through which we can understand and control macromolecular architecture in polyethers. Different parameters such as charge density, monomer sequence, polymer architecture, counter-ions, hydrophobicity affect complex coacervation process

while each of these parameters have been explored to some degree, they have not been investigated in the context of one single unified polymer platform. It is worthwhile to explore this single synthetic platform that can tune each parameter independently to understand and control polyelectrolyte self-assembly.

Lastly, P(PGE-*stat*-ECH) is a highly functional polymer with pendant alkyne and chloromethyl groups. With MOB polymerization platform, we can achieve accurately controlled molecular weights without any chain transfer and controlled chain-end functionality. Even tailored architecture is possible using combinations of spacer monomer and multi-site initiator. We can utilize this to develop coating of charged polyethers on the surface of reverse osmosis polyamide membrane. Increasing surface charges will increase the donnan potential and helps to reduce fouling tendency and minimize maintenance costs.

Figure 98: Proposed scheme for polyamide membrane modification using charged polyethers A statistical copolymer of PGE and epichlorohydrin can be considered a key factor for the synthesis of multifunctional charged polymers. Now keeping this platform as a central importance, we explored new charged polymers in these different contexts to better understand ion transport through membrane and charge polymer self-assembly.